Contents

Voorwoord **iii**

Samenvatting **vii**

Abstract **xi**

List of Abbreviations **xv**

List of Symbols **xvii**

List of Figures **xxi**

List of Tables **xxvii**

1 Introduction **1**
1.1 A short history of ionic liquids 2
1.2 Why should electrodeposition be carried out in ionic liquids? . . . 4
1.3 Electrochemical windows of ionic liquids 6
1.3.1 Experimental determination of electrochemical windows . . 7
1.3.2 Comparison with organic solvents 11
1.3.3 Electrochemical decomposition of ionic liquids 12
1.4 Reference electrodes for use in ionic liquids 16
1.5 Viscosity, conductivity and ionicity of ionic liquids 17
1.5.1 Application of hole theory on viscosity and conductivity . . 18
1.5.2 The Walden rule in ionic liquids and ionicity 19
1.5.3 Transport of ions in ionic liquids 22
1.6 Ionic liquids in high vacuum 24
1.6.1 Volatility and distillability of ionic liquids 24
1.6.2 Solubility of gases in ionic liquids 26
1.6.3 Examples of high vacuum applications for ionic liquids . . . 26
1.7 Additives for electroplating from ionic liquids 27
1.8 Liquid metal salts 29

1.9 Drying of ionic liquids 30
1.10 Outline and objectives 31
1.11 Properties of the used ionic liquids 33

2 Electrodeposition from cationic cuprous organic complexes: ionic liquids for high current density electroplating 55

3 High current density electrodeposition from silver complex ionic liquids 83

4 Electrodeposition from a liquid cationic cuprous organic complex for seed layer deposition 121

5 Direct Cu-on-Ta electroplating from ionic liquids in high vacuum 135

6 Oscillating electrochemical reaction in copper-containing imidazolium ionic liquids 149

7 Modeling of aluminium deposition from chloroaluminate ionic liquids 169

8 Conclusions and outlook 191
8.1 Conclusions 192
8.1.1 General conclusions 192
8.1.2 Breakthroughs 193
8.2 Outlook for further research 194

Appendix I

A Derivations I
A.1 Average hole size $\langle r_{hole} \rangle$ II
A.2 Stokes - Einstein equation III

List of Publications V

List of Contributions to International Conferences VII

Voorwoord

Het werk voor een doctoraat is onmogelijk alleen uit te voeren, zeker als het een experimenteel werk betreft. Er zijn dan ook een heleboel mensen die een oprechte bedanking verdienen.

In de eerste plaats wil ik mijn promotoren, Jan en Koen, bedanken voor de kans die ze mij hebben gegeven met dit doctoraat en hun niet-aflatende stroom aan wetenschappelijke ideeën tijdens de vele meetings, vergaderingen en occasionele ontmoetingen in het labo. Ook de traktaties met cake of zelfgekweekte kersen (en bananen) werden ten zeerste geapprecieerd. De andere leden van mijn jury zou ik willen bedanken voor hun opmerkingen en tips tijdens de *Ionic Liquid Days*, buitenlandse conferenties en/of preliminaire verdediging. Ook de voorzitter van mijn examencommissie, prof. Yves Willems wil ik danken voor de efficiënte manier waarop hij mijn preliminaire en publieke verdediging in goede banen stuurde. Het agentschap voor Innovatie door Wetenschap en Techniek (IWT) mag ik hier niet vergeten voor de 4 jaar van financiële steun.

In de voorbije jaren heb ik lokaal 01.55 met een heleboel collega's mogen delen. Allereerst is er Linda, de steun en toeverlaat voor elke doctoraatsstudent bij Jan[1], en Dimi die steeds te vinden was voor een humoristisch een-tweetje (vaak tot frustratie van de andere aanwezigen). Hai, the second cookie monster in the office and local Wifi installer, was always willing to help solve LaTeX-problems, and Ganapathi stood always ready when I needed a second pair of hands near my glove box and who was always eager to find out how I did my experiments. Uiteraard mag ik niet de andere personen vergeten die nu of in het verleden deel uitmaakten van de elektrodepositiegroep: Christian, Minxian, Gert, Eleonora, Wouter, Wagner, Michael, Annelien, Andrey, Lucia, Annelies en Evgeny.

Een groot voordeel van promotoren te hebben uit verschillende departementen is dat dit snel tot interdisciplinair onderzoek leidt. Neil, thank you for the nice

[1] Ik kan het niet beter verwoorden dan zoals Dimi het beschreef in het voorwoord van zijn thesis ;)

collaboration on the liquid metal salts. I believe that we can call the work fruitful, considering all the mutual papers (and more to come).

An, Marc, Pieter, en Wout: een welgemeend "dankuwel" voor jullie hulp bij analyses, onderhoud van de handschoenkasten, een handje toe te steken bij experimenten, de gezamenlijke wandeltochtjes naar het chemische magazijn en de babbels tussendoor. Ook Eddy, Gert en Joop, a.k.a. *de mannen van de werkplaats*, verdienen een pluim voor alle bestelbonnen die steeds met veel zorg en kunde werden afgewerkt, en Danny voor alle TGA-experimenten. Ik wil trouwens ook van de gelegenheid gebruik maken om me bij Paul te excuseren voor de talrijke keren dat ik hem vroeg: "*Waar is Olivier?*" Zodra die laatste opgespoord was, werden elektronische problemen snel opgelost zodat er tijd gespendeerd kon worden aan het bespreken van fotografie, de recentste voetbaluitslagen en andere belangrijke bijzaken des levens.

Andere bewoners van het labo die door hun aanwezigheid het labowerk verlichtten en daarom een eervolle vermelding verdienen zijn Bram, co-auteur van talrijke lijstjes op het labobord en partner tijdens vele practicasessies over chemisch gedrag, en Annabel en Tina, gekend onder de gemeenschappelijke naam van de *biobabes*. Ook Tina's toestemming om haar 2WD-fiets te gebruiken werd ten zeerste geapprecieerd.

Het hele FoF-team verdient om hier even in de spotlights te verschijnen. Dank u Kim, Lieven, Joop, Yann, Olivier, Dieter, Ling, Kobe, Oksana, Niels, Hai, Xiebin, Xuan, Gregory, Houcine, Yentl, Koen, Bin, Thomas, Bey, Dieter, and everybody else who joined voor wonderlijke wedstrijden, schitterende schoten, dolle dribbels, prachtige passes, geweldige goals en toverachtige tackles. Ondanks dat de matchen vaak op het scherp van de snee werden beslecht, waren ze telkens een hoogtepunt van de werkweek. Ook de sportievelingen die tijdens zomerse middagpauzes mee in het zand gingen duikelen voor een partijtje beachvolleybal, wil ik vereren met een bedankje. Verder mag ik ook het loopteam (Annelies, Lieven, Akhilesh en Yann) hier niet vergeten: ze hebben lang mogen aandringen voordat ik besloot de loopschoenveters aan te binden!

Het DTOC team, zowel de vorige als huidige generaties: dank u voor de met koekjes gespijsde vergaderingen, inefficiënte doch hilarische brainstormsessies en de uitstapjes en weekends om gekozen bestemmingen te gaan verkennen. Samengevat: de voorbereidingen waren al net zo plezant als de departementsreis zelf!

Verder mag ik niet vergeten om Olivier M. te bedanken voor het gebruik van zijn 2WD-fiets en de talrijke besprekingen over telescopische observaties van sterren,

planeten en andere wonderen aan het hemelgewelf: het hoeft namelijk niet altijd over microscopische waarnemingen te gaan.

Wie ook een eervolle vermelding verdient is Lore om mij in te wijden in de geneugten van *Jungle Speed*, *Regenwormen*, *Saboteur* en andere spellen. Uiteraard moet ik dan ook Bey, Maria, Victoria, Dieter, e.a. vermelden voor de talloze keren dat de pauze uitliep door het onschuldig lijkende zinnetje "*Ach, als we snel zijn kunnen we nog één rondje spelen.*"

Aan iedereen die momenteel nog bezig is aan zijn/haar leven als doctoraatsstudent (of er misschien nog aan moet beginnen), en opziet tegen het moment dat hij/zij moet beginnen aan het schrijven van de finale tekst: laat onderstaande strip een tip zijn.

"*Piled Higher and Deeper*" by Jorge Cham, www.phdcomics.com

Figure 1: The advantages of combining papers for a thesis.

Tenslotte aan mijn ouders en zus, die zich waarschijnlijk vaak hebben afgevraagd wat ik eigenlijk deed aan de universiteit: ik hoop dat jullie ondertussen een idee hebben gekregen van wat ik de voorbije 5 $\frac{1}{2}$ jaar heb uitgespookt.

Stijn Schaltin
Heverlee, maart 2012

Samenvatting

Elektrodepositie is een interessante en veel gebruikte techniek om dunne metaallagen aan te brengen op elektrisch geleidende materialen. De morfologie en samenstelling van zulke deklagen kan gecontroleerd worden door een juiste keuze van de procesparameters zoals badsamenstelling, temperatuur en de aangelegde waarde van potentiaal of stroomdichtheid. Tijdens de voorbije tien jaar was de elektrodepositie van metalen uit ionische vloeistoffen een populair onderzoekstopic. Niettemin zijn er nog heel wat uitdagingen die opgelost dienen te worden. Het grootste deel van dit doctoraat is gericht op volgende drie onderwerpen:

1. De karakterisering van vloeibare metaalzouten om de oplosbaarheid, en daardoor massatransport, van metalen in ionische vloeistoffen te verhogen
2. Het gebruik van hoog vacuüm als omgeving voor elektrodepositie
3. Invloed van snelheidsconstanten in chloroaluminaat-gebaseerde ionische vloeistoffen

Verder wordt de allereerste elektrochemische oscillator voorgesteld die bij toeval ontdekt werd in een ionische vloeistof. De technieken die tijdens dit doctoraat zijn gebruikt, zijn o. a.: Cyclische Voltammetrie (CV), Chronoamperometrie, Raster- (SEM) en Transmissie-elektronenmicroscopie (TEM), Atomaire Kracht Microscopie (AFM), Kwartskristal Microbalans (QCM), Optische Spectroscopie, Raman-spectroscopie en Eindige-Elementenmodellering.

Vloeibare metaalzouten zoals tetrakis(acetonitril) copper(I) bis(trifluoromethylsulfonyl)imide ($[Cu(MeCN)_4][Tf_2N]$) en tetrakis(benzonitril) copper(I) bis(trifluoromethylsulfonyl)imide ($[Cu(PhCN)_4][Tf_2N]$), bis(tetrakis(acetonitril) silver(I)) tris((trifluoromethylsulfonyl)imide) silver(I) ($[Ag(MeCN)_4]_2[Ag(Tf_2N)_3]$) en bis(1-ethylimidazole) silver(I) bis(trifluoromethylsulfonyl)imide ($[Ag(EtIm)_2][Tf_2N]$) werden elektrochemisch gekarakteriseerd. In een elektrochemisch proces zijn positief geladen complexen voordeliger dan negatief geladen complexen. Complexen gebaseerd op MeCN bleken het makkelijkst te reduceren, en stroomdichtheden tot 25 A dm^{-2} waren haalbaar, zelfs in ongeroerde oplossingen. De bij hoge

stroomdichtheid aangemaakte deklagen hadden een vlakke morfologie, vertoonden geen scheuren en bevatten geen onzuiverheden. Bij lage stroomdichtheden waren de deklagen nodulair, maar de morfologie kon worden verbeterd door het toevoegen van de additieven thioureum of 1*H*-benzotriazool. Het goede massatransport wordt waarschijnlijk veroorzaakt door enerzijds de hoge concentratie aan metaalionen in vloeibare metaalzouten en anderzijds door elektrische interactie tussen de positief geladen metaalcomplexen en de kathode. Hierdoor zijn vloeibare metaalzouten interessant voor elektrochemische toepassingen waar een hoge stroomdichtheid is vereist. Het feit dat gelijkaardige resultaten worden bekomen voor zowel koper als zilver geeft aan dat complexen, bestaande uit een metaal met acetonitril als ligand, gebruikt kunnen worden voor elektrodepositie aan een hoge stroomdichtheid. Een tweede interessante eigenschap van de vloeibare metaalzouten is het feit dat hoge overpotentialen kunnen aangelegd worden. Dit heeft als voordeel dat de kritische grootte van een nucleatiekiem wordt verkleind. Dat is interessant voor de elektrodepositie van koper op barrièrelagen zoals tantaal. Door $[Cu(MeCN)_2][Tf_2N]$ te gebruiken als solvent voor koper-op-tantaaldepositie, kan een nucleatiedichtheid van $8{\cdot}10^{14}$ m^{-2} gehaald worden, waarmee gesloten deklagen kunnen afgezet worden van 19 nm dik.

Elektrochemische vacuumdepositie is een techniek die gebruik maakt van een bijzondere eigenschap van de meeste ionische vloeistoffen: een erg lage dampspanning. Daardoor kunnen ionische vloeistoffen geplaatst worden in een omgeving van hoog vacuüm zonder verdamping van de ionische vloeistof, dit in tegenstelling met waterige oplossingen of organische solventen. In zulk een omgeving is de hoeveelheid water en zuurstofgas sterk verminderd. Een mogelijke toepassing is de elektrodepositie van koper op tantaal, maar de experimenten geven aan dat, zelfs in hoog vacuüm, er oxidatie van het tantaal optreedt.

Een eindige-elementenmodel beschrijft de elektrodepositie van aluminium uit chloroaluminaat-gebaseerde ionische vloeistoffen. Het bleek dat de snelheidsconstanten van de evenwichtsvergelijking tussen $Al_2Cl_7^-$, $AlCl_4^-$ en Cl^- een sterke invloed hebben op de stroomdichtheid tijdens het afzetten van aluminium. Dit wordt veroorzaakt doordat de thermodynamica en kinetica van de reductiereactie in tegengestelde zin evolueren als functie van k_b. Dit leidt tot een minimum in de berekende stroomdichtheid. Een vergelijking tussen deze berekende stroomdichtheid en de experimenteel bepaalde stroomdichtheid geeft aan dat de waarde voor k_b zich bevindt tussen $10^{-7.5}$ en $10^{-6.7}$ $m^3\ mol^{-1}\ s^{-1}$.

Elektrochemische oscillaties zijn het verschijnsel waarbij een aangelegde constante potentiaal aanleiding geeft tot een oscillerende stroom, of waarbij een oscillerende spanning veroorzaakt wordt door een aangelegde constante stroom. Een elektrochemische oscillator van het eerste type werd ontdekt in de ionische vloeistof

1-ethyl-3-methylimidazolium chloride waarin zowel één- als tweewaardige koperionen waren opgelost. De oscillator kon worden gecatalogeerd als een N-NDR-type enerzijds omdat het impedantiespectrum negatieve impedanties vertoont voor lage frequenties en anderzijds omdat het stroomsignaal een sterke terugval liet zien tijdens een potentiaalscan. De detectie van een oscillerend signaal vereist de aanwezigheid van chloride-ionen, en ook is het imidazoliumkation betrokken bij de reacties die leiden tot het oscillerend gedrag.

Abstract

Electrodeposition is an interesting and often used technique to deposit thin films of metals onto conducting substrates. During electrodeposition, film properties such as morphology or composition can be adjusted by controlling process parameters such as bath composition, temperature and applied potential or current density. The electrodeposition of metals from ionic liquids has become a heavily studied topic in the last decade but still lots of challenges remain. This thesis investigates three main topics:

1. The use of liquid metal salts to increase the solubility of metals in ionic liquids, hereby improving the mass transport
2. The application of high vacuum as an environment for electrodeposition
3. Influence of rate constants in chloroaluminates

Furthermore, the first electrochemical oscillator in ionic liquids was discovered by serendipity. The techniques, used in this PhD thesis, consist of Cyclic Voltammetry (CV), Chronoamperometry, Scanning Electron Microscopy (SEM), Transmission Electron Microscopy (TEM), Atomic Force Microscopy (AFM), Quartz Crystal Microbalance (QCM), Optical Spectroscopy, Raman Spectroscopy and Finite Element Modeling.

The liquid metal salts tetrakis(acetonitrile) copper(I) bis(trifluoromethylsulfonyl)imide ($[Cu(MeCN)_4][Tf_2N]$) and tetrakis(benzonitrile) copper(I) bis(trifluoromethylsulfonyl)imide ($[Cu(PhCN)_4][Tf_2N]$), bis(tetrakis(acetonitrile) silver(I)) tris((trifluoromethylsulfonyl)imide) silver(I) ($[Ag(MeCN)_4]_2[Ag(Tf_2N)_3]$) and bis(1-ethylimidazole) silver(I) bis(trifluoromethylsulfonyl)imide ($[Ag(EtIm)_2][Tf_2N]$) were electrochemically characterized: for electrodeposition purposes, low melting salts with a cationic complex are preferred over anionic complexes. The MeCN complexes are the easiest to be reduced and current densities up to 25 A dm^{-2} in unstirred solutions could be achieved. The resulting copper or silver deposits, made at high current densities, have a smooth appearance, did not show cracks and were free from entrapped organic compounds. Lower current densities result

in nodular deposits. The use of thiourea or 1*H*-benzotriazole as additive resulted in smooth morphologies at 1 A dm^{-2}. It is believed that excellent mass transport in this system is due to the high metal concentration and to the favorable electrostatic interactions between the cationic electroactive species and the cathode. This makes the use of liquid metal salts with electrochemically active cationic complexes interesting for electrochemical applications where mass transport is important. The fact that comparable results are obtained for two metals, indicates that the complexes with a metal center, surrounded by acetonitrile, lead to ionic liquids that can be used for high current density electroplating. A second interesting property of liquid metal salts is that high overpotentials can be applied during electrodeposition. This leads to a small critical size for nucleation, which is advantageous during the plating of copper on barrier materials such as tantalum. By using $[Cu(MeCN)_2][Tf_2N]$ as medium for copper electrodeposition on a tantalum substrate, a nucleation density of $8{\cdot}10^{14}$ m^{-2} is reached. The resulting deposits contain very few pinholes and have thicknesses of $\pm$19 nm.

Electrochemical vacuum deposition is a technique which exploits the low vapor pressure of ionic liquids. In contrast with aqueous solutions or organic solvents, ionic liquids can be placed in a high vacuum environment, without noticeable loss of ionic liquid, to strongly decrease the amount of oxygen gas and water. Possible applications are the deposition of copper on tantalum, but results indicate that even at the low pressure of a high vacuum environment, the oxidation of tantalum cannot be avoided.

A finite element model of the electrodeposition of aluminium from chloroaluminate ionic liquids was made to study the influence of the rate constants k_b and k_f on the electrodeposition rate of aluminium. These rate constants determine the equilibrium between $Al_2Cl_7^-$, $AlCl_4^-$ and Cl^-. It was found that thermodynamics and kinetics change in opposite directions for variations in k_b or k_f and these opposing effects lead to a minimum in the calculated current density as a function of k_b. A comparison of the calculated data and the experimental limiting current densities indicates that the value of k_b lies between $10^{-7.5}$ and $10^{-6.7}$ m^3 mol^{-1} s^{-1}.

Electrochemical oscillations are a phenomenon in which a constant applied potential leads to an oscillating current or that a constant applied current gives rise to an oscillating potential. A former type of electrochemical oscillator was found in a mixture of monovalent with divalent copper ions in 1-ethyl-3-methylimidazolium chloride. The oscillator is an N-NDR-type because the low frequency-end of the impedance spectrum has negative real impedances and the steep decrease in current in the potential-current curve. The presence of chloride is also a necessary, yet not a sufficient condition for the occurrence of current oscillations and the

imidazolium cation also plays a role in the reactions leading to the oscillatory behavior.

List of Abbreviations

Abbreviation	Meaning
AFM	atomic force microscopy
$[BBnP]^+$	*N*-butyl-*N*-butylnitrilepyrrolidinium
$[BEnP]^+$	*N*-butyl-*N*-ethylnitrilepyrrolidinium
$[BEP]^+$	*N*-butyl-*N*-ethylpyrrolidinium
$[BMP]^+$	*N*-butyl-*N*-methylpyrrolidinium
$[BnMP]^+$	*N*-butylnitrile-*N*-methylpyrrolidinium
bpy	2,2'-bipyridine
BuIm	1-butylimidazole
$[C_4dmim]^+$	1-butyl-2,3-dimethylimidazolium
$[C_4pyr]^+$	*N*-butylpyridinium
$[C_nmim]^+$	1-*n*-alkyl-3-methylimidazolium
CV	Cyclic voltammetry
DMSO	dimethyl sulfoxide
DSC	differential scanning calorimetry
EDX	energy dispersive X-ray spectroscopy
EIS	electrochemical impedance spectroscopy
$[EMP]^+$	*N*-ethyl-*N*-methylpyrrolidinium
$[EnMP]^+$	*N*-ethylnitrile-*N*-methylpyrrolidinium
EtIm	1-ethylimidazole
EVD	electrochemical vacuum deposition
Fc	ferrocene
Fc^+	ferrocenium
$[HnMP]^+$	*N*-hexylnitrile-*N*-methylpyrrolidinium
ICP-AES	inductively coupled plasma - atomic emission spectrometry
IR	infrared
MeCN	acetonitrile
MeIm	1-methylimidazole

(*Continued on next page*)

Abbreviation	Meaning
$[MPPip]^+$	1-methyl-1-propylpiperidinium
NDR	negative differential resistance
NHE	normal hydrogen electrode
OPD	overpotential deposition
$[P_{4,4,4,14}]^+$	tributyltetradecylphosphonium
PhCN	benzonitrile
$[PMP]^+$	*N*-propyl-*N*-methylpyrrolidinium
PrIm	1-propylimidazole
PTFE	polytetrafluoroethylene
PVD	physical vapor deposition
py	pyridine
QCM	quartz crystal microbalance
RDE	rotating disk electrode
RT	room temperature
SCE	saturated calomel electrode
SEM	scanning electron microscopy
SERS	surface enhanced raman spectroscopy
TEM	transmission electron microscopy
$[Tf_2N]^-$	bis(trifluoromethylsulfonyl)imide, $N(SO_2CF_3)^-$
$[TfO]^-$	trifluoromethanesulfonate, $CF_3SO_3^-$
TGA	thermogravimetrical analysis
TSV	through-silicon-via
UPD	underpotential deposition
XPS	X-ray photoelectron spectroscopy

List of Symbols

Symbol	Meaning	[Unit]
c	molar concentration	[mol m^{-3}]
d	deposit thickness	[m]
e	elementary charge	[C]
f	frequency	[Hz]
j	current density	[A m^{-2}]
j_L	limiting current density	[A m^{-2}]
k	Boltzmann constant	[J K^{-1}]
k_b	backward reaction rate constant	[m^3 mol^{-1} s^{-1}]
k_f	forward reaction rate constant	[m^3 mol^{-1} s^{-1}]
k^o_{ox}	heterogeneous rate constant for oxidation	[mol m^{-2} s^{-1}]
k^o_{red}	heterogeneous rate constant for reduction	[m s^{-1}]
l	length	[m]
n	number of exchanged electrons	
p	partial pressure	[Pa]
r	(a) radius	[m]
	(b) radial coordinate	[m]
r_c	critical radius for nucleation	[m]
r_{dc}	radius of diffusing complex	[m]
t	time	[s]
$\mathbf{u}$	fluid velocity vector	[m s^{-1}]
u	scalar fluid velocity	[m s^{-1}]
x	molar fraction	
z	axial coordinate	[m]
A	pre-exponential constant	
C_{dl}	double layer capacitance	[F]
D	diffusion coefficient	[m^2 s^{-1}]

(*Continued on next page*)

Symbol	Meaning	[Unit]
E	potential	[V]
E_{act}	activation energy	[J mol^{-1}]
F	Faraday constant	[C mol^{-1}]
G	Gibbs free energy	[J mol^{-1}]
H	Henry coefficient	[Pa]
J	molar flux	[mol m^{-2} s^{-1}]
K_{eq}	equilibrium constant	
N	nucleation density	[m^{-2}]
N_a	Avogadro constant	[mol^{-1}]
P	vapor pressure	[Pa]
P_r	probability	
R	(a) resistance	[Ω]
	(b) bulk reaction rate	[mol m^{-3}]
R_a	arithmetic mean roughness	[m]
R_{ct}	charge transfer resistance	[Ω]
R_g	gas constant	[J mol^{-1} K^{-1}]
R_q	root mean square roughness	[m]
T	temperature	[K]
T_b	boiling temperature	[K]
T_c	critical temperature	[K]
T_g	glass-transition temperature	[K]
T_m	melting temperature	[K]
V_{mol}	molar volume	[m^3 mol^{-1}]
W	Warburg impedance	[Ω]
Z_{Im}	imaginary impedance	[Ω]
Z_{Re}	real impedance	[Ω]
α	charge transfer coefficient for reduction	
β	charge transfer coefficient for oxidation	
γ	surface energy	[J m^{-2}]
η	overpotential	[V]
η_c	concentration overpotential	[V]
θ	(a) phase angle	[°]
	(b) angular coordinate	[rad]
μ	dynamic viscosity	[Pa s]
ν	kinematic viscosity	[m^2 s^{-1}]
ξ	coefficient of sliding friction	
σ	electrical conductivity	[Ω^{-1} m^{-1}]
ω	angular frequency of rotation	[rad s^{-1}]

(*Continued on next page*)

Symbol	Meaning	[Unit]
Θ	Sutherland coefficient	
Λ	molar conductivity	$[m^2\ \Omega^{-1}\ mol^{-1}]$

List of Figures

1 The advantages of combining papers for a thesis. v

1.1 Molecular structure of popular cations for ionic liquids: (a) 1-alkyl-3-methylimidazolium, (b) *N*-alkyl-*N*-methylpyrrolidinium, (c) 1-alkylpyridinium, (d) 1-alkyl-1-methylpiperidinium, (e) tetraalkylammonium, (f) tetraalkylphosphonium. 3

1.2 Potential window of [BMP][Tf_2N] measured at 90 °C on a Pt working electrode using a scan rate of 20 mV s^{-1}. Figure (a) shows the potential window measured in the glove box, figure (b) gives the potential window in high vacuum ($2{\cdot}10^{-6}$ mbar) [90]. 8

1.3 Electrochemical windows of ionic liquids measured at 90 °C on a Pt working electrode [90]. 9

1.4 Molecular structure of the $[BnMP]^+$ cation. 10

1.5 Comparison of the electrochemical windows of seven organic solvents. All data are valid for platinum working electrodes. dimethylsulfoxide (DMSO), dimethylformamide (DMF), hexamethylphosphorotriamide (HMPT), dimethoxyethane (DME), tetrahydrofuran (THF), acetonitrile (MeCN) and propylene carbonate (PC). These data are from reference [119]. 13

1.6 Cathodic decomposition reactions of $[C_4mim]^+$ as described by Kroon *et al.* [120] 14

1.7 Cathodic decomposition reactions of $[BMP]^+$ as described by Kroon *et al.* [120] 15

1.8 Schematic representation of the Fc/Fc^+-reference electrode. 17

1.9 If the radius of the complete ion is considered (r_1), calculations lead to an underestimation of the conductivity, when only the size of the ring is considered (r_2) more reliable results are found. 19

1.10 Walden plot of three hypothetical ionic liquids and an aqueous solution of KCl. 21

1.11 (a) Coordinate system on a rotating disk electrode, (b) fluid flow on a rotating disk electrode. 24

2.1 Structural formulae of the cations of the copper-containing ionic liquids (a) $[Cu(MeCN)_4][Tf_2N]$ and (b) $[Cu(PhCN)_4][Tf_2N]$. 58
2.2 TGA curve of $[Cu(MeCN)_4][Tf_2N]$: the temperature was scanned from room temperature to 300 °C at 5 °C per minute. The dotted lines indicate the theoretical mass losses leading to the formation of the different $[Cu(MeCN)_x][Tf_2N]$ complexes. 60
2.3 TGA curve of $[Cu(PhCN)_4][Tf_2N]$: the temperature was scanned from room temperature to 300 °C at 5 °C per minute. The dotted lines indicate the theoretical mass losses leading to the formation of the different $[Cu(PhCN)_x][Tf_2N]$ complexes. 61
2.4 Cyclic voltammograms of (a) $[Cu(MeCN)_2][Tf_2N]$ and (b) $[Cu(PhCN)_2]$-$[Tf_2N]$ on a Pt working electrode at 90 °C. The scan rate was 50 mV s^{-1}. 62
2.5 Potential scan versus a home-made reference electrode (see text) on a Pt working electrode at 90 °C for $[Cu(MeCN)_2][Tf_2N]$ and $[Cu(PhCN)_2][Tf_2N]$. The scan rate was 50 mV s^{-1}. 63
2.6 Copper deposit from $[Cu(PhCN)_2][Tf_2N]$ on a Pt working electrode at 90 °C. The deposition potential was -0.25 V and it was applied until a theoretical thickness of 1 μm was reached (135 C dm^{-2}). . 64
2.7 Preliminary experiment on $[Cu(MeCN)_2][Tf_2N]$ on a Pt working electrode at 90 °C: (a) linear potential scan at 50 mV s^{-1}, (b) dendritic copper deposit from $[Cu(MeCN)_2][Tf_2N]$. 65
2.8 Schematic of the electrochemical cell: (a) Overview of the electrochemical cell, (b) Cross-section of the electrochemical cell with isopotential lines. 66
2.9 Electrochemical impedance spectrum of $[Cu(MeCN)_2][Tf_2N]$ on a Pt working electrode at 90 °C at +0.1 V vs Cu for the frequency range 100 kHz − 1 Hz. 67
2.10 (a) Cyclic voltammogram of $[Cu(MeCN)_2][Tf_2N]$ on a Pt working electrode at 90 °C and (b) cyclic voltammogram (solid line) and potential scan (dotted line, see also figure 2.11), corrected for iR drop. 68
2.11 Linear potential scan of $[Cu(MeCN)_2][Tf_2N]$ on a Pt working electrode at 90 °C. This scan was not corrected for iR drop. See also figure 2.10(b). 69
2.12 Copper deposits from $[Cu(MeCN)_2][Tf_2N]$ on a Pt working electrode at 90 °C for (a) 1 A dm^{-2}, (b) 5 A dm^{-2} and (c) 25 A dm^{-2}. Theoretical thickness of 1 μm (135 C dm^{-2}). 70
2.13 EDX spectrum of a copper deposit obtained at 25 A dm^{-2} from $[Cu(MeCN)_2][Tf_2N]$ at 90 °C (see figure 2.12(c)). 70

2.14 Experiments performed on a platinum rotating disk in $[Cu(MeCN)_2]$-$[Tf_2N]$ at 90 °C: (a) linear potential scans at 5 mV s^{-1} and (b) Steady-state current j_L as a function of $\sqrt{\omega}$. 72
2.15 Cyclic voltammograms of $[Cu(MeCN)_2][Tf_2N]$ on a Pt working electrode at 90 °C. $(\cdots)$ no additive, $(--)$ 0.05 mol dm^{-3} thiourea, $(-)$ 0.1 mol dm^{-3} 1*H*-benzotriazole. 74
2.16 Deposits from $[Cu(MeCN)_2][Tf_2N]$ at 90 °C on a Pt working electrode at 1 A dm^{-2}: (a) no additive, (b) 0.05 mol dm^{-3} thiourea, (c) 0.1 mol dm^{-3} 1*H*-benzotriazole. The theoretical thickness is 1 μm. 75
2.17 AFM topologies of deposits from $[Cu(MeCN)_2][Tf_2N]$ at 90 °C on a Pt working electrode at 1 A dm^{-2}: (a) no additive, (b) 0.05 mol dm^{-3} thiourea, (c) 0.1 mol dm^{-3} 1*H*-benzotriazole. See also figure 2.16. 77
2.18 Roughness profiles of deposits from $[Cu(MeCN)_2][Tf_2N]$ at 90 °C on a Pt working electrode at 1 A dm^{-2}: (a) no additive, (b) 0.05 mol dm^{-3} thiourea, (c) 0.1 mol dm^{-3} 1*H*-benzotriazole. See also figure 2.17. 78

3.1 View of the crystal structure of $[Ag(MeCN)_4]_2[Ag(Tf_2N)_3]$. 89
3.2 View of the packing in the crystal structure of $[Ag(MeCN)_4]_2[Ag(Tf_2N)_3]$, viewed along the crystallographic *c* axis. 90
3.3 View of the crystal structure of $[Ag(MeCN)][Tf_2N]$ showing the polymeric structure. The longer Ag−O bond is shown in green. . . 91
3.4 View of the crystal structure of $[Ag(EtIm)_2][Tf_2N]$. 92
3.5 Thermogravimetrical analysis data for (a) $[Ag(MeCN)_4]_2[Ag(Tf_2N)_3]$ with the temperature program on the right vertical axis, and (b) $[Ag(EtIm)_2][Tf_2N]$ (heating rate: 5 °C $min.^{-1}$). 93
3.6 Voltammetry experiments in $[Ag(MeCN)_4]_2[Ag(Tf_2N)_3]$ at 50 °C and $[Ag(EtIm)_2][Tf_2N]$ at 90 °C on a Au working electrode: (a) cyclic voltammogram (corrected for iR drop); (b) linear potential scan (not corrected for iR drop). 94
3.7 Silver deposits from $[Ag(MeCN)_4]_2[Ag(Tf_2N)_3]$ on a Au working electrode at 50 °C for different current densities: (a) 1 A dm^{-2}, (b) 5 A dm^{-2}, and (c) 25 A dm^{-2}. The theoretical thickness is 1 μm. 97
3.8 Silver deposits from $[Ag(EtIm)_2][Tf_2N]$ on a Au working electrode at 90 °C for different current densities: (a) 1 A dm^{-2}, (b) 5 A dm^{-2}, and (c) 25 A dm^{-2}. The theoretical thickness is 1 μm. . . . 98
3.9 EDX spectrum of a silver deposit obtained at 25 A dm^{-2} from $[Ag(MeCN)_4]_2[Ag(Tf_2N)_3]$ at 50 °C (see figure 3.7(c)). A similar EDX spectrum was observed for a deposit from $[Ag(EtIm)_2][Tf_2N]$ at 90 °C. 99

3.10 Silver deposits from $[Ag(MeCN)_4]_2[Ag(Tf_2N)_3]$ on a Au working electrode at 50 °C for 1 A dm^{-2} with 0.05 mol dm^{-3} of (a) thiourea or (b) 1*H*-benzotriazole. The theoretical thickness is 1 μm. 100

3.11 AFM topologies of silver deposits from $[Ag(MeCN)_4]_2[Ag(Tf_2N)_3]$ at 50 °C on a Au working electrode at 1 A dm^{-2}: (a) no additive, (b) 0.05 mol dm^{-3} thiourea, (c) 0.05 mol dm^{-3} 1*H*-benzotriazole. 102

3.12 Roughness profiles, based on AFM data, of silver deposits from $[Ag(MeCN)_4]_2[Ag(Tf_2N)_3]$ at 50 °C on a Au working electrode at 1 A dm^{-2}: (a) no additive, (b) 0.05 mol dm^{-3} thiourea, (c) 0.05 mol dm^{-3} 1*H*-benzotriazole. 103

3.13 Raman spectra of (a) $[Ag(MeCN)_4]_2[Ag(Tf_2N)_3]$ (see ESI), (b) 1*H*-benzotriazole, (c) 0.1 mol dm^{-3} 1*H*-benzotriazole in $[Ag(MeCN)_4]_2$-$[Ag(Tf_2N)_3]$. (d) SERS spectrum of 0.1 mol dm^{-3} 1*H*-benzotriazole in $[Ag(MeCN)_4]_2[Ag(Tf_2N)_3]$ on a silver foil. The dashed lines indicate wavenumber values mentioned in the text. 104

3.14 Raman spectrum of solid $[Ag(MeCN)_4]_2[Ag(Tf_2N)_3]$. 106

3.15 Raman spectrum of liquid $[Ag(MeCN)_4]_2[Ag(Tf_2N)_3]$. 107

3.16 View of the packing in the crystal structure of $[Ag(MeCN)][Tf_2N]$, viewed along the crystallographic *a* axis. 108

3.17 View of the packing in the crystal structure of $[Ag(EtIm)_2][Tf_2N]$, viewed along the crystallographic *b* axis. 109

3.18 Silver deposits from $[Ag(MeCN)_4]_2[Ag(Tf_2N)_3]$, saturated with water, on a Au working electrode at 50 °C for different current densities: (a) 1 A dm^{-2}, (b) 5 A dm^{-2}, and (c) 25 A dm^{-2}. The theoretical thickness is 1 μm. 110

3.19 Cyclic voltammograms of $[Ag(MeCN)_4]_2[Ag(Tf_2N)_3]$ on a Au working electrode at 50 °C. $(\cdots)$ no additive, $(--)$ 0.05 mol dm^{-3} thiourea, $(-)$ 0.05 mol dm^{-3} 1*H*-benzotriazole. 111

3.20 Silver deposits from $[Ag(MeCN)_4]_2[Ag(Tf_2N)_3]$ on a Au working electrode at 50 °C for 5 A dm^{-2} and 25 A dm^{-2} with 0.05 mol dm^{-3} of the mentioned additive. The theoretical thickness is 1 μm. 112

3.21 Silver deposits from $[Ag(EtIm)_2][Tf_2N]$ on a Au working electrode at 90 °C for 1 A dm^{-2}, 5 A dm^{-2} and 25 A dm^{-2} with 0.05 mol dm^{-3} of the mentioned additive. The theoretical thickness is 1 μm. 113

4.1 Structural formula of the cation of the copper-containing ionic liquid $[Cu(MeCN)_4][Tf_2N]$. 124

4.2 (a) Seed layer stripping at +0.5 V. (b) Cyclic voltammograms of the ionic liquid $[Cu(MeCN)_2][Tf_2N]$ on a tantalum working electrode at 90 °C. The scan rate was 50 mV s^{-1}. 127

4.3 SEM micrographs of copper deposits from the ionic liquid $[Cu(MeCN)_2]$-$[Tf_2N]$ on a tantalum working electrode after seed layer stripping at +0.5 V at 90 °C: (a) 0.5 s at -3.0 V, (b) 0.25 s at -4.0 V, (c) 0.25 s at -5.0 V. 129
4.4 TEM cross-section of a copper deposit from the ionic liquid $[Cu(MeCN)_2]$-$[Tf_2N]$ on a tantalum working electrode at 90 °C: 0.25 s at -5.0 V. The white lines mark the tantalum oxide layer. 130

5.1 Absorption spectra at room temperature of the stabilized [BMP]-$[Tf_2N]$-$Cu(Tf_2N)$ solution (dashed line) and six Cu^{2+} solutions with different concentrations (solid lines). Insert: absorbance as function of Cu^{2+} concentration at a wavelength of 955 nm. 139
5.2 Amount of O_2 that has reacted with the electrode per unit area as a function of time. 141
5.3 Cyclic voltammograms of 1 mol dm^{-3} of $Cu(Tf_2N)$ in $[BMP][Tf_2N]$ at 90 °C on (a) a Pt working electrode, (b) a Ta working electrode. The scan rate was 50 mV s^{-1}. 142
5.4 TEM cross section of a deposit made in 1 mol dm^{-3} of $Cu(Tf_2N)$ in $[BMP][Tf_2N]$-[BMP]Cl (50-50 mol%) at 90 °C. The deposition potential was -3 V and was applied for 500 ms. The white circles indicate the renucleated layer. The oxide layer is marked by two lines on the Cu-Ta interface. 143

6.1 Schematic of the experimental setup, with relative positions of the working (WE), reference (RE) and counter electrode (CE). 153
6.2 (a): Polarization at -1.0 V. $(--)$ cupric solution, $(\cdot\cdot)$ cuprous solution, $(-)$ mixed Cu^{2+}/Cu^{+} solution. (b): Extended view for the mixed Cu^{2+}/Cu^{+} solution of Fig. 6.2(a) 154
6.3 Rotating disk electrode experiment at 250 rpm at -1.0 V on the mixed Cu^{2+}/Cu^{+} solution. 155
6.4 Polarization at -1.0 V in the equilibrated mixed Cu^{2+}/Cu^{+} solution. (a) no cupric solution added, (b) two drops of cupric solution added, (c) three drops of cupric solution added, (d) four drops of cupric solution added. 156
6.5 Current density (upper curve) and growth rate of the deposited copper layer (lower curve) as a function of time in the mixed Cu^{2+}/Cu^{+} solution. 157
6.6 Potential scan $(-)$ at 20 mV s^{-1} and current scan $(\cdot\cdot)$ at 20 mA dm^{-2} s^{-1} in the mixed Cu^{2+}/Cu^{+} solution. The $j-E$ curve under potential control clearly resembles the shape of the letter N. $(--)$: Potential scan of the cupric solution. 157

6.7 Impedance spectrum (0.1−1000 Hz) of the mixed Cu^{2+}/Cu^{+} solution at two polarization potentials. (- -) -0.5 V, (−) -1.0 V. (a) Nyquist plot, (b) Bode plot. 159
6.8 Simple equivalent circuit of an electrode indicating the meaning of the double layer capacitance C_{dl}, the charge transfer resistance R_{ct} and the Warburg impedance W. 159
6.9 Polarization at -1.0 V for different temperatures in the mixed Cu^{2+}/Cu^{+} solution. 160

7.1 Schematic representation of the one-dimensional model: point A represents the active area of a rotating disk electrode and point B the bulk solution. 172
7.2 Calculated current densities for different rotation speeds. Only the first 10 s are shown. The numbers on the graph indicate different values for n in $k_b = 10^n$ m^3 mol^{-1} s^{-1}. 176
7.3 Calculated concentration profiles for $Al_2Cl_7^-$, $AlCl_4^-$ and Cl^- after 100 s at -0.75 V. (- -) $k_b = 10^{-25}$ m^3 mol^{-1} s^{-1}, (−) $k_b = 10^{-8}$ m^3 mol^{-1} s^{-1}, (··) $k_b = 10^{-5}$ m^3 mol^{-1} s^{-1}. The graphs are explained in the text. Please note that the scale on the horizontal axis is different for the two rotation speeds. 177
7.4 Calculated concentration ratios after 100 s at -0.75 V for the stirred solution. The numbers on the graph indicate different values for n in $k_b = 10^n$ m^3 mol^{-1} s^{-1}. 179
7.5 Linear potential scans for different rotation speeds at 20 mV s^{-1} and Koutecky-Levich plot of $AlCl_3$ - $[C_2mim]Cl$ (60-40 mol%) at 40 °C. 181
7.6 Calculated limiting current density j_L as a function of k_b for different rotation rates. The + and × signs indicate the intersection with the experimental j_L values (figure 7.5(a)). 182

8.1 Complexes used for germanium deposition: (a) $GeCl_4(py)_2$, (b) $GeCl_4(bpy)$, (c) $GeCl_4(DMSO)_2$, (d) $GeCl_4(BuIm)_2$. 195

A.1 Motion of spherical particle with velocity v through a medium with viscosity μ. III

List of Tables

1.1 Comparison of organic solvents with ionic liquids [4] 5
1.2 Melting points (T_m), viscosities (μ) and electrical conductivities (σ) of ionic liquids used in this thesis 33

2.1 R_a and R_q values for deposits from $[Cu(MeCN)_2][Tf_2N]$ at 90 °C on a Pt working electrode at 1 A dm^{-2}, obtained in the absence and presence of additives. 76

3.1 Melting points (T_m), viscosities (μ) and electrical conductivities (κ) of the three silver complexes 95
3.2 R_a and R_q values for deposits from $[Ag(MeCN)_4]_2[Ag(Tf_2N)_3]$ at 50 °C on a Au working electrode at 1 A dm^{-2}, obtained in the absence and presence of additives. 101

6.1 Influence of the temperature on the oscillating behavior 161
6.2 Mixtures investigated for oscillations 162

7.1 Values for the equilibrium constant K_{eq} at different temperatures . 173
7.2 Experimental j_L values for different rotation speeds. Also given are the k_b values for which the calculated limiting current density corresponds to the experimental value. 182

Chapter 1

Introduction

This introductory chapter gives an overview of ionic liquid properties that are of importance for the electrodeposition and electrochemistry in ionic liquids.

After a short history of ionic liquids (§1.1), a summary of the reasons why electrodeposition should be carried out from ionic liquids is given in §1.2. It also indicates the place that ionic liquids take in the field of the electrodeposition of metals. This is followed by a section on an important electrochemical property of ionic liquids: their electrochemical window (§1.3). It mentions how they are determined, how electrochemical windows of ionic liquids compare to those of other solvents, and what possible decomposition paths of ionic liquids are. Because of the non-aqueous nature of ionic liquids, water-based reference electrodes are often unusable, so electrochemical studies in ionic liquids require specific reference potentials and electrodes (§1.4). Several methods to measure potential differences in ionic liquids are presented. §1.5 discusses transport phenomena in ionic liquids. This is based on theories concerning the viscosity of ionic liquids such as hole theory and the Walden rule, but this section also deals with conductivity and ionicity as these properties are strongly related to viscosity. §1.6 gives an overview of ionic liquids in a high vacuum environment. A first subsection deals with the behavior of ionic liquids in a high vacuum environment: their volatility. Other subsections are about the solubility of gases in ionic liquids when they are exposed to vacuum conditions and possible applications of ionic liquids for vacuum techniques. A summary of electrodeposition additives for ionic liquids is given in §1.7. This section mentions which additives have already been studied for metal deposition from ionic liquids. §1.8 discusses liquid metal salts, a class of ionic liquids in which metal ions are incorporated into the structure of the ionic liquids, and §1.9 shows how ionic liquids are dried: a necessity to use their properties to the fullest.

Finally, §1.10 gives an outline of this thesis and §1.11 summarizes the ionic liquids that have been used and in which experiments they are applied.

1.1 A short history of ionic liquids

The following summary of the history of ionic liquids is based on the introduction of several review articles on ionic liquids [1–5]. The molecular structures of the cations of mentioned ionic liquids are shown in figure 1.1.

The first compound that can be considered as an ionic liquid was synthesized and described by Paul Walden in 1914 [6]. In that paper he described the physical properties of a compound that was formed by the neutralization of ethylamine and concentrated nitric acid. This compound, ethylammonium nitrate or $[C_2H_5NH_3][NO_3]$, has a melting point of 12 °C and is thus no doubt an ionic liquid,

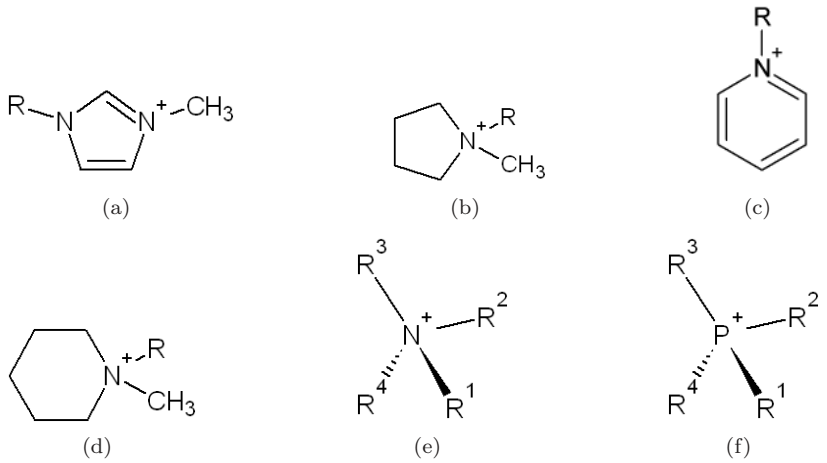

Figure 1.1: Molecular structure of popular cations for ionic liquids: (a) 1-alkyl-3-methylimidazolium, (b) *N*-alkyl-*N*-methylpyrrolidinium, (c) 1-alkylpyridinium, (d) 1-alkyl-1-methylpiperidinium, (e) tetraalkylammonium, (f) tetraalkylphosphonium.

although the name *ionic liquids*, or *room-temperature molten salts* only appeared at the end of the twentieth century.

A next step in the development of ionic liquids was taken in 1951 when Hurley and Wier published about liquids that formed when 1-ethylpyridinium bromide was mixed with $AlCl_3$, and their use as media for the electrodeposition of metals [7, 8]. This mixture of bromide and chloride salts was chemically complicated, due tot the presence of two types of anions, and later replaced by 1-butylpyridinium chloride - $AlCl_3$ baths. These solutions were themselves replaced by imidazolium-based mixtures due to the larger electrochemical window of the imidazolium cation and a larger liquid range as a function of the $AlCl_3$ concentration. The ionic liquids based on organic halides and $AlCl_3$ were named *first-generation ionic liquids*. This was chosen badly, because the first ionic liquid ever made, $[C_2H_5NH_3][NO_3]$, does not belong into this class.

The introduction of ionic liquids, stable to water and air by Wilkes and Zaworotko meant a new milestone [9]. These ionic liquids were based on anions such as $[CH_3CO_2]^-$ and $[BF_4]^-$, later followed by $[PF_6]^-$, and are considered the *second generation ionic liquids*. Later it became clear that they still needed to be handled in a dry atmosphere, because the latter two anions can release HF when exposed

to moisture. Such problems were circumvented by the introduction of ionic liquids with even more hydrophobic anions such as trifluoromethanesulfonate ($[TfO]^-$) and bis(trifluoromethylsulfonyl)imide ($[Tf_2N]^-$), ... first for imidazolium ionic liquids [10] and later for ammonium and pyrrolidinium ionic liquids [11].

Ionic liquids were later adjusted to contain functional groups which lead to so-called *task-specific* or *functionalized* ionic liquids [12, 13]. Hereby it became possible to introduce particular capabilities to ionic liquids, e.g. the ability to interact with a metal center and thus to contribute to an enhanced solubility of metal salts [14, 15].

An overview of ionic liquids would not be complete without mentioning the mixtures made by Abbott *et al.* [16], and especially the ones based on choline chloride [16–18], the so-called *deep-eutectic solvents* which have been used for the electrodeposition of e.g. zinc and chromium, and for the electropolishing of stainless steel [19]. It is sometimes claimed that deep eutectic solvents are not ionic liquids, because they contain non-ionic species. On the other hand, their properties are very similar to ionic liquids. Examples are their low melting point, water-stability and wide electrochemical window.

1.2 Why should electrodeposition be carried out in ionic liquids?

Electrodeposition is an interesting technique to deposit thin films of metals. Compared to other deposition techniques, electrodeposition gives the ability to control the composition and morphology of the deposit through the composition of the bath, applied potential and temperature [20–22]. Industrial plating is focused mainly on deposition from aqueous media, but besides water, electrodeposition can also be performed from molten salts and organic solvents. Molten salts require however high temperatures (>800 °C), increasing the costs of this process and the elevated temperature might lead to thermal stress and deformation due to mismatch between the thermal expansion coefficients of the deposited layer and the substrate. Furthermore, many types of substrates cannot withstand such high temperatures (e.g. polymers and semi-conductor wafers). On the other hand, the electric conductivity of organic solvents is intrinsically low, therefore they require large concentrations of supporting electrolyte. Most of the organic solvents are also volatile and flammable which leads to safety and health hazards.

In non-aqueous electroplating, ionic liquids offer therefore an alternative for organic solvents. Table 1.1 gives a comparison of some properties which are important for electrodeposition:

Table 1.1: Comparison of organic solvents with ionic liquids [4]

Property	Organic solvents	Ionic liquids
Number of solvents	>1000	>1000000
Vapor pressure	Obeys the Clausius-Clapeyron equation	Negligible vapor pressure under ambient conditions
Solvation	Weakly solvating	Strongly solvating
Cost	Normally cheap	Typically between 2 and 100 times the cost of organic solvents
Recyclability	Green imperative	Economic imperative
Viscosity	0.2−100 mPa s	22−40000 mPa s

Ionic liquids were first used as solvents for the electrodeposition of aluminium and its alloys (chloroaluminate solutions). The introduction of new anions, such as $[TfO]^-$, $[Tf_2N]^-$, $N(CN)_2^-$, ... and cations (mostly functionalized forms of the basic imidazolium, pyridinium, pyrrolidinium, ... structure) lead to an enormous number of available solvents as medium for electrodeposition. Nonetheless, the basic requirements for an ionic liquid suited for electrodeposition remained the same:

- a wide electrochemical window, see §1.3
- solubilizing power for metal salts (liquid metal salts are an exception to this rule: see chapters 2, 3 and 4)
- low water content (or: have the possibility to be easily dried), see §1.9
- high enough electrical conductivity

How stringent these requirements are depends on the metal that is to be deposited and the nature of the substrate:

- The electrodeposition of aluminium and rare earth metals requires a well-dried ionic liquid with a large electrochemical window
- The width of the electrochemical window, or the water content are less important when e.g. copper is being deposited, except when the substrate (e.g. tantalum) is sensitive to water (see chapters 4 and 5)
- When germanium is deposited, the ionic liquid needs to be well-dried to avoid the evolution of hydrogen gas and the width of the electrochemical window is only of secondary importance.

While it is very unlikely that ionic liquids will overtake electrochemical processes for which aqueous solutions have proven their value (e.g. the electrowinning of zinc or electrorefining for copper), they can offer an alternative for processes where the substrate is water-sensitive, or where ionic liquids can provide a *green* alternative. Examples are the deposition of chromium (which is often carried out from aqueous solution containing carcinogenic Cr(VI) [22]) or for the aqueous electrodeposition of silver which suffers from the use of highly toxic cyanides [22]. These cyanides increase the conductivity and electrode polarization for a sufficient anode corrosion, but the presence of cyanide places a large burden on the disposal of the plating bath and waste water.

However, most research on the electrodeposition of metals from ionic liquids focused on reducing metals that cannot be plated from aqueous solutions. Studies have been made on the electrodeposition of titanium [23, 24], tantalum [25–28], magnesium [29], silicon [30, 31], germanium [32, 33], gallium [34] and cesium [35], but the most successful and convincing results were obtained for aluminium and some of its alloys [8, 25, 33, 36–68]. Research towards the electroplating of rare earths, and especially their alloys with iron, cobalt or nickel, is also an important topic. There are claims that alloys of the iron-group elements with rare earths (e.g. cerium, neodymium, samarium, gadolinium and terbium) can be deposited from aqueous solutions [69–73], but the results indicate large concentrations of oxygen, so that it is unlikely that all deposited rare earth atoms are in the zero-valence state. Ionic liquids, and deep-eutectic solvents, are therefore a better alternative as a medium for the investigation of the reduction of rare earth alloys. Examples of studies concern the electroreduction of lanthanum, cerium, neodymium, dysprosium, samarium, europium, gadolinium and ytterbium [74–88].

1.3 Electrochemical windows of ionic liquids

A key property of solvents used in electrochemistry is their electrochemical window. According to Bard and Faulkner [89], the electrochemical window corresponds to the useful working range of electric potential with sufficiently low background currents. Often an arbitrary current density of 0.2 A dm^{-2} is used to define the potential window. Terms as *potential window* are therefore not precisely defined. More generally: it corresponds to the useful working range of a solvent. For non-aqueous solvents, this range is critically dependent on purity and in particular on elimination of traces of water [89].

1.3.1 Experimental determination of electrochemical windows

Figure 1.2 shows two cyclic voltammograms of [BMP][Tf_2N]. One is measured in a glove box (figure 1.2(a)) and the other in high vacuum (figure 1.2(b)). At potentials more negative than -2.8 V vs Fc/Fc^+, the $[BMP]^+$ cation is reduced; at potentials more positive than 2.3 V vs Fc/Fc^+, the $[Tf_2N]^-$ anion is oxidized. The small reduction wave near -2.1 V vs Fc/Fc^+ in figure 1.2(a) is believed to be a reaction of the $[Tf_2N]^-$ anion [91], but when the experiment is conducted in high vacuum (figure 1.2(b)), that reduction wave has disappeared. Howlett *et al.* claimed that the smal reduction wave is caused by a reaction of the $[Tf_2N]^-$ anion. They used *N*-methyl-*N*-propylpyrrolidinium bis(trifluoromethylsulfonyl)imide ([PMP][Tf_2N]) as an example of an electrochemically stable cation combined with $[Tf_2N]^-$. Although there will be differences between different families (quaternary phosphoniums salts, quaternary ammonium salts, ...) they believe that their findings are broadly applicable to other $[Tf_2N]^-$ based ionic liquids. The accepted electrochemical window of [PMP][Tf_2N] suggests that the ionic liquid is stable at potentials more positive than -3.5 V. However, there have been suggestions of interactions between the ionic liquid and metal surfaces at potentials positive to the rapported cathodic limit [91] (and references therein). This may also explain some of the examples of high interfacial impedance, poor stripping of deposits, deposition only at elevated temperatures and extended cathodic limits in the electrodeposition literature. Howlett *et al.* calculated the theoretical stability of the $[Tf_2N]^-$ anion and the $[PMP]^+$ cation using molecular orbital theory and density functional theory. If they assumed that the measured cathodic limit was caused by the reduction of the cation, the calculations suggested that the anion reduction should start at around -1.3 V vs Fc/Fc^+. Though this is somewhat less negative than the position of the experimental peaks (compare with figure 1.2, although this is for [BMP][Tf_2N], not for [PMP][Tf_2N]), it certainly supports the hypothesis that the $[Tf_2N]^-$ anion is less stable towards reduction as compared to the $[PMP]^+$ cation and is responsible for the electrochemical behavior around -2.1 V vs Fc/Fc^+. The proposed reduction reaction of $[Tf_2N]^-$ is:

$$N(SO_2CF_3)_2^- + e^- \rightleftharpoons N(SO_2CF_3)_2^{2-\bullet} \rightleftharpoons {}^{\bullet}NSO_2CF_3^- + SO_2CF_3^- \qquad (1.1)$$

Although Howlett *et al.* [91] noticed that the peak is relatively insensitive to the water content, their claim is contradicted by results reported by Randström *et al.* [92] They found that the peak does not occur in ionic liquids with a very low water content (<1 ppm) and which have been thoroughly degassed under vacuum in a glass oven. At higher water concentrations, decomposition of the bis(trifluoromethylsulfonyl)imide anion can happen, catalyzed by the presence of water and without degassing, oxygen can be reduced to superoxide. The results of Randström *et al.* explain the differences in the voltammograms of [BMP][Tf_2N] shown in figure 1.2: the voltammogram recorded in a high vacuum environment

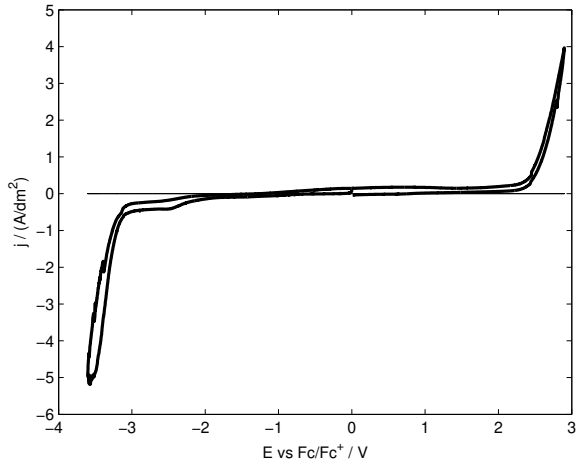

(a)

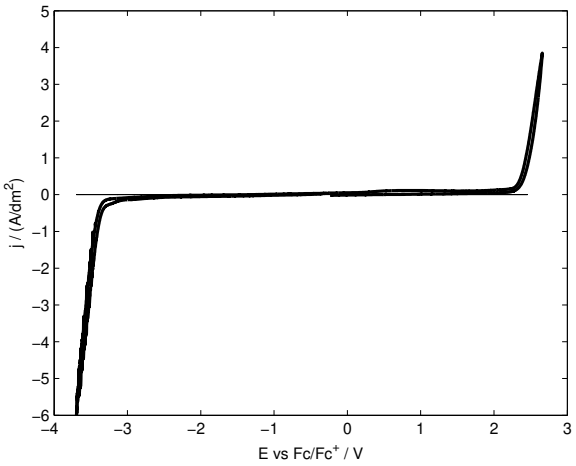

(b)

Figure 1.2: Potential window of [BMP][Tf_2N] measured at 90 °C on a Pt working electrode using a scan rate of 20 mV s^{-1}. Figure (a) shows the potential window measured in the glove box, figure (b) gives the potential window in high vacuum ($2{\cdot}10^{-6}$ mbar) [90].

does not have a shoulder around -2.5 V, whereas the voltammogram measured in a glove box does. In another report [93], Randström *et al.* investigated the influence of air and its components on the cathodic stability of [BMP][Tf_2N]. They concluded that an argon atmosphere, or vacuum environments are excellent circumstances which enable the use of the entire electrochemical window of [BMP][Tf_2N]. Both lead to a strong depression, and even disappearance of peaks associated with the presence of water, oxygen or nitrogen.

Figure 1.3 gives a schematic overview of the electrochemical windows of nine ionic liquids. In this list, the anion was kept constant as it is generally accepted that the cathodic limit is determined by reduction of the cation, if the anion is stable against reduction as is the case for $[Tf_2N]^-$. This is the reason why all

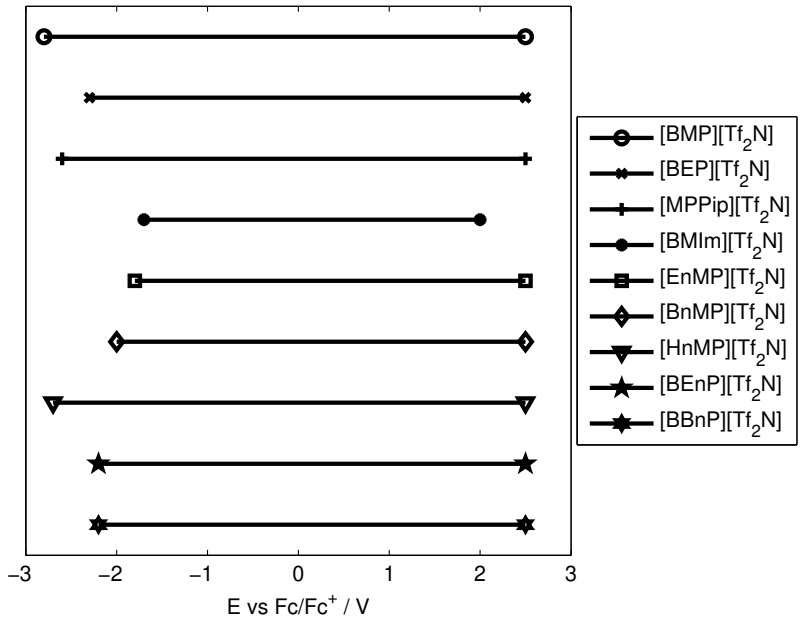

Figure 1.3: Electrochemical windows of ionic liquids measured at 90 °C on a Pt working electrode [90].

ionic liquids but one have a anodic limit of 2.5 V vs Fc/Fc^+. The exception is 1-butyl-3-methylimidazolium bis(trifluoromethylsulfonyl)imide ([C_4mim][Tf_2N]), for which the $[C_4mim]^+$ cation also determines the oxidation limit. This is a general property of imidazolium ionic liquids: despite their widespread use, their elec-

trochemical stability is limited compared to other classes of ionic liquids [94–98]. The fact that the imidazolium ionic liquids seem to have a lower resistance towards reduction than the alkylammonium ionic liquids, is one of the reasons for the growing interest in quaternary ammonium ionic liquids: they have a lower cathodic limit compared to the 1,3-dialkylimidazolium cations. Zhou *et al.* found that the cathodic limit of quaternary ammonium salts is determined by the reduction of the quaternary ammonium cations while their anodic limit is governed by the oxidation of the respective anions [99]. However, in the case of the 1,3-dialkylimidazolium ionic liquids, both the cathodic and anodic decomposition are limited by the 1,3-dialkylimidazolium cations [100, 101]. Therefore it seems reasonable that the anions such as $[BF_4]^-$ and $[Tf_2N]^-$ are more stable against reduction and oxidation than 1,3-dialkylimidazolium cations [101]. Sun *et al.* also found that alkylammonium cations have a greater electrochemical stability than a comparable imidazolium ion [102]. McEwen *et al.* also found that different anions have little effect on the anodic stability of imidazolium ionic liquids [103]. The effect of the water content on the electrochemical window of twelve ionic liquids was investigated by O'Mahony *et al.* [104] The ionic liquid 1-methyl-1-propylpiperidinium bis(trifluoromethylsulfonyl)imide ([MPPip][Tf_2N]) was tested since it was believed that this cation had less ring strain, compared to [BMP][Tf_2N], because of the extra carbon atom inside its ring structure. The decrease in strain could lead to an increase in electrochemical stability. Unfortunately this was not the case. No ionic liquid with a higher cathodic stability than [BMP][Tf_2N] was found, although several types of ionic liquids were synthesized and/or tested.

As no molecular structure could be found which is more stable against reduction than pyrrolidinium, research was concentrated on changing the alkyl chains on the nitrogen of the $[BMP]^+$ cation. A first approach was the addition of a nitrile group [14, 105–108]. This ionic liquid was called 1-butylnitrile-1-methylpyrrolidinium bis(trifluoromethylsulfonyl)imide ([BnMP][Tf_2N], see figure 1.4). An added ad-

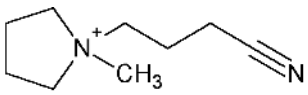

Figure 1.4: Molecular structure of the $[BnMP]^+$ cation.

vantage of such nitrile-functionalized ionic liquids is their higher solubilizing power towards metal salts due to the coordinating power of the functional group. Unfortunately the nitrile group reduces the electrochemical stability of the ionic liquid (figure 1.3). A decreasing electrochemical stability after the addition of functional groups was also noticed by Han *et al.* [109] Decreasing the distance between the positively charged nitrogen of the pyrrolidinium structure and the nitrile group by removing two $-CH_2-$ groups decreases the electrochemical stability

(1-ethylnitrile-1-methylpyrrolidinium bis(trifluoromethylsulfonyl)imide, [EnMP][Tf_2N]) and in the same manner the electrochemical stability increases when extra $-CH_2-$ groups are added (1-hexylnitrile-1-methylpyrrolidinium bis(trifluoromethylsulfonyl)imide, [HnMP][Tf_2N]). But the cathodic limit does not extend beyond the value of non-functionalized [BMP][Tf_2N]. These findings indicated that adding $-CH_2-$ groups to the positively charged nitrogen could extend the cathodic decomposition limit towards more negative potentials. Such behavior is not only observed for functionalized pyrrolidinium, but also for non-functionalized pyrrolidiniums, imidazolium and piperidinium based ionic liquids [98, 110–112].

Surprisingly, an increase in length of the second alkyl chain (mostly a methyl group) does not increase the electrochemical stability of the cation. Experimental evidence even points out that the electrochemical window becomes smaller: compare the ionic liquid 1-butyl-1-ethylpyrrolidinium bis(trifluoromethylsulfonyl)imide ([BEP][Tf_2N]) to [BMP][Tf_2N] in figure 1.3. An explanation for this behavior was given by Montanino *et al.* based on experiments with piperidinium ionic liquids [112]. If the following scheme is assumed for the decomposition of a piperidinium cation Pip^+ with two alkyl chains of length m and n:

$$Pip^+_{mn} + e^- \rightarrow Pip_m + n^\bullet \tag{1.2}$$

then both alkyl chains play opposite roles on the stability of the cation. At first, a long chain provides a shielding effect for the positive charge on the nitrogen, thereby stabilizing the cation. This effect is enhanced by the length of the alkyl chain. However, the radical $n^\bullet$ becomes more stable if the chain length increases. Such a long radical is thus a better leaving group and reduces the electrochemical stability. When one of the two side chains is very short (a methyl group), the dominating effect is the shielding by the longer chain which increases by increasing length of this chain because the short chain is not a good leaving group. On the other hand, increasing the length of the shorter chain makes it a better leaving group thereby reducing the electrochemical stability of the cation. In addition, the steric hindrance of two bulky alkyl side chains favors the exit of one of them.

1.3.2 Comparison with organic solvents

It is difficult to compare different solvents because the experimental conditions used by researchers can differ significantly. Buzzeo *et al.* [1] mention the most occuring reasons for these differences:

- Presence of (electroactive) impurities
- The use of different working electrodes (platinum, glassy carbon, tungsten, gold, ... and even mercury [113]) can lead to significant changes in the electrochemical window, see e.g. the work of Suarez *et al.* [114, 115] and Howlett *et al.* [91]

- The data are reported against several (quasi)reference electrodes which can not always be interconverted

Nonetheless, trends are apparent: the oxidation of anions such as $[BF_4]^-$, $[PF_6]^-$ or $[Tf_2N]^-$ are very similar whereas the cathodic limit varies much more, depending on the nature of the cation. Imidazolium-based ionic liquids can be attacked on their acidic proton on the C2-position (leading to the formation of carbenes [116]) and are therefore more vulnerable for reduction than e.g. tetraalkylammonium, or pyrrolidinium ionic liquids [10]. Alkylation of the C2-position of imidazolium ionic liquids shifts the cathodic decomposition to more negative potentials [103, 117, 118].

Figure 1.5 presents the electrochemical window of seven organic solvents [119]. The electrochemical windows are measured using supporting electrolytes that permit the largest oxidizing and reducing range in the solvent. Such typical supporting electrolytes are (a.o.) $NaClO_4$, tetramethylammonium chloride, tetraethylammonium bromide and tetraethylammonium tetrafluoroborate. The figure shows that several organic solvents have a more negative cathodic limit than the ionic liquids.

1.3.3 Electrochemical decomposition of ionic liquids

The cathodic decomposition of imidazolium or pyrrolidinium ionic liquids is described by Kroon *et al.* [120]. The possible reaction products were predicted by quantumchemical calculations and the reactions that were experimentally validated are given in figures 1.6 and 1.7. Markevich [121] made an experimental study on the decomposition of [BMP][Tf_2N]. They considered both the cathodic and anodic reactions of this ionic liquid.

Ionic liquids for which the (cathodic) decomposition is a useful reaction, are discussed in chapters 2, 3 and 4.

Cathodic decomposition

Imidazolium based ionic liquids Several decomposition paths were quantumchemically calculated for $[C_4mim]^+$, but only a few were also experimentally found. They are shown in figure 1.6 with the reaction of figure 1.6(c) being the most probable.

Pyrrolidinium based ionic liquids The decomposition paths for $[BMP]^+$ are shown in figure 1.7. This leads eventually to following products being found in the ionic liquid:

- 1-methylpyrrolidine

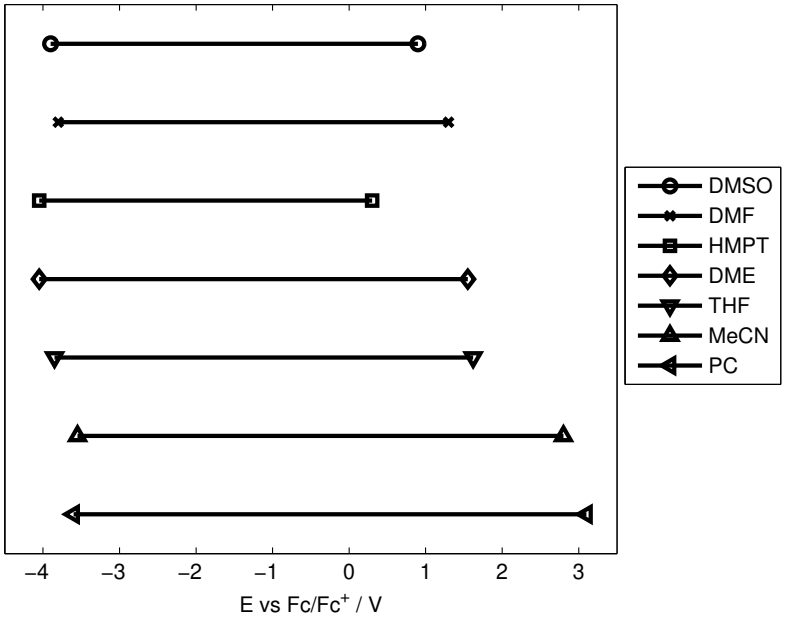

Figure 1.5: Comparison of the electrochemical windows of seven organic solvents. All data are valid for platinum working electrodes. dimethylsulfoxide (DMSO), dimethylformamide (DMF), hexamethylphosphorotriamide (HMPT), dimethoxyethane (DME), tetrahydrofuran (THF), acetonitrile (MeCN) and propylene carbonate (PC). These data are from reference [119].

- octanes
- octenes
- 2-butanol
- dibutylmethylamine
- 1-butylpyrrolidine

Probably also butane is formed but it is not detected because of its low boiling point. The presence of 1-methylpyrrolidine, 1-butylpyrrolidine and dibutylmethylamine is obvious from figures 1.7(a), (c) and (b) respectively. Octanes are formed by radical-radical coupling and their main product is 3,4-dimethylhexane since

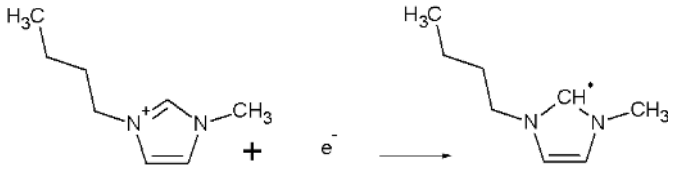

(a) Formation of the 1-butyl-3-methylimidazolium radical

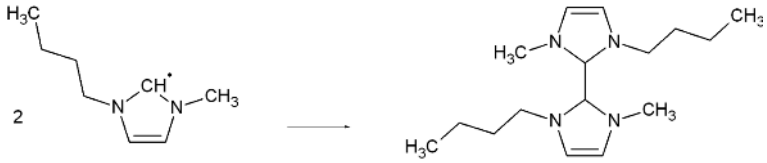

(b) Coupling reaction of two 1-butyl-3-methylimidazolium radicals

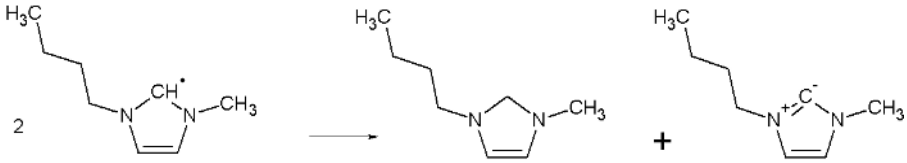

(c) Disproportionation reaction of two 1-butyl-3-methylimidazolium radicals

Figure 1.6: Cathodic decomposition reactions of $[C_4mim]^+$ as described by Kroon *et al.* [120]

secondary radicals are more stable than primary ones. The presence of secondary radicals is also indicated by the detection of 2-butanol which is formed from the reaction of the secondary radical with chloride followed by a reaction with water. Both water and chloride are present in the ppm-range in the ionic liquid. Butenes form due to disproportionation of two radicals, and can react further with another radical, leading to octenes. A similar decomposition scheme is presented by Markevich *et al.* [121]. Instead of a one-electron decomposition as in figure 1.7, the reduction reaction requires in this case two electrons. This leads to identical reaction products, except that carbanions are formed instead of radicals. These carbanions can deprotonate the $[BMP]^+$ cation, which leads to the formation of e.g. methylpyrrolidine, 1-butene or ethene.

Anodic decomposition

Except for imidazolium-based ionic liquids, the anodic decomposition consists of the oxidation of the anion. The oxidation of the bis(trifluoromethylsulfonyl)imide anion $[Tf_2N]^-$ was already given in reaction (1.1). Markevich *et al.* also proposed

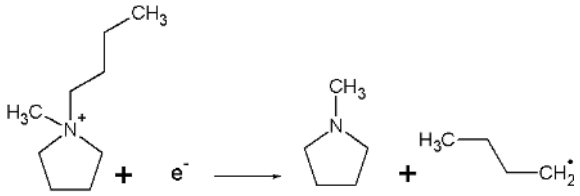

(a) Formation of methylpyrrolidine and the butyl radical

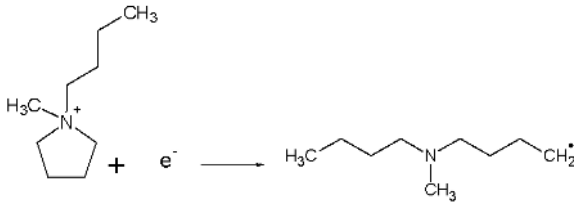

(b) Formation of the dibutylmethylamine radical

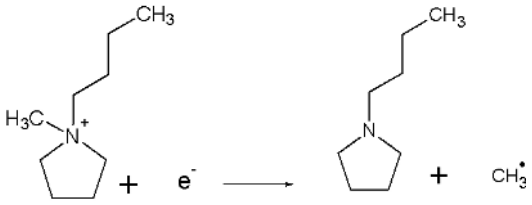

(c) Formation of butylpyrrolidine and the methyl radical

Figure 1.7: Cathodic decomposition reactions of $[BMP]^+$ as described by Kroon *et al.* [120]

another decomposition scheme [121]:

$$N(SO_2CF_3)_2^- + e^- \rightleftharpoons N(SO_2CF_3)_2^{2-\bullet} \rightleftharpoons {}^{\bullet}SO_2NSO_2CF_3^- + CF_3^- \tag{1.3}$$

The reaction products of schemes (1.1) and (1.3) can then undergo further reduction:

$${}^{\bullet}NSO_2CF_3^- + e^- \rightleftharpoons NSO_2^- + CF_3^- \tag{1.4}$$

$${}^{\bullet}SO_2NSO_2CF_3^- + e^- \rightleftharpoons NS_2O_4^- + CF_3^- \tag{1.5}$$

$$SO_2CF_3^- + e^- \rightleftharpoons SO_2^{-\bullet} + CF_3^- \tag{1.6}$$

after which the formed CF_3^- can deprotonate a cation forming trifluoromethane.

The anodic decomposition of ionic liquids which contain Cl^- as the anionic species is the formation of Cl_2.

1.4 Reference electrodes for use in ionic liquids

Selecting a suitable reference electrode for experiments in ionic liquids can be a troublesome task, because standard laboratory electrodes (e.g. SCE) are based on aqueous solutions. A wide diversity of reference potentials is used in literature, although most can be placed in one of the following categories:

1. **Pseudo-reference electrodes** are a type of reference electrode, in which a metallic wire is brought into contact with the solution under investigation. They can be further divided into:

   - Noble metal reference electrodes such as platinum, are often used as pseudo-reference electrode. It is stable and reproducible, but the main disadvantage is the uncertainty about the potential determining redox couple
   - A more logical choice is the use of a pseudo-reference electrode made out of the same metal M as the one under investigation. The potential determining reaction is then assumed to be M/M^{x+} in which M^{x+} is an ion in solution. An advantage of this type of pseudo-reference electrode is the a priori knowledge on the stability region of the metal or its ions (at negative and positive potentials respectively), while a disadvantage is that they are only suitable for metal reduction and oxidation, and not in situations where one is investigating the electrochemistry of e.g. organic molecules. In such a case, an inert metal is more appropriate.

   The main disadvantage of pseudo-reference electrodes is the absence of any link to the Normal Hydrogen Electrode (NHE)

2. **Real reference electrodes** give the opportunity to compare measured potentials between different solutions and to the Normal Hydrogen Electrode. This is mostly done by the use of a redox couple with a well-known reaction potential. Examples of such redox couples are bis(biphenyl)chromium(I)/bis-(biphenyl)chromium(0) [122], $Ag/AgCl/Cl^-$ [123, 124], Ag/Ag^+ [124–128] and bis(η-cyclopentadienyl)-cobalt(II) (cobaltocene) [129, 130]. However, the mostly used compound is indisputably bis(η-cyclopentadienyl)-iron(II) (ferrocene, Fc) [122, 129–131]. Even more, ferrocene is often used to calibrate other electrodes [124, 125, 132], as the redox potential of the Fc/Fc^+ couple is +0.400 V vs NHE [133] and this value is assumed to be solvent-independent [122]. Real reference electrodes can again be divided into two subcategories:

   - Internal references are almost solely based on ferrocene. It consists of measuring the solution of interest before and after the addition of ferrocene. A cyclic voltammogram of the solution with ferrocene will have two more peaks compared to an identical voltammogram without Fc,

due the oxidation to, and reduction of Fc^+. All other peaks can then easily be calibrated to the Fc/Fc^+ redox potential. A disadvantage of this method is that the solution gets poisoned by the presence of ferrocene, and that the peaks caused by ferrocene may coincide with peaks of the solution.

- Home made reference electrodes: Several research groups constructed their own reference electrodes for use in ionic liquids. They all have in common that a metal wire is inserted in a reference solution. This solution is separated from the working solution by a fritted disk. Possible setups include the insertion of a silver wire into a solution containing Ag^+ [124–126], reference electrodes based on Ag/AgCl [123, 124] or a reference electrode whose setup is presented in figure 1.8. A platinum wire

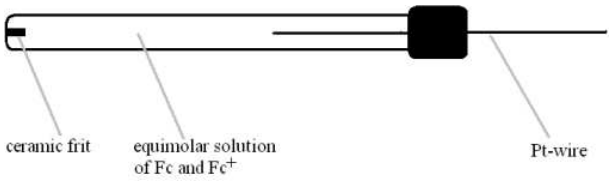

Figure 1.8: Schematic representation of the Fc/Fc^+-reference electrode.

is inserted in a solution containing an equimolar mixture of ferrocene and ferrocenium (the latter is added as $FcPF_6$). The potential of this type of electrode is 0.0 V vs Fc/Fc^+.

1.5 Viscosity, conductivity and ionicity of ionic liquids

During electrodeposition, metal ions are constantly being consumed and thus to keep current flowing, ions must be transported from the bulk of the solution to the electrode. Mass transport is thus crucial. An important property in the description of mass transport is a solvent's viscosity μ which is strongly correlated to the conductivity σ or molar conductivity Λ of a solution. A comparison of the theoretically expected conductivity and the experimentally determined value gives insight in the ionicity (fraction of ions contributing to ionic conduction) of an ionic liquid. That is why these three properties are discussed in the same section.

An overview of values for conductivity and viscosity of the ionic liquids used in this thesis is given in table 1.2 in §1.11.

1.5.1 Application of hole theory on viscosity and conductivity

The reason that conductivity and viscosity are strongly related is because they both depend on the movement of species: movement of ions for conductivity and movement of ions and neutral species for viscosity. This movement is described by three models [134]:

- Schottky-vacancy models
- hole theory
- gas-oriented models

but it is *hole theory* that appears to yield more agreement to experiments than the two others, so this is the theory that will be discussed here. The application of hole theory for ionic liquids was developed by Abbott and Zhao *et al.* [135–137]

In hole theory, holes arise from thermally induced fluctuations in the local density and they are random in size and location. The average size $\langle r_{hole} \rangle$ of a hole is given by [134] (a derivation of this equation is given in appendix A.1):

$$4\pi \langle r_{hole}^2 \rangle = 3.5 \frac{\mathrm{k}T}{\gamma} \tag{1.7}$$

The surface tension γ is comparable for ionic liquids and molten salts, so that equation (1.7) proves that the average hole size is smaller for ionic liquids due the lower temperatures that are involved. This point, together with the larger ionic radii causes the larger viscosity of ionic liquids. Simply stated: the viscosity and conductivity are functions of the probability $P_r(r_{ion} < r_{hole})$ because the motion of ions is only possible when the size of an adjacent hole is larger than the size of the ion. The probability of finding a hole of large enough radius is

$$P_r(r_{ion} < r_{hole}) = \int_{r_{ion}}^{\infty} P_r(r)\, \mathrm{d}r \tag{1.8}$$

in which $P_r(r)$ is given by [134]:

$$P_r(r) = \frac{16}{15\sqrt{\pi}} \left(\frac{4\pi\gamma}{\mathrm{k}T} \right)^{\frac{7}{2}} r^6 \exp\left(-\frac{4\pi\gamma}{\mathrm{k}T} r^2 \right) \tag{1.9}$$

The fraction of holes of sufficient size is very low (about 10^{-6}). This means that they can be considered to be at infinite dilution so that the holes move independently of each other. The independent hopping of holes causes that the Walden rule is applicable in ionic liquids, as explained in the next section. An application of hole theory to predict viscosities is, for instance, used in reference [138].

Differences in calculated and expected conductivity values are attributed to the fact that the species of interest deviate from being a perfect sphere: cations as, for instance, octyltrimethylammonium cannot be considered spherical [136]. Zhao *et al.* tried to resolve this issue [137]. They looked at ionic liquids based on imidazolium, pyridinium and pyrrolidinium, which all have a bulky, rigid ring with an attached alkyl chain (see figure 1.1). They claim that an ion can hop if the adjacent hole is large enough to accept only the ring structure. The alkyl chain then takes over the place previously occupied by the ring. The differences between both models is made more clear in figure 1.9. In figure 1.9(a), movement of an ion

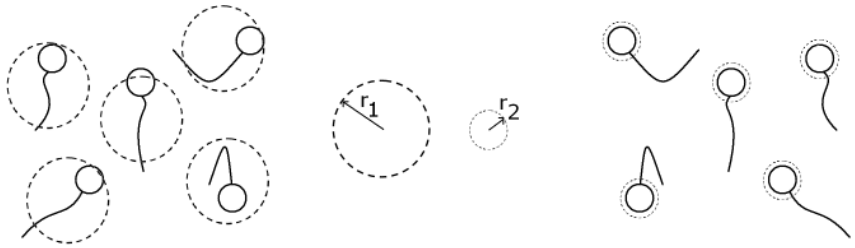

(a) (b)

Figure 1.9: If the radius of the complete ion is considered (r_1), calculations lead to an underestimation of the conductivity, when only the size of the ring is considered (r_2) more reliable results are found.

requires a free hole of size r_1, while hopping of the ring (figure 1.9(b)) only needs a hole of size r_2, with $r_2 < r_1$ so that more holes are available for ion hopping because $P_r(r_{hole} > r_2) > P_r(r_{hole} > r_1)$. The results of this modified hole theory model reduced the difference between estimated and measured conductivity from -27% to -2%.

1.5.2 The Walden rule in ionic liquids and ionicity

Intuitively, one would think that adding electrolytes to a solvent will increase the conductivity. Although this is true for aqueous solutions, where adding salts increases the concentration of charge carriers, this is not necessarily true for ionic liquids where the concentration of charge carriers is already high. Katase *et al.* added several M[Tf_2N]$_n$ salts (M = H, Li, Mg, Ni, Cu, Zn, La, Dy) to the ionic liquid trimethyl-*n*-hexylammonium bis(trifluoromethylsulfonyl)imide and noticed that the electrical conductivity of the pure ionic liquid was always higher than after the addition of M[Tf_2N]$_n$ [139]. The decrease became larger with increasing concentration of the metal salt and metal ion valence. The authors also mention

that the conductivity of the solution is inversely proportional to the viscosity, independent of the concentration of $M[Tf_2N]_n$.

This relationship between viscosity and conductivity of a solution is called the Walden rule

$$\Lambda\mu = \mathrm{cte}_1 \tag{1.10}$$

The Walden rule was originally developed for diluted aqueous solutions, but has since then been validated for molten salts and other non-aqueous solutions too, as shown by the results of Katase *et al.* [139]. The validity is caused by the almost infinite dilution of holes as described above. The Walden rule predicts that molar conductivity and viscosity are inversely proportional. The validity of such a prediction is easily tested by plotting Λ and μ on a $\log - \log$ plot:

$$\log\Lambda = \mathrm{cte}_2 + \log\left(\frac{1}{\mu}\right) \tag{1.11}$$

Experimental data of molar conductivity and viscosity should then lead to a straight line. Ideally, which means in the absence of any ion-ion interactions, the slope should be unity and if the ionic liquids can be well represented as an ensemble of independent ions then the Walden plot will correspond closely with the ideal line. The position of this ideal line is established using aqueous KCl solutions at high dilution [140]. Most ionic liquids obey the requirement that the slope should be unity: a hypothetical example is given in figure 1.10, while experimental data can be found in literature [141]. From the figure, it is clear that the data for ionic liquids are parallel to the reference line, but that they are shifted downwards: the molar conductivities are lower than expected. That is caused by the incomplete dissociation of the ionic liquids into its constituents ions:

$$[\mathrm{cation}][\mathrm{anion}] \rightleftharpoons [\mathrm{cation}]^+ + [\mathrm{anion}]^- \tag{1.12}$$

The equilibrium of equation (1.12) for most ionic liquids lies far, but not completely, to the right. This means that the expected molar conductivity, calculated by the Nernst-Einstein equation

$$\Lambda_{NE} = \frac{\mathrm{N}_a \mathrm{e}^2 (D_+ + D_-)}{\mathrm{k}T} \tag{1.13}$$

is an overestimation of the experimentally determined molar conductivity because it assumes that all of the diffusing species contribute to the molar conductivity. On the other hand, Λ_{exp} is based on the migration of the charged species under an electric field while an undissociated ionic liquid does not contribute to Λ_{exp}. In equation (1.13) N_a represents Avogadro's number, e the elementary charge, D_+ and D_- the diffusion coefficients for the cation and anion respectively, k the Boltzmann constant and T the temperature. The ratio $\frac{\Lambda_{exp}}{\Lambda_{NE}}$ is therefore a measure

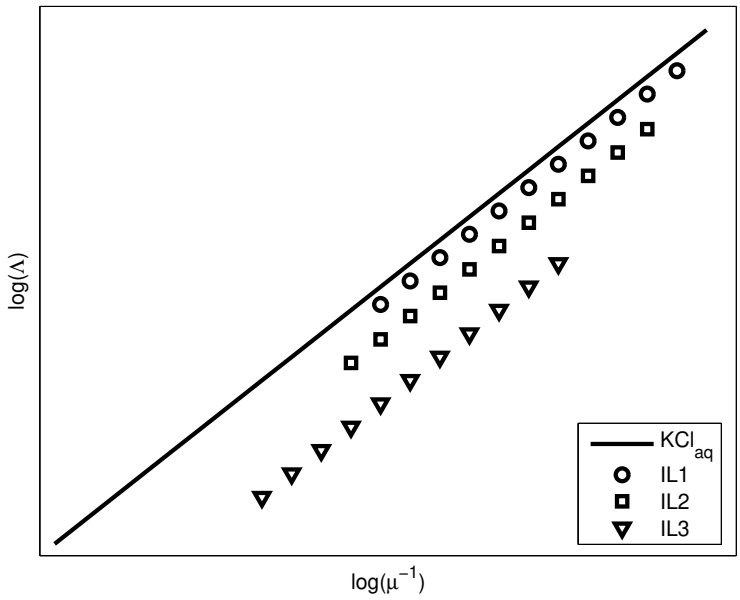

Figure 1.10: Walden plot of three hypothetical ionic liquids and an aqueous solution of KCl.

of the ionicity of ionic liquids [141, 142] and indicates the percentage of ions contributing to the ionic conduction in the diffusing species on the time scale of the experiments. Tokuda *et al.* investigated the ionicity by measuring Λ_{exp} by impedance measurements and Λ_{NMR} is calculated by measuring the self-diffusion coefficients, obtained by pulse-field-gradient spin-echo NMR (PGSE-NMR), and using them in equation (1.13). For all investigated ionic liquids, the $\frac{\Lambda_{exp}}{\Lambda_{NMR}}$ ratio was smaller than unity, indicating that not all of the diffusive species in the ionic liquids contribute to the ionic conduction: ionic aggregates and/or clusters are formed. Typical values for the ionicity are 0.5−0.8, but it can drop as low as 0.3 [143–146]. For the hypothetical ionic liquids shown in figure 1.10, the following order is valid for ionicity: IL1 > IL2 > IL3.

Sometimes a Walden plot will not lead to a line parallel to the KCl reference line. This means that the viscosity μ, and hence molar conductivity Λ do not

depend on temperature in an Arrhenius fashion:

$$\Lambda(T) = A_{Arr} \exp\left(-\frac{E_{act}}{\mathrm{R}_g T}\right) \tag{1.14}$$

An alternative relationship for the temperature dependence is the Vogel-Tamman-Fulcher relationship. The simplest version of this equation states:

$$\Lambda(T) = A_{VTF} \exp\left(-\frac{B_{VTF}}{T - T_g}\right) \tag{1.15}$$

This equation is valid at temperatures not much different from the glass-transition temperature T_g. Often, T_g is considered as an extra parameter and then the VTF relationship has three parameters which can be fitted to experimental data, in contrast to the two parameters of the Arrhenius relationship. Other versions of the VTF equation are

$$\Lambda(T) = \frac{A_{VTF}}{\sqrt{T}} \exp\left(-\frac{B_{VTF}}{T - T_g}\right) \tag{1.16}$$

$$\Lambda(T) = \frac{A_{VTF}}{T} \exp\left(-\frac{B_{VTF}}{T - T_g}\right) \tag{1.17}$$

Here, an explicit temperature dependence of the pre-exponential factor is included.

1.5.3 Transport of ions in ionic liquids

Ions in solution can change their position by either diffusion (due to concentration gradients), migration (because of the presence of an electric field) or convection (natural or forced by e.g. a rotating disk or stirring magnet). It does not matter whether the ions are part of an ionic liquid or that they originate from dissolved salts. Of the three transport methods, diffusion is the most important during electrodeposition and will therefore be discussed first.

The role of viscosity in diffusional mass transport is clarified by the Stokes-Einstein equation [147]:

$$D = \frac{\mathrm{k}T}{\Theta \pi \mu r_{dc}} \tag{1.18}$$

which directly links the viscosity to diffusivity. A derivation of this equation is given in appendix A.2. r_{dc} is the radius of the diffusing complex and Θ a constant which depends on the shape of the diffusing entity. Often, it is assumed that $\Theta = 6$. The Stokes-Einstein equation is mostly used to determine the value of r_{dc} after D is determined by either rotating-disk experiments and the Levich equation, or by chronoamperometry and the Cottrell equation. There are however two major disadvantages concerning the Stokes-Einstein equation:

- What does r_{dc} mean? The use of r_{dc} assumes a spherical complex. So what if the complex is disk-like or rod-like? In that case, r_{dc} gives an hydrodynamic radius: the size of a sphere that has the same diffusivity as the non-spherical entity, but it contains no information on, for instance, the distance between a metal ion and the ligands it carries.

- Is the assumption of $\Theta = 6$ valid? Sutherland proposed the following formula, with ξ the coefficient of sliding friction [148]:

$$\Theta = 6 \left(\frac{1 + \frac{2\mu}{\xi r_{dc}}}{1 + \frac{3\mu}{\xi r_{dc}}} \right) \tag{1.19}$$

  For a large solute moving amongst smaller solvent molecules, the so-called *sticking sphere* model, $\xi = \infty$ and $\Theta = 6$. If $\xi = 0$ (no friction on the surface of the moving sphere: *perfect sliding sphere* model), $\Theta = 4$. This is valid when a small solute is moving in a solvent with large molecules. Intermediate values for Θ are found in a *partially sticking sphere* model with $0 < \xi < \infty$. Vorotyntsev *et al.* applied this theory to ionic liquids by using the diffusion of ferrocene [149]. They concluded that ferrocene-diffusion can be described with $\Theta = 4$, and that a strict interpretation of the Stokes-Einstein equation (for which $\Theta = 6$) is not valid.

A second element that contributes to mass transport is migration. Migration is almost always neglected during electrochemical experiments because of the addition of supporting electrolytes. The ideal supporting electrolyte is electrochemically inactive, highly soluble and dissociates completely as to increase the electrical conductivity of the solution. This lowers the electric field which is the driving force for migration. Ionic liquids used for electrochemistry, combine the function of solvent and supporting electrolyte so that the addition of an external supporting electrolyte is not necessary. Liquid metal salts (see §1.8, and chapters 2, 3 and 4) combine three functions: they are the solvent, the supporting electrolyte and they also are the source of metal ions. For these compounds, migration might play a roll too, besides diffusion. This was already stated by Brown *et al.* [150]

The third process of mass transport is convection: here the focus will be on forced convection. The simplest way to achieve forced convection consists of magnetic stirring. This is an ideal method to get a completely mixed solution, but the flow of liquid is not always reproducible and depends on the electrode's position as well. Stirring methods which permit more control of the fluid flow are the rotating cylinder electrode and, especially, the rotating disk electrode (RDE). The equations describing the fluid flow, mostly formulated in cylindrical coordinates, r, θ and z, on and around a rotating disk electrode have been published [151]. The coordinates are shown in figure 1.11(a), while figure 1.11(b) gives a schematic

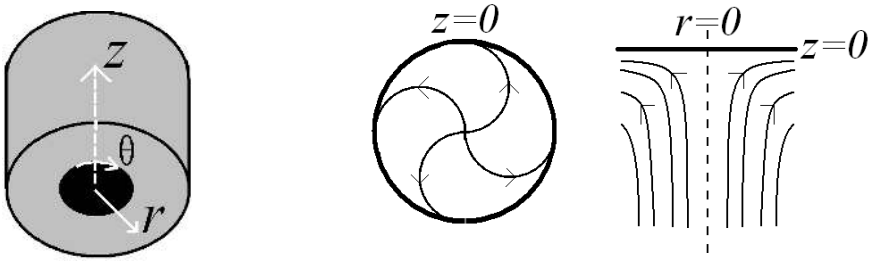

(a) (b)

Figure 1.11: (a) Coordinate system on a rotating disk electrode, (b) fluid flow on a rotating disk electrode.

representation of the fluid flow in the vicinity of the electrode area. In this thesis, rotating disk electrodes were not used for electroplating but for electroanalytical experiments in chapters 3, 6 and 7.

1.6 Ionic liquids in high vacuum

1.6.1 Volatility and distillability of ionic liquids

Until only a few years ago, it was widely believed that a defining characteristic of ionic liquids was that they have a negligible vapor pressure. This was a key factor in their increasing popularity. Though, this involatility seems to have been presumed rather than tested. Starting from 2005, papers were published in which it was stated that ionic liquids could be vaporized [152] and even distilled [153]. Rebelo *et al.* estimated the normal boiling temperature T_b and vapor pressure of imidazolium ionic liquids with $[BF_4]^-$, $[PF_6]^-$ and $[Tf_2N]^-$ anions by the prediction of the critical temperature T_c since, for most substances, $T_b = 0.6\ T_c$ [152]. They succeeded in predicting the critical/normal boiling temperature with an accuracy better than 10%. Normal boiling temperatures of ionic systems are inherently high because strong, long-range Coulomb interactions prevent the particles' separations into the gas phase, even more so as the ion size decreases and charge density increases. The boiling point decreases as the alkyl chain length on the cation increases or if the anion becomes bulkier. This way, ionic liquids can be identified for which the decomposition temperature T_d is higher than T_b and $[Tf_2N]^-$ based ionic liquids constitute a very promising case for the measurement of vapor pressure.

The vapor pressure of $[C_4mim][Tf_2N]$ and other imidazolium bis(trifluoromethylsulfonyl)imides was experimentally determined by Paulechka *et al.* [154] and Zaitsau *et al.* [155] and theoretically by Diedenhofen *et al.* [156], but these calculated vapor pressures systematically underestimated the experimental data. Paulechka *et al.* reported that the temperature dependence of the vapor pressure P for $[C_4mim][Tf_2N]$ is (with $[T]$ = K, $[P]$ = Pa):

$$\ln P = 27.11 - \frac{14.42 \cdot 10^3}{T} \tag{1.20}$$

which gives a value of $5.7{\cdot}10^{-12}$ mbar at 25 °C and $3.3{\cdot}10^{-8}$ mbar at 90 °C. They believed that the vapor consisted of ion pairs of $[C_4mim][Tf_2N]$. This assumption is supported by the results of Armstrong *et al.* [157] who successfully evaporated imidazolium based ionic liquids in ultra-high vacuum ($\sim 5{\cdot}10^{-10}$ mbar) and analyzed the vapor with line of sight mass spectrometry. The conclusion was that the vapor consisted of ion pairs and not as individual ions or ion clusters. Similar conclusions were drawn by Leal *et al.* [158] Relative volatilities of ionic liquids were determined by the distillation of mixtures [159]. It was found that the volatility of imidazolium or pyridinium ionic liquids is higher than for ammonium or pyrrolidinium based ionic liquids. For anions, the volatility increases as $[PF_6]^- < [TfO]^- < [Tf_2N]^-$.

The vapor pressure also depends on the ionicity of the ionic liquid. An ionicity of less than 1 indicates the presence of aggregates (see §1.5) and ionic liquids having a large amount of aggregates may have higher vapor pressures than ideally unassociated salts: the vapor pressure seems to increase with a decrease of C_{eff} which is the product of ionicity and the molar concentration of the ionic liquid [142].

The distillability and volatility of ionic liquids was investigated by Earle *et al.* at temperatures up to 300 °C and pressures down to 0.001 mbar [153]. Their results also point out that ionic liquids volatilize as ion aggregates rather than single ions. It was possible to vaporize the ionic liquids and then condense them on colder parts of the experimental setup. Generally, the bis(trifluoromethylsulfonyl)imide ionic liquids distilled without significant decomposition. The vapor pressures for triflates however, seemed lower than for similar bis(trifluoromethylsulfonyl)imides salts as shown by their lower distillation rates. Ionic liquids with other anions as halides, sulfates or carboxylates decomposed on distillation.

It seems that ionic liquids do not always have a negligible vapor pressure and this should open up new ways for exploiting their properties. However, near ambient temperature, their vapor pressure remains negligible. More information on the volatility of ionic liquids can be found in two review papers [160, 161].

1.6.2 Solubility of gases in ionic liquids

The low vapor pressure of ionic liquids permits to purify them from volatile compounds, including atmospheric gases.

The solubility of these gases, at pressures close to atmospheric presssure, in ionic liquids has been investigated by several researchers. Most of the research has been done on the solubility of CO_2 [162–166]. It has been found that CO_2 has one of the highest solubilities (up to concentrations of several mol%), compared with other gases as O_2, N_2 and H_2 whose solubility is in the range 10^{-2} mol%. The solubility of all gases decreases with increasing temperature. Solubility studies suggest that the nature of the anion has the most significant influence on gas solubilities, compared with the cation [162, 164]. Ionic liquids based on the bis(trifluoromethylsulfonyl)imide anion had more affinity for CO_2 than $[BF_4]^-$ or $[PF_6]^-$ ionic liquids, regardless of whether the cation was imidazolium, pyrrolidinium or tetraalkylammonium [162].

Solubility data are most often determined at pressures above atmospheric pressure, so that information about the solubility in high vacuum conditions can only be found by extrapolation.

1.6.3 Examples of high vacuum applications for ionic liquids

Johnston *et al.* gave the first proof that ionic liquids can be used as solvents for electrochemistry in a high vacuum environment [167]. They investigated the underpotential deposition (UPD) of aluminium on tungsten and gold from $AlCl_3$ - $[C_2mim]Cl$-solutions. The results on gold electrodes were similar to measurements carried out in gloveboxes under an inert gas atmosphere. On tungsten electrodes, which are more reactive, the voltammetric features ascribed to the stripping of underpotential-deposited aluminium could be observed following a single scan whereas in glovebox atmospheres extensive potential cycling was required to make all electrochemical features visible.

Arimoto *et al.* showed that ionic liquids could be placed in a Scanning Electron Microscope (SEM) for in-situ observations of electrochemical processes such as the electrochemically induced volume changes of a polypyrrole film or the electrodeposition of a silver film [168–170].

An extended overview of the possible applications of ionic liquids in a high vacuum environment is given by Kuwabata *et al.* [171] They divide the possibilities into two categories: production methods and analysis techniques.

1. **Material production** under vacuum conditions:

- **Electrodeposition** See the above mentioned example by Johnston *et al.* [167] Ideally, working in a high vacuum conditions should lead to an environment which is as good as completely free of O_2: see chapter 5
- **Magnetron sputtering** In theory, this method should allow to produce nanoparticles of any element that can be ejected by either an Ar^+ or N_2^+ plasma
- **Plasma deposition** In this technique, a direct current gas discharge is being used as a gaseous electrode. Electrons from the plasma, are accelerated to the interface with the ionic liquid and reduce the available metal ions
- **Physical vapor deposition**
- **Electron beam and γ-ray irradiation**

2. **Analyses** under vacuum conditions:

- **XPS analysis** Ionic liquids have been investigated by X-ray photoelectron spectroscopy (XPS) e.g. as a means of in-situ monitoring of catalytic processes, for the study of liquid surfaces or the detection of electrochemically generated species [172–174]. A comprehensive review on XPS of ionic liquids is written by Lovelock *et al.* [175].
- **MALDI mass spectrometry** In matrix-assisted laser desorption/ionization mass spectrometry (MALDI-MS), the matrix (i.e. the ionic liquid) that contains the sample should strongly absorb at the wavelength of the laser and thereby promote ionization of the sample
- **SEM observation and EDX analysis** Ionic liquids have also been used as electrically conductive coating for the analysis of non-conducting samples by SEM [170].
- **TEM observation** This is the ideal tool to characterize the nanoparticles that were produced in ionic liquids. By leaving them in the ionic liquid, aggregation can be delayed or even prevented.

More information on the mentioned techniques can be found in the paper of Kuwabata *et al.* [171] and references therein.

1.7 Additives for electroplating from ionic liquids

Despite the increasing interest in ionic liquids as a solvent for electrodeposition, the resulting quality of the deposits' morphology often leaves room for improvement. In aqueous electroplating, the surface quality of deposits is controlled by using additives in the plating solution. It is well known that small additions of organic additives to plating baths can lead to changes in morphology, structure,

composition or internal stress distribution. The activity of additives mainly depends on the presence of unsaturated bonds on/between carbon, nitrogen, oxygen or sulfur atoms. Although additives are used for decades, knowledge about their function, and how they effect the deposit morphology (or other properties) remains mostly empirical. The use of additives in ionic liquids is often based on knowledge of the additive in aqueous electroplating wherever such knowledge is available. For metals that are impossible to reduce from water, research of functional additives is often trial-and-error. In this regard, the following quote from reference [176] seems very appropriate:

> "*There is a phalanx of different additives available in aqueous electroplating. We have often had the experience that aqueous electroplaters add personal additive recipes to ionic liquids and are surprised, or even disappointed, that they do not work. One has to bear in mind that all known additives were developed over several decades and their mode of action in aqueous solutions is still not fully understood. How can it be expected that one can just replace water by the ionic liquid and get the same or even better results? In our opinion a deep understanding of cation/anion interactions with dissolved substances is required to develop additives that are suited for ionic liquids.*"

It is indeed known that ionic liquids themselves can function as an additive, so that no external compound needs to be added to the solution: aluminium deposits made from N-butyl-N-methylpyrrolidinium bistriflimide ([BMP][Tf_2N]) were nanocrystalline, whereas deposits from 1-butyl-3-methylimidazolium bistriflimide ([C_4mim][Tf_2N]) were microcrystalline [177]. This is caused by the stronger interaction of $[BMP]^+$ with the substrate compared to $[C_4mim]^+$. It has also been reported that the cathodic decomposition can lead to an improved morphology: a transition of microcrystalline to nanocrystalline aluminium deposits was observed in $[C_4mim]^+$ based ionic liquids if sufficiently negative potentials are applied, possibly caused by decomposition products of the cation that act as grain refiner [51].

It is no coincidence that the above mentioned studies all concern the deposition of aluminium. This metal is by far the most used one in the research of additives in ionic liquids. Other examples are the addition of benzene to pyridinium chloroaluminate ionic liquids [38] and imidazolium chloroaluminate ionic liquids [178]. Toluene has also been used in imidazolium-based chloroaluminates [68]. Another additive that has been used in imidazolium chloroaluminates is nicotinic acid [54], while a series of other carboxylic acids was tested by Natter *et al.* [55] Aluminium can also be deposited in a nanocrystalline structure from the ionic liquid 1-(2-methoxyethyl)-3-methylimidazolium chloride [53].

An example of the use of an additive in electroplating from ionic liquids for other metals than aluminium is the addition of LiCl to a plating bath of choline chloride and $CrCl_3$. LiCl made the resulting chromium deposits nanocrystalline [179]. Another example is the addition of acetonitrile to a solution of $Ni(Tf_2N)_2$ in [BMP][Tf_2N] which leads to finer-grained and smoother nickel deposits [180] or the change in morphology of nickel deposits from choline chloride-based eutectic mixtures after adding ethylenediamine or sodium acetylacetonate [181]. Ding *et al.* discovered that pyrrole induces the electrodeposition of titanium from the ionic liquid [C_2mim][Tf_2N] in which $TiCl_4$ was dissolved as titanium source [23].

1.8 Liquid metal salts

Liquid metal salts are ionic liquids in which a metal ion is incorporated into the structure of the ionic liquid. Although, for example, mixtures of metal chlorides with chloride based ionic liquids can lead to ionic liquids which contain metal complexes such as $[AlCl_4]^-$, $[CoCl_4]^{2-}$, $[ZnCl_4]^{2-}$ and $[MnCl_4]^{2-}$ [182–185], only positively charged complexes will be discussed here. Such cationic complexes are reported for silver [186–188], zinc [188], aluminium [189], iron [190] and ruthenium [191].

The work on ionic liquids which contain an iron complex cation $[Fe((OHCH_2CH_2)_2NH)_6][CF_3SO_3]_3$ by Anderson *et al.* [190] reports voltammograms on the Fe^{3+}/Fe^{2+} reaction, but does not comment whether the electrodeposition of iron is possible. Iida *et al.* [186, 187] synthesized silver salts such as [Ag(*N*-2-ethylhexylethylenediamine)$_2$]NO_3, [Ag(*N*-hexylethylenediamine)$_2$]PF_6 and *N*-alkylethylenediamine-Ag^+ complexes with bis(trifluoromethylsulfonyl)imide as counter anion, from which nanoparticles could be made but the electrical conductivity of their complexes was too low for any useful electrochemical experiments. This is caused by the very viscous nature of the complex, though no numerical value is given. However, the silver complexes that Huang *et al.* synthesized, $[Ag(H_2NC_3H_7)_2][Tf_2N]$, $[Ag(H_2NC_2H_5)_2][Tf_2N]$ and $[Ag(H_2NCH_3)(H_2NC_2H_5)][Tf_2N]$, are electrochemically active and the authors also succeeded in producing a zinc analog $[Zn(H_2NC_4H_9)_2][Tf_2N]_2$, from which deposition can take place as well [188]. The properties of a tris(bipyridine) complex of ruthenium are described in reference [191]. These complexes, consisting of attached poly(ethylene glycol)-mono(methyl ether) to a $[Ru(bpy)_3]^{2+}$ complex (with bpy = 2,2'-bipyridine), are concentrated molten salts and despite the low conductivities (10^{-4} Ω^{-1} m^{-1} and lower), peaks for the Ru^{3+}/Ru^{2+} and Ru^{2+}/Ru^{+} couples are observed. The results obtained by Abood *et al.* [189] prove that it is even possible to form an ionic liquid of the form $[AlCl_2 \cdot n\text{Amide}][AlCl_4]$ of which both the cation and anion contain a metal ion. From these liquid, aluminium could be electrodeposited. It is believed that only the cation is electrochemically active in this type of ionic liquids

because it is known from chloroaluminate solutions that $AlCl_4^-$ is not electrochemically active. It is further mentioned that these aluminium complexes hydrolyze less readily in moist air than chloroaluminate ionic liquids, an observation that is in agreement with the findings by Means *et al.* [192]

An extensive list of metal complexes is given by Welleman *et al.* [193] They synthesized complexes of the form $[M(alkylimidazole)_n^{m+}X_m^-]$ in which M stands for manganese, cobalt, nickel, copper, zinc or cadmium and the counter anion X is either ClO_4^-, BF_4^-, NO_3^-, Br^- or Cl^-. Some of their metal complexes have melting points in the range 100−200 °C and a few even below 100 °C. For example: $[Zn(BuIm)_2(NO_3)_2]$ has a melting point of 64 °C and $[Cu(PrIm)_4(NO_3)_2]$ has a melting point of 85 °C (BuIm = 1-butylimidazole, PrIm = 1-propylimidazole). However, the electrochemical properties were not tested.

Chapters 2, 3 and 4 will give more information on newly developed liquid metal salts of copper and silver, respectively, and their possibilities for electrodeposition. Chapter 3 also contains an example of an ionic liquid with a metal containing cation and anion: $[Ag(MeCN)_4]_2[Ag(Tf_2N)_3]$.

1.9 Drying of ionic liquids

Ionic liquids are often used to perform reactions (chemical, electrochemical, catalytical, ...) that are difficult, or even impossible, in aqueous solutions. To take advantage of their non-aqueous properties, ionic liquids need to be dried before use since water can have a dramatic influence on the physical properties of ionic liquids. This is not only true for the chloroaluminates, but also for the air- and water-stable ionic liquids which, despite their name, are hygroscopic and can absorb large amounts of moisture from the ambient atmosphere [111, 194]. This absorbed water can have a significant influence on their physicochemical and electrochemical properties as viscosity, diffusivity and the electrochemical window [91, 93, 111, 195–199]. Even the chemistry can be effected, especially in chloroaluminates [200] because they will react exothermically with the evolution of hydrochloric acid. For the latter type of ionic liquids, it has been reported that phosgene can be used to remove protons and water [201]. Phosgene is however an extremely toxic chemical and its use should be discouraged. An alternative is the organoaluminium compound $EtAlCl_2$ [202].

An often applied drying procedure is to heat the ionic liquid to temperatures above 100 °C while applying a vacuum over the ionic liquid, although the exact value for the remaining pressure is seldomly mentioned. But these conditions never lead to an ionic liquid with a ppm concentration of water, although bulk water

would have evaporated under these circumstances. The water that remains in solution no longer acts as having the properties of bulk water: it can be assumed that it is chemically complexed by the ions present in solution. It has been reported earlier [199, 203] that for low concentrations water is "*in a special state, linked to the salt, and that the hydrogen bonds are perturbed or even broken by the strong electric field of the ions.*" This means that free water is present only if the water concentration is high (>50 mol%) so if one wants to apply ionic liquids to use materials which are highly water sensitive, a strict drying procedure needs to be followed. Simply drying in a low vacuum (pressure of 10^{-1} mbar and above) and/or only moderately heating is not sufficient to achieve a really dry ionic liquid.

Another reported drying procedure is the decomposition of the water present in the ionic liquid by electrolysis [204]. The authors analyzed the water content of ionic liquids as received from the supplier, and after deliberately adding water and drying by electrolysis. Despite the claim that electrolysis is an excellent approach to dry an ionic liquid, the results do not seem to support this claim: the amount of water that remains after the drying procedure is hardly different from the ionic liquid *as received*.

1.10 Outline and objectives

The electrodeposition of sufficiently thick layers of metals from ionic liquids suffers from the lower maximum achievable current density compared to aqueous solutions. This means that longer deposition times are required. The low current densities in ionic liquids are mainly caused by the low solubility of metal salts in ionic liquids (except the dicyanamide ionic liquids [205]) and the high viscosity which is, even for heated low-viscosity ionic liquids, higher than in aqueous solutions. The difficulty of solubilizing metals in ionic liquids can be circumvented by either applying a common ion effect [206] or by incorporating the metal of interest into the molecular structure of the ionic liquid. In the former method, Chiappe *et al.* demonstrated that high concentrations of metal salts in both hydrophilic and hydrophobic ionic liquids could be obtained by directly dissolving the salts in ionic liquids which have the same anion. The latter approach was used in synthesizing so called *liquid metal salts*, and is presented in Chapters 2 and 3 for copper and silver respectively. In these chapters it is shown that high current densities can be achieved in **unstirred** deposition baths without decomposition of the ionic liquid. That is: the decomposition is the actual electrodeposition of metal. It is also shown that the morphology of deposited copper or silver from these liquid metal salts can be strongly improved by the addition of a suitable additive. In the aqueous electroplating of these metals, often used additives are 1*H*-benzotriazole and thiourea. Thiourea acts as a brightening and levelling agent [207–218] while 1*H*-benzotriazole functions as a corrosion inhibitor [212, 213, 219–223]. In chap-

ters 2 and 3 the effect of 1*H*-benzotriazole and thiourea on the morphology of copper and silver deposited from the liquid metal salts $[Cu(MeCN)_2][Tf_2N]$ and $[Ag(MeCN)_4]_2[Ag(Tf_2N)_3]$, is reported.

In Chapter 4, another use of the liquid metal salt $[Cu(MeCN)_2][Tf_2N]$ is shown: the electrodeposition of copper onto a tantalum barrier. For this application it is not the high achievable current density which is offered by the ionic liquid that is used, but the possibility to apply high overpotentials. High overpotentials are advantageous in achieving large nucleation densities. In aqueous electroplating on tantalum surfaces, nucleation is strongly hampered by the presence of a naturally occuring oxide layer. By using $[Cu(MeCN)_2][Tf_2N]$, extreme overpotentials as negative as -5 V can be applied.

The electrodeposition of copper on tantalum from more *traditional* ionic liquids is discussed in Chapter 5. The described experiments exploit an important property of ionic liquids: most of them (but not all) have a much lower vapor pressure than water or organic solvents so that they can by placed in high-vacuum environments. The high vacuum aids in decreasing the concentrations of water and oxygen to the lowest amounts possible, so that the oxidation of tantalum can be retarded or even avoided.

In Chapter 6, the first electrochemical oscillator in ionic liquids is described. The existence of this oscillating behavior was discovered with some good fortune during the testing of the $[C_2mim]Cl$ - $CuCl_2$ mixture for the deposition of copper on tantalum: it happened unexpectedly but turned out to be an interesting topic. In this chapter it is shown that, for oscillations to occur, both Cu^+ and Cu^{2+} need to be present, as well as chloride ions. Imidazolium ions also play a role in the reactions leading to the oscillations under potentiostatic conditions.

Chapter 7 presents a finite-element model of the electrodeposition of aluminium from chloroaluminate ionic liquids. This chapter tries to explain why reasonable current densities can be achieved in the electrodeposition from chloroaluminate ionic liquids despite the fact that, in the net reduction reaction, aluminium ions are trapped in an electrochemically inactive complex during the deposition of aluminium. The reactions which happen at the electrode and in the bulk of the solution are represented by the appropriate mathematical equations in a finite-element model.

In the end, general conclusions and suggestions for further research are discussed in Chapter 8.

1.11 Properties of the used ionic liquids

For this thesis, several ionic liquids were used. While some of these liquids are commercially available, others needed to be synthesized: especially the liquid metal salts. An overview of the used ionic liquids is given in table 1.2, together with their melting point, viscosity μ and electrical conductivity σ.

Table 1.2: Melting points (T_m), viscosities (μ) and electrical conductivities (σ) of ionic liquids used in this thesis

	T_m (°C)	μ (mPa s)	σ (Ω^{-1} m^{-1})	data from
$[Cu(MeCN)_4][Tf_2N]$	66			Ch. 2, [224]
$[Cu(MeCN)_2][Tf_2N]$		9.0 (80 °C)	1.62 (90 °C)	Ch. 2, [224]
$[Cu(PhCN)_4][Tf_2N]$	66			Ch. 2
$[Ag(MeCN)_4]_2[Ag(Tf_2N)_3]$	18	40 (25 °C)		Ch. 3
		16.6 (50 °C)	1.58 (50 °C)	Ch. 3
		7.8 (80 °C)		Ch. 3
$[Ag(MeCN)][Tf_2N]$	90			Ch. 3
$[Ag(EtIm)_2][Tf_2N]$	65	14.1 (80 °C)	0.27 (90 °C)	Ch. 3
$[BMP][Tf_2N]$	-18	85 (25 °C)	0.22 (25 °C)	[11]
			1.1 (90 °C)	[90]
[BMP]Cl	203			[225]
$[C_2mim]Cl$	89			[226]
$[C_2mim][Tf_2N]$	-3	34 (20 °C)	0.88 (20 °C)	[10]
$[C_4mim]Cl$	65			[226]
$[P_{4,4,4,14}]Cl$	45			
$[C_4pyr]Cl$	162			
$[C_4dmim]Cl$	89			
$AlCl_3$-$[C_2mim]Cl$ (60-40 mol%)	<-40	18 (30 °C)	1.5 (32 °C)	[39]

The electrochemical properties of the liquid metal salts containing copper are discussed in Chapters 2 and 4, and a discussion on the crystallographic properties of $[Cu(MeCN)_x][Tf_2N]$ ($x = 2-4$) is presented in [224]. The liquid silver salts are described in Chapter 3.

[BMP][Tf_2N], an ionic liquid which is widely used due to its wide electrochemical window (§1.3), was used as solvent for the electrodeposition of copper on tantalum with $Cu(Tf_2N)_2$ as copper source. It was used either as pure solvent, or in a mixture with [BMP]Cl because the melting point of the latter ionic liquid is high.

The addition of [BMP][Tf_2N] to [BMP]Cl did not bring a new ion in solution as the cation is shared by both compounds and the $[Tf_2N]^-$ ion was already in solution as counter ion for Cu^{2+}. These experiments are presented in Chapter 5.

[C_2mim]Cl is also used for Cu-on-Ta electrodeposition (Chapter 5), but it was mostly used for experiments on electrochemical oscillations (Chapter 6). The ionic liquids [C_2mim][Tf_2N], [C_4mim]Cl, [$P_{4,4,4,14}$]Cl, [C_4pyr]Cl and [C_4dmim]Cl were used in the same chapter to investigate the influence of different ionic liquids on the detected electrochemical oscillations. Despite the mentioned melting point of 162 °C for [C_4pyr]Cl, it could be used at 150 °C. This means that the addition of $CuCl_2$ decreased the melting point, forming a eutectic mixture.

[C_2mim]Cl, with 60 mol% of $AlCl_3$ was also used as example solution for the modelling of aluminium electrodeposition from chloroaluminate ionic liquids. Some experimental tests were conducted on this mixture to measure input data for the model.

References

[1] M. C. Buzzeo, R. G. Evans, R. G. Compton, Non-haloaluminate room-temperature ionic liquids in electrochemistry - a review, *ChemPhysChem*, **5**, 1106 (2004).

[2] S. Zein El Abedin, F. Endres, Electrodeposition of metals and semiconductors in air-and water-stable ionic liquids, *ChemPhysChem*, **7**, 58 (2006).

[3] F. Endres, S. Zein El Abedin, Air and water stable ionic liquids in physical chemistry, *Phys. Chem. Chem. Phys.*, **8**, 2101 (2006).

[4] N. V. Plechkova, K. R. Seddon, Applications of ionic liquids in the chemical industry, *Chem. Soc. Rev.*, **37**, 123 (2008).

[5] F. Endres, Physical chemistry of ionic liquids, *Phys. Chem. Chem. Phys.*, **12**, 1648 (2010).

[6] P. Walden, Ueber die Molekulargrösse und elektrische Leitfähigkeit einiger geschmolzenen Salze, *Bull. Acad. Imper. Sci. St. Petersbourg*, **8**, 405 (1914).

[7] F. H. Hurley, T. P. Wier Jr., Electrodeposition of metals from fused quaternary ammonium salts, *J. Electrochem. Soc.*, **98**, 203 (1951).

[8] F. H. Hurley, T. P. Wier Jr., The electrodeposition of aluminum from nonaqueous solutions at room temperature, *J. Electrochem. Soc.*, **98**, 207 (1951).

[9] J. S. Wilkes, M. J. Zaworotko, Air and water stable 1-ethyl-3-methylimidazolium based ionic liquids, *J. Chem. Soc., Chem. Commun.*, , 965 (1992).

[10] P. Bonhôte, A.-P. Dias, N. Papageorgiou, K. Kalyanasundaram, M. Grätzel, Hydrophobic, highly conductive ambient-temperature molten salts, *Inorg. Chem.*, **35**, 1168 (1996).

[11] D. R. MacFarlane, J. Sun, J. Golding, P. Meakin, M. Forsyth, High conductivity molten salts based on the imide ion, *Electrochim. Acta*, **45**, 1271 (2000).

[12] J. H. Davis Jr., Task-specific ionic liquids, *Chem. Lett.*, **33**, 1072 (2004).

[13] A. E. Visser, R. P. Swatloski, W. M. Reichert, R. Mayton, S. Sheff, A. Wierzbicki, J. H. Davis Jr., R. D. Rogers, Task-specific ionic liquids incorporating novel cations for the coordination and extraction of Hg^{2+} and Cd^{2+}: Synthesis, characterization, and extraction studies, *Environ. Sci. Technol.*, **36**, 2523 (2002).

[14] P. Nockemann, M. Pellens, K. Van Hecke, L. Van Meervelt, J. Wouters, B. Thijs, E. Vanecht, T. N. Parac-Vogt, H. Mehdi, S. Schaltin, J. Fransaer, S. Zahn, B. Kirchner, K. Binnemans, Cobalt(II) complexes of nitrile-functionalized ionic liquids, *Chem. Eur. J.*, **16**, 1849 (2010).

[15] P. Nockemann, B. Thijs, S. Pittois, J. Thoen, C. Glorieux, K. Van Hecke, L. Van Meervelt, B. Kirchner, K. Binnemans, Task-specific ionic liquid for solubilizing metal oxides, *J. Phys. Chem. B*, **110**, 20978 (2006).

[16] A. P. Abbott, G. Capper, D. L. Davies, H. L. Munro, R. K. Rasheed, V. Tambyrajah, Preparation of novel, moisture-stable, Lewis-acidic ionic liquids containing quaternary ammonium salts with functional side chains, *Chem. Commun.*, , 2010 (2001).

[17] A. P. Abbott, G. Capper, D. L. Davies, R. K. Rasheed, Ionic liquid analogues formed from hydrated metal salts, *Chem. Eur. J.*, **10**, 3769 (2004).

[18] A. P. Abbott, D. Boothby, G. Capper, D. L. Davies, R. K. Rasheed, Deep eutectic solvents formed between choline chloride and carboxylic acids: Versatile alternatives to ionic liquids, *J. Am. Chem. Soc.*, **126**, 9142 (2004).

[19] A. P. Abbott, G. Capper, B. G. Swain, D. A. Wheeler, Electropolishing of stainless steel in an ionic liquid, *Trans. Inst. Metal. Finish.*, **83**, 51 (2005).

[20] A. Brenner, *Electrodeposition of alloys*, Academic press, New York (1963).

[21] J. O. Bockris, A. K. N. Reddy, *Modern Electrochemistry*, Plenum press, New York (1970).

[22] Ed.: M. Schlesinger, M. Paunovic, *Modern electroplating*, John Wiley & sons, Inc., New York (2000).

[23] J. Ding, J. Wu, D. R. MacFarlane, W. E. Price, G. Wallace, Induction of titanium reduction using pyrrole and polypyrrole in the ionic liquid ethyl-methyl-imidazolium bis(trifluoromethanesulphonyl)amide, *Electrochem. Commun.*, **10**, 217 (2008).

[24] F. Endres, S. Zein El Abedin, A. Y. Saad, E. M. Moustafa, N. Borissenko, W. E. Price, G. G. Wallace, D. R. MacFarlane, P. J. Newman, A. Bund, On the electrodeposition of titanium in ionic liquids, *Phys. Chem. Chem. Phys.*, **6**, 2189 (2008).

[25] S. Zein El Abedin, Electrodeposition of tantalum and aluminium in ionic liquid [$Py_{1,4}$] TFSA, *Trans. Inst. Metal. Finish.*, **86**, 220 (2008).

[26] N. Borissenko, A. Ispas, E. Zschippang, Q. Liu, S. Zein El Abedin, A. Bund, F. Endres, In situ STM and EQCM studies of tantalum electrodeposition from TaF_5 in the air- and water-stable ionic liquid 1-butyl-1-methylpyrrolidinium bis(trifluoromethylsulfonyl)amide, *Electrochim. Acta*, **54**, 1519 (2009).

[27] S. Zein El Abedin, U. Welz-Biermann, F. Endres, A study on the electrodeposition of tantalum on NiTi alloy in an ionic liquid and corrosion behaviour of the coated alloy, *Electrochem. Commun.*, **7**, 941 (2005).

[28] A. Ispas, B. Adolphi, A. Bund, F. Endres, On the electrodeposition of tantalum from three different ionic liquids with the bis(trifluoromethyl sulfonyl) amide anion, *Phys. Chem. Chem. Phys.*, **12**, 1793 (2010).

[29] G. T. Cheek, W. E. O'Grady, S. Zein El Abedin, E. M. Moustafa, F. Endres, Studies on the electrodeposition of magnesium in ionic liquids, *J. Electrochem. Soc.*, **155**, D91 (2008).

[30] S. Zein El Abedin, N. Borissenko, F. Endres, Electrodeposition of nanoscale silicon in a room temperature ionic liquid, *Electrochem. Commun.*, **6**, 510 (2004).

[31] Y. Nishimura, Y. Fukunaka, T. Nishida, T. Nohira, R. Hagiwara, Electrodeposition of Si thin film in a hydrophobic room-temperature molten salt, *Electrochem. Solid-State Lett.*, **11**, D75 (2008).

[32] F. Endres, Electrodeposition of nanosized germanium from $GeBr_4$ and $GeCl_4$ in an ionic liquid, *Electrochem. Solid-State Lett.*, **5**, C38 (2002).

[33] W. Freyland, C. A. Zell, S. Zein El Abedin, F. Endres, Nanoscale electrodeposition of metals and semiconductors from ionic liquids, *Electrochim. Acta*, **48**, 3053 (2003).

[34] L. H. S. Gasparotto, N. Borissenko, O. Höfft, R. Al-Salman, W. Maus-Friedrichs, N. Bocchi, S. Zein El Abedin, F. Endres, In situ STM studies of Ga electrodeposition from $GaCl_3$ in the air- and water-stable ionic liquid 1-butyl-1-methylpyrrolidinium bis(trifluoromethylsulfonyl)amide, *Electrochim. Acta*, **55**, 218 (2009).

[35] P.-Y. Chen, C. L. Hussey, Electrodeposition of cesium at mercury electrodes in the tri-1-butylmethylammonium bis((trifluoromethyl)sulfonyl)imide room-temperature ionic liquid, *Electrochim. Acta*, **49**, 5125 (2004).

[36] L. G. Boxall, H. L. Jones, R. A. Osteryoung, Solvent equilibria of AlCl -NaCl melts, *J. Electrochem. Soc.*, **120**, 223 (1973).

[37] P. Rolland, G. Mamantov, Electrochemical reduction of $Al_2Cl_7^-$ ions in chloroaluminate melts, *J. Electrochem. Soc.*, **123**, 1299 (1976).

[38] J. Robinson, R. A. Osteryoung, The electrochemical behavior of aluminum in the low temperature molten salt system n butyl pyridinium chloride: Aluminum chloride and mixtures of this molten salt with benzene, *J. Electrochem. Soc.*, **127**, 122 (1980).

[39] J. S. Wilkes, J. A. Levisky, R. A. Wilson, C. L. Hussey, Dialkylimidazolium chloroaluminate melts: a new class of room-temperature ionic liquids for electrochemistry, spectroscopy, and synthesis, *Inorg. Chem.*, **21**, 1263 (1982).

[40] C. J. Dymek Jr., J. L. Williams, D. J. Groeger, J. J. Auborn, An aluminum acid-base concentration cell using room temperature chloroaluminate ionic liquids, *J. Electrochem. Soc.*, **131**, 2887 (1984).

[41] C. L. Hussey, T. B. Scheffler, J. S. Wilkes, A. A. Fannin, Chloroaluminate equilibria in the aluminum chloride-l-methyl-3-ethylimidazolium chloride ionic liquid, *J. Electrochem. Soc.*, **133**, 1389 (1986).

[42] P. K. Lai, M. Skyllas-Kazacos, Aluminium deposition and dissolution in aluminium chloride-*n*-butylpyridinium chloride melts, *Electrochim. Acta*, **32**, 1443 (1987).

[43] P. K. Lai, M. Skyllas-Kazacos, Electrodeposition of aluminium in aluminium chloride/1-methyl-3-ethylimidazolium chloride, *J. Electroanal. Chem.*, **248**, 431 (1988).

[44] R. T. Carlin, W. Crawford, M. Bersch, Nucleation and morphology studies of aluminum deposited from an ambient-temperature chloroaluminate molten salt, *J. Electrochem. Soc.*, **139**, 2720 (1992).

[45] G. R. Stafford, C. L. Hussey, *Advances in Electrochemical science and engineering*, volume 7, chapter Electrodeposition of transition metal-aluminum alloys from chloroaluminate molten salts, 275, Wiley-VCH Verlag GmbH, Weinheim (2002).

[46] Y. Zhao, T. J. Vandernoot, Electrodeposition of aluminium from nonaqueous organic electrolytic systems and room temperature molten salts, *Electrochim. Acta*, **42**, 3 (1997).

[47] A. P. Abbott, C. A. Eardley, N. R. S. Farley, A. Pratt, Novel room temperature molten salts for aluminium electrodeposition, *Trans. Inst. Metal. Finish.*, **77**, 26 (1999).

[48] T. Jiang, M. J. Chollier Brym, G. Dubé, A. Lasia, G. M. Brisard, Electrodeposition of aluminium from ionic liquids: Part I - electrodeposition and surface morphology of aluminium from aluminium chloride ($AlCl_3$)-1-ethyl-3-methylimidazolium chloride ([EMIm]Cl) ionic liquids, *Surf. Coat. Technol.*, **201**, 1 (2006).

[49] T. Jiang, M. J. Chollier Brym, G. Dubé, A. Lasia, G. M. Brisard, Electrodeposition of aluminium from ionic liquids: Part II - studies on the electrodeposition of aluminum from aluminum chloride ($AlCl_3$) - trimethylphenylammonium chloride (TMPAC) ionic liquids, *Surf. Coat. Technol.*, **201**, 10 (2006).

[50] J. Vaughan, D. Dreisinger, Electrodeposition of aluminum from aluminum chloride-trihexyl(tetradecyl) phosphonium chloride, *J. Electrochem. Soc.*, **155**, D68 (2008).

[51] Q. X. Liu, S. Zein El Abedin, F. Endres, Electrodeposition of nanocrystalline aluminum: Breakdown of imidazolium cations modifies the crystal size, *J. Electrochem. Soc.*, **155**, D357 (2008).

[52] G. Yue, S. Zhang, Y. Zhu, X. Lu, S. Li, Z. Li, A promising method for electrodeposition of aluminium on stainless steel in ionic liquid, *AIChE Journal*, **55**, 783 (2009).

[53] S. Zein El Abedin, P. Giridhar, P. Schwab, F. Endres, Electrodeposition of nanocrystalline aluminium from a chloroaluminate ionic liquid, *Electrochem. Commun.*, **12**, 1084 (2010).

[54] F. Endres, M. Bukowski, R. Hempelmann, H. Natter, Electrodeposition of nanocrystalline metals and alloys from ionic liquids, *Angew. Chem. Int. Ed.*, **42**, 3428 (2003).

[55] H. Natter, M. Bukowski, R. Hempelmann, S. Zein El Abedin, E. M. Moustafa, F. Endres, Electrochemical deposition of nanostructured metals and alloys from ionic liquids, *Z. Phys. Chem.*, **220**, 1275 (2006).

[56] A. P. Abbott, C. A. Eardley, N. R. S. Farley, G. A. Griffith, A. Pratt, Electrodeposition of aluminium and aluminium/platinum alloys from $AlCl_3$/benzyltrimethylammonium chloride room temperature ionic liquids, *J. Appl. Electrochem.*, **31**, 1345 (2001).

[57] R. T. Carlin, H. C. De Long, J. Fuller, P. C. Trulove, Microelectrode evaluation of transition metal-aluminum alloy electrodepositions in chloroaluminate ionic liquids, *J. Electrochem. Soc.*, **145**, 1598 (1998).

[58] J. A. Mitchell, W. R. Pitner, C. L. Hussey, G. R. Stafford, Electrodeposition of cobalt and cobalt-aluminum alloys from a room temperature chloroaluminate molten salt, *J. Electrochem. Soc.*, **143**, 3448 (1996).

[59] M. R. Ali, A. Nishikata, T. Tsuru, Electrodeposition of Co-Al alloys of different composition from the $AlCl_3$-BPC-$CoCl_2$ room temperature molten salt, *Electrochim. Acta*, **42**, 1819 (1997).

[60] B. J. Tierney, W. R. Pitner, J. A. Mitchell, C. L. Hussey, G. R. Stafford, Electrodeposition of copper and copper-aluminum alloys from a room-temperature chloroaluminate molten salt, *J. Electrochem. Soc.*, **145**, 3110 (1998).

[61] W. R. Pitner, C. L. Hussey, Electrodeposition of zinc from the Lewis acidic aluminum chloride-1-methyl-3-ethylimidazolium chloride room temperature molten salt, *J. Electrochem. Soc.*, **44**, 3095 (1997).

[62] Y.-F. Lin, I.-W. Sun, Electrodeposition of zinc from a Lewis acidic zinc chloride-1-ethyl-3-methylimidazolium chloride molten salt, *Electrochim. Acta*, **44**, 2771 (1999).

[63] H. C. De Long, J. S. Wilkes, R. T. Carlin, Electrodeposition of palladium and adsorption of palladium chloride onto solid electrodes from room temperature molten salts, *J. Electrochem. Soc.*, **141**, 1000 (1994).

[64] G. R. Stafford, G. M. Haarberg, The electrodeposition of Al-Nb alloys from chloroaluminate electrolytes, *Plasmas & Ions*, **1**, 35 (1999).

[65] C. A. Zell, F. Endres, W. Freyland, Electrochemical in situ STM study of phase formation during Ag and Al electrodeposition on Au(111) from a room temperature molten salt, *Phys. Chem. Chem. Phys.*, **1**, 697 (1999).

[66] S. Zein El Abedin, E. M. Moustafa, R. Hempelmann, H. Natter, F. Endres, Additive free electrodeposition of nanocrystalline aluminium in a water and air stable ionic liquid, *Electrochem. Commun.*, **7**, 1111 (2005).

[67] S. Zein El Abedin, E. M. Moustafa, R. Hempelmann, H. Natter, F. Endres, Electrodeposition of nano- and microcrystalline aluminium in three different air and water stable ionic liquids, *ChemPhysChem*, **7**, 1535 (2006).

[68] A. P. Abbott, F. Qiu, H. M. A. Abood, M. R. Ali, K. S. Ryder, Double layer, diluent and anode effects upon the electrodeposition of aluminium from chloroaluminate based ionic liquids, *Phys. Chem. Chem. Phys.*, **12**, 1862 (2010).

[69] M. Schwartz, N. V. Myung, K. Nobe, Electrodeposition of iron group-rare earth alloys from aqueous media, *J. Electrochem. Soc.*, **151**, C468 (2004).

[70] J. Zhang, P. Evans, G. Zangari, Electrodeposition of Sm-Co nanoparticles from aqueous solutions, *J. Magn. Magn. Mater.*, **283**, 89 (2004).

[71] L. Wang, L. Tang, G. Huang, W.-Q. Huang, J. Peng, Preparation of amorphous rare-earth films of Ni-Re-P (Re=Ce, Nd) by electrodeposition from an aqueous bath, *Surf. Coat. Technol.*, **192**, 208 (2005).

[72] R. Mishra, E. J. Podlaha, Coupled partial current density behavior of cobalt-terbium alloy codeposition, *J. Electrochem. Soc.*, **153**, C422 (2006).

[73] J. C. Wei, M. Schwartz, K. Nobe, Aqueous electrodeposition of SmCo alloys: I. Hull cell studies, *J. Electrochem. Soc.*, **155**, D660 (2008).

[74] L. Liu, Y. Tong, Q. Yang, Electroreduction of Co(II), Ni(II) and co-deposition with La(III) in urea-NaBr melt, *Rare Met.*, **19**, 237 (2000).

[75] T. Tsuda, T. Nohira, Y. Ito, Electrodeposition of lanthanum in lanthanum chloride saturated $AlCl_3$-1-ethyl-3-methylimidazolium chloride molten salts, *Electrochim. Acta*, **46**, 1891 (2001).

[76] Y.-X. Tong, L.-Z. Liu, C.-W. Xu, G.-H. Liu, Q.-Q. Yang, Preparation of Gd-Ni alloy film in urea-NaBr melt, *Trans. Nonferrous Met. Soc. China*, **11**, 451 (2001).

[77] H.-Y. Hsu, C.-C. Yang, Conductivity, electrodeposition and magnetic property of cobalt(II) and dysprosium chloride in zinc chloride-1-ethyl-3-methylimidazolium chloride room temperature molten salt, *Z. Naturforsch.*, **58**, 139 (2003).

[78] C.-W. Xu, W.-J. Pan, D.-S. Yuan, Y.-X. Tong, G.-K. Liu, Preparation of Gd-Co alloy film in acetamide-urea-NaBr melt, *Trans. Nonferrous Met. Soc. China*, **12**, 1007 (2002).

[79] A. I. Bhatt, I. May, V. A. Volkovich, D. Collison, M. Helliwell, I. B. Polovov, R. G. Lewin, Structural characterization of a lanthanum bistriflimide complex, $La(N(SO_2CF_3)_2)_3(H_2O)_3$, and an investigation of La, Sm, and Eu electrochemistry in a room-temperature ionic liquid, $[Me_3N\mathit{n}Bu][N(SO_2CF_3)_2]$, *Inorg. Chem.*, **44**, 4934 (2005).

[80] C.-Y. Guo, J.-C. Wang, B.-Q. Chen, J.-G. Wang, Electrochemical studies on La-Co alloy film in acetamide-urea-NaBr melt system, *Trans. Nonferrous Met. Soc. China*, **15**, 1190 (2005).

[81] P. Liu, Y.-P. Du, Q.-Q. Yang, G.-R. Li, Y.-X. Tong, Electrochemical behavior of Fe(II) in acetamide-urea-NaBr-KBr melt and magnetic properties of inductively codeposited Nd-Fe film, *Electrochim. Acta*, **52**, 710 (2006).

[82] P. Liu, Y. Du, Q. Yang, Y. Tong, G. A. Hope, Induced codeposition of Sm-Co amorphous films in urea melt and their magnetism, *J. Electrochem. Soc.*, **153**, C57 (2006).

[83] M. Yamagata, T. Katayama, Y amd Miura, Electrochemical behavior of samarium, europium, and ytterbium in hydrophobic room-temperature molten salt systems, *J. Electrochem. Soc.*, **153**, E5 (2006).

[84] J. Lodermeyer, M. Multerer, M. Zistler, S. Jordan, H. J. Gores, K. W, E. Diaconu, M. sperl, G. Bayreuther, Electroplating of dysprosium, electrochemical investigations, and study of magnetic properties, *J. Electrochem. Soc.*, **153**, C242 (2006).

[85] G.-R. Li, Q.-F. Ke, G.-K. Liu, Y.-X. Tong, Studies on the electrodeposition of Ce-Co rare earth alloy thin films in urea-DMSO systems, *J. Electrochem. Soc.*, **153**, C411 (2006).

[86] S. Legeai, S. Diliberto, N. Stein, C. Boulanger, J. Estager, N. Papaiconomou, M. Draye, Room-temperature ionic liquid for lanthanum electrodeposition, *Electrochem. Commun.*, **10**, 1661 (2008).

[87] S.-L. Wang, J.-B. Lin, Q.-Y. Cai, Y. Zhang, Electro-deposition of Co-La alloy films in urea melt and their performances, *J. Alloys Compd.*, **450**, 142 (2008).

[88] E. Gómez, P. Cojocaru, L. Magagnin, E. Valles, Electrodeposition of Co, Sm and SmCo from a deep eutectic solvent, *J. Electroanal. Chem.*, **658**, 18 (2011).

[89] A. J. Bard, L. R. Faulkner, *Electrochemical methods*, p. 'back flap', John Wiley & Sons, New York (2001).

[90] S. Schaltin, K. Binnemans, J. Fransaer, Unpublished results, (2009).

[91] P. C. Howlett, E. I. Izgorodina, M. Forsyth, D. R. MacFarlane, Electrochemistry at negative potentials in bis(trifluoromethanesulfonyl)amide ionic liquids, *Z. Phys. Chem.*, **220**, 1483 (2006).

[92] S. Randström, M. Montanino, G. B. Appetecchi, C. Lagergren, A. Moreno, S. Passerini, Effect of water and oxygen traces on the cathodic stability of *N*-alkyl-*N*-methylpyrrolidinium bis(trifluoromethanesulfonyl)imide, *Electrochim. Acta*, **53**, 6397 (2008).

[93] S. Randström, G. B. Appetecchi, C. Lagergren, A. Moreno, S. Passerini, The influence of air and its components on the cathodic stability of *N*-butyl-*N*-methylpyrrolidinium bis(trifluoromethanesulfonyl)imide, *Electrochim. Acta*, **53**, 1837 (2007).

[94] H. Sakaebe, H. Matsumoto, *N*-methyl-*N*-propylpiperidinium bis(trifluoromethanesulfonyl)imide (PP13-TFSI) novel electrolyte base for Li battery, *Electrochem. Commun.*, **5**, 594 (2003).

[95] H. Matsumoto, H. Sakaebe, K. Tatsumi, Preparation of room temperature ionic liquids based on aliphatic onium cations and asymmetric amide anions and their electrochemical properties as a lithium battery electrolyte, *J. Power Sources*, **146**, 45 (2005).

[96] H. Matsumoto, H. Sakaebe, K. Tatsumi, M. Kikuta, E. Ishiko, M. Kono, Fast cycling of $Li/LiCoO_2$ cell with low-viscosity ionic liquids based on bis(fluorosulfonyl)imide $[FSI]^-$, *J. Power Sources*, **160**, 1308 (2006).

[97] A. S. Best, A. I. Bhatt, A. F. Hollenkamp, Ionic liquids with the bis(fluorosulfonyl)imide anion: Electrochemical properties and applications in battery technology, *J. Electrochem. Soc.*, **157**, A903 (2010).

[98] G. B. Appetecchi, M. Montanino, M. Carewska, A. Moreno, F. Alessandrini, S. Passerini, Chemicalphysical properties of bis(perfluoroalkylsulfonyl)imide-based ionic liquids, *Electrochim. Acta*, **56**, 1300 (2011).

[99] Z.-B. Zhou, H. Matsumoto, K. Tatsumi, Low-melting, low-viscous, hydrophobic ionic liquids: Aliphatic quaternary ammonium salts with perfluoroalkyltrifluoroborates, *Chem. Eur. J.*, **11**, 752 (2005).

[100] Z.-B. Zhou, M. Takeda, M. Ue, New hydrophobic ionic liquids based on perfluoroalkyltrifluoroborate anions, *J. Fluorine Chem.*, **125**, 471 (2004).

[101] Z.-B. Zhou, H. Matsumoto, K. Tatsumi, Low-melting, low-viscous, hydrophobic ionic liquids: 1-alkyl(alkyl ether)-3-methylimidazolium perfluoroalkyltrifluoroborate, *Chem. Eur. J.*, **10**, 6581 (2004).

[102] J. Sun, M. Forsyth, D. R. MacFarlane, Room-temperature molten salts based on the quaternary ammonium ion, *J. Phys. Chem. B*, **102**, 8858 (1998).

[103] A. B. McEwen, H. L. Ngo, K. LeCompte, J. L. Goldman, Electrochemical properties of imidazolium salt electrolytes for electrochemical capacitor applications, *J. Electrochem. Soc.*, **146**, 1687 (1999).

[104] A. M. O'Mahony, D. S. Silvester, L. Aldous, C. Hardacre, R. G. Compton, Effect of water on the electrochemical window and potential limits of room-temperature ionic liquids, *J. Chem. Eng. Data*, **53**, 2884 (2008).

[105] D. Zhao, Z. Fei, R. Scopelliti, P. J. Dyson, Synthesis and characterization of ionic liquids incorporating the nitrile functionality, *Inorg. Chem.*, **43**, 2197 (2004).

[106] M. Egashira, S. Okada, J. Yamaki, D. A. Dri, F. Bonadies, B. Scrosati, The preparation of quaternary ammonium-based ionic liquid containing a cyano group and its properties in a lithium battery electrolyte, *J. Power Sources*, **138**, 240 (2004).

[107] Q. Zhang, Z. Li, J. Zhang, S. Zhang, L. Zhu, J. Yang, X. Zhang, Y. Deng, Physicochemical properties of nitrile-functionalized ionic liquids, *J. Phys. Chem. B*, **111**, 2864 (2007).

[108] Y. Cui, I. Biondi, M. Chaubey, X. Yang, Z. Fei, R. Scopelliti, C. G. Hartinger, Y. Li, C. Chiappe, P. J. Dyson, Nitrile-functionalized pyrrolidinium ionic liquids as solvents for cross-coupling reactions involving in situ generated nanoparticle catalyst reservoirs, *Phys. Chem. Chem. Phys.*, **12**, 1834 (2010).

[109] H.-B. Han, J. Nie, K. Liu, W.-K. Li, W.-F. Feng, M. Armand, H. Matsumoto, Z.-B. Zhou, Ionic liquids and plastic crystals based on tertiary sulfonium and bis(fluorosulfonyl)imide, *Electrochim. Acta*, **55**, 1221 (2010).

[110] G. B. Appetecchi, M. Montanino, D. Zane, M. Carewska, F. Alessandrini, S. Passerini, Effect of the alkyl group on the synthesis and the electrochemical properties of *N*-alkyl-*N*-methyl-pyrrolidinium bis(trifluoromethanesulfonyl)imide ionic liquids, *Electrochim. Acta*, **54**, 1325 (2009).

[111] B. D. Fitchett, T. N. Knepp, J. C. Conboy, 1-alkyl-3-methylimidazolium bis(perfluoroalkylsulfonyl)imide water-immiscible ionic liquids, *J. Electrochem. Soc.*, **151**, E219 (2004).

[112] M. Montanino, M. Carewska, F. Alessandrini, S. Passerini, G. B. Appetecchi, The role of the cation aliphatic side chain length in piperidinium bis(trifluoromethansulfonyl)imide ionic liquids, *Electrochim. Acta*, , in press (2011).

[113] E. I. Rogers, B. Šljukić, C. Hardacre, R. G. Compton, Electrochemistry in room-temperature ionic liquids: Potential windows at mercury electrodes, *J. Chem. Eng. Data*, **54**, 2049 (2009).

[114] P. A. Z. Suarez, V. M. Selbach, J. E. L. Dullius, S. Einloft, C. M. S. Piatnicki, D. S. Azambuja, R. F. de Souza, J. Dupont, Enlarged electrochemical window in dialkyl-imidazolium cation based room-temperature air and molten salts, *Electrochim. Acta*, **42**, 2533 (1997).

[115] P. A. Z. Suarez, C. S. Consorti, R. F. de Souza, J. Dupont, R. S. Gonçalves, Electrochemical behavior of vitreous glass carbon and platinum electrodes in the ionic liquid 1-*n*-butyl-3-methylimidazolium trifluoroacetate, *J. Braz. Chem. Soc.*, **13**, 106 (2002).

[116] B. Gorodetsky, T. Ramnial, N. R. Branda, J. A. C. Clyburne, Electrochemical reduction of an imidazolium cation: a convenient preparation of imidazol-2-ylidenes and their observation in an ionic liquid, *Chem. Commun.*, , 1972 (2004).

[117] P. R. Gifford, J. B. Palmisano, A substituted imidazolium chloroaluminate molten salt possessing an increased electrochemical window, *J. Electrochem. Soc.*, **134**, 610 (1987).

[118] C. Maton, N. De Vos, B. I. Roman, E. Vanecht, N. R. Brooks, K. Binnemans, S. Schaltin, J. Fransaer, C. V. Stevens, Continuous synthesis of peralkylated imidazoles and their transformation into ionic liquids, *To be submitted to ChemPhysChem*, .

[119] C. K. Mann, Nonaqueous solvents for electrochemical use, In: *Electroanalytical chemistry,* Eds.: A. J. Bard, volume 3. Marcel Dekker, Inc. (1969).

[120] M. C. Kroon, W. Buijs, C. J. Peters, G.-J. Witkamp, Decomposition of ionic liquids in electrochemical processing, *Green. Chem.*, **8**, 241 (2006).

[121] E. Markevich, R. Sharabi, V. Borgel, H. Gottlieb, G. Salitra, D. Aurbach, G. Semrau, M. A. Schmidt, In situ FTIR study of the decomposition of *N*-butyl-*N*-methylpyrrolidinium bis(trifluoromethanesulfonyl)amide ionic liquid during cathodic polarization of lithium and graphite electrodes, *Electrochim. Acta*, **55**, 2687 (2010).

[122] G. Gritzner, J. Küta, Recommendations on reporting electrode potentials in nonaqueous solvents, *Pure & Appl. Chem.*, **56**, 461 (1984).

[123] P. Koronaios, R. A. Osteryoung, Use of the $Ag/AgCl/Cl_2$ electrode to estimate solubility products in ambient temperature ionic liquids, *J. Electrochem. Soc.*, **147**, 3414 (2000).

[124] A. Saheb, J. Janata, M. Josowicz, Reference electrode for ionic liquids, *Electroanalysis*, **18**, 405 (2006).

[125] G. A. Snook, A. S. Best, A. G. Pandolfo, A. F. Hollenkamp, Evaluation of a Ag/Ag^+ reference electrode for use in room temperature ionic liquids, *Electrochem. Commun.*, **8**, 1405 (2006).

[126] A. Lewandowski, M. Osińska, A. Swiderska-Mocek, M. Galinski, A cryptate reference electrode for ionic liquids, *Electroanalysis*, **20**, 1903 (2008).

[127] B. Huber, B. Roling, Development of a Ag/Ag^+ micro-reference electrode for electrochemical measurements in ionic liquids, *Electrochim. Acta*, **56**, 6569 (2011).

[128] E. I. Rogers, D. S. Silvester, S. E. Ward Jones, L. Aldous, C. Hardacre, A. J. Russell, S. G. Davies, R. G. Compton, Electrochemical kinetics of Ag/Ag^+ and $TMPD/TMPD^{+\cdot}$ in the room-temperature ionic liquid $[C_4mpyrr][NTf_2]$; toward optimizing reference electrodes for voltammetry in RTILs, *J. Phys. Chem. C*, **111**, 13957 (2007).

[129] S. K. Sukardi, J. Zhang, I. Burgar, M. D. Horne, A. F. Hollenkamp, D. R. MacFarlane, A. M. Bond, Prospects for a widely applicable reference potential scale in ionic liquids based on ideal reversible reduction of the cobaltocenium cation, *Electrochem. Commun.*, **10**, 250 (2008).

[130] E. I. Rogers, D. S. Silvester, D. L. Poole, L. Aldous, C. Hardacre, R. G. Compton, Voltammetric characterization of the ferrocene/ferrocenium and cobaltocenium/cobaltocene redox couples in RTILs, *J. Phys. Chem. C*, **112**, 2729 (2008).

[131] R. R. Gagné, C. A. Koval, G. C. Lisensky, Ferrocene as an internal standard for electrochemical measurements, *Inorg. Chem.*, **19**, 2854 (1980).

[132] A. M. Bond, K. B. Oldham, G. A. Snook, Use of the ferrocene oxidation process to provide both reference electrode potential calibration and a simple measurement (via semiintegration) of the uncompensated resistance in cyclic voltammetric studies in high resistance organic solvents, *Anal. Chem.*, **72**, 3492 (2000).

[133] H. M. Koepp, H. Wendt, H. Strehlow, Der Vergleich der Spannungsreihen in verschiedenen Solventien, *Z. Elektrochem.*, **64**, 483 (1960).

[134] J. O. Bockris, A. K. N. Reddy, *Modern Electrochemistry*, volume 1, chapter 6 - Ionic liquids, Plenum press, New York (1970).

[135] A. P. Abbott, Application of hole theory to the viscosity of ionic and molecular liquids, *ChemPhysChem*, **5**, 1242 (2004).

[136] A. P. Abbott, Model for the conductivity of ionic liquids based on a infinite dilution of holes, *ChemPhysChem*, **6**, 2502 (2005).

[137] H. Zhao, Z.-C. Liang, F. Li, An improved model for the conductivity of room-temperature ionic liquids based on hole theory, *J. Mol. Liq.*, **149**, 55 (2009).

[138] A. P. Abbott, G. Capper, D. L. Davies, R. Rasheed, Ionic liquids based upon metal halide/substituted quaternary ammonium salt mixtures, *Inorg. Chem.*, **43**, 3447 (2004).

[139] T. Katase, S. Imashuku, K. Murase, T. Hirato, Y. Awakura, Water content and related physical properties of aliphatic quaternary ammonium imide-type ionic liquid containing metal ions, *Sci. Technol. Adv. Mater.*, **7**, 502 (2006).

[140] M. Yoshizawa, W. Xu, C. A. Angell, Ionic liquids by proton transfer: Vapor pressure, conductivity, and the relevance of $\Delta \mathrm{p}k_a$ from aqueous solutions, *J. Am. Chem. Soc.*, **125**, 15411 (2003).

[141] D. R. MacFarlane, M. Forsyth, E. I. Izgorodina, A. P. Abbott, G. Annat, K. Fraser, On the concept of ionicity in ionic liquids, *Phys. Chem. Chem. Phys.*, **11**, 4962 (2009).

[142] H. Tokuda, S. Tsuzuki, M. A. B. H. Susan, K. Hayamizu, M. Watanabe, How ionic are room-temperature ionic liquids? An indicator of the physicochemical properties, *J. Phys. Chem. B*, **110**, 19593 (2006).

[143] A. Noda, K. Hayamizu, M. Watanabe, Pulsed-gradient spin-echo ^{1}H and ^{19}F NMR ionic diffusion coefficient, viscosity and ionic conductivity of non-chloroaluminate room-temperature ionic liquids, *J. Phys. Chem. B*, **105**, 4603 (2001).

[144] H. Tokuda, K. Hayamizu, K. Ishii, M. Abu Bin Hasan Susan, M. Watanabe, Physicochemical properties and structures of room temperature ionic liquids. 1. variation of anionic species, *J. Phys. Chem. B*, **108**, 16593 (2004).

[145] H. Tokuda, K. Hayamizu, K. Ishii, M. Abu Bin Hasan Susan, M. Watanabe, Physicochemical properties and structures of room temperature ionic liquids. 2. variation of alkyl chain length in imidazolium cation, *J. Phys. Chem. B*, **109**, 6103 (2005).

[146] H. Tokuda, K. Ishii, M. Abu Bin Hasan Susan, S. Tsuzuki, K. Hayamizu, M. Watanabe, Physicochemical properties and structures of room-temperature ionic liquids. 3. variation of cationic structures, *J. Phys. Chem. B*, **110**, 2833 (2006).

[147] R. B. Bird, W. E. Stewart, E. N. Lightfoot, *Transport phenomena*, p. 529, John Wiley & Sons, New York, 2nd edition (2002).

[148] W. Sutherland, A dynamical theory of diffusion for non-electrolytes and the molecular mass of albumin, *Phil. Mag.*, **9**, 781 (1905).

[149] M. A. Vorotyntsev, V. A. Zinovyeva, M. Picquet, Diffusional transport in ionic liquids: Stokes-Einstein relation or "sliding sphere" model? Ferrocene (Fc) in imidazolium liquids, *Electrochim. Acta*, **55**, 5063 (2010).

[150] R. J. C. Brown, P. J. Dyson, D. J. Ellis, T. Welton, 1-butyl-3-methylimidazolium cobalt tetracarbonyl [bmim][$Co(CO)_4$]: a catalytically active organometallic ionic liquid, *Chem. Commun.*, , 1862 (2001).

[151] J. Fransaer, J. R. Roos, J. P. Celis, Fluid flow past a rotating disk, *Chem. Eng. Sci.*, **46**, 1194 (1991).

[152] L. P. N. Rebelo, J. N. C. Lopes, J. M. S. S. Esperança, E. Filipe, On the critical temperature, normal boiling point, and vapor pressure of ionic liquids, *J. Phys. Chem. B*, **109**, 6040 (2005).

[153] M. J. Earle, J. M. S. S. Esperança, M. A. Gilea, J. N. C. Lopes, L. P. N. Rebelo, J. W. Magee, K. R. Seddon, J. A. Widegren, The distillation and volatility of ionic liquids, *Nature*, **439**, 831 (2006).

[154] Y. U. Paulechka, D. H. Zaitsau, G. J. Kabo, A. A. Strechan, Vapor pressure and thermal stability of ionic liquid 1-butyl-3-methylimidazolium bis(trifluoromethylsulfonyl)amide, *Thermochim. Acta*, **439**, 158 (2005).

[155] D. H. Zaitsau, G. J. Kabo, A. A. Strechan, Y. U. Paulechka, A. Tschersich, S. P. Verevkin, A. Heintz, Experimental vapor pressures of 1-alkyl-3-methylimidazolium bis(trifluoromethylsulfonyl)imides and a correlation scheme for estimation of vaporization enthalpies of ionic liquids, *J. Phys. Chem. A*, **110**, 7303 (2006).

[156] M. Diedenhofen, A. Klamt, K. Marsh, A. Schäfer, Prediction of the vapor pressure and vaporization enthalpy of 1-*n*-alkyl-3-methylimidazolium-bis-(trifluoromethanesulfonyl) amide ionic liquids, *Phys. Chem. Chem. Phys.*, **9**, 4653 (2007).

[157] J. P. Armstrong, C. Hurst, R. G. Jones, P. Licence, K. R. J. Lovelock, C. J. Satterley, I. J. Villar-Garcia, Vapourisation of ionic liquids, *Phys. Chem. Chem. Phys.*, **9**, 982 (2007).

[158] J. P. Leal, J. M. S. S. Esperança, M. E. Minas da Piedade, J. N. Canongia Lopes, L. P. N. Rebelo, K. R. Seddon, The nature of ionic liquids in the gas phase, *J. Phys. Chem. A*, **111**, 6176 (2007).

[159] J. A. Widegren, Y.-M. Wang, W. A. Henderson, J. W. Magee, Relative volatilities of ionic liquids by vacuum distillation of mixtures, *J. Phys. Chem. B*, **111**, 8959 (2007).

[160] R. Ludwig, U. Kragl, Do we understand the volatility of ionic liquids?, *Angew. Chem. Int. Ed.*, **46**, 6582 (2007).

[161] J. M. S. S. Esperança, J. N. Canongia Lopes, M. Tariq, L. M. N. B. F. Santos, J. W. Magee, L. P. N. Rebelo, Volatility of aprotic ionic liquids - a review, *J. Chem. Eng. Data*, **55**, 3 (2010).

[162] J. L. Anthony, J. L. Anderson, E. J. Maginn, J. F. Brennecke, Anion effects on gas solubility in ionic liquids, *J. Phys. Chem. B*, **109**, 6366 (2005).

[163] J. Jacquemin, M. F. Costa Gomes, P. Husson, V. Majer, Solubility of carbon dioxide, ethane, methane, oxygen, nitrogen, hydrogen, argon, and carbon monoxide in 1-butyl-3-methylimidazolium tetrafluoroborate between temperatures 283 K and 343 K and at pressures close to atmospheric, *J. Chem. Thermodyn.*, **38**, 490 (2006).

[164] J. Jacquemin, P. Husson, V. Majer, M. F. Costa Gomes, Influence of the cation on the solubility of CO_2 and H_2 in ionic liquids based on the bis(trifluoromethylsulfonyl)imide anion, *J. Solution Chem.*, **36**, 967 (2007).

[165] J. Jacquemin, P. Husson, V. Majer, M. F. Costa Gomes, Low-pressure solubilities and thermodynamics of solvation of eight gases in 1-butyl-3-methylimidazolium hexafluorophosphate, *Fluid Phase Equilib.*, **240**, 87 (2006).

[166] G. Hong, J. Jacquemin, M. Deetlefs, C. Hardacre, P. Husson, M. F. Costa, Solubility of carbon dioxide and ethane in three ionic liquids based on the bis(trifluoromethylsulfonyl)imide anion, *Fluid Phase Equilib.*, **257**, 27 (2007).

[167] M. Johnston, J.-J. Lee, G. S. Chottiner, B. Miller, T. Tsuda, C. L. Hussey, D. A. Scherson, Electrochemistry in ultrahigh vacuum: Underpotential deposition of Al on polycrystalline W and Au from room temperature $AlCl_3$/1-ethyl-3-methylimidazolium chloride melts, *J. Phys. Chem. B*, **109**, 11296 (2005).

[168] S. Arimoto, D. Oyamatsu, T. Torimoto, S. Kuwabata, Development of in situ electrochemical scanning electron microscopy with ionic liquids as electrolytes, *ChemPhysChem*, **9**, 763 (2008).

[169] S. Arimoto, H. Kageyama, T. Torimoto, S. Kuwabata, Development of in situ scanning electron microscope system for real time observation of metal deposition from ionic liquid, *Electrochem. Commun.*, **10**, 1901 (2008).

[170] S. Arimoto, M. Sugimura, H. Kageyama, T. Torimoto, S. Kuwabata, Development of new techniques for scanning electron microscope observation using ionic liquid, *Electrochim. Acta*, **53**, 6228 (2008).

[171] S. Kuwabata, T. Tsuda, T. Torimoto, Room-temperature ionic liquid. a new medium for material production and analyses under vacuum conditions, *J. Phys. Chem. Lett.*, **1**, 3177 (2010).

[172] E. F. Smith, I. J. Villar-Garcia, D. Briggs, P. Licence, Ionic liquids in vacuo; solution-phase x-ray photoelectron spectroscopy, *Chem. Commun.*, , 5633 (2005).

[173] E. F. Smith, F. J. M. Rutten, I. J. Villar-Garcia, D. Briggs, P. Licence, Ionic liquids in vacuo: Analysis of liquid surfaces using ultra-high-vacuum techniques, *Langmuir*, **22**, 9386 (2006).

[174] A. W. Taylor, F. Qiu, I. J. Villar-Garcia, P. Licence, Spectroelectrochemistry at ultrahigh vacuum: in situ monitoring of electrochemically generated species by X-ray photoelectron spectroscopy, *Chem. Commun.*, , 5817 (2009).

[175] K. R. J. Lovelock, I. J. Villar-Garcia, F. Maier, H.-P. Steinrück, P. Licence, Photoelectron spectroscopy of ionic liquid-based interfaces, *Chem. Rev.*, **110**, 5158 (2010).

[176] Ed.: F. Endres, A. P. Abbott, D. R. MacFarlane, *Electrodeposition from ionic liquids*, p. 118, Wiley-VCH, Weinheim (2008).

[177] R. Atkin, S. Zein El Abedin, R. Hayes, L. H. S. Gasparotto, N. Borisenko, F. Endres, AFM and STM studies on the surface interaction of [BMP]TFSA and [EMIm]TFSA ionic liquids with Au(111), *J. Phys. Chem. C*, **113**, 13266 (2009).

[178] Q. Liao, W. R. Pitner, G. Stewart, C. L. Hussey, G. R. Stafford, Electrodeposition of aluminum from the aluminum chloride-1-methyl-3-ethylimidazolium chloride room temperature molten salt + benzene, *J. Electrochem. Soc.*, **144**, 936 (1997).

[179] A. P. Abbott, G. Capper, D. L. Davies, R. K. Rasheed, J. Archer, C. John, Electrodeposition of chromium black from ionic liquids, *Trans. Inst. Metal. Finish.*, **82**, 14 (2004).

[180] Y.-L. Zhu, Y. Katayama, T. Miura, Effects of acetonitrile on electrodeposition of Ni from a hydrophobic ionic liquid, *Electrochim. Acta*, **55**, 9019 (2010).

[181] A. P. Abbott, K. El Ttaib, K. S. Ryder, E. L. Smith, Electrodeposition of nickel using eutectic based ionic liquids, *Trans. Inst. Metal. Finish.*, **86**, 234 (2008).

[182] C. L. Hussey, T. M. Laher, Electrochemical and spectroscopic studies of cobalt(II) in molten aluminum chloride-*N*-*n*-butylpyridinium chloride, *Inorg. Chem.*, **20**, 4201 (1981).

[183] S. Schaltin, P. Nockemann, B. Thijs, K. Binnemans, J. Fransaer, Influence of the anion on the electrodeposition of cobalt from imidazolium ionic liquids, *Electrochem. Solid-State Lett.*, **10**, D104 (2007).

[184] S.-I. Hsiu, J.-F. Huang, I.-W. Sun, C.-H. Yuan, J. Shiea, Lewis acidity dependency of the electrochemical window of zinc chloride - 1-ethyl-3-methylimidazolium chloride ionic liquids, *Electrochim. Acta*, **47**, 4367 (2002).

[185] R. E. Del Sesto, T. M. McCleskey, A. K. Burrell, G. A. Baker, J. D. Thompson, B. L. Scott, J. S. Wilkes, P. Williams, Structure and magnetic behavior of transition metal based ionic liquids, *Chem. Commun.*, , 447 (2008).

[186] M. Iida, C. Baba, M. Inoue, H. Yoshida, E. Taguchi, H. Furusho, Ionic liquids of bis(alkylethylenediamine)silver(I) salts and the formation of silver(0) nanoparticles from the ionic liquid system, *Chem. Eur. J.*, **14**, 5047 (2008).

[187] M. Iida, S. Kawakami, E. Syouno, H. Er, E. Taguchi, Properties of ionic liquids containing silver(I) or protic alkylethylenediamine cations with a bis(trifluoromethanesulfonyl)amide anion, *J. Colloid Interface Sci.*, **356**, 630 (2011).

[188] J.-F. Huang, H. Luo, S. Dai, A new strategy for synthesis of novel classes of room-temperature ionic liquids based on complexation reaction of cations, *J. Electrochem. Soc.*, **153**, J9 (2006).

[189] H. M. A. Abood, A. P. Abbott, A. D. Ballantyne, K. S. Ryder, Do all ionic liquids need organic cations? Characterisation of $[AlCl_2{\cdot}n$ amide$]^+$ $AlCl_4^-$ and comparison with imidazolium based systems, *Chem. Commun.*, **47**, 3523 (2011).

[190] T. M. Anderson, D. Ingersoll, A. J. Rose, C. L. Staiger, J. C. Leonard, Synthesis of an ionic liquid with an iron coordination cation, *Dalton Trans.*, **39**, 8609 (2010).

[191] H. Masui, R. W. Murray, Room-temperature molten salts of ruthenium tris(bipyridine), *Inorg. Chem.*, **36**, 5118 (1997).

[192] N. C. Means, C. M. Means, S. G. Bott, J. L. Atwood, Interaction of $AlCl_3$ with tetrahydrofuran - formation and crystal-structure of $[AlCl_2(THF)_4][AlCl_4]$, *Inorg. Chem.*, **26**, 1466 (1987).

[193] J. A. Welleman, F. B. Hulsbergen, J. Verbiest, J. Reedijk, Influence of alkyl chain length in N-alkyl imidazoles upon the complex formation with transition-metal salts, *J. Inorg. Nucl. Chem.*, **40**, 143 (1978).

[194] J. G. Huddleston, A. E. Visser, W. M. Reichert, H. D. Willauer, G. A. Broker, R. D. Rogers, Characterization and comparison of hydrophilic and hydrophobic room temperature ionic liquids incorporating the imidazolium cation, *Green. Chem.*, **3**, 156 (2001).

[195] S. Sahami, R. A. Osteryoung, Voltammetric determination of water in an aluminum chloride-N-normal-butylpyridinium chloride ionic liquid, *Anal. Chem.*, **55**, 1970 (1983).

[196] R. G. Evans, O. V. Klymenko, C. Hardacre, K. R. Seddon, R. G. Compton, Oxidation of N,N,N',N'-tetraalkyl-para-phenylenediamines in a series of room temperature ionic liquids incorporating the bis(trifluoromethylsulfonyl)imide anion, *J. Electroanal. Chem.*, **556**, 179 (2003).

[197] D. S. Silvester, R. G. Compton, Electrochemistry in room temperature ionic liquids: A review and some possible applications, *Z. Phys. Chem.*, **220**, 1247 (2006).

[198] U. Schröder, J. D. Wadhawan, R. G. Compton, F. Marken, P. A. Z. Suarez, C. S. Consorti, R. F. de Souza, J. Dupont, Water-induced accelerated ion diffusion: voltammetric studies in 1-methyl-3-[2,6-(S)-dimethylocten-2-yl]imidazolium tetrafluoroborate, 1-butyl-3-methylimidazolium tetrafluoroborate and hexafluorophosphate ionic liquids, *New J. Chem.*, **24**, 1009 (2000).

[199] K. R. Seddon, A. Stark, M.-J. Torres, Influence of chloride, water, and organic solvents on the physical properties of ionic liquids, *Pure & Appl. Chem.*, **72**, 2275 (2000).

[200] H. Linga, Z. Stojek, R. A. Osteryoung, Electrochemistry of titanium(IV) in basic normal-butylpyridinium chloride-aluminum chloride in the presence of oxide, *J. Am. Chem. Soc.*, **103**, 3754 (1981).

[201] M. A. M. Noël, P. C. Trulove, R. A. Osteryoung, Removal of protons from ambient-temperature chloroaluminate ionic liquids, *Anal. Chem.*, **63**, 2892 (1991).

[202] T. A. Zawodzinski, R. T. Carlin, R. A. Osteryoung, Removal of protons from ambient-temperature chloroaluminate ionic liquids, *Anal. Chem.*, **59**, 2639 (1987).

[203] M. Abraham, M. C. Abraham, Electrolytic conductance and viscosity of some mixed nitrate water-systems from fused-salts to dilute-solutions, *Electrochim. Acta*, **31**, 921 (1986).

[204] M. M. Islam, T. Okajima, S. Kojima, T. Ohsaka, Water electrolysis: an excellent approach for the removal of water from ionic liquids, *Chem. Commun.*, , 5330 (2008).

[205] M.-J. Deng, P.-Y. Chen, T.-I. Leong, I.-W. Sun, J.-K. Chang, W.-T. Tsai, Dicyanamide anion based ionic liquids for electrodeposition of metals, *Electrochem. Commun.*, **10**, 213 (2008).

[206] C. Chiappe, M. Malvaldi, B. Melai, S. Fantini, U. Bardi, S. Caporali, An unusual common ion effect promotes dissolution of metal salts in room-temperature ionic liquids: a strategy to obtain ionic liquids having organic-inorganic mixed cations, *Green. Chem.*, **12**, 77 (2010).

[207] N. Alodan, W. Smyrl, Effect of thiourea on copper dissolution and deposition, *Electrochim. Acta*, **44**, 299 (1998).

[208] V. San Martín, S. Sanllorente, S. Palmero, Optimization of influent factors on nucleation process of copper in solutions containing thiourea using an experimental design, *Electrochim. Acta*, **44**, 579 (1998).

[209] N. Tantavichet, M. D. Pritzker, Effect of plating mode, thiourea and chloride on the morphology of copper deposits produced in acidic sulphate solutions, *Electrochim. Acta*, **50**, 1849 (2005).

[210] N. Tantavichet, S. Damronglerd, O. Chailapakul, Influence of the interaction between chloride and thiourea on copper electrodeposition, *Electrochim. Acta*, **55**, 240 (2009).

[211] M. S. Kang, S.-K. Kim, K. Kim, J. J. Kim, The influence of thiourea on copper electrodeposition: Adsorbate identification and effect on electrochemical nucleation, *Thin Solid Films*, **516**, 3761 (2008).

[212] E. E. Farndon, F. C. Walsh, S. A. Campbell, Effect of thiourea, benzotriazole and 4,5-dithiaoctane-1,8-disulfonic acid on the kinetics of copper deposition from dilute-acid sulfate-solutions, *J. Appl. Electrochem.*, **25**, 574 (1995).

[213] E. J. Ahn, J. J. Kim, Additives for superconformal electroplating of Ag thin film for ULSIs, *Electrochem. Solid-State Lett.*, **7**, C118 (2004).

[214] A. G. Zelinsky, S. K. Ershov, Using an electrode with renewable surface for study of silver reduction from acid thiourea solutions, *J. Appl. Electrochem.*, **38**, 273 (2008).

[215] E. Gómez, J. García-Torres, E. Vallés, Study and preparation of silver electrodeposits at negative potentials, *J. Electroanal. Chem.*, **594**, 89 (2006).

[216] O. Azzaroni, P. L. Schilardi, R. C. Salvarezza, A. J. Arvia, Smoothening mechanism of thiourea on silver electrodeposition. Real time imaging of the growth front evolution, *Langmuir*, **15**, 1508 (1999).

[217] B. Reents, W. Plieth, V. A. Macagno, G. I. Lacconi, Influence of thiourea on silver deposition: Spectroscopic investigation, *J. Electroanal. Chem.*, **453**, 121 (1998).

[218] G. I. Lacconi, V. A. Macagno, Electrochemical study of thiourea in relation to the silver electrodeposition process, *Electrochim. Acta*, **39**, 2605 (1994).

[219] T. P. Moffat, J. E. Bonevich, W. H. Huber, A. Stanishevsky, D. R. Kelly, G. R. Stafford, D. Josell, Superconformal electrodeposition of copper in 500-90 nm features, *J. Electrochem. Soc.*, **147**, 4524 (2000).

[220] R. M. Rynders, R. C. Alkire, Use of in-situ atomic-force microscopy to image copper electrodeposits on platinum, *J. Electrochem. Soc.*, **141**, 1166 (1994).

[221] J. Kim, S.-K. Kim, J.-U. Bae, Investigation of copper deposition in the presence of benzotriazole, *Thin Solid Films*, **415**, 101 (2002).

[222] D. Tromans, R. Sun, Anodic polarization behavior of copper in aqueous chloride benzotriazole solutions, *J. Electrochem. Soc.*, **138**, 3235 (1991).

[223] J. C. Rubim, I. G. R. Gutz, O. Sala, Surface-enhanced raman-spectra of benzotriazole adsorbed on a silver electrode, *J. Mol. Struct.*, **101**, 1 (1983).

[224] N. R. Brooks, S. Schaltin, K. Van Hecke, L. Van Meervelt, K. Binnemans, J. Fransaer, Copper(I)-containing ionic liquids for high-rate electrodeposition, *Chem. Eur. J.*, **17**, 5054 (2011).

[225] O. B. Babushkina, S. Ekres, Spectroscopic study of the electrochemical behaviour of tantalum(V) chloride and oxochloride species in 1-butyl-1-methylpyrrolidinium chloride, *Electrochim. Acta*, **56**, 867 (2010).

[226] M. Galiński, A. Lewandowski, I. Stępniak, Ionic liquids as electrolytes, *Electrochim. Acta*, **55**, 5567 (2006).

Chapter 2

Electrodeposition from cationic cuprous organic complexes: ionic liquids for high current density electroplating

Published as S. Schaltin, N.R. Brooks, K. Binnemans and J. Fransaer, *J. Electrochem. Soc.*, **158**, D21-D27 (2011)

Abstract

The electrochemical behavior of the low-melting copper salts $[Cu(MeCN)_x][Tf_2N]$ and $[Cu(PhCN)_x][Tf_2N]$ ($x = 2-4$), where MeCN is acetonitrile and PhCN is benzonitrile, is presented. In these compounds, the copper(I) ion is a main component of the ionic liquid cation. Consequently, the copper concentration is the highest achievable for an ionic liquid and this permits to obtain a good mass transport and high current densities for electrodeposition. The cathodic limit of the ionic liquid is the reduction of copper(I) to copper metal instead of the breakdown of the cation as in conventional ionic liquids. It is shown that pure, crack-free copper layers can be deposited from these copper-containing ionic liquids in unstirred solutions at current densities up to 25 A dm^{-2}.

Introduction

Ionic liquids are useful solvents for electrochemical applications because of their wide electrochemical window and the presence of intrinsic ionic charge carriers [1–3]. Examples of such applications are their use as electrolytes in batteries, in photovoltaic devices, and for the electrodeposition of metals. In all of these applications, good mass transfer is needed. However, as the viscosity of most ionic liquids is a lot higher than most molecular solvents, the mass transport in ionic liquids is rather poor. Moreover, the mass transport is limited even further by the poor solubility of simple metal salts (e.g. chlorides) in most ionic liquids suitable for electrodeposition, except for the dicyanamide ionic liquids [4–7]. The limited solubility is due to the poor coordinating power of anions such as $[BF_4]^-$, $[PF_6]^-$ or bis(trifluoromethylsulfonyl)imide ($[Tf_2N]^-$).

To increase the solubility, functionalized ionic liquids can be used. These ionic liquids have a built-in coordinating unit such as a nitrile group which can complex the metal ion, thereby increasing its solubility [8, 9]. Another way to improve the solubility of metal ions in ionic liquids is to design ionic liquids with a metal complex as part of their composition [10]. Most ionic liquids of this type contain anionic metal complexes: typical examples of such anionic complexes are $[AlCl_4]^-$, $[CoCl_4]^{2-}$, $[ZnCl_4]^{2-}$, $[MnCl_4]^{2-}$ [11–14]. The synthesis of an anionic complex $[Co(CO)_4^-]$ without chloroligands is given in reference [15].

In this paper we present ionic liquids in which the cation is a metal complex and we illustrate their use as medium for the electrodeposition of metals in non-aqueous solutions. Examples of other cationic complexes, based on amine ligands, are already reported in reference [16]. The complexes under investigation in this paper are $[Cu(MeCN)_4][Tf_2N]$ (figure 2.1(a)) and $[Cu(PhCN)_4][Tf_2N]$ (figure 2.1(b)). In both these complexes the copper ions are in the monovalent oxidation state, as often observed for non-aqueous solvents such as acetonitrile and ionic liquids. The chemical characterization of $[Cu(MeCN)_4][Tf_2N]$ will be presented elsewhere. The electrochemical behavior of copper in organic solvents is already described in references [17–23] and the electrochemistry of copper in ionic liquids in references [7, 24–28].

Experimental

We have synthesized tetrakis(acetonitrile) copper(I) bis(trifluoromethylsulfonyl)-imide (bistriflimide), $[Cu(MeCN)_4][Tf_2N]$. The cation consists of four acetonitrile molecules coordinating to the copper(I) ion in a tetrahedral arrangement. The charge balance is provided by the $[Tf_2N]^-$ counter anion. This compound was prepared by reacting copper(II) oxide with bis(trifluoromethylsulfonyl)imidic acid

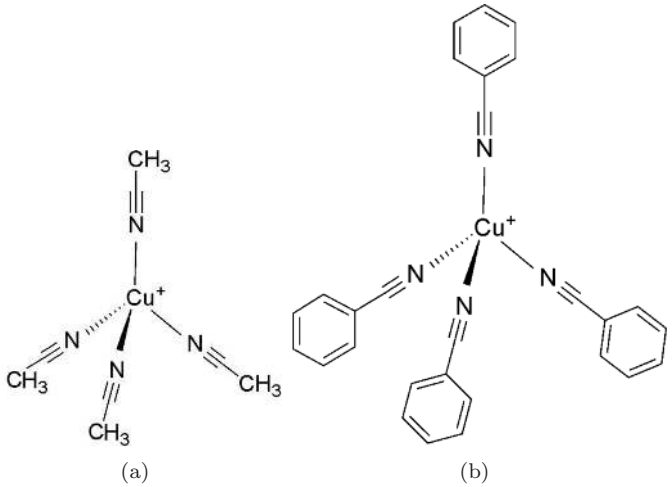

Figure 2.1: Structural formulae of the cations of the copper-containing ionic liquids (a) $[Cu(MeCN)_4][Tf_2N]$ and (b) $[Cu(PhCN)_4][Tf_2N]$.

in water to yield copper(II) bistriflimide. The Cu(II) salt $Cu(Tf_2N)_2(H_2O)_4$ was isolated by drying in vacuo and then redissolved in acetonitrile. Because copper(I) is the stable copper species in acetonitrile solutions [17, 19, 22], a comproportionation reaction between copper metal (added as a powder) and the copper(II) ions yielded $[Cu(MeCN)_4][Tf_2N]$, which was then isolated by removing solvent MeCN in vacuo. The reaction sequence is:

$$CuO + 2\ H[Tf_2N]_{aq} \rightarrow Cu(Tf_2N)_2 + H_2O \tag{2.1}$$

$$Cu(Tf_2N)_2 + Cu + 8\ CH_3CN \rightarrow 2\ [Cu(CH_3CN)_4][Tf_2N] \tag{2.2}$$

$[Cu(PhCN)_4][Tf_2N]$ is prepared in an analogous way.

The electrochemical experiments were performed in an argon-filled glove box (with O_2 and H_2O concentrations below 1 ppm) because the tested low-melting salts are sensitive to moisture and oxygen and can undergo disproportionation or oxidation of copper(I). Platinum-covered silicon wafers (Si, 500 nm SiO_2, 10 nm Ti, 100 nm Pt) have been used as the substrates for electrodeposition. Before use, these substrates were cleaned by rinsing with acetone and dried. After the deposition of a copper layer, they were rinsed with acetone and ethanol, and dried. The solution was contained in a copper crucible, which also served as counter-electrode, and it was not stirred during the experiments. The experiments were done using a

Solartron instruments SI 1287 Electrochemical interface controlled by a computer with Corrware software. All potentials in this paper are relative to a copper wire directly immersed in solution (pseudo-reference electrode), unless stated otherwise. If required, the potential values were corrected for the *iR* drop in real time by using the *current interrupt* technique, or post-experimental using a value for the electrolyte resistance *R*. This value was determined both experimentally (by Electrochemical Impedance Spectroscopy with a Solartron instruments SI 1255 HF frequency response analyzer) and theoretically (by finite elements analysis of the experimental setup). During all electrochemical experiments, the temperature was kept at 90 °C, except for the electrogravimetrical analysis which was performed at room temperature. Thermogravimetrical analyses were done in an argon atmosphere with a Q 600 instrument from TA Instruments. The viscosity was measured on a Brookfield cone plate viscosimeter (LVDV-II+ programmable viscosimeter) with a cone spindle CPE-40. The sample holder was purged with dry nitrogen gas and heated to 80 °C by a circulating water bad. Morphology and elemental composition of the copper deposits were determined by scanning electron microscopy (SEM) and energy-dispersive X-ray analysis (EDX) (Philips XL 30 FEG).

Results and discussion

Characterization

Both $[Cu(MeCN)_4][Tf_2N]$ and $[Cu(PhCN)_4][Tf_2N]$ are white crystalline solids at room temperature. Upon melting (at 66 °C for both $[Cu(MeCN)_4][Tf_2N]$ and $[Cu(PhCN)_4][Tf_2N]$) they form colorless liquids. In figures 2.2 and 2.3, the thermogravimetrical (TGA) curves of $[Cu(MeCN)_4][Tf_2N]$ and $[Cu(PhCN)_4][Tf_2N]$ are shown respectively. Upon heating, the ligands are gradually lost from the complexes, but full dissociation is complete only at temperatures which are higher than the boiling points of MeCN (82 °C) and PhCN (188 °C). It can also be seen that the decrease in mass starts at higher temperatures for $[Cu(PhCN)_4][Tf_2N]$ as compared to $[Cu(MeCN)_4][Tf_2N]$, indicating that the bond between copper(I) and MeCN is thermally more labile than that between copper(I) and PhCN. A possible explanation is the higher molecular mobility of MeCN, which is a much smaller molecule than PhCN with no $\pi - \pi$ interactions, that causes its easy removal from the copper(I) ions. To determine the long-term stability of the $[Cu(MeCN)_4][Tf_2N]$ compound, an electrogravimetrical analysis of the product was performed after it was heated at 90 °C for several days. This temperature was chosen because it is the temperature at which the electrochemical experiments have been performed (*vide infra*). A carefully weighed amount of $[Cu(MeCN)_4][Tf_2N]$ was dissolved in a 1:1 mixture of demineralized water and concentrated nitric acid. Nitric acid was required to dissolve the metallic copper that resulted from the disproportionation

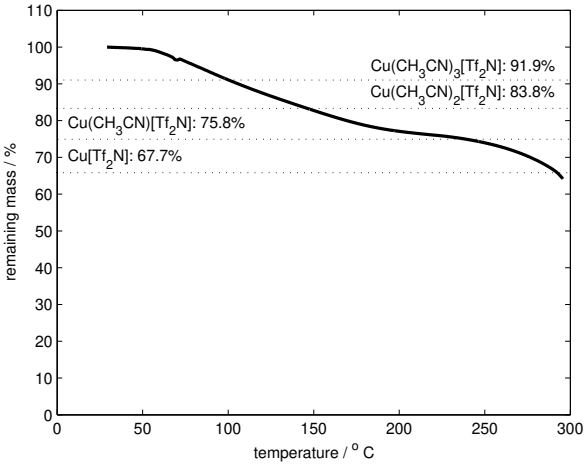

Figure 2.2: TGA curve of $[Cu(MeCN)_4][Tf_2N]$: the temperature was scanned from room temperature to 300 °C at 5 °C per minute. The dotted lines indicate the theoretical mass losses leading to the formation of the different $[Cu(MeCN)_x]$-$[Tf_2N]$ complexes.

reaction when the cuprous ions in $[Cu(MeCN)_4][Tf_2N]$ are dissolved in water (reverse of reaction (2.2)). A platinum gauze electrode was polarized at -0.2 V vs Ag/AgCl overnight until no more copper was deposited. The deposited amount of copper corresponded to 15.3 wt% of the original mass which is close to the theoretical value of 14.9 wt% for $[Cu(MeCN)_2][Tf_2N]$. Therefore, in the remainder of the paper the copper(I) acetonitrile complex used for electrochemical studies will be denoted by $[Cu(MeCN)_2][Tf_2N]$. In an analogous way, the long-term stability of $[Cu(PhCN)_4][Tf_2N]$ was determined. The electrogravimetrical analysis indicates a copper content of 11.0 wt%, in between the values for $x = 2$ and $x = 3$ (11.6 and 9.74 wt% respectively). Since the measured value is closer to $x = 2$ than $x = 3$, the compound will be denoted by $[Cu(PhCN)_2][Tf_2N]$.

Voltammetry

Because the cuprous ion is part of the cation it will move toward the cathode during electrodeposition experiments by electromigration. This gives liquid metal salts with a metal-containing cation an advantage over those with a metal-containing anion. Furthermore, since the cuprous ion is an integral part of the ionic liquid there is no need to solubilize a copper salt: the ionic liquid itself contains

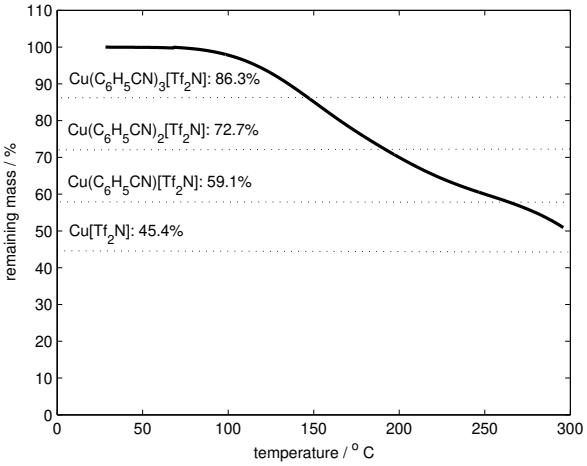

Figure 2.3: TGA curve of $[Cu(PhCN)_4][Tf_2N]$: the temperature was scanned from room temperature to 300 °C at 5 °C per minute. The dotted lines indicate the theoretical mass losses leading to the formation of the different $[Cu(PhCN)_x]$-$[Tf_2N]$ complexes.

a relatively high amount of cuprous ions. A third advantage is that the cathodic decomposition is the desired cathodic reaction: electrodeposition of metal instead of breakdown of an organic cation. Since the density of $[Cu(MeCN)_4][Tf_2N]$ is 1.59 10^3 g dm^{-3} at room temperature (based on crystallographic data), the concentration c of copper(I) ions is $c = 1.59\ 10^3$ g $(507.89\ g\ mol^{-1})^{-1}$ $(1\ dm^{-3})^{-1} = 3.1$ mol dm^{-3}. No data are available for $[Cu(MeCN)_2][Tf_2N]$.

Figures 2.4(a) and 2.4(b) show the cyclic voltammograms of $[Cu(MeCN)_2]$-$[Tf_2N]$ and $[Cu(PhCN)_2][Tf_2N]$ respectively. The overall appearance of these cyclic voltammograms is typical for an electrode reaction involving the electrodeposition and stripping of bulk metal. From a comparison of these figures, one can see that the electrochemical behavior of $[Cu(MeCN)_2][Tf_2N]$ distinctly differs from $[Cu(PhCN)_2][Tf_2N]$. First, the current density in $[Cu(MeCN)_2][Tf_2N]$ is remarkably higher and, secondly, the voltammogram for $[Cu(MeCN)_2][Tf_2N]$ does not have a peak on the cathodic side which would indicate a diffusion-limited process. One possibility is that the higher electrochemical activity of the acetonitrile complex is linked to the weaker bond between the cuprous ions and the acetonitrile ligands as compared to the benzonitrile ligands. This means that copper can be extracted more easily from the acetonitrile complex and be reduced, because the

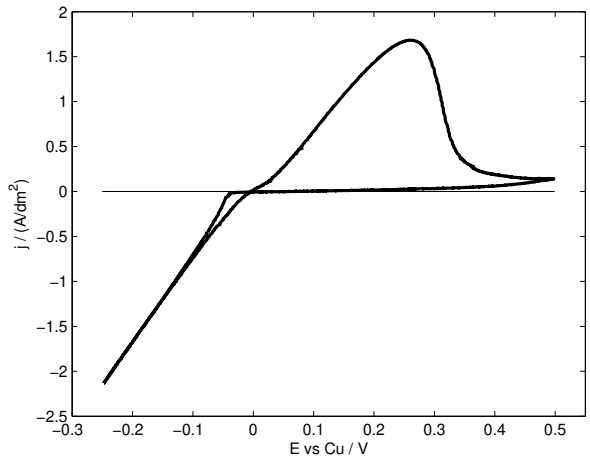

(a)

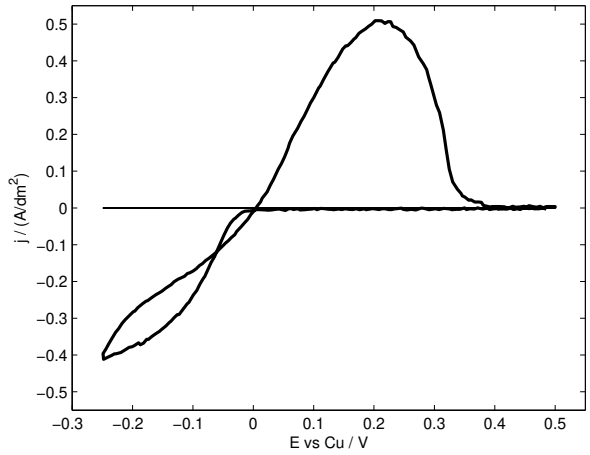

(b)

Figure 2.4: Cyclic voltammograms of (a) $[Cu(MeCN)_2][Tf_2N]$ and (b) $[Cu(PhCN)_2][Tf_2N]$ on a Pt working electrode at 90 °C. The scan rate was 50 mV s^{-1}.

electrodeposition process requires that the bonds between the cuprous ions and the ligands are broken.

To test this hypothesis, linear potential scans were measured versus a common reference electrode, so that potential values could be compared between the different solutions. The reference electrode consisted of a glass tube with a ceramic frit. This tube was filled with *N*-butyl-*N*-methylpyrrolidinium bistriflimide ([BMP][Tf_2N]), which is an electrochemically stable ionic liquid with high electrical conductivity [29]. [BMP][Tf_2N] has the advantage that it shares its anion with the low-melting copper salts under investigation, so that potential drops over the ceramic frit will be decreased. It is also assumed that this potential drop is comparable for both tested low-melting copper salts. The resulting potential scans for [$Cu(MeCN)_2$][Tf_2N] and [$Cu(PhCN)_2$][Tf_2N] are shown in figure 2.5. It

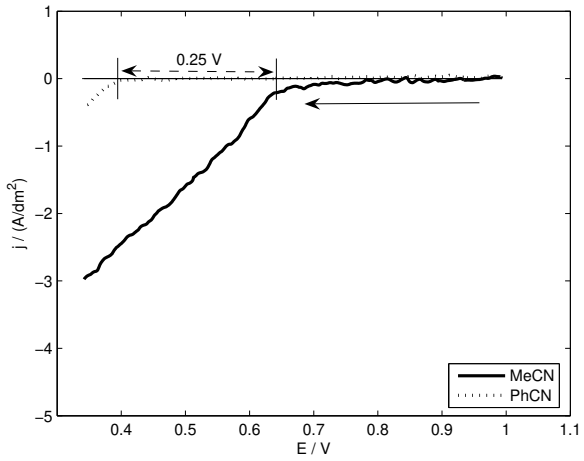

Figure 2.5: Potential scan versus a home-made reference electrode (see text) on a Pt working electrode at 90 °C for [$Cu(MeCN)_2$][Tf_2N] and [$Cu(PhCN)_2$][Tf_2N]. The scan rate was 50 mV s^{-1}.

is evident that the reduction of copper(I) in [$Cu(PhCN)_2$][Tf_2N] shifts towards more negative potentials than is the case for [$Cu(MeCN)_2$][Tf_2N], indicating the higher stability of the former complex. The difference in reduction potential is 0.25 V. Based on the formula $\Delta G = n\mathrm{F}\Delta E$, in which n is the number of exchanged electrons and F is the Faraday constant, the difference in free energy of both low melting salts $\Delta G = 24.1$ kJ mol^{-1}. A copper deposit from [$Cu(PhCN)_2$][Tf_2N] with a thickness of 1 μm on a Pt working electrode is shown in figure 2.6. The

deposition potential was -0.25 V. The total time required to achieve a thickness of 1 μm was 4 minutes, much longer than for deposits made from $[Cu(MeCN)_2][Tf_2N]$ (*vide infra*). Because we are interested in compounds which permit a large mass

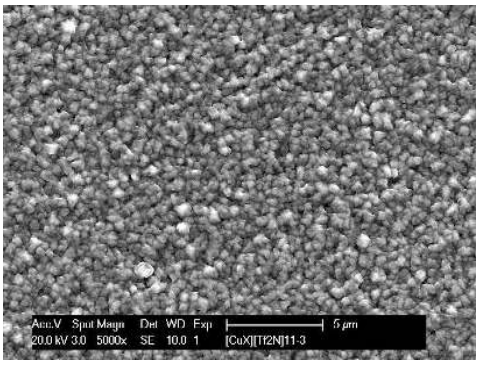

Figure 2.6: Copper deposit from $[Cu(PhCN)_2][Tf_2N]$ on a Pt working electrode at 90 °C. The deposition potential was -0.25 V and it was applied until a theoretical thickness of 1 μm was reached (135 C dm^{-2}).

transport during electrodeposition, the remainder of the discussion will mainly focus on $[Cu(MeCN)_2][Tf_2N]$.

Detailed experiments on $[Cu(MeCN)_2][Tf_2N]$

As it seemed that high current densities could be reached in $[Cu(MeCN)_2]$-$[Tf_2N]$, this system was pushed to find the maximum achievable current density. The outcome of these initial experiments gave the impression that an astonishingly high current density of 170 A dm^{-2} could be applied (figure 2.7(a)). A closer look of the resulting deposit showed a rough, strongly dendritic morphology (figure 2.7(b)). Therefore, the real current density had to be much lower than the value, calculated on the basis of the geometrical size of the electrode, and these results indicate that one cannot rely solely on voltammetry data. To be able to control the real current density, the experimental setup was adjusted.

If disk electrodes are used, the high current density on the edges of the disk leads to an uncontrollable surface area since the deposit grows radially and a rough morphology arises due to dendritic growth. To decrease the tendency for dendritic growth, a cell was built in which a cylindrical channel made out of PTFE was placed in front of the disk electrode. The cell is schematically shown in figure 2.8. The disk electrode had a diameter of 3 mm while the channel was 6 mm long. With this setup, the current density profile becomes uniform minimizing

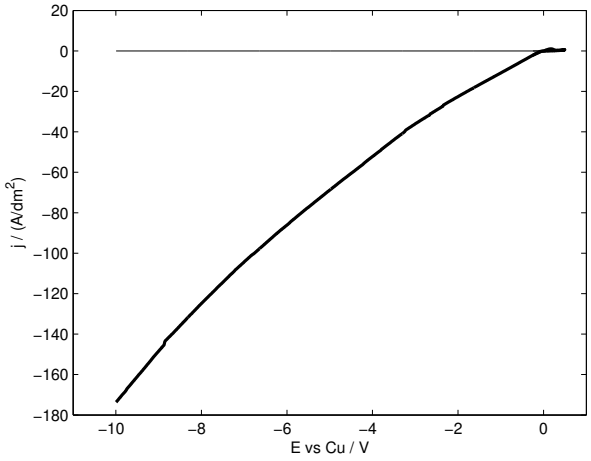

(a)

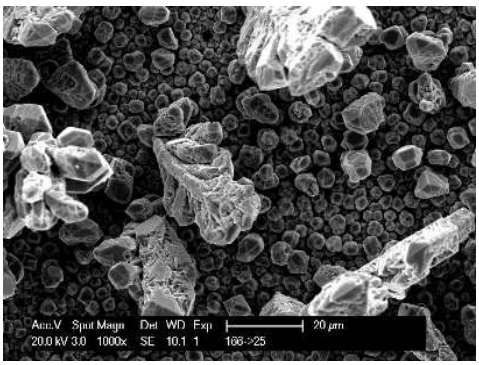

(b)

Figure 2.7: Preliminary experiment on $[Cu(MeCN)_2][Tf_2N]$ on a Pt working electrode at 90 °C: (a) linear potential scan at 50 mV s^{-1}, (b) dendritic copper deposit from $[Cu(MeCN)_2]$-$[Tf_2N]$.

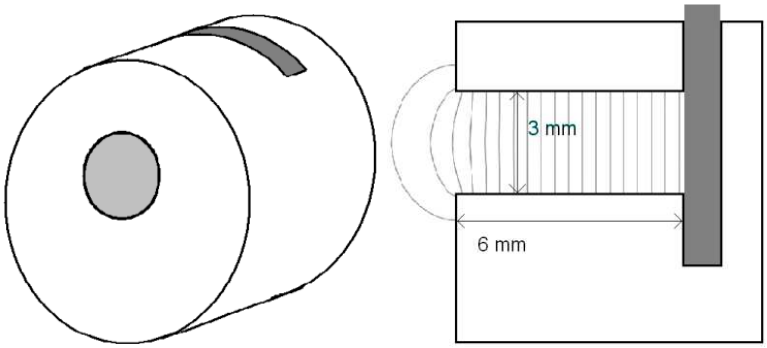

Figure 2.8: Schematic of the electrochemical cell: (a) Overview of the electrochemical cell, (b) Cross-section of the electrochemical cell with isopotential lines.

the tendency for dendritic growth. Of course, this configuration increased the iR drop. Where possible the iR drop was corrected for during the measurement by the current-interrupt technique. Otherwise, the measured j vs E curves were corrected post-experimentally using a constant electrolyte resistance R. In a first approximation, R consists of two parts: $R = R_1 + R_2$. R_1 is the resistance of infinity to the entrance of the channel and is approximately equal to $R_1 = (4\sigma r)^{-1}$, as calculated by Newman [30]. R_2 is the resistance in the channel, modeled as a straight conductor whose resistance is equal to $R_2 = l\left[(\pi r^2)\sigma\right]^{-1}$ in which l is the length of the channel, r is the radius of the channel and σ is the solution's conductivity (1.62 Ω^{-1} m^{-1}). The total value for the resistance R is therefore 627 Ω. This value was also found by the finite-element model and experimentally by electrochemical impedance spectroscopy (EIS). The experimental EIS value was determined by extrapolating the high frequency end of the measured curve to the real axis (figure 2.9). A cyclic voltammogram of $[Cu(MeCN)_2][Tf_2N]$, not corrected for iR drop is shown in figure 2.10(a), the corrected voltammogram (by a current interrupt technique) can be seen in figure 2.10(b). One can immediately notice the much lower current densities and inclination versus the baseline in the uncorrected CV. At negative potentials vs Cu, the copper(I) ion can be extracted from the cation and reduced to copper metal. This metallic copper layer can be stripped at positive potentials. It is clear that even for small overpotentials, a remarkably high current density could be achieved. When the system was pushed to higher overpotentials, current densities up to 25 A dm^{-2} could be reached (figure 2.11). This potential scan could only be corrected for iR drop post-experimentally as the current interrupt method becomes unstable at higher current densities. The

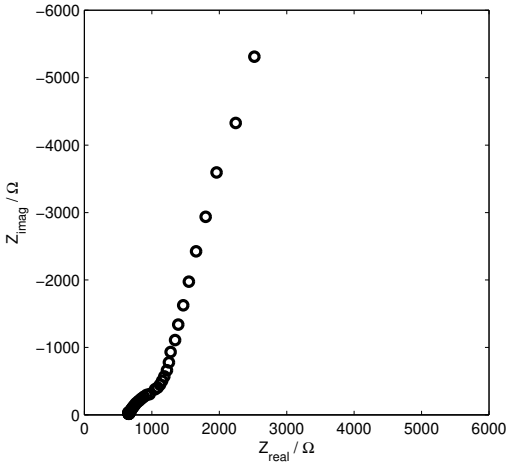

Figure 2.9: Electrochemical impedance spectrum of $[Cu(MeCN)_2][Tf_2N]$ on a Pt working electrode at 90 °C at +0.1 V vs Cu for the frequency range 100 kHz − 1 Hz.

low overpotential region of the potential scan should be compared to the cyclic voltammogram in figure 2.10(b). At the start of the measurement the resemblance is satisfactory.

Copper deposition

As mentioned in reference [15], one should realize that the electrochemical experiments are performed in a pure ionic liquid that acts as both the supporting electrolyte and the electrochemically active species, which is therefore present in a high concentration. It also follows that migrational processes might occur. In contrast with other ionic liquids that often contain negatively charged electroactive species, in our ionic liquids the migrational flux helps to increase the mass transport due to the positively charged copper complex. Based on the information obtained by voltammetry, deposition experiments were performed for three different current densities: 1, 5 and 25 A dm^{-2}. The SEM micrographs of these deposits are shown in figure 2.12. All layers have a theoretical thickness of 1 μm (135 C dm^{-2}). For a current density of 1 A dm^{-2} the morphology of the deposit was rough and nodular. The grain size exceeded 1 μm. Based on the formula $N = (\pi d^2)^{-1}$, in which N represents the nucleation density and d the deposit's thickness, and the fact that the substrate is not fully covered with deposited copper, N is lower than $3{\cdot}10^{11}$ m^{-2}. The higher the current density, the higher the

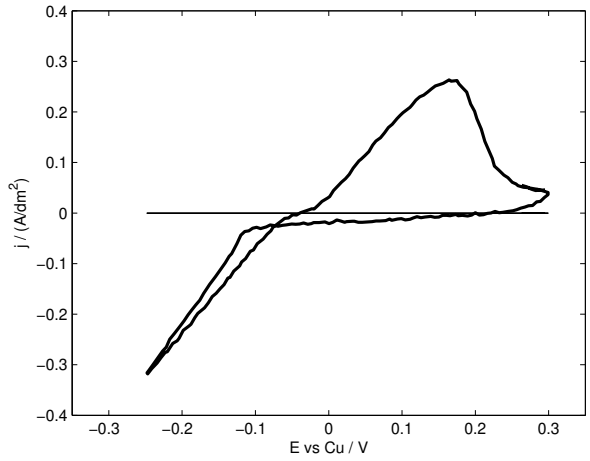

(a)

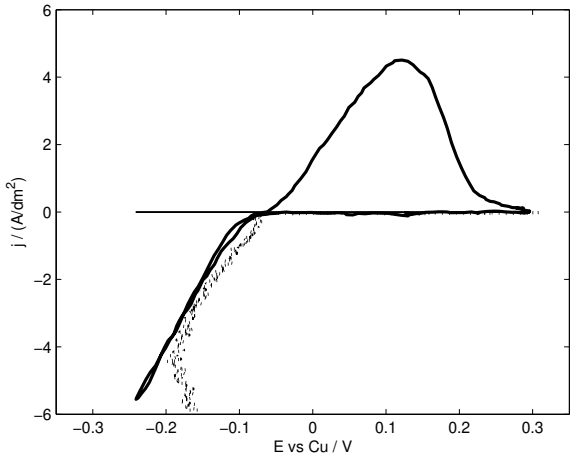

(b)

Figure 2.10: (a) Cyclic voltammogram of $[Cu(MeCN)_2]$-$[Tf_2N]$ on a Pt working electrode at 90 °C and (b) cyclic voltammogram (solid line) and potential scan (dotted line, see also figure 2.11), corrected for iR drop.

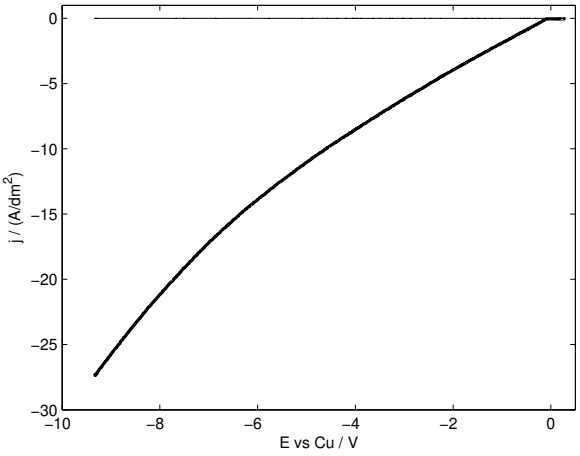

Figure 2.11: Linear potential scan of $[Cu(MeCN)_2][Tf_2N]$ on a Pt working electrode at 90 °C. This scan was not corrected for iR drop. See also figure 2.10(b).

nucleation density and the smoother the layers become: for 5 A dm^{-2} the layer had a fine cauliflower like morphology whereas for 25 A dm^{-2}, the surface was wavy yet uniform. No cracks were visible, indicating the absence of large internal stresses. The value for the nucleation density was not determined for the higher current densities but based on the smooth appearance it is considerably higher than $3{\cdot}10^{11}$ m^{-2}.

Figure 2.13 displays the EDX analysis of the deposit made at 25 A dm^{-2} (see figure 2.12(c)). The spectrum contains only copper peaks, without any signs of carbon, sulfur, fluorine or oxygen which could indicate the decomposition of the bistriflimide anion or acetonitrile molecules. Since the solution was contained in a copper crucible that also served as counter-electrode, the anodic reaction was the dissolution of copper. In a recent paper [31], it was reported that that the $[Tf_2N]^-$ anion can be decomposed during the anodic dissolution of copper, leading to the formation of CuF_2 which remains in the ionic liquid as a white suspension. During our experiments, the solution kept its clear appearance so we believe that no significant decomposition occurred. A first possible explanation for this discrepancy is the large ratio of anode area to cathode area so that the current density and overpotential at the anode is kept small. Secondly, the deposition time to reach 1 μm thickness is 135 s, 27 s and 5.4 s for 1, 5 and 25 A dm^{-2}, respectively. Much shorter than the two hours of continuous anodization reported in reference

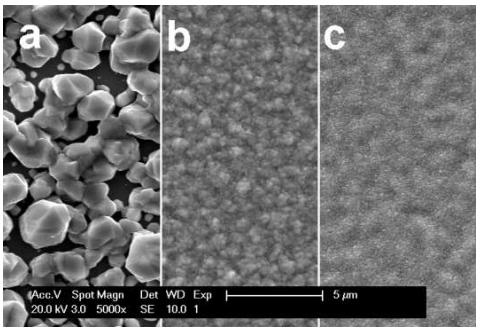

Figure 2.12: Copper deposits from $[Cu(MeCN)_2][Tf_2N]$ on a Pt working electrode at 90 °C for (a) 1 A dm^{-2}, (b) 5 A dm^{-2} and (c) 25 A dm^{-2}. Theoretical thickness of 1 μm (135 C dm^{-2}).

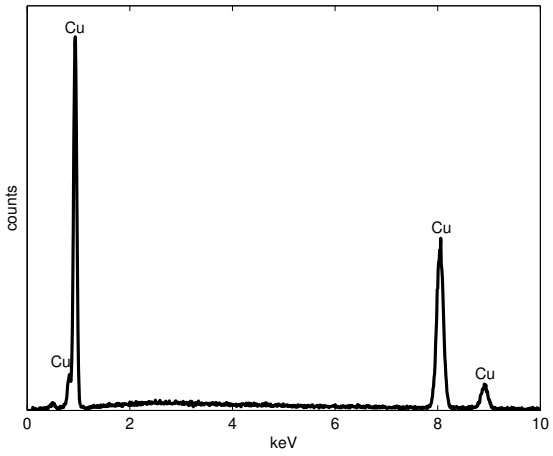

Figure 2.13: EDX spectrum of a copper deposit obtained at 25 A dm^{-2} from $[Cu(MeCN)_2][Tf_2N]$ at 90 °C (see figure 2.12(c)).

[31].

Diffusion coefficient

The diffusion coefficient for Cu^+ was measured by using a rotating disk electrode and the well known Levich equation [32]:

$$j_L = 0.62nFD^{2/3}\nu^{-1/6}c\sqrt{\omega} \tag{2.3}$$

In this equation j_L (A dm^{-2}) is the limiting current density, D is the diffusivity (dm^2 s^{-1}), ν the kinematic viscosity ($5.7{\cdot}10^{-4}$ dm^2 s^{-1}), c the concentration (mol dm^{-3}) and ω the angular frequency of rotation (rad s^{-1}). To circumvent the interference of the electrodeposition reaction and possible change in the electrode's surface area, Cu^+ was oxidized to Cu^{2+} instead of being reduced to metallic copper. Linear potential scans at 5 mV s^{-1} for different rotational speeds are plotted in figure 2.14(a) while figure 2.14(b) shows j_L as a function of $\sqrt{\omega}$. A straight line is fitted through the data points. The diffusion coefficient D can calculated from the slope of this fit and its value is $4.9{\cdot}10^{-10}$ dm^2 s^{-1}. The value for D is rather low. In the authors' opinion, the oxidative reaction of Cu^+ is quite different from the reduction to copper metal. In the latter case ligand bonds need to be broken and the liberated acetonitrile molecules can influence complex forming by Cu^+ and attribute a migrational component into the transport of Cu^+ ions.

Conclusion

The electrochemical behavior of the liquid copper salts $[Cu(MeCN)_x][Tf_2N]$ and $[Cu(PhCN)_x][Tf_2N]$ ($x = 2{-}4$) is presented. For electrodeposition purposes, low melting salts with a cationic complex are preferred over anionic complexes. The $[Cu(MeCN)_2][Tf_2N]$ complex is the easiest to be reduced to copper and current densities up to 25 A dm^{-2} in unstirred solutions could be achieved. The resulting copper deposits from $[Cu(MeCN)_2][Tf_2N]$ had a smooth appearance, did not show cracks and were free from incorporated species. Due to stronger ligand interaction, $[Cu(PhCN)_2][Tf_2N]$ did not show the same behavior. We believe that the much better mass transport in this system is due to the high metal concentration and to the favorable electrostatic interactions between the cationic electroactive species and the cathode. This makes the use of liquid metal salts with electrochemically active cationic complexes interesting for electrochemical applications where mass transport is important.

Acknowledgments

Research funded by a Ph.D grant of the Institute for the Promotion of Innovation through Science and Technology in Flanders (IWT-Vlaanderen) to S.S. This

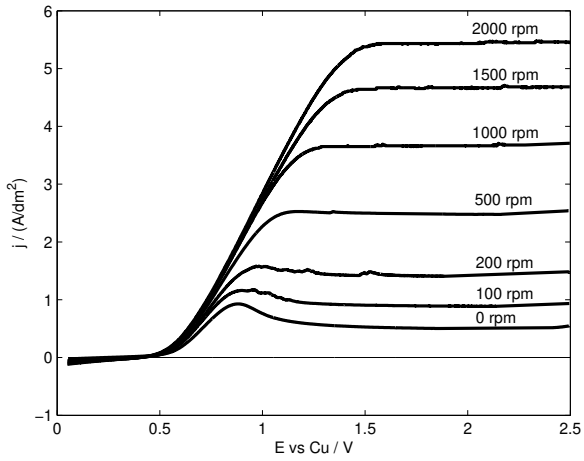

(a)

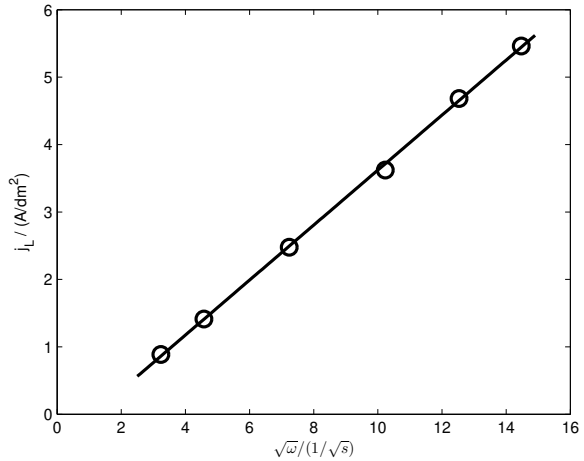

(b)

Figure 2.14: Experiments performed on a platinum rotating disk in $[Cu(MeCN)_2][Tf_2N]$ at 90 °C: (a) linear potential scans at 5 mV s^{-1} and (b) Steady-state current j_L as a function of $\sqrt{\omega}$.

work is supported in part by the European Commissions Seventh Framework Programme (FP7) under Grant Agreement number 216474 (CopPeR). The authors acknowledge financial support by the K.U.Leuven (projects IDO/05/005 and GOA 08/05), by the FWO-Flanders (research community "Ionic Liquids") and by the IWT-Flanders (SBO-project IWT 80031 "MAPIL"). Support by IoLiTec (Denzlingen, Germany) is also acknowledged.

Supplementary information

This section contains results of experiments that were performed after publication of the paper "*Electrodeposition from cationic cuprous organic complexes: ionic liquids for high current density electroplating*", presented in this chapter. Considering the strong influence that thiourea and 1*H*-benzotriazole showed on the morphology of silver (see Chapter 3), their effect was also studied during the electrodeposition of copper from $[Cu(MeCN)_2][Tf_2N]$. These results are shown here.

Figure 2.15 shows the cyclic voltammograms with and without both additives. From this figure, it is clear that these additives change the electrodeposition of cop-

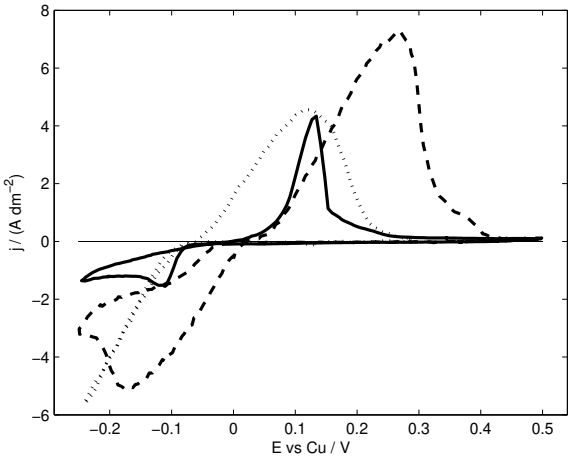

Figure 2.15: Cyclic voltammograms of $[Cu(MeCN)_2][Tf_2N]$ on a Pt working electrode at 90 °C. $(\cdots)$ no additive, $(--)$ 0.05 mol dm^{-3} thiourea, $(-)$ 0.1 mol dm^{-3} 1*H*-benzotriazole.

per: thiourea shifts the deposition potential slightly to more anodic potentials and depresses the current at potentials more negative than -0.2 V. 1*H*-benzotriazole leads to an even stronger decrease in the observed current.

Metal deposits at 1 A dm^{-2} from solutions containing thiourea or 1*H*-benzotriazole are presented in figure 2.16. This figure shows the strong influence that both additives have on the deposit morphology of copper. Thiourea is able to smoothen the morphology but it is 1*H*-benzotriazole that gives the best results with a mirror-like visual appearance of the deposit. To quantify the roughness of the deposits,

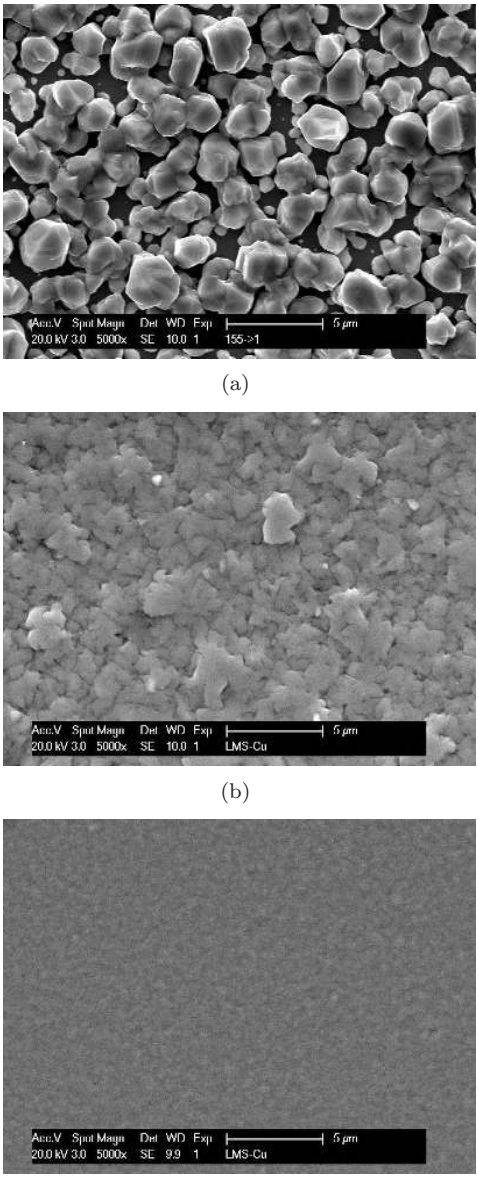

Figure 2.16: Deposits from $[Cu(MeCN)_2][Tf_2N]$ at 90 °C on a Pt working electrode at 1 A dm^{-2}: (a) no additive, (b) 0.05 mol dm^{-3} thiourea, (c) 0.1 mol dm^{-3} 1*H*-benzotriazole. The theoretical thickness is 1 μm.

atomic force microscopy was applied. The AFM topologies of the copper deposits are shown in figure 2.17. These pictures clearly show a rough morphology from the additive-free solution, while the deposit from the solution containing thiourea consists of a combination of smaller and larger grains. The mirror-like appearance of the deposit from the 1*H*-benzotriazole containing solution is caused by the very flat deposit. This is obvious from the roughness profiles shown in figure 2.18, and the R_a and R_q values mentioned in table 2.1. The addition of thiourea

Table 2.1: R_a and R_q values for deposits from $[Cu(MeCN)_2][Tf_2N]$ at 90 °C on a Pt working electrode at 1 A dm^{-2}, obtained in the absence and presence of additives.

Additive	R_a (nm)	R_q (nm)
none	362 ± 49	454 ± 59
0.05 mol dm^{-3} thiourea	30 ± 4	40 ± 5
0.1 mol dm^{-3} 1*H*-benzotriazole	5.4 ± 0.2	7.0 ± 0.4

to $[Cu(MeCN)_2][Tf_2N]$ leads to a more than tenfold decrease in the roughness profile: R_q decreases from 454 nm to 40 nm. Adding 1H-benzotriazole leads to an R_q value of only 7 nm. Based on these results, it seems that the function of 1*H*-benzotriazole and thiourea in $[Cu(MeCN)_2][Tf_2N]$ is not much different from their behavior in aqueous solutions. In aqueous copper plating, there are strong indications that thiourea bonds to the copper surface by its unsaturated sulfur atom, inhibiting the surface diffusion of the copper adatoms which promotes a smaller-grained structure [33, 34]. 1*H*-benzotriazole on the other hand, might adsorb at the active sites of the copper surface and because these active sites are now blocked by adsorbates of 1H-benzotriazole, the reduction of copper proceeds randomly over the surface. Furthermore, the adsorbed 1*H*-benzotriazole inhibits the lateral diffusion of the adsorbed ions. Thereby, growth occurs mainly by small nuclei. A description of the deposition mechanism in presence of 1*H*-benzotriazole or thiourea from aqueous solutions is given by Schmidt *et al.* [35]

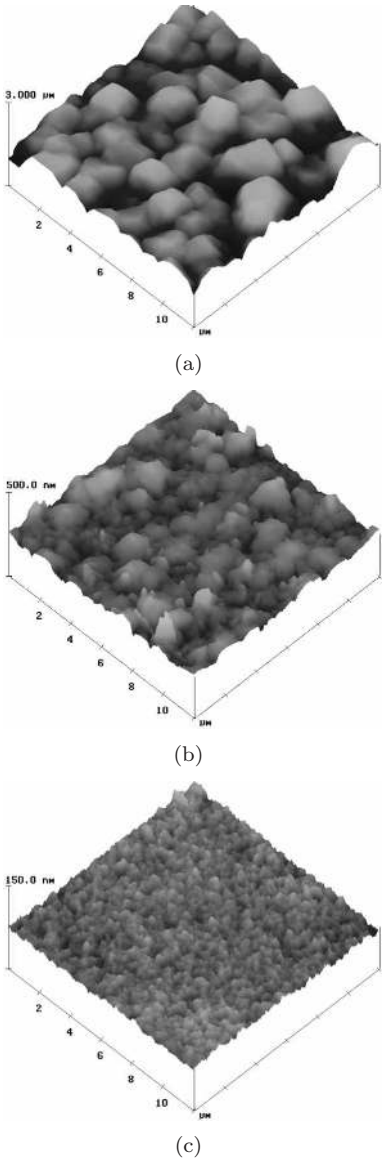

Figure 2.17: AFM topologies of deposits from $[Cu(MeCN)_2][Tf_2N]$ at 90 °C on a Pt working electrode at 1 A dm^{-2}: (a) no additive, (b) 0.05 mol dm^{-3} thiourea, (c) 0.1 mol dm^{-3} 1*H*-benzotriazole. See also figure 2.16.

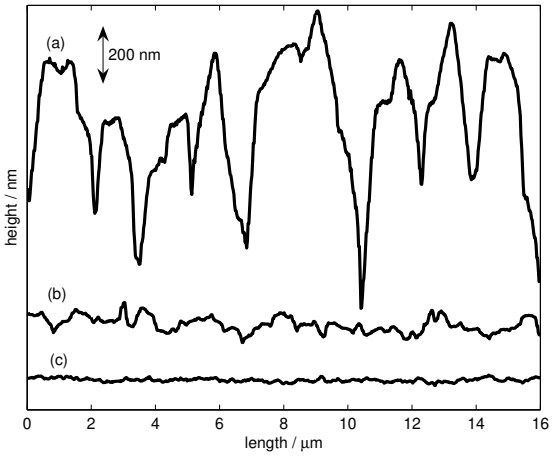

Figure 2.18: Roughness profiles of deposits from $[Cu(MeCN)_2][Tf_2N]$ at 90 °C on a Pt working electrode at 1 A dm^{-2}: (a) no additive, (b) 0.05 mol dm^{-3} thiourea, (c) 0.1 mol dm^{-3} 1*H*-benzotriazole. See also figure 2.17.

References

[1] S. A. Forsyth, J. M. Pringle, D. R. MacFarlane, Ionic liquids - an overview, *Aust. J. Chem.*, **57**, 113 (2004).

[2] F. Endres, Ionic liquids: solvents for the electrodeposition of metals and semiconductors, *ChemPhysChem*, **3**, 144 (2002).

[3] A. P. Abbott, K. J. McKenzie, Application of ionic liquids to the electrodeposition of metals, *Phys. Chem. Chem. Phys.*, **8**, 4265 (2006).

[4] M.-J. Deng, P.-Y. Chen, T.-I. Leong, I.-W. Sun, J.-K. Chang, W.-T. Tsai, Dicyanamide anion based ionic liquids for electrodeposition of metals, *Electrochem. Commun.*, **10**, 213 (2008).

[5] D.-X. Zhuang, M.-J. Deng, P.-Y. Chen, I.-W. Sun, Electrochemistry of manganese in the hydrophilic *N*-butyl-*N*-methylpyrrolidinium dicyanamide room-temperature ionic liquid, *J. Electrochem. Soc.*, **155**, D575 (2008).

[6] M.-J. Deng, I.-W. Sun, P.-Y. Chen, J.-K. Chang, W.-T. Tsai, Electrodeposition behavior of nickel in the water- and air-stable 1-ethyl-3-methylimidazolium-dicyanamide room-temperature ionic liquid, *Electrochim. Acta*, **53**, 5812 (2008).

[7] T.-I. Leong, I.-W. Sun, M.-J. Deng, C.-M. Wu, P.-Y. Chen, Electrochemical study of copper in the 1-ethyl-3-methylimidazolium dicyanamide room temperature ionic liquid, *J. Electrochem. Soc.*, **155**, F55 (2008).

[8] P. Nockemann, B. Thijs, S. Pittois, J. Thoen, C. Glorieux, K. Van Hecke, L. Van Meervelt, B. Kirchner, K. Binnemans, Task-specific ionic liquid for solubilizing metal oxides, *J. Phys. Chem. B*, **110**, 20978 (2006).

[9] P. Nockemann, M. Pellens, K. Van Hecke, L. Van Meervelt, J. Wouters, B. Thijs, E. Vanecht, T. N. Parac-Vogt, H. Mehdi, S. Schaltin, J. Fransaer, S. Zahn, B. Kirchner, K. Binnemans, Cobalt(II) complexes of nitrile-functionalized ionic liquids, *Chem. Eur. J.*, **16**, 1849 (2010).

[10] I. J. B. Lin, C. S. Vasam, Metal-containing ionic liquids and ionic liquid crystals based on imidazolium moiety, *J. Organomet. Chem.*, **690**, 3498 (2005).

[11] C. L. Hussey, T. M. Laher, Electrochemical and spectroscopic studies of cobalt(II) in molten aluminum chloride-*N*-*n*-butylpyridinium chloride, *Inorg. Chem.*, **20**, 4201 (1981).

[12] S. Schaltin, P. Nockemann, B. Thijs, K. Binnemans, J. Fransaer, Influence of the anion on the electrodeposition of cobalt from imidazolium ionic liquids, *Electrochem. Solid-State Lett.*, **10**, D104 (2007).

[13] S.-I. Hsiu, J.-F. Huang, I.-W. Sun, C.-H. Yuan, J. Shiea, Lewis acidity dependency of the electrochemical window of zinc chloride - 1-ethyl-3-methylimidazolium chloride ionic liquids, *Electrochim. Acta*, **47**, 4367 (2002).

[14] R. E. Del Sesto, T. M. McCleskey, A. K. Burrell, G. A. Baker, J. D. Thompson, B. L. Scott, J. S. Wilkes, P. Williams, Structure and magnetic behavior of transition metal based ionic liquids, *Chem. Commun.*, , 447 (2008).

[15] R. J. C. Brown, P. J. Dyson, D. J. Ellis, T. Welton, 1-butyl-3-methylimidazolium cobalt tetracarbonyl [bmim][$Co(CO)_4$]: a catalytically active organometallic ionic liquid, *Chem. Commun.*, , 1862 (2001).

[16] J.-F. Huang, H. Luo, S. Dai, A new strategy for synthesis of novel classes of room-temperature ionic liquids based on complexation reaction of cations, *J. Electrochem. Soc.*, **153**, J9 (2006).

[17] S. G. Biallozor, Electrodeposition of copper on platinum from non-aqueous solutions, *Electrochim. Acta*, **17**, 1243 (1972).

[18] D. M. Muir, A. J. Parker, J. H. Sharp, W. E. Waghorne, Cuprous hydrometallurgy, Part I: Electrorefining copper via acidic solutions of cuprous sulphate containing organic nitriles, *Hydrometallurgy*, **1**, 61 (1975).

[19] S. G. Biallozor, D. Poletek, Electrochemical behavior of copper in nonaqueous solutions. I, *Élektrokhimiya*, **15**, 472 (1979).

[20] S. G. Biallozor, A. Lisowska, Electrochemical behavior of copper in nonaqueous solutions. II, *Élektrokhimiya*, **15**, 634 (1979).

[21] I. D. MacLeod, A. J. Parker, P. Singh, Electrochemistry of copper in aqueous acetonitrile, *J. Solution Chem.*, **10**, 757 (1981).

[22] N. Petrescu, L. Ganovici, M. Britchi, Electrolytic copper refining from cuprous sulphate solutions containing organic nitriles, *Rev. Roum. Chim.*, **29**, 407 (1984).

[23] A. Vaskevich, I. Rubinstein, Underpotential deposition of copper in acetonitrile, *J. Electroanal. Chem.*, **491**, 87 (2000).

[24] L. G. Boxall, H. L. Jones, R. A. Osteryoung, Electrochemical studies on Ag, Fe, and Cu species in AlCl -NaCl melts, *J. Electrochem. Soc.*, **121**, 212 (1974).

[25] C. L. Hussey, L. A. King, R. A. Carpio, The electrochemistry of copper in a room temperature acidic chloroaluminate melt, *J. Electrochem. Soc.*, **126**, 1029 (1979).

[26] P.-Y. Chen, I.-W. Sun, Electrochemical study of copper in a basic 1-ethyl-3-methylimidazolium tetrafluoroborate room temperature molten salt, *Electrochim. Acta*, **45**, 441 (1999).

[27] K. Murase, K. Nitta, T. Hirato, Y. Awakura, Electrochemical behaviour of copper in trimethyl-*n*-hexylammonium bis((trifluoromethyl)sulfonyl)amide, an ammonium imide-type room temperature molten salt, *J. Appl. Electrochem.*, **31**, 1089 (2001).

[28] T. Katase, K. Murase, T. Hirato, Y. Awakura, Redox and transport behaviors of Cu(I) ions in TMHA-Tf_2N ionic liquid solution, *J. Appl. Electrochem.*, **37**, 339 (2007).

[29] D. R. MacFarlane, J. Sun, J. Golding, P. Meakin, M. Forsyth, High conductivity molten salts based on the imide ion, *Electrochim. Acta*, **45**, 1271 (2000).

[30] J. Newman, Resistance for flow of current to a disk, *J. Electrochem. Soc.*, **113**, 501 (1966).

[31] A. S. Ismail, S. Zein El Abedin, O. Höfft, F. Endres, Unexpected decomposition of the bis (trifluoromethylsulfonyl) amide anion during electrochemical copper oxidation in an ionic liquid, *Electrochem. Commun.*, **12**, 909 (2010).

[32] A. J. Bard, L. R. Faulkner, *Electrochemical methods*, p. 339, John Wiley & Sons (2001).

[33] B. H. Loo, Molecular-orientation of thiourea chemisorbed on copper and silver surfaces, *Chem. Phys. Lett.*, **89**, 346 (1982).

[34] S. A. Campbell, E. E. Farndon, F. C. Walsh, M. Kalaji, Electrochemical and spectroscopic studies of the influence of thiourea on copper deposition from acid sulphate solution, *Trans. Inst. Metal. Finish.*, **75**, 10 (1997).

[35] W. U. Schmidt, R. C. Alkire, A. A. Gewirth, Mechanic study of copper deposition onto gold surfaces by scaling and spectral analysis of in situ atomic force microscopic images, *J. Electrochem. Soc.*, **143**, 3122 (1996).

Chapter 3

High current density electrodeposition from silver complex ionic liquids

Published as S. Schaltin, N.R. Brooks, L. Stappers, K. Van Hecke, L. Van Meervelt, K. Binnemans and J. Fransaer, *Phys. Chem. Chem. Phys.*, **14**, 1706-1715 (2012)

Abstract

Liquid metals salts are electrolytes with the highest possible metal concentration for electrodeposition, because the metal ion is an integral part of the solvent. This paper introduces the new ionic silver complexes $[Ag(MeCN)_4]_2[Ag(Tf_2N)_3]$, $[Ag(MeCN)][Tf_2N]$ and $[Ag(EtIm)_2][Tf_2N]$, where MeCN stands for acetonitrile, EtIm for 1-ethylimidazole and Tf_2N is bis(trifluoromethylsulfonyl)imide. These complexes have been characterized by differential scanning calorimetry, single crystal X-ray crystallography, thermogravimetrical analysis, Raman spectroscopy and cyclic voltammetry. $[Ag(MeCN)_4]_2[Ag(Tf_2N)_3]$ is a room temperature ionic liquid. Smooth silver layers of a good quality could be deposited from it, at current densities up to 25 A dm^{-2} in unstirred solutions. $[Ag(EtIm)_2][Tf_2N]$ melts at 65 °C, and can be used as electrolyte for silver deposition above this temperature. $[Ag(MeCN)][Tf_2N]$ has a melting point that is too high to be useful in electrodeposition. Addition of thiourea or 1*H*-benzotriazole to the electrolyte decreased the surface roughness of the silver coatings. The morphology of the metal layers was investigated by atomic force microscopy (AFM). Adsorption of 1*H*-benzotriazole on the silver metal surface has been proven by Raman spectroscopy. This work shows the usefulness of additives to improve the quality of metal films electrodeposited from ionic liquids.

Introduction

Ionic liquids are becoming increasingly important in applications such as electrolytes in batteries and supercapacitors, in photovoltaic devices, and for the electrodeposition of metals due to their wide electrochemical window and the presence of intrinsic ionic charge carriers [1–3]. In these applications, a good mass transfer is needed. However, as the viscosity of most ionic liquids is quite high compared to most molecular solvents, the mass transport in ionic liquids is often rather poor. This problem is complicated by the poor solubility of simple metal salts (e.g. chlorides) in most ionic liquids suitable for electrodeposition, except for dicyanamide ionic liquids [4–7]. The limited solubility is due to the weakly coordinating ability of anions such as $[BF_4]^-$, $[PF_6]^-$ or bistriflimide ($[Tf_2N]^-$).

One way to circumvent the problem of low solubility is the use of functionalized ionic liquids. These ionic liquids have a built-in coordinating unit, such as a nitrile group which can bind to the metal ion, thereby increasing its solubility [8, 9]. Another way to improve the solubility of metal ions in ionic liquids is to design ionic liquids with a metal complex as part of their composition [10–13]. Most ionic liquids of this type contain anionic metal complexes. Examples of such anionic complexes are $[AlCl_4]^-$, $[CoCl_4]^{2-}$, $[ZnCl_4]^{2-}$ and $[MnCl_4]^{2-}$ [14–17]. Descriptions of anionic complexes such as $[WO_4]^{2-}$ and $[Co(CO)_4]^-$ without chloro ligands are given by Brown *et al.* [18] and Qiao *et al.* [19] The advantages of complexing a metal ion with organic ligands and the use of the formed complexes as the cation in an ionic liquid has already been reported for copper [20, 21]. In those papers we showed that acetonitrile complexes of copper(I) are able to sustain high current densities. Silver is an interesting metal for its high electrical conductivity [22], good corrosion resistance [22] and as antimicrobial agent [23, 24]. Unfortunately, the electrodeposition of silver from most aqueous solutions suffers from the use of highly toxic cyanides [25]. Cyanides increase the conductivity and electrode polarization for a sufficient anode corrosion, but the presence of cyanide places a large burden on the disposal of the plating bath and waste water. The electrodeposition of silver from other solvents such as ionic liquids is therefore an interesting topic.

In this paper we present two new silver containing ionic liquids $[Ag(MeCN)_4]_2$-$[Ag(Tf_2N)_3]$ and $[Ag(EtIm)_2][Tf_2N]$ (MeCN = acetonitrile, EtIm = 1-ethylimidazole). The first ionic liquid contains both silver-complex cations and anions, while the second contains only silver-complex cations. We show that the methodology developed for Cu^+ of creating ionic liquids containing metal cations complexed by organic ligands [20, 21] is generally more applicable and the morphology of deposits can be altered by the use of additives. Other examples of cationic silver complexes, based on amine ligands, have been reported by Huang *et al.* [26] and

Iida *et al.* [27, 28] but these authors do not mention nor show that these complexes can sustain high current densities. Additional papers on the electrodeposition of silver from ionic liquids can be found in literature [29–44].

Experimental

Material and methods

All chemicals purchased were of reagent grade and used without further purification. TGA studies were preformed on a TA instruments Q600 thermogravimeter. For $[Ag(EtIm)_2][Tf_2N]$ the temperature was scanned from room temperature up to 400 °C at a heating rate of 5 °C per minute. The temperature programme used for the analysis of $[Ag(MeCN)_4]_2[Ag(Tf_2N)_3]$ consisted of a combination of 10 °C temperature steps and temperature ramps (see discussion for full details). Elemental analyses (C, H, N) were carried out using a CE Instruments EA-1110 elemental analyzer or by ICP-AES (Ag) on a Varian 720-ES ICP Optical Emission Spectrometer. The IR and Raman spectra were recorded on a Bruker Vertex 70 FTIR spectrometer, coupled with a Ram II Raman module, at a resolution of 4 cm^{-1}. SERS spectra were recorded by immersing a rough silver foil in the ionic liquid or ionic liquid containing additive, removing the foil from the liquid and irradiating the wet foil. Melting points were determined on a Mettler-Toledo 822 DSC instrument. Viscosities have been measured on a Brookfield cone plate viscosimeter (LVDV-II+ Programmable Viscometer) with a cone spindle CPE-40. The ionic liquid was kept under dry nitrogen atmosphere during the measurement and the temperature of the sample was controlled by a circulating water bath. The morphology and elemental composition of the silver deposits were determined by scanning electron microscopy (SEM) and energy-dispersive X-ray analysis (EDX) (Philips XL 30 FEG) and atomic force microscopy (AFM) (Digital Instruments Nanoscope III AFM).

Synthesis

$[Ag(MeCN)_4]_2[Ag(Tf_2N)_3]$: To Ag_2O (10.13 g, 43.7 mmol) in acetonitrile (100 ml) was added $H[Tf_2N]$ (80% solution in water, 30.74 g, 87.5 mmol) and the mixture stirred at room temperature for 1 hour. Remaining solids were removed by filtration and the acetonitrile removed on a rotary evaporator. The resulting liquid was cooled to -78 °C which resulted in solidification. The remaining liquid was removed *in vacuo* overnight as the mixture was allowed to slowly come to room temperature to give $[Ag(MeCN)_4]_2[Ag(Tf_2N)_3]$ (42.11 g, 28.2 mmol, yield 96.7%) as a white solid. Melting point: 18 °C. IR: ν/cm^{-1} 3008 and 2945 (C−H), 2130 and 2279 (C≡N), 1344, 1179, 1128, 1055, 1013 ($[Tf_2N]^-$), 932, 790, 764, 742, 655, 612, 599, 569, 510 and 406. Found: Ag, 22.8%. Calc. for $C_{22}H_{24}Ag_3F_{18}N_{11}O_{12}S_6$:

Ag, 21.7%

[Ag(MeCN)][Tf_2N]: [$Ag(MeCN)_4]_2[Ag(Tf_2N)_3$] (1.17 g, 0.78 mmol) was placed *in vacuo* and the temperature was raised at approximately 10 °C per hour to 90 °C and then left overnight to give [Ag(MeCN)][Tf_2N] (0.99 g, 2.31 mmol, yield 98.2%) as a white solid. Melting point: 90 °C. IR: ν/cm^{-1}: 3011 and 2949 (C−H), 2320 and 2291 (C≡N), 1366, 1350, 1182, 1122 and 991 ($[Tf_2N]^-$), 1046, 939, 800, 766, 752, 647, 599, 567, 507. Found: C, 10.8%; N, 6.5%. Calc. for $C_4H_3AgF_6N_2O_4S_2$: C, 11.2%; N, 6.5%

[$Ag(EtIm)_2$][Tf_2N]: To [$Ag(MeCN)_4]_2[Ag(Tf_2N)_3$] (15.78 g, 10.6 mmol) was added 1-ethylimidazole (6.10 g, 63.4 mmol) and resulting displaced acetonitrile was removed *in vacuo* to give [$Ag(EtIm)_2$][Tf_2N] (17.94 g, 30.9 mmol, yield 97.5%) as a white solid. Melting point: 65 °C. IR: ν/cm^{-1}: 3145, 3130, 2981 and 2941 (C−H), 1342, 1330, 1177, 1132, 1113, 1095, 1047 ($[Tf_2N]^-$), 1603, 1531, 1520, 1468, 1452, 1384, 1292, 1239, 958, 865, 854, 843, 831, 787, 771, 753, 739, 650, 632, 594, 568, 531, 505, 434, 405. Found: C, 25.1%; N, 11.7%. Calc. for $C_{12}H_{16}AgF_6N_5O_4S_2$: C, 24.8%; N, 11.8%

Crystal structures

Crystals of [$Ag(MeCN)_4]_2[Ag(Tf_2N)_3$], [Ag(MeCN)][$Tf_2N$] and [$Ag(EtIm)_2$][$Tf_2N$] suitable for single crystal X-ray diffraction were mounted on a nylon loop attached to a copper pin and placed in the cold N_2 stream on a Bruker SMART 6000 diffractometer at 100(2) K using Cu K_α radiation ($\lambda = 1.54178$ Å). Absorption corrections were applied using SADABS [45]. All structures were solved using direct methods and refined by the full-matrix least-squares procedure in SHELXL [46]. H atoms were placed in calculated positions, or for CH_3 groups placed based on the difference electron density around the CH_3 group, and refined using a riding model. In [$Ag(MeCN)_4]_2[Ag(Tf_2N)_3$], some thermal parameter restraints were required for atoms of a MeCN molecule that sits along a three-fold rotation axis. A summary of the crystallographic data can be found below and the complete data in the CIF. The program OLEX2 was also used in refinement and making pictures [47].

Crystal data for [$Ag(MeCN)_4]_2[Ag(Tf_2N)_3$]: $C_{22}H_{24}Ag_3F_{18}N_{11}O_{12}S_6$, $M = 1492.49$ g mol^{-1}, trigonal, $a = b = 12.9281(11)$, $c = 16.8181(12)$ Å, $V = 2434.3(5)$ Å^3, $T = 100(2)$ K, space group $P\bar{3}c1$ (no.158), $Z = 2$, $\rho_{calc} = 2.036$ g cm^{-3}, μ(Cu-Kα) = 13.222 mm^{-1}, $F(000) = 1456$, 17040 reflections measured, 1583 unique ($R_{int} = 0.0892$) which were used in all calculations. Final $R = 0.0367$ for 1383 reflections with $I > 2\sigma(I)$ and $wR2 = 0.0875$ for all data.

Crystal data for [Ag(MeCN)][Tf_2N]: $C_4H_3AgF_6N_2O_4S_2$, $M = 429.07$ g mol^{-1}, monoclinic, $a = 7.6535(3)$, $b = 18.7315(8)$, $c = 8.4452(4)$ Å, $\beta = 99.254(2)$ °, $V = 1194.96(9)$ Å^3, $T = 100(2)$ K, space group $P2_1/c$ (no.14), $Z = 4$, $\rho_{calc} = 2.385$ g cm^{-3}, μ(Cu-Kα) = 17.758 mm^{-1}, $F(000) = 824$, 10410 reflections measured, 2277

unique ($R_{\text{int}} = 0.0696$) which were used in all calculations. Final $R = 0.0387$ for 2073 reflections with $I > 2\sigma(I)$ and $wR2 = 0.0974$ for all data.

Crystal data for $[Ag(EtIm)_2][Tf_2N]$: $C_{12}H_{16}AgF_6N_5O_4S_2$, $M = 580.31$ g mol^{-1}, monoclinic, $a = 14.9257(3)$, $b = 8.6793(2)$, $c = 16.5837(3)$ Å, $\beta = 108.6980(10)$ °, $V = 2034.94(7)$ Å^3, $T = 100(2)$ K, space group $P2_1/n$ (no.14), $Z = 4$, $\rho_{\text{calc}} = 1.894$ g cm^{-3}, μ(Cu-Kα) = 10.673 mm^{-1}, $F(000) = 1152$, 17211 reflections measured, 3911 unique ($R_{\text{int}} = 0.0622$) which were used in all calculations. Final $R = 0.0297$ for 3500 reflections with $I > 2\sigma(I)$ and $wR2 = 0.0731$ for all data.

Electrochemistry

Gold-covered silicon wafers were used as substrates for electrodeposition (Si, 500 nm SiO_2, 10 nm Ti, 100 nm Au). In order to make the current density uniform across the whole electrode area, the electrode was recessed by placing it inside a PTFE-sample holder, which decreased the tendency for dendritic growth. The presence of dendrites increases the real surface area which means that the real current density is lower than the value based on the geometrical surface area of the electrode. A complete description of the electrochemical cell is given elsewhere [20]. Before use, the substrates were cleaned by rinsing with acetone and dried. After the deposition of a silver layer, the deposit was rinsed with acetone and dried. The electrolyte was contained in a platinum crucible, and it was not stirred during the experiments. Thiourea (99.5%) was bought from Merck and 1*H*-benzotriazole (99%) was purchased from Acros Organics. For $[Ag(MeCN)_4]_2$-$[Ag(Tf_2N)_3]$, the electrochemical experiments were conducted at 50 °C, while for $[Ag(EtIm)_2][Tf_2N]$, the temperature was held at 90 °C due to its higher melting point. The experiments were done using a Solartron instruments SI 1287 Electrochemical interface controlled by a computer with Corrware software. All potential values in this paper are relative to a silver wire directly immersed in solution (pseudo-reference electrode). If required, the potential values were corrected for the *iR* drop in real time by using the *current interrupt* technique. A silver coil was used as counter electrode. It is known that ionic liquids, even the hydrophobic ones, can take up atmospheric moisture which might alter the deposit morphology, depending on the amount of absorbed water [39]. Therefore, all electrochemical experiments were performed in an argon-filled glove box (with O_2 and H_2O concentrations below 1 ppm), despite the air and moisture stability of the liquids presented in this study (*vide infra*).

Results and discussion

Structure Description

$[Ag(MeCN)_4]_2[Ag(Tf_2N)_3]$ was prepared by reaction of $H[Tf_2N]$ with Ag_2O in an excess of MeCN, giving the compound $[Ag(MeCN)_4][Tf_2N]$ in solution. On removal of the solvent *in vacuo*, the $[Ag(MeCN)_4]^+$ cations were found with complex anions consisting of Ag^+ ions coordinated by three $[Tf_2N]^-$ anions, as determined by single crystal X-ray diffraction on a crystal grown from cooling the pure liquid in a fridge (Fig. 3.1). This compound with an overall formula of $[Ag(MeCN)_4]_2$-

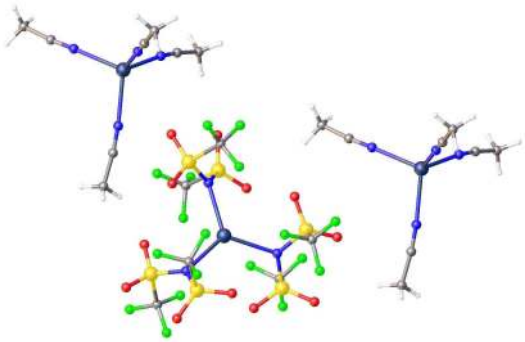

Figure 3.1: View of the crystal structure of $[Ag(MeCN)_4]_2$-$[Ag(Tf_2N)_3]$.

$[Ag(Tf_2N)_3]$ has a melting point of 18 °C and is hence a room temperature ionic liquid. Raman spectroscopy showed that the structure is the same in the solid and the liquid state (see ESI[1]). The formulation was somewhat unexpected, with the compound $[Ag(MeCN)_4][Tf_2N]$ expected in analogy to the $[Ag(MeCN)_4]^+$ complexes with $[BF_4]^-$ and $[ClO_4]^-$ anions [48–50]. However, it is not without precedent as two other $[Ag(MeCN)_4]^+$ cations have been characterized with silver-complex anions in the solid state, namely $[Ag(MeCN)_4][Ag((MeSO_2)_2N)_2]$ and $[Ag(MeCN)_4][Ag_3(NO_2)_2N)_4]$ [51, 52]. If the compound is continually left *in vacuo*, a solid is formed which corresponds to the formula $[Ag(MeCN)][Tf_2N]$.

Liquid $[Ag(MeCN)_4]_2[Ag(Tf_2N)_3]$ is stable to air and when mixed with water forms a biphasic system. On heating to 70 °C the water and ionic liquid phases mix to become one phase and then separate into two phases again on cooling. Similar behavior has been seen before in other ionic liquid/water mixtures [8, 53, 54]. The viscosity of $[Ag(MeCN)_4]_2[Ag(Tf_2N)_3]$ is 40 mPa s at 25 °C and decreases to 16.6 mPa s at 50 °C and 7.8 mPa s at 80 °C.

[1]Electronic supplementary information at the end of this chapter: Figs. 3.14 and 3.15

$[Ag(MeCN)_4]_2[Ag(Tf_2N)_3]$ crystallizes in the highly symmetrical space group $P\bar{3}c1$ with both ions lying on crystallographic special positions giving two Ag−N distances of 2.250(5) and 2.273(3) Å for the cation and one for the anion, Ag−N = 2.298(3) Å. The cation is approximately tetrahedral (N−Ag−N = 106.67(8) and 112.15(7) °) and the anion is trigonal planar enforced by the space group symmetry. Usually in order to decrease their melting points ionic liquids are designed to have unsymmetrical ions, so it is somewhat surprising that $[Ag(MeCN)_4]_2$-$[Ag(Tf_2N)_3]$ should have such a low melting point considering that the ions are highly symmetrical. The low melting point must come from the lack of intermolecular interactions, which can be seen by looking at the crystal packing (Fig. 3.2). There are no hydrogen bonds observed and the anions stack on top each

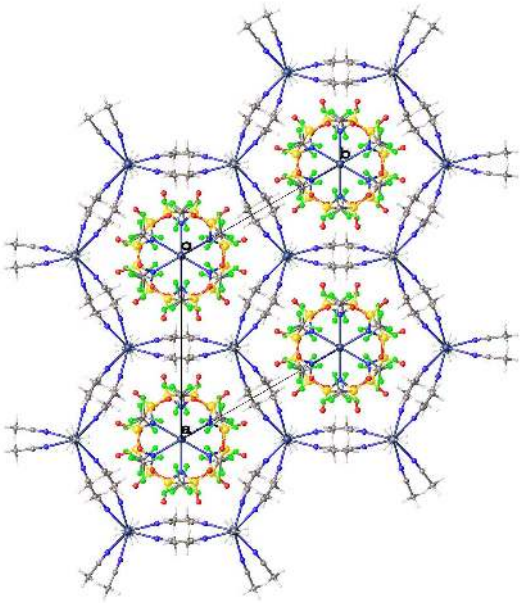

Figure 3.2: View of the packing in the crystal structure of $[Ag(MeCN)_4]_2[Ag(Tf_2N)_3]$, viewed along the crystallographic c axis.

other, as viewed along the c axis. The cations also stack along the c axis with the MeCN molecules from neighboring cations interdigitating to form the channels which contain anions.

Crystals of $[Ag(MeCN)][Tf_2N]$ could also be isolated and studied by X-ray diffraction showing that it consists of a one-dimensional polymeric structure of silver

ions linked by $[Tf_2N]^-$ anions (Fig. 3.3). The $[Tf_2N]^-$ anions link two Ag^+ ions by

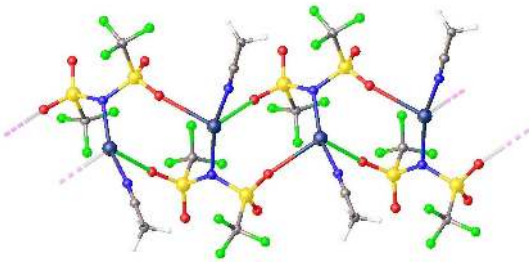

Figure 3.3: View of the crystal structure of [Ag(MeCN)]-$[Tf_2N]$ showing the polymeric structure. The longer Ag−O bond is shown in green.

coordinating to one through the N atom (Ag−N = 2.236(3) Å) and one through an O atom (Ag−O = 2.526(3) Å). The Ag^+ ion is additionally coordinated by the MeCN (Ag−N = 2.153(4) Å) molecule. There is a longer contact between the Ag^+ ion and an O atom of the $[Tf_2N]^-$ anion (Ag−O = 2.632(3) Å), this distance is longer than the sum of the ionic radii of Ag and O (2.55 Å) but only slightly longer than the Ag−O bond so it could be considered a bond. Thus, the total coordination number of the Ag^+ ions can be considered [3+1]. The melting point of $[Ag(MeCN)][Tf_2N]$ is 90 °C.

$[Ag(MeCN)_4]_2[Ag(Tf_2N)_3]$ could be reacted with an appropriate amount of 1-ethylimidazole (EtIm) to give a compound of formula $[Ag(EtIm)_2][Tf_2N]$ with a melting point of 65 °C and a viscosity of 14.1 mPa s at 80 °C. Single crystals of $[Ag(EtIm)_2][Tf_2N]$ were grown by allowing an MeCN solution of the compound to slowly evaporate. The crystals structure analysis of $[Ag(EtIm)_2][Tf_2N]$ revealed a two coordinate Ag^+ ion and an uncoordinated $[Tf_2N]^-$ anion (Fig. 3.4). The Ag−N distances are 2.102(2) and 2.107(2) Å, which are shorter than those seen in the MeCN structures but similar to those seen in other two-coordinate silver(I) complexes [55]. The N-Ag-N bond angle is 173.65(8) ° making the complex almost linear. Packing views of $[Ag(MeCN)][Tf_2N]$ and $[Ag(EtIm)_2][Tf_2N]$ are given in the Supporting information (see ESI[2]).

Thermal stability

By TGA it is possible to check whether the acetonitrile molecules stay bound to the silver ion or how easily they can be removed. The TGA experiment of $[Ag(MeCN)_4]_2[Ag(Tf_2N)_3]$ consisted of holding the temperature constant for 2

[2]Electronic supplementary information at the end of this chapter: Figs. 3.16 and 3.17

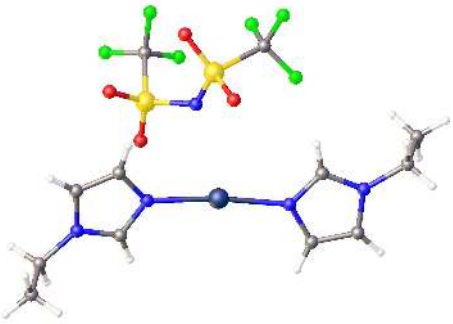

Figure 3.4: View of the crystal structure of $[Ag(EtIm)_2][Tf_2N]$.

hours at 10 °C intervals between 30 °C and 150 °C. The temperature function is shown in Figure 3.5(a). This complex temperature program was chosen because $[Ag(MeCN)_4]_2[Ag(Tf_2N)_3]$ loses MeCN fairly easily (Fig. 3.5(a)). Even whilst the sample is held at 30 °C in an open container it is already losing MeCN molecules. The first four molecules are gradually lost by the time the temperature reaches 60 °C. At 90 °C, the four remaining molecules are driven off the complex. The remaining substance is $Ag(Tf_2N)$, which remains stable up to 300 °C. The thermal decomposition of $[Ag(MeCN)_4]_2[Ag(Tf_2N)_3]$ was further investigated because the electrodepositions are carried out at a temperature of 50 °C and at this temperature it is expected that some MeCN would be lost. However, the behavior of the bulk solution in the plating bath is not expected to be the same as is found in the few milligrams of sample in the TGA analyzer due to the proportionally much lower surface area. Therefore, samples were taken from the plating bath after 4 hours, 8 hours, 1 day and 2 days at 50 °C. Between 4 hours and 8 hours a solid layer appeared on top of the bath which was found to be $[Ag(MeCN)][Tf_2N]$. The amount of $[Ag(MeCN)][Tf_2N]$ that was formed increased with time. $[Ag(MeCN)][Tf_2N]$ was easy to identify because it crystallized readily and several crystals from several different conditions were investigated by X-ray diffraction and they all corresponded to the $[Ag(MeCN)][Tf_2N]$ described above. The remaining liquid could be separated and was found to have the composition $Ag(MeCN)_2(Tf_2N)$, which would correspond to an ionic liquid of formula $[Ag(MeCN)_4][Ag(Tf_2N)_2]$, which is quite likely from the precedent of $[Ag(MeCN)_4][Ag((MeSO_2)_2N)_2]$ [52]. Attempts to isolate $[Ag(MeCN)_4][Ag(Tf_2N)_2]$ as a solid have been unsuccessful, however, it is useful to start with the ionic liquid $[Ag(MeCN)_4]_2[Ag(Tf_2N)_3]$ because it can be isolated as a solid.

The TGA analysis of $[Ag(EtIm)_2][Tf_2N]$ is presented in Figure 3.5(b), and this figure shows that the thermal decomposition of $[Ag(EtIm)_2][Tf_2N]$ only starts at

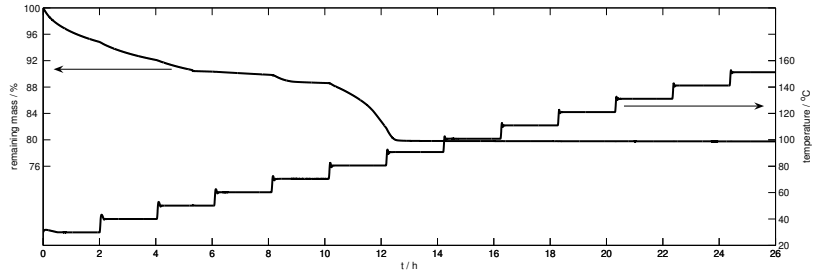

(a)

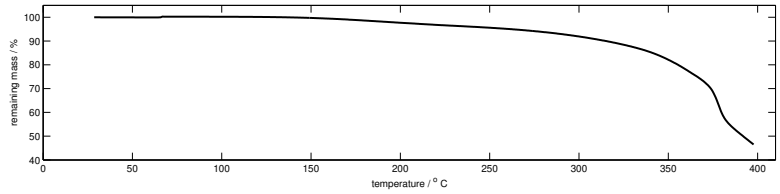

(b)

Figure 3.5: Thermogravimetrical analysis data for (a) $[Ag(MeCN)_4]_2[Ag(Tf_2N)_3]$ with the temperature program on the right vertical axis, and (b) $[Ag(EtIm)_2][Tf_2N]$ (heating rate: 5 °C min.$^{-1}$).

150 °C. At 90 °C, the temperature at which the electrochemical experiments were conducted, $[Ag(EtIm)_2][Tf_2N]$ is thermally stable. At higher temperatures, 1-ethylimidazole is slowly expelled. Table 3.1 summarizes the mentioned properties of the silver complexes.

Electrochemistry

Figure 3.6(a) shows the cyclic voltammograms of $[Ag(MeCN)_4]_2[Ag(Tf_2N)_3]$ and $[Ag(EtIm)_2][Tf_2N]$. The potential values in this figure are corrected for iR drop since the solutions' conductivity is 1.58 Ω^{-1} m^{-1} for $[Ag(MeCN)_4]_2[Ag(Tf_2N)_3]$ at 50 °C and 0.27 Ω^{-1} m^{-1} for $[Ag(EtIm)_2][Tf_2N]$ at 90 °C (Table 3.1). This large difference in conductivity between the two ionic liquids might be caused by the weaker bond between Ag^+ and MeCN compared to the bond between Ag^+ and EtIm and the fact that the concentration of Ag^+ ions is higher in $[Ag(MeCN)_4]_2$-$[Ag(Tf_2N)_3]$ than in $[Ag(EtIm)_2][Tf_2N]$. The cyclic voltammograms display the typical characteristics for the electrodeposition and stripping of bulk metal: at negative potentials vs Ag, the Ag^+ ion is extracted from the cation and reduced

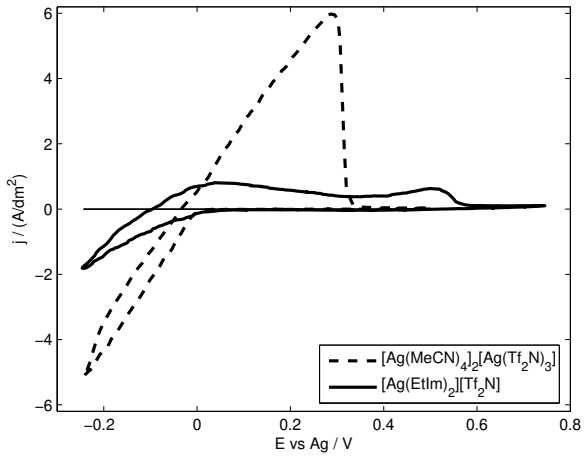

(a)

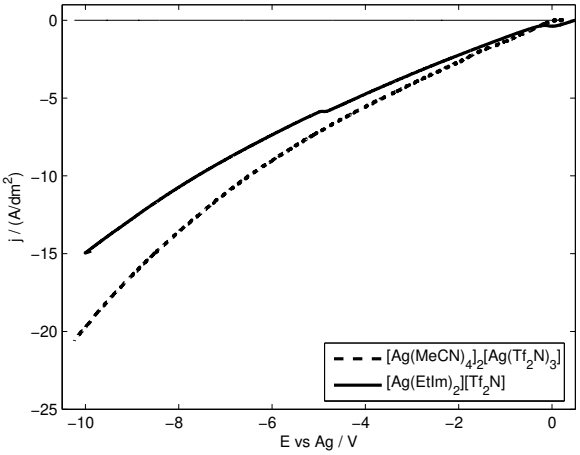

(b)

Figure 3.6: Voltammetry experiments in $[Ag(MeCN)_4]_2$-$[Ag(Tf_2N)_3]$ at 50 °C and $[Ag(EtIm)_2][Tf_2N]$ at 90 °C on a Au working electrode: (a) cyclic voltammogram (corrected for iR drop); (b) linear potential scan (not corrected for iR drop).

Table 3.1: Melting points (T_m), viscosities (μ) and electrical conductivities (κ) of the three silver complexes

	T_m (°C)	μ (mPa s)	κ (Ω^{-1} m^{-1})
$[Ag(MeCN)_4]_2[Ag(Tf_2N)_3]$	18	40 (25 °C)	
		16.6 (50 °C)	1.58 (50 °C)
		7.8 (80 °C)	
$[Ag(MeCN)][Tf_2N]$	90		
$[Ag(EtIm)_2][Tf_2N]$	65	14.1 (80 °C)	0.27 (90 °C)

to silver metal. At positive potentials, this metallic silver layer is stripped. Fig. 3.6 indicates that the electrodeposition of silver proceeds slower in $[Ag(EtIm)_2][Tf_2N]$, compared to $[Ag(MeCN)_4]_2[Ag(Tf_2N)_3]$, and the second stripping peak (at +0.5 V) can be assigned to alloying between the deposited silver and the gold substrate as it was not observed on platinum working electrodes. Such alloying between deposited silver and gold substrates has been reported before [40, 41]. Both studies use imidazolium-based ionic liquids which might explain why surface alloying is not observed for $[Ag(MeCN)_4]_2[Ag(Tf_2N)_3]$ as this compound does not contain the imidazole or imidazolium structure. Another explanation could be the higher temperature used for the experiments in $[Ag(EtIm)_2][Tf_2N]$. The reduction of silver ions, and the oxidation of deposited silver is reversible for both $[Ag(MeCN)_4]_2[Ag(Tf_2N)_3]$ and $[Ag(EtIm)_2][Tf_2N]$: by integrating the current of the cyclic voltammogram, it was found that the charges consumed during reduction and oxidation are equal. This means that reversible stripping of the deposited silver is achieved.

Just as for similar copper containing ionic liquids [20], remarkably high current densities (up to 5 A dm^{-2}) can be achieved for small overpotentials (0.25 V) if acetonitrile is used as ligand. Despite the high current densities, the voltammogram does not show a peak current on the cathodic side due to diffusion limitation. Such a peak does not even appear when the potential is increased to much more negative values (the current interrupt method becomes unstable at higher current densities so these potentials could not be corrected for *iR* drop). Figure 3.6(b) shows that currents beyond 15 A dm^{-2} can be reached in $[Ag(EtIm)_2][Tf_2N]$ and even beyond 20 A dm^{-2} for $[Ag(MeCN)_4]_2[Ag(Tf_2N)_3]$. $[Ag(MeCN)_4]_2[Ag(Tf_2N)_3]$ and $[Ag(EtIm)_2][Tf_2N]$ act as both the supporting electrolyte and the electrochemically active species, which is therefore present in a high concentration. As mentioned by Brown *et al.* [18], this means that electromigrational processes might occur besides diffusion. In contrast with other ionic liquids that often contain negatively charged electroactive species, in $[Ag(MeCN)_4]_2[Ag(Tf_2N)_3]$ the electromigrational flux helps to increase the mass transport due to the positively charged silver complex. It is not known yet whether the cathodic current in $[Ag(MeCN)_4]_2$-

$[Ag(Tf_2N)_3]$ is solely supported by reduction of silver from the $[Ag(MeCN)_4]^+$ cation or that the silver ion in $[Ag(Tf_2N)_3]^{2-}$ can also be reduced. Most likely, both silver anions and cations are electrochemically active. That is: Ag^+ can be removed from the argentate anion by the MeCN molecules liberated after reduction of the silver ion in the cation. This means that the Ag^+ in both the cations and anions is available for reduction even if migration processes would expel the anions from the electrode.

Based on the information obtained by voltammetry, deposition experiments were performed at three different current densities: 1, 5 and 25 A dm^{-2}. A current density of 25 A dm^{-2} is higher than the currents seen in Figure 3.6(b), but even for this high current density, the deposits contained only silver (*vide infra*). The SEM micrographs of these deposits are shown in Figures 3.7 and 3.8. All layers had a theoretical thickness of 1 μm (93 C dm^{-2}). The trend in morphology for the deposits from $[Ag(MeCN)_4]_2[Ag(Tf_2N)_3]$ as a function of applied current density is similar to that for the deposition of copper from $[Cu(MeCN)_2][Tf_2N]$ [20]: a rough and nodular morphology for a current density of 1 A dm^{-2} (Fig. 3.7(a)). The higher the current density, the higher the nucleation density and the smoother the layers become (Figs. 3.7(b,c). No cracks were visible, indicating the absence of large internal stresses. Even at thicknesses up to 5 μm, the quality of the deposits was good. The morphology of deposits from $[Ag(MeCN)_4]_2[Ag(Tf_2N)_3]$, saturated with water, was very similar the the deposits shown in Fig. 3.7 (see ESI[3]). This makes $[Ag(MeCN)_4]_2[Ag(Tf_2N)_3]$ suitable for the deposition of silver outside the protective atmosphere of a glovebox.

For the deposits from $[Ag(EtIm)_2][Tf_2N]$, the influence of the current density is opposite. The smoothest deposit is made at 1 A dm^{-2} (Fig. 3.8(a)) and for higher current densities a dendritic structure appears (Figs. 3.8(b,c)). The different morphology for the deposits from both ionic liquids at 1 A dm^{-2} might be explained by the electrochemical Kelvin equation [56]

$$r_c = \frac{2\gamma V_{mol}}{n\mathrm{F}|\eta|} \tag{3.1}$$

in which γ is the surface energy between deposit and electrolyte (J m^{-2}), V_{mol} the molar volume of the deposited metal (m^3 mol^{-1}), n the ion charge, F the Faraday constant (C mol^{-1}) and r_c is the critical radius for nucleation (m). A nucleus is only stable and able to grow if its size is equal to, or exceeds r_c. If it is smaller than r_c, it is energetically favorable to dissolve again. From the voltammograms in Fig. 3.6(a) it is clear that a current density of 1 A dm^{-2} requires a larger overpotential η in $[Ag(EtIm)_2][Tf_2N]$ than in $[Ag(MeCN)_4]_2[Ag(Tf_2N)_3]$.

[3]Electronic supplementary information at the end of this chapter: Fig. 3.18

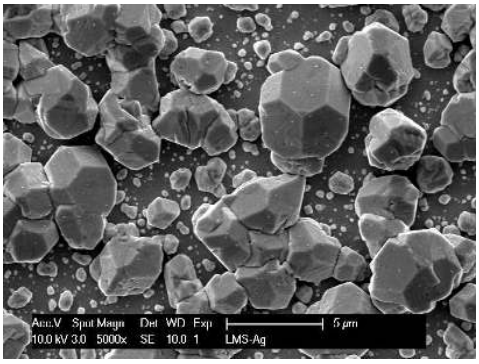

(a)

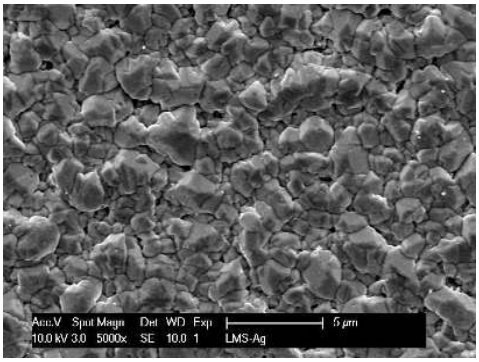

(b)

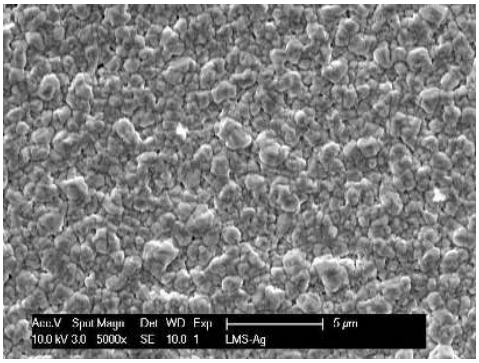

(c)

Figure 3.7: Silver deposits from $[Ag(MeCN)_4]_2[Ag(Tf_2N)_3]$ on a Au working electrode at 50 °C for different current densities: (a) 1 A dm^{-2}, (b) 5 A dm^{-2}, and (c) 25 A dm^{-2}. The theoretical thickness is 1 μm.

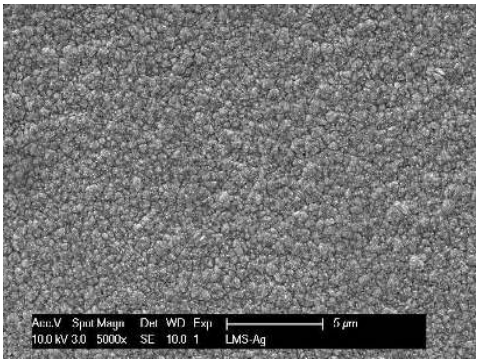

(a)

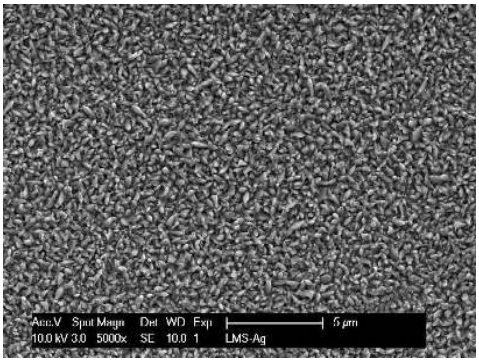

(b)

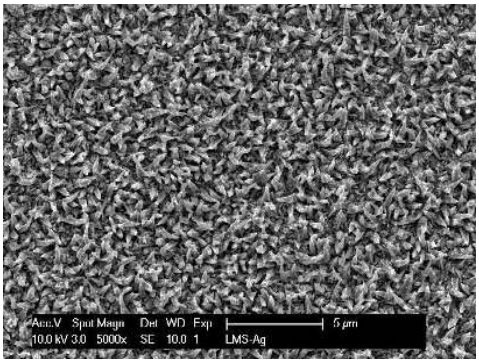

(c)

Figure 3.8: Silver deposits from $[Ag(EtIm)_2][Tf_2N]$ on a Au working electrode at 90 °C for different current densities: (a) 1 A dm^{-2}, (b) 5 A dm^{-2}, and (c) 25 A dm^{-2}. The theoretical thickness is 1 μm.

Consequently, the resulting grain size will be smaller. Fig. 3.9 displays the EDX analysis of the deposit made at 25 A dm^{-2} from $[Ag(MeCN)_4]_2[Ag(Tf_2N)_3]$ (see Fig. 3.7(c)). The spectrum contains only peaks due to silver, without any signs of

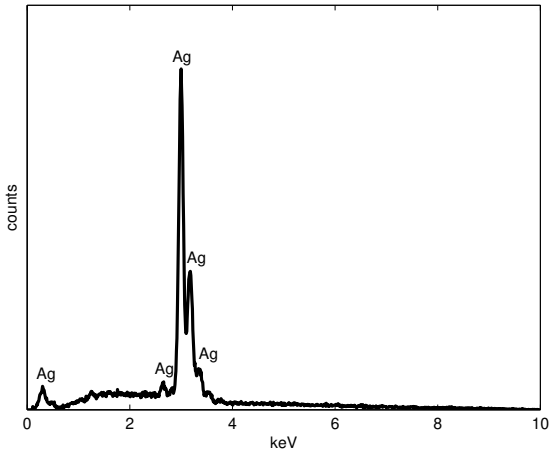

Figure 3.9: EDX spectrum of a silver deposit obtained at 25 A dm^{-2} from $[Ag(MeCN)_4]_2[Ag(Tf_2N)_3]$ at 50 °C (see figure 3.7(c)). A similar EDX spectrum was observed for a deposit from $[Ag(EtIm)_2][Tf_2N]$ at 90 °C.

carbon, sulfur, fluorine or oxygen which would indicate the decomposition of the bistriflimide anion or acetonitrile molecules. A similar EDX spectrum was found for a deposit obtained at 25 A dm^{-2} from $[Ag(EtIm)_2][Tf_2N]$.

To improve the morphology of the deposited silver layers, the additives thiourea and 1*H*-benzotriazole were tested. Thiourea is known to act as a brightener and suppressor in aqueous silver plating [57–62], while 1*H*-benzotriazole can adsorb on silver [63] and act as an accelerator [57]. These two additives were added to $[Ag(MeCN)_4]_2[Ag(Tf_2N)_3]$ or $[Ag(EtIm)_2][Tf_2N]$ in a concentration of 0.05 mol dm^{-3}. The addition of thiourea led to a turbid deposition bath in the case of $[Ag(MeCN)_4]_2[Ag(Tf_2N)_3]$, so 0.05 mol dm^{-3} might be higher than the solubility limit of thiourea in this electrolyte. In the case of $[Ag(EtIm)_2][Tf_2N]$, the addition of thiourea led to a dark solution. 1*H*-benzotriazole quickly dissolved in $[Ag(MeCN)_4]_2[Ag(Tf_2N)_3]$, but gave a turbid solution in $[Ag(EtIm)_2][Tf_2N]$. A concentration of 0.05 mol dm^{-3} is high compared to aqueous solutions, but it is known that in ionic liquids the solvent itself can act as an additive [64] so that external additives need to be dissolved in high enough concentrations (for

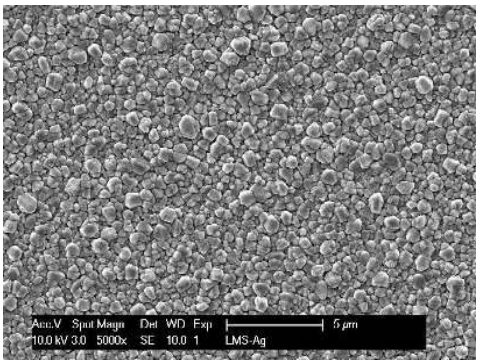

(a)

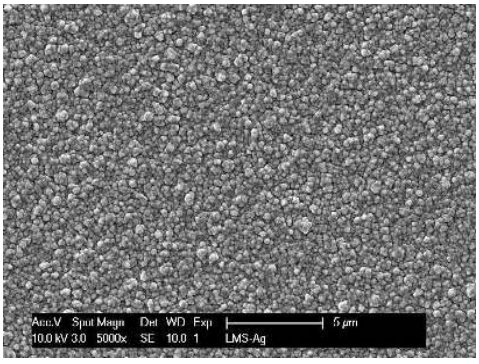

(b)

Figure 3.10: Silver deposits from $[Ag(MeCN)_4]_2[Ag(Tf_2N)_3]$ on a Au working electrode at 50 °C for 1 A dm^{-2} with 0.05 mol dm^{-3} of (a) thiourea or (b) 1*H*-benzotriazole. The theoretical thickness is 1 μm.

the cyclic voltammograms of solutions with additives: see ESI[4]). The morphologies of the deposits from $[Ag(MeCN)_4]_2[Ag(Tf_2N)_3]$ with added thiourea or 1*H*-benzotriazole at a current density of 1 A dm^{-2} are shown in Figure 3.10 (for the deposits at 5 and 25 A dm^{-2}: see ESI[5]). When the morphologies of the silver coatings obtained with and without additives are compared, it is clear that the use of thiourea and 1*H*-benzotriazole strongly influences the resulting morphology. Both additives have a grain-refining effect, lead to an increased nucleation density and smoothen the deposit. In $[Ag(EtIm)_2][Tf_2N]$, the addition of thiourea or 1*H*-benzotriazole is much less clear (see ESI[6]). Atomic force microscopy (AFM) was used to quantify the roughness of the deposits. The AFM topologies of the silver deposits from $[Ag(MeCN)_4]_2[Ag(Tf_2N)_3]$ are shown in Fig. 3.11. Individual nodules are observed in the AFM topology from the additive-free solution and the roughness decreases for the deposits made from solutions containing thiourea or 1*H*-benzotriazole. The smoothest profile is found after the addition of 1*H*-benzotriazole. The roughness profiles are presented in Fig. 3.12, and the R_a and R_q values are summarized in Table 3.2. R_a (arithmetic mean roughness) and R_q

Table 3.2: R_a and R_q values for deposits from $[Ag(MeCN)_4]_2[Ag(Tf_2N)_3]$ at 50 °C on a Au working electrode at 1 A dm^{-2}, obtained in the absence and presence of additives.

Additive	R_a (nm)	R_q (nm)
none	318 ± 41	391 ± 47
0.05 mol dm^{-3} thiourea	62 ± 5	78 ± 6
0.05 mol dm^{-3} 1*H*-benzotriazole	36 ± 2	45 ± 3

(root mean square roughness) are defined as:

$$R_a = \frac{1}{L}\int_0^L |h(l)|\ \mathrm{d}l \tag{3.2}$$

$$R_q = \sqrt{\frac{1}{L}\int_0^L h^2(l)\ \mathrm{d}l} \tag{3.3}$$

in which $h(l)$ are the roughness profiles of Fig. 3.12. The addition of thiourea to $[Ag(MeCN)_4]_2[Ag(Tf_2N)_3]$ leads to a fivefold decrease in the roughness profile: R_q decreases from 391 nm to 78 nm. Adding 1*H*-benzotriazole leads to an R_q value of only 45 nm.

[4]Electronic supplementary information at the end of this chapter: Fig. 3.19
[5]Electronic supplementary information at the end of this chapter: Fig. 3.20
[6]Electronic supplementary information at the end of this chapter: Fig. 3.21

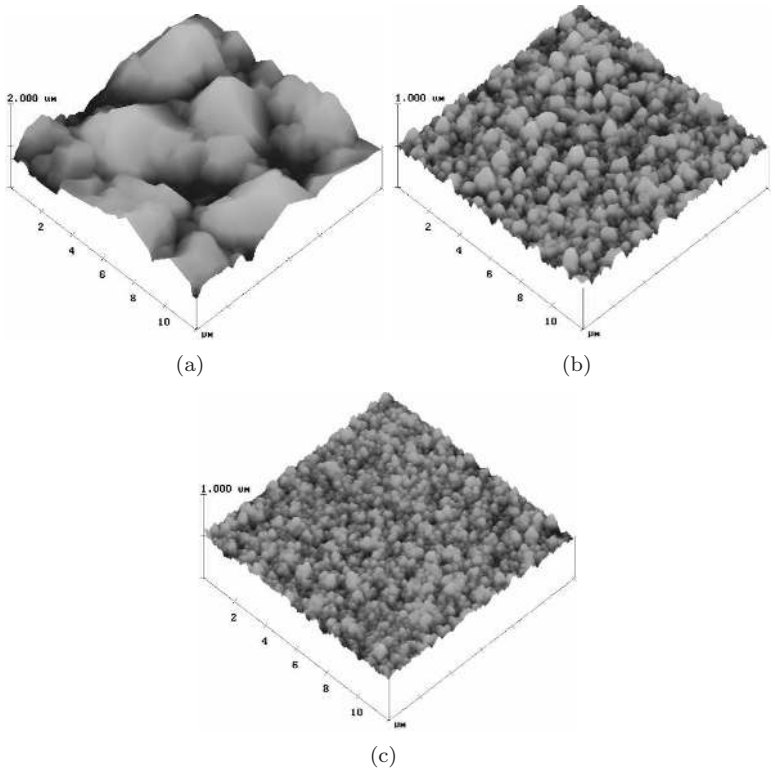

(a) (b)

(c)

Figure 3.11: AFM topologies of silver deposits from $[Ag(MeCN)_4]_2[Ag(Tf_2N)_3]$ at 50 °C on a Au working electrode at 1 A dm^{-2}: (a) no additive, (b) 0.05 mol dm^{-3} thiourea, (c) 0.05 mol dm^{-3} 1*H*-benzotriazole.

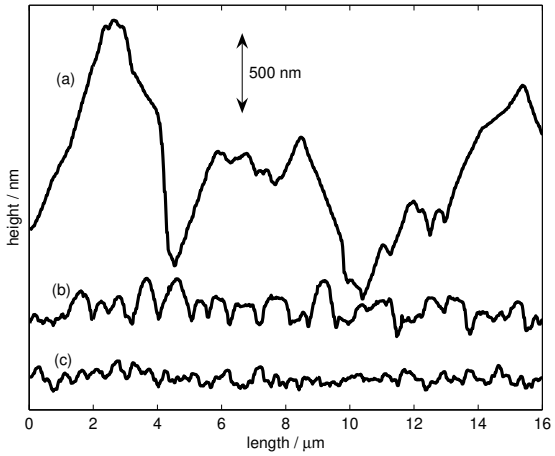

Figure 3.12: Roughness profiles, based on AFM data, of silver deposits from $[Ag(MeCN)_4]_2[Ag(Tf_2N)_3]$ at 50 °C on a Au working electrode at 1 A dm^{-2}: (a) no additive, (b) 0.05 mol dm^{-3} thiourea, (c) 0.05 mol dm^{-3} 1*H*-benzotriazole.

Raman spectroscopy

The addition of 1*H*-benzotriazole or thiourea to the ionic liquid $[Ag(MeCN)_4]_2$-$[Ag(Tf_2N)_3]$ gives noticeable improvements to the morphology of the deposits. To investigate the possible adsorption of the additives Surfaced Enhanced Raman Spectroscopy (SERS) was performed to see if these additives could be seen to be interacting with the silver surface. SERS has already been used to detect additives on silver deposits electroplated from ionic liquids [43]. Examples of SERS on solutions of 1*H*-benzotriazole or thiourea can also be found in literature [61, 63, 65, 66]. The Raman spectrum (Fig. 3.13) of a bulk sample of $[Ag(MeCN)_4]_2$-$[Ag(Tf_2N)_3]$ with 0.1 mol dm^{-3} 1*H*-benzotriazole shows very little difference to that of pure $[Ag(MeCN)_4]_2[Ag(Tf_2N)_3]$ because the 1*H*-benzotriazole is at low concentration and the $[Ag(MeCN)_4]_2[Ag(Tf_2N)_3]$ has several bands between 1500 to 200 cm^{-1}. A notable exception is the band from 1*H*-benzotriazole at 1600 cm^{-1} which appears as a very small peak (Fig. 3.13(c)). In the SERS spectrum there are some very notable differences to that of the bulk sample. Peak assignments are taken from literature [65, 66]. Firstly, the peak at around 1600 cm^{-1}, which is due to benzene ring stretch of 1*H*-benzotriazole, has become relatively much more intense and shifted by 22 cm^{-1} to 1578 cm^{-1}. There is still a small peak at the original position (now 1598 cm^{-1}) which is probably due to the 1*H*-benzotriazole in the small amount of bulk solution remaining. Additionally there are new peaks

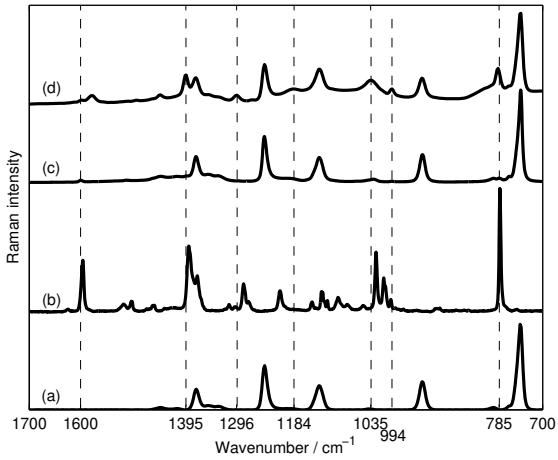

Figure 3.13: Raman spectra of (a) $[Ag(MeCN)_4]_2$-$[Ag(Tf_2N)_3]$ (see ESI), (b) 1*H*-benzotriazole, (c) 0.1 mol dm^{-3} 1*H*-benzotriazole in $[Ag(MeCN)_4]_2[Ag(Tf_2N)_3]$. (d) SERS spectrum of 0.1 mol dm^{-3} 1*H*-benzotriazole in $[Ag(MeCN)_4]_2[Ag(Tf_2N)_3]$ on a silver foil. The dashed lines indicate wavenumber values mentioned in the text.

in the SERS spectrum corresponding to benzotriazole at 1395 cm^{-1}, 1296 cm^{-1}, 1184 cm^{-1}, 1035 cm^{-1}, 994 cm^{-1} and 785 cm^{-1}. The peaks at 1395 cm^{-1} and 785 cm^{-1} correspond with intense peaks in the pure sample of benzotriazole and can be assigned to triazole ring stretch and the benzene ring breathing mode, respectively. The peaks at 1296, 1184, 1035 and 994 cm^{-1} do not directly correspond with peaks from the pure substance but do appear in the SERS spectra of Kapoor *et al.* [65, 66] Bands from the bulk IL do not show any significant changes in position or relative intensity between the bulk sample and the SERS spectra indicating that the 1*H*-benzotriazole is certainly absorbed to the silver surface. This would also explain the affect on the electrodeposition process. Similar experiments were conducted with thiourea in $[Ag(MeCN)_4]_2[Ag(Tf_2N)_3]$. In this case, the SERS spectrum was no different from the spectrum without thiourea, which indicates that its adsorption is too weak to be detected or that the effect of thiourea on the morphology is caused by a process other than adsorption.

Conclusions

The electrochemical behavior of the liquid silver salts $[Ag(MeCN)_4]_2[Ag(Tf_2N)_3]$ and $[Ag(EtIm)_2][Tf_2N]$ is presented. For electrodeposition purposes, low melting salts with a cationic complex are preferred over anionic complexes. The ionic liquids $[Ag(MeCN)_4]_2[Ag(Tf_2N)_3]$ and $[Ag(EtIm)_2][Tf_2N]$, based on silver(I) complexes, can sustain current densities up to 25 A dm^{-2} in unstirred solutions. The resulting silver deposits from $[Ag(MeCN)_4]_2[Ag(Tf_2N)_3]$ did not show cracks, were free from incorporated species and had a smooth appearance for current densities of 5 or 25 A dm^{-2}. Lower current densities result in nodular deposits. The use of thiourea or 1*H*-benzotriazole as additive in $[Ag(MeCN)_4]_2[Ag(Tf_2N)_3]$ permits to achieve smooth morphologies at 1 A dm^{-2}. In $[Ag(EtIm)_2][Tf_2N]$, the addition of additives did not improve the resulting morphology. A third silver(I) complex, $[Ag(MeCN)][Tf_2N]$ was characterized, but its melting point was too high to make this complex of use for electrodeposition of silver. This work on $[Ag(MeCN)_4]_2$-$[Ag(Tf_2N)_3]$ and $[Ag(EtIm)_2][Tf_2N]$ is an extension of recent work on the copper complex $[Cu(MeCN)_2][Tf_2N]$ [20, 21]. The fact that comparable results are obtained, indicates that the complexes with a metal core, surrounded by acetonitrile lead to ionic liquids that can be used for high current density electroplating.

Acknowledgements

This research was funded by a Ph.D grant of the Institute for the Promotion of Innovation through Science and Technology in Flanders (IWT-Vlaanderen) to S.S. The authors acknowledge financial support by the K.U.Leuven (projects IDO/05/005 and GOA 08/05), by the FWO-Flanders (research community "Ionic Liquids") and by the IWT-Flanders (SBO-project IWT 80031 "MAPIL"). We thank Danny Winant for his assistance with TGA measurements and Dirk Henot for performing the CHN analyses. Support by IoLiTec (Heilbronn, Germany) is also acknowledged.

Electronic supplementary information

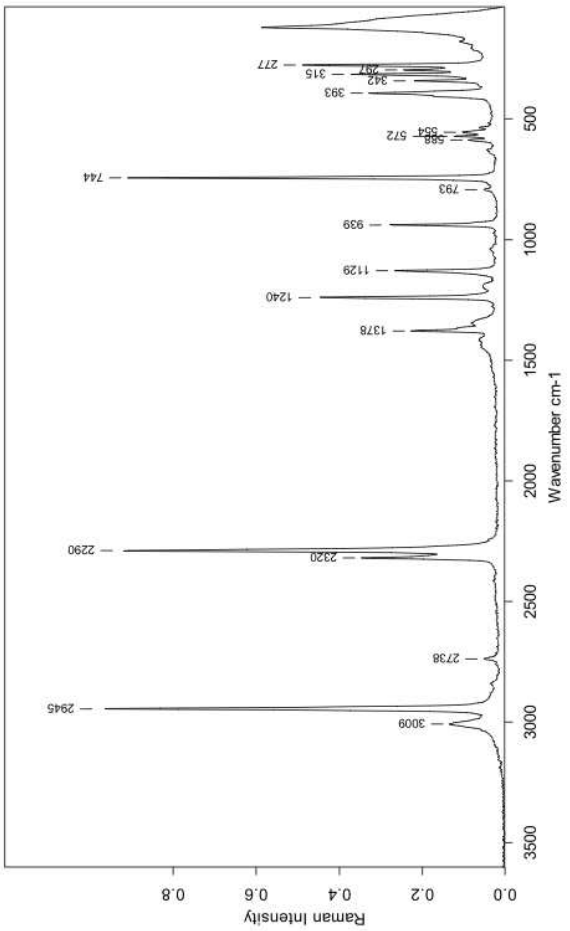

Figure 3.14: Raman spectrum of solid $[Ag(MeCN)_4]_2$-$[Ag(Tf_2N)_3]$.

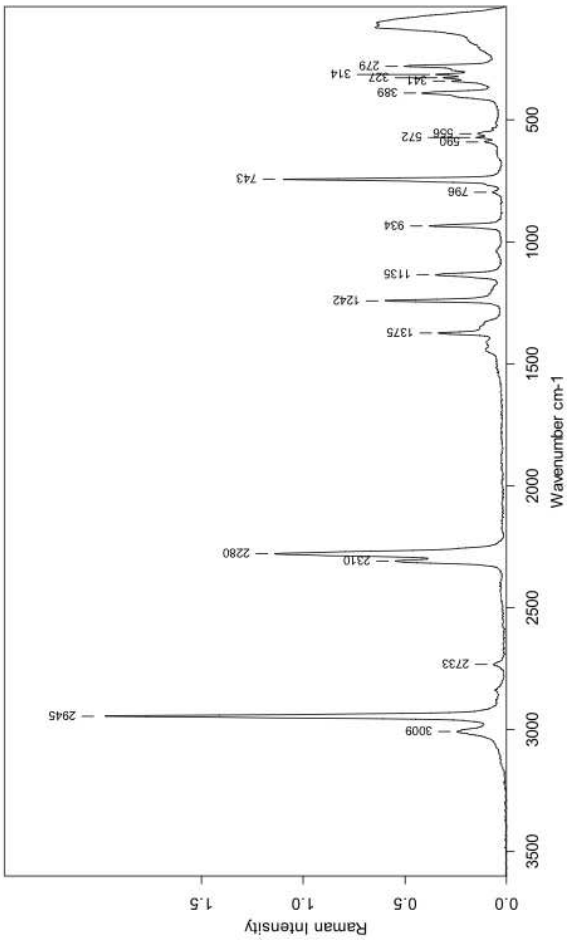

Figure 3.15: Raman spectrum of liquid $[Ag(MeCN)_4]_2$-$[Ag(Tf_2N)_3]$.

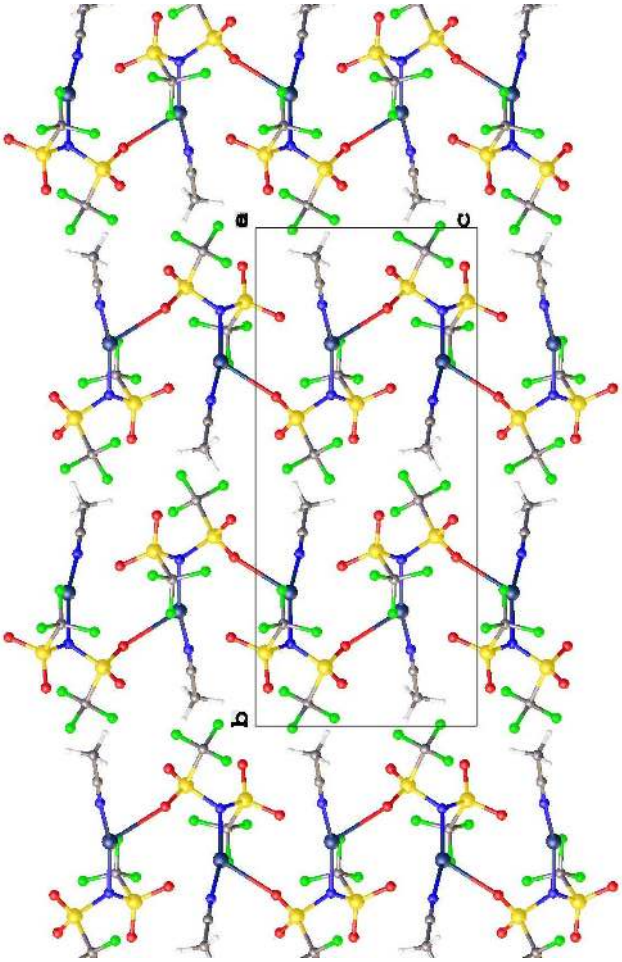

Figure 3.16: View of the packing in the crystal structure of [Ag(MeCN)][Tf_2N], viewed along the crystallographic *a* axis.

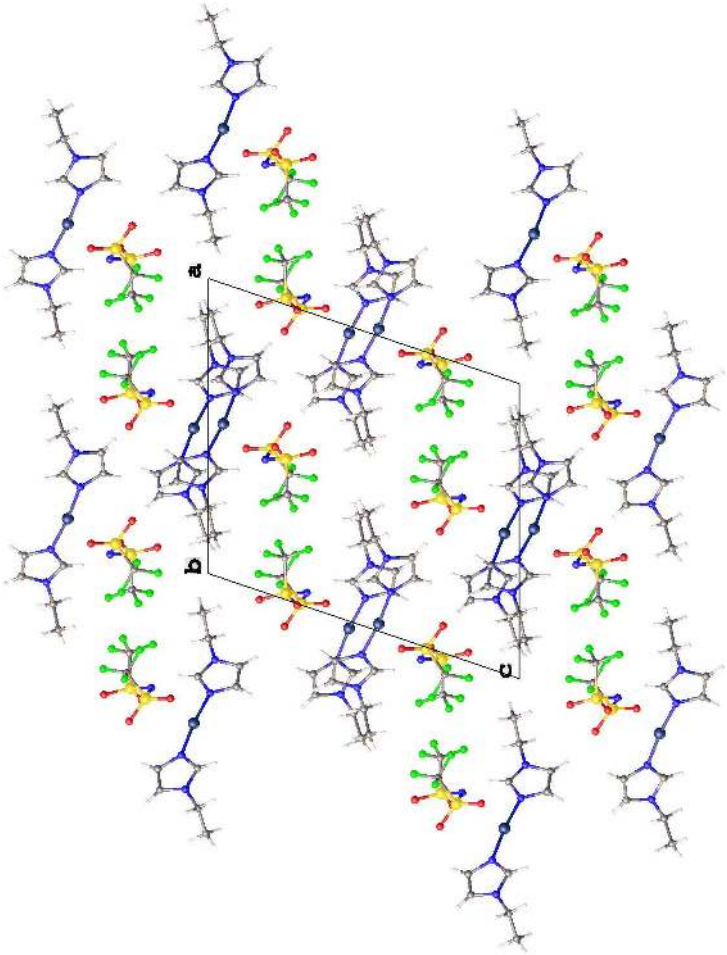

Figure 3.17: View of the packing in the crystal structure of $[Ag(EtIm)_2][Tf_2N]$, viewed along the crystallographic b axis.

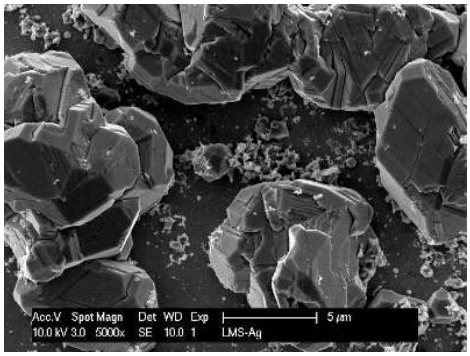

(a)

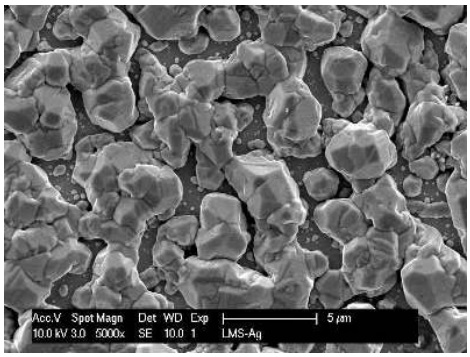

(b)

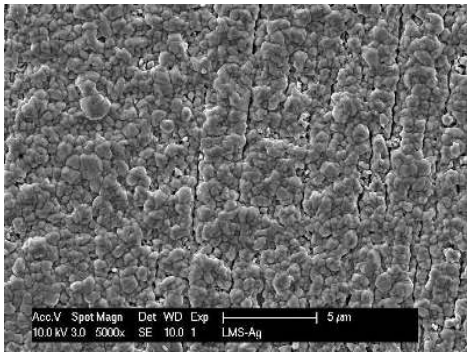

(c)

Figure 3.18: Silver deposits from $[Ag(MeCN)_4]_2$-$[Ag(Tf_2N)_3]$, saturated with water, on a Au working electrode at 50 °C for different current densities: (a) 1 A dm^{-2}, (b) 5 A dm^{-2}, and (c) 25 A dm^{-2}. The theoretical thickness is 1 μm.

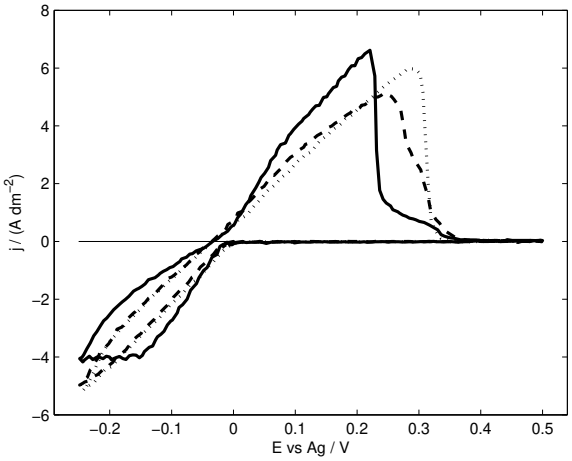

Figure 3.19: Cyclic voltammograms of $[Ag(MeCN)_4]_2$-$[Ag(Tf_2N)_3]$ on a Au working electrode at 50 °C. $(\cdots)$ no additive, $(--)$ 0.05 mol dm^{-3} thiourea, $(-)$ 0.05 mol dm^{-3} 1*H*-benzotriazole.

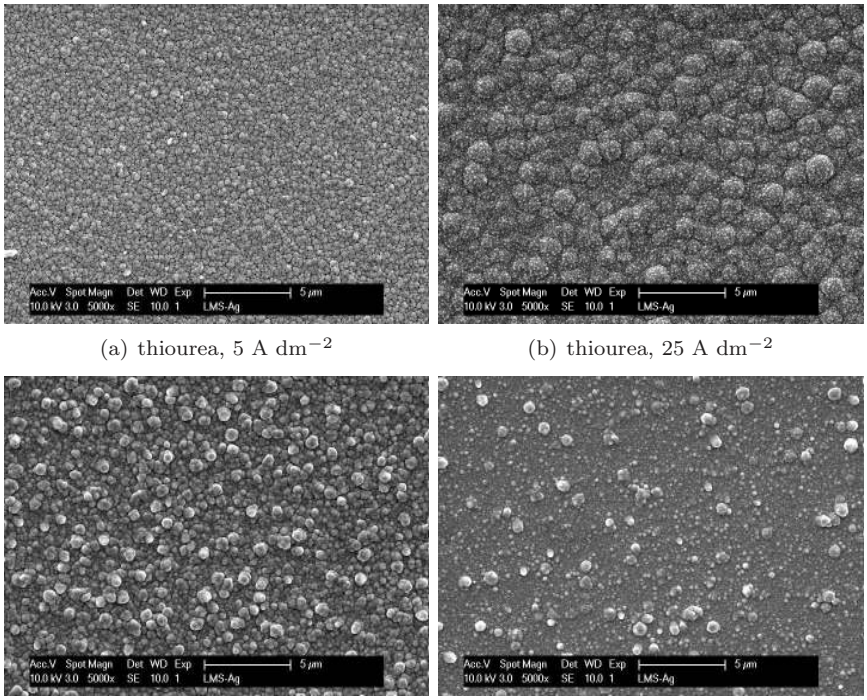

(a) thiourea, 5 A dm^{-2}

(b) thiourea, 25 A dm^{-2}

(c) 1*H*-benzotriazole, 5 A dm^{-2}

(d) 1*H*-benzotriazole, 25 A dm^{-2}

Figure 3.20: Silver deposits from $[Ag(MeCN)_4]_2[Ag(Tf_2N)_3]$ on a Au working electrode at 50 °C for 5 A dm^{-2} and 25 A dm^{-2} with 0.05 mol dm^{-3} of the mentioned additive. The theoretical thickness is 1 μm.

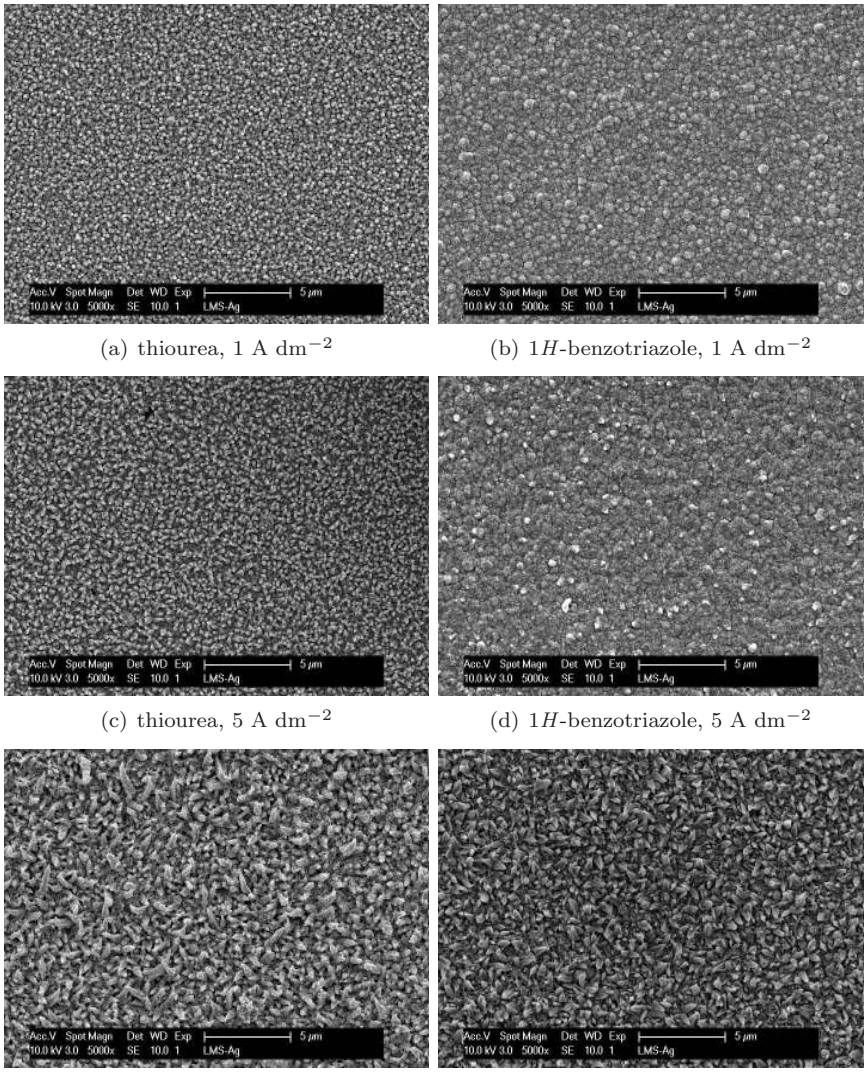

(a) thiourea, 1 A dm^{-2} (b) 1*H*-benzotriazole, 1 A dm^{-2}

(c) thiourea, 5 A dm^{-2} (d) 1*H*-benzotriazole, 5 A dm^{-2}

(e) thiourea, 25 A dm^{-2} (f) 1*H*-benzotriazole, 25 A dm^{-2}

Figure 3.21: Silver deposits from $[Ag(EtIm)_2][Tf_2N]$ on a Au working electrode at 90 °C for 1 A dm^{-2}, 5 A dm^{-2} and 25 A dm^{-2} with 0.05 mol dm^{-3} of the mentioned additive. The theoretical thickness is 1 μm.

References

[1] S. A. Forsyth, J. M. Pringle, D. R. MacFarlane, Ionic liquids - an overview, *Aust. J. Chem.*, **57**, 113 (2004).

[2] F. Endres, S. Zein El Abedin, Air and water stable ionic liquids in physical chemistry, *Phys. Chem. Chem. Phys.*, **8**, 2101 (2006).

[3] A. P. Abbott, K. J. McKenzie, Application of ionic liquids to the electrodeposition of metals, *Phys. Chem. Chem. Phys.*, **8**, 4265 (2006).

[4] M.-J. Deng, P.-Y. Chen, T.-I. Leong, I.-W. Sun, J.-K. Chang, W.-T. Tsai, Dicyanamide anion based ionic liquids for electrodeposition of metals, *Electrochem. Commun.*, **10**, 213 (2008).

[5] D.-X. Zhuang, M.-J. Deng, P.-Y. Chen, I.-W. Sun, Electrochemistry of manganese in the hydrophilic *N*-butyl-*N*-methylpyrrolidinium dicyanamide room-temperature ionic liquid, *J. Electrochem. Soc.*, **155**, D575 (2008).

[6] M.-J. Deng, I.-W. Sun, P.-Y. Chen, J.-K. Chang, W.-T. Tsai, Electrodeposition behavior of nickel in the water- and air-stable 1-ethyl-3-methylimidazolium-dicyanamide room-temperature ionic liquid, *Electrochim. Acta*, **53**, 5812 (2008).

[7] T.-I. Leong, I.-W. Sun, M.-J. Deng, C.-M. Wu, P.-Y. Chen, Electrochemical study of copper in the 1-ethyl-3-methylimidazolium dicyanamide room temperature ionic liquid, *J. Electrochem. Soc.*, **155**, F55 (2008).

[8] P. Nockemann, B. Thijs, S. Pittois, J. Thoen, C. Glorieux, K. Van Hecke, L. Van Meervelt, B. Kirchner, K. Binnemans, Task-specific ionic liquid for solubilizing metal oxides, *J. Phys. Chem. B*, **110**, 20978 (2006).

[9] P. Nockemann, M. Pellens, K. Van Hecke, L. Van Meervelt, J. Wouters, B. Thijs, E. Vanecht, T. N. Parac-Vogt, H. Mehdi, S. Schaltin, J. Fransaer, S. Zahn, B. Kirchner, K. Binnemans, Cobalt(II) complexes of nitrile-functionalized ionic liquids, *Chem. Eur. J.*, **16**, 1849 (2010).

[10] I. J. B. Lin, C. S. Vasam, Metal-containing ionic liquids and ionic liquid crystals based on imidazolium moiety, *J. Organomet. Chem.*, **690**, 3498 (2005).

[11] C. Chiappe, M. Malvaldi, Highly concentrated "solutions"of metal cations in ionic liquids: current status and future challenges, *Phys. Chem. Chem. Phys.*, **12**, 11191 (2010).

[12] H. M. A. Abood, A. P. Abbott, A. D. Ballantyne, K. S. Ryder, Do all ionic liquids need organic cations? Characterisation of $[AlCl_2{\cdot}n$ amide$]^+$ $AlCl_4^-$ and comparison with imidazolium based systems, *Chem. Commun.*, **47**, 3523 (2011).

[13] T. M. Anderson, D. Ingersoll, A. J. Rose, C. L. Staiger, J. C. Leonard, Synthesis of an ionic liquid with an iron coordination cation, *Dalton Trans.*, **39**, 8609 (2010).

[14] C. L. Hussey, T. M. Laher, Electrochemical and spectroscopic studies of cobalt(II) in molten aluminum chloride-*N*-*n*-butylpyridinium chloride, *Inorg. Chem.*, **20**, 4201 (1981).

[15] S. Schaltin, P. Nockemann, B. Thijs, K. Binnemans, J. Fransaer, Influence of the anion on the electrodeposition of cobalt from imidazolium ionic liquids, *Electrochem. Solid-State Lett.*, **10**, D104 (2007).

[16] S.-I. Hsiu, J.-F. Huang, I.-W. Sun, C.-H. Yuan, J. Shiea, Lewis acidity dependency of the electrochemical window of zinc chloride - 1-ethyl-3-methylimidazolium chloride ionic liquids, *Electrochim. Acta*, **47**, 4367 (2002).

[17] R. E. Del Sesto, T. M. McCleskey, A. K. Burrell, G. A. Baker, J. D. Thompson, B. L. Scott, J. S. Wilkes, P. Williams, Structure and magnetic behavior of transition metal based ionic liquids, *Chem. Commun.*, , 447 (2008).

[18] R. J. C. Brown, P. J. Dyson, D. J. Ellis, T. Welton, 1-butyl-3-methylimidazolium cobalt tetracarbonyl [bmim][$Co(CO)_4$]: a catalytically active organometallic ionic liquid, *Chem. Commun.*, , 1862 (2001).

[19] Y. Qiao, J. Hu, H. Li, H. Li, Y. Hu, B. Feng, Z. Hou, Physicochemical properties of tungstate-based room-temperature ionic liquids, *J. Electrochem. Soc.*, **157**, F124 (2010).

[20] S. Schaltin, N. R. Brooks, K. Binnemans, J. Fransaer, Electrodeposition from cationic cuprous organic complexes: Ionic liquids for high current density electroplating, *J. Electrochem. Soc.*, **158**, D21 (2011).

[21] N. R. Brooks, S. Schaltin, K. Van Hecke, L. Van Meervelt, K. Binnemans, J. Fransaer, Copper(I)-containing ionic liquids for high-rate electrodeposition, *Chem. Eur. J.*, **17**, 5054 (2011).

[22] Ed.: R. C. Weast, M. J. Astle, W. H. Beyer, *Handbook of chemistry and physics*, CRC Press, Boca Raton, Florida (1986).

[23] I. Chopra, The increasing use of silver-based products as antimicrobial agents: a useful development or a cause for concern?, *J. Antimicrob. Chemother.*, **59**, 587 (2007).

[24] R. M. Slawson, M. I. Van Dyke, H. Lee, J. T. Trevors, Germanium and silver resistance, accumulation, and toxicity in microorganisms, *Plasmid*, **27**, 72 (1992).

[25] Ed.: M. Schlesinger, M. Paunovic, *Modern electroplating*, John Wiley & sons, Inc., New York (2000).

[26] J.-F. Huang, H. Luo, S. Dai, A new strategy for synthesis of novel classes of room-temperature ionic liquids based on complexation reaction of cations, *J. Electrochem. Soc.*, **153**, J9 (2006).

[27] M. Iida, C. Baba, M. Inoue, H. Yoshida, E. Taguchi, H. Furusho, Ionic liquids of bis(alkylethylenediamine)silver(I) salts and the formation of silver(0) nanoparticles from the ionic liquid system, *Chem. Eur. J.*, **14**, 5047 (2008).

[28] M. Iida, S. Kawakami, E. Syouno, H. Er, E. Taguchi, Properties of ionic liquids containing silver(I) or protic alkylethylenediamine cations with a bis(trifluoromethanesulfonyl)amide anion, *J. Colloid Interface Sci.*, **356**, 630 (2011).

[29] R. T. Carlin, R. A. Osteryoung, Microelectrodes in the examination of anodic and cathodic limit reactions of an ambient-temperature molten-salt, *J. Electroanal. Chem.*, **252**, 81 (1988).

[30] M.-C. Tsai, D.-X. Zhuang, P.-Y. Chen, Electrodeposition of macroporous silver films from ionic liquids and assessment of these films in the electrocatalytic reduction of nitrate, *Electrochim. Acta*, **55**, 1019 (2010).

[31] N. Serizawa, Y. Katayama, T. Miura, EQCM measurement of Ag(I)/Ag reaction in an amide-type room-temperature ionic liquid, *J. Electrochem. Soc.*, **156**, D503 (2009).

[32] S. Zein El Abedin, F. Endres, Electrodeposition of nanocrystalline silver films and nanowires from the ionic liquid 1-ethyl-3-methylimidazolium trifluoromethylsulfonate, *Electrochim. Acta*, **54**, 5673 (2009).

[33] A. I. Bhatt, A. M. Bond, Electrodeposition of silver from the distillable ionic liquid, DIMCARB in the absence and presence of chemically induced nanoparticle formation, *J. Electroanal. Chem.*, **619-620**, 1 (2008).

[34] R. Bomparola, S. Caporali, A. Lavacchi, U. Bardi, Silver electrodeposition from air and water-stable ionic liquid: An environmentally friendly alternative to cyanide baths, *Surf. Coat. Technol.*, **201**, 9485 (2007).

[35] F.-H. Yeh, C.-C. Tai, J. F. Huang, I.-W. Sun, Formation of porous silver by electrochemical alloying/dealloying in a water-insensitive zinc chloride-1-ethyl-3-methyl imidazolium chloride ionic liquid, *J. Phys. Chem. B*, **110**, 5215 (2006).

[36] C.-C. Tai, F.-Y. Su, I.-W. Sun, Electrodeposition of palladium-silver in a lewis basic 1-ethyl-3-methylimidazolium chloride-tetrafluoroborate ionic liquid, *Electrochim. Acta*, **50**, 5504 (2005).

[37] Q. Zhu, C. L. Hussey, G. R. Stafford, Electrodeposition of silver-aluminum alloys from a room-temperature chloroaluminate molten salt, *J. Electrochem. Soc.*, **148**, C88 (2001).

[38] Y. Katayama, S. Dan, T. Miura, T. Kishi, Electrochemical behavior of silver in 1-ethyl-3-methylimidazolium tetrafluoroborate molten salt, *J. Electrochem. Soc.*, **148**, C102 (2001).

[39] A. Basile, A. I. Bhatt, A. P. O'Mullane, S. K. Bhargava, An investigation of silver electrodeposition from ionic liquids: Influence of atmospheric water uptake on the silver electrodeposition mechanism and film morphology, *Electrochim. Acta*, **56**, 2895 (2011).

[40] C. A. Zell, F. Endres, W. Freyland, Electrochemical in situ STM study of phase formation during Ag and Al electrodeposition on Au(111) from a room temperature molten salt, *Phys. Chem. Chem. Phys.*, **1**, 697 (1999).

[41] X.-H. Xu, C. L. Hussey, Electrodeposition of silver on metallic and nonmetallic electrodes from the acidic aluminum chloride-1-methyl-3-ethylimidazolium chloride molten salt, *J. Electrochem. Soc.*, **139**, 1295 (1992).

[42] F. Endres, W. Freyland, Electrochemical scanning tunneling microscopy investigation of HOPG and silver electrodeposition on HOPG from the acid room-temperature molten salt aluminum chloride-1-methyl-3-butylimidazolium chloride, *J. Phys. Chem. B*, **102**, 10229 (1998).

[43] P. He, H. T. Liu, Z. Y. Li, Y. Liu, X. D. Xu, J. H. Li, Electrochemical deposition of silver in room-temperature ionic liquids and its surface-enhanced raman scattering effect, *Langmuir*, **20**, 10260 (2004).

[44] R. Fukui, Y. Katayama, T. Miura, The influence of potential on electrodeposition of silver and formation of silver nanoparticles in some ionic liquids, *J. Electrochem. Soc.*, **158**, D567 (2011).

[45] *SADABS, version 5.0, An empirical absorption correction program from the SAINTPlus NT*, Bruker AXS, Madison (USA) (1998).

[46] *SHELXTL, version 5.1*, Bruker AXS, Madison (USA) (1998).

[47] A. V. Dolomanov, L. J. Bourhis, R. J. Gildea, J. A. K. Howard, H. Puschmann, OLEX2: a complete structure solution, refinement and analysis program, *J. Appl. Crystallogr.*, **42**, 339 (2009).

[48] K. Nilsson, A. Oskarsson, The crystal-structure of tetraacetonitrile silver(I) perchlorate at 240 K, *Acta Chem. Scand. A*, **38**, 79 (1984).

[49] P. G. Jones, E. Bembenek, Redetermination of the structure of tetrakis(acetonitrilo)silver(I) perchlorate at 173 K, *Z. Kristallogr.*, **208**, 213 (1993).

[50] A. A. M. Aly, B. Walfort, H. Lang, Crystal structure of tetrakis(acetonitrile)silver(I) tetrafluoroborate, $[Ag(C_2H_3N)_4][BF_4]$, *Z. Kristallogr.-New Cryst. Struct.*, **219**, 489 (2004).

[51] H.-G. Ang, W. Fraenk, K. Karaghiosoff, T. M. Klapotke, P. Mayer, H. Noth, J. Sprott, M. Warchhold, Synthesis, characterization, and crystal structures of Cu, Ag, and Pd dinitramide salts, *Z. Anorg. Allg. Chem.*, **628**, 2894 (2002).

[52] A. Blaschette, P. G. Jones, T. Hamman, M. Naveke, D. Schomburg, H. K. Cammenga, M. Epple, I. Steppuhn, Polysulfonylamine. XL Darstellung von Silber(I)-disulfonylamid-Acetonitril-Komplexen. R´ontgenstrukturanalytische und thermochemische Charakterisierung von Tetraacetonitrilsilber(I)-bis(dimesylamido)argentat(I) und von (1,1,3,3-Tetraoxo-1,3,2-benzodithiazolido)acetonitrilsilber(I), *Z. Anorg. Allg. Chem.*, **619**, 912 (1993).

[53] P. Nockemann, K. Binnemans, B. Thijs, T. N. Parac-Vogt, K. Merz, A.-V. Mudring, P. C. Menon, R. N. Rajesh, G. Cordoyiannis, J. Thoen, J. Leys, C. Glorieux, Temperature-driven mixing-demixing behavior of binary mixtures of the ionic liquid choline bis(trifluoromethylsulfonyl)imide and water, *J. Phys. Chem. B*, **113**, 1429 (2009).

[54] K. Fukumoto, H. Ohno, LCST-type phase changes of a mixture of water and ionic liquids derived from amino acids, *Angew. Chem. Int. Ed.*, **46**, 1852 (2007).

[55] F. H. Allen, The Cambridge Structural Database: a quarter of a million crystal structures and rising, *Acta Cryst.*, **B58**, 380 (2002).

[56] E. Budevski, G. Staikov, J. W. Lorenz, *Electrochemical phase transformation and growth*, VCH, Weinheim (1996).

[57] E. J. Ahn, J. J. Kim, Additives for superconformal electroplating of Ag thin film for ULSIs, *Electrochem. Solid-State Lett.*, **7**, C118 (2004).

[58] A. G. Zelinsky, S. K. Ershov, Using an electrode with renewable surface for study of silver reduction from acid thiourea solutions, *J. Appl. Electrochem.*, **38**, 273 (2008).

[59] E. Gómez, J. García-Torres, E. Vallés, Study and preparation of silver electrodeposits at negative potentials, *J. Electroanal. Chem.*, **594**, 89 (2006).

[60] O. Azzaroni, P. L. Schilardi, R. C. Salvarezza, A. J. Arvia, Smoothening mechanism of thiourea on silver electrodeposition. Real time imaging of the growth front evolution, *Langmuir*, **15**, 1508 (1999).

[61] B. Reents, W. Plieth, V. A. Macagno, G. I. Lacconi, Influence of thiourea on silver deposition: Spectroscopic investigation, *J. Electroanal. Chem.*, **453**, 121 (1998).

[62] G. I. Lacconi, V. A. Macagno, Electrochemical study of thiourea in relation to the silver electrodeposition process, *Electrochim. Acta*, **39**, 2605 (1994).

[63] J. C. Rubim, I. G. R. Gutz, O. Sala, Surface-enhanced raman-spectra of benzotriazole adsorbed on a silver electrode, *J. Mol. Struct.*, **101**, 1 (1983).

[64] R. Atkin, S. Zein El Abedin, R. Hayes, L. H. S. Gasparotto, N. Borisenko, F. Endres, AFM and STM studies on the surface interaction of [BMP]TFSA and [EMIm]TFSA ionic liquids with Au(111), *J. Phys. Chem. C*, **113**, 13266 (2009).

[65] S. Naumov, S. Kapoor, S. Thomas, S. Venkateswaran, T. Mukherjee, SERS of benzotriazole on Ag colloid: surface structure characterization using the DFT approach, *J. Mol. Struct.: THEOCHEM*, **685**, 127 (2004).

[66] S. Thomas, S. Venkateswaran, S. Kapoor, R. D'Cunha, T. Mukherjee, Surface enhanced raman scattering of benzotriazole: a molecular orientational study, *Spectrochim. Acta, Part A*, **60**, 25 (2004).

Chapter 4

Electrodeposition from a liquid cationic cuprous organic complex for seed layer deposition

Published as S. Schaltin, N. R. Brooks, L. Stappers, L. D'Urzo, H. Plank, G. Kothleitner, C. Gspan, K. Binnemans and J. Fransaer, *J. Electrochem. Soc.*, **158**, D647-D650 (2011)

Abstract

Smooth layers of 20 nm of copper have been deposited on a tantalum substrate from the liquid cationic cuprous organic complex $[Cu(MeCN)_2][Tf_2N]$. This type of ionic liquid, with a high concentration of copper(I) ions permits to achieve high nucleation densities. Furthermore, extremely high overpotentials (up to 5.0 V) can be applied without decomposition of the ionic liquid. The deposition of copper has been investigated by cyclic voltammetry (CV), atomic force microscopy (AFM), scanning electron microscopy (SEM) and transmission electron microscopy (TEM). The resulting copper deposits can be useful as seed layers for aqueous copper filling.

Introduction

Due to their intrinsic ionic conductivity and wide electrochemical window, ionic liquids are interesting non-aqueous electrolytes for the electrodeposition of reactive metals which cannot be deposited from aqueous solutions [1–5]. At first sight, there seems to be no advantages associated with the electrodeposition from ionic liquids of metals which can also be deposited from water e.g. zinc, copper, silver or gold. However, in ionic liquids the deposition of alloys of these metals with compositions not obtainable from aqueous solutions is possible, and these solvents also allow the use of electrodes made of materials that are passivated in the presence of water, such as titanium, niobium or tantalum. A useful application is the deposition of a thin copper metal layer on a tantalum electrode. The possibility of direct deposition of copper on a tantalum barrier is of great importance for the microelectronics industry. In state-of-the-art wafer technology, a barrier layer of Ta/TaN prevents the diffusion of copper into silicon [6–8]. Presently, the copper layer is fabricated via a two-step process. First, a copper seed layer is grown by Physical Vapor Deposition (PVD) and this layer protects the underlying tantalum against oxidation. On top of this seed layer, copper is deposited electrochemically from an aqueous copper(II) sulfate solution until the desired thickness is reached. For through-silicon-vias (TSV), the fabrication of the copper seed layers through vapor techniques is troublesome because of the high aspect ratio, resulting in an uneven distribution of the vapor deposited copper. This leads to further difficulties in the consecutive electrodeposition from aqueous solution.

The electrodeposition and nucleation of copper from aqueous solutions on the naturally oxidized surface of tantalum is described by Emery *et al.* [9], Radisic *et al.* [10] and Zheng *et al.* [11] The nucleation of copper on tantalum, free of an intervening oxide film, is presented by Wang *et al.* [12] In their study, this oxide layer is removed by galvanic displacement. To achieve a closed film an electroless step was needed and the presence of the interfacial suboxide TaO could not be excluded. Starosvetsky *et al.* presented an electrochemical procedure to deposit copper on tantalum without a seed layer [13]. An activation step was used to reduce *in situ* the oxide layer to tantalum metal. Although qualitative copper layers were deposited, visual proof of the absence of an oxide layer between the tantalum barrier and the deposited copper has not been given. Kim described the electroplating of copper on tantalum, from which the oxide skin is dissolved anodically in a saturated KOH solution [14]. Although the removal of oxide was not complete due to the presence of interfacial TaO, the wetting of copper on tantalum was significantly improved. A disadvantage of this method is the partial loss of the barrier material in the dissolution step.

In this study we present an electrochemical alternative for vapor deposition techniques to achieve a thin copper seed layer, since electrodeposition is not a line-of-sight process like PVD. If this layer is grown in a through-silicon-via, the TSV can later be filled electrochemically with copper from classic aqueous copper plating baths [15–18], because yet, the required superfilling process has not been developed for ionic liquids. We describe how copper can be electrodeposited on tantalum from the liquid metal salt $[Cu(MeCN)_2][Tf_2N]$. Liquid metal salts are ionic liquids in which a metal ion is incorporated into the structure of the ionic liquid, preferably in the cation. A detailed chemical and electrochemical characterization of $[Cu(MeCN)_2][Tf_2N]$ has been reported elsewhere [19, 20]. Other examples of cationic liquid metal salts can be found in literature [21–24].

Experimental

The electrolyte $[Cu(MeCN)_2][Tf_2N]$ was prepared starting from the copper(I) complex tetrakis(acetonitrile) copper(I) bis(trifluoromethylsulfonyl)imide (bistriflimide)
$[Cu(MeCN)_4][Tf_2N]$ (figure 4.1). The cation of $[Cu(MeCN)_4][Tf_2N]$ consists of four

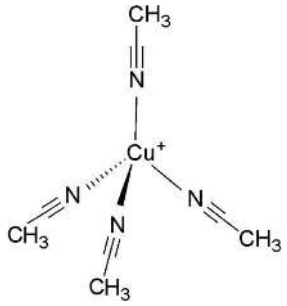

Figure 4.1: Structural formula of the cation of the copper-containing ionic liquid $[Cu(MeCN)_4][Tf_2N]$.

acetonitrile molecules coordinating to the copper(I) ion in a tetrahedral arrangement. The charge balance is provided by the $[Tf_2N]^-$ counter anion. This compound was prepared by reacting copper(II) oxide with bis(trifluoromethylsulfonyl)-imidic acid in water to yield copper(II) bistriflimide. The Cu(II) salt $Cu(Tf_2N)_2(H_2O)_4$ was isolated by drying in vacuo and then redissolved in acetonitrile. Because copper(I) is the stable copper species in acetonitrile solutions [25–27], a comproportionation reaction between copper metal (added as a powder) and the copper(II) ions yielded $[Cu(MeCN)_4][Tf_2N]$, which was then isolated by removing solvent MeCN in vacuo. The reaction sequence is:

$$CuO + 2\ H[Tf_2N]_{aq} \rightarrow Cu(Tf_2N)_2 + H_2O \tag{4.1}$$

$$Cu(Tf_2N)_2 + Cu + 8\ CH_3CN \rightarrow 2\ [Cu(CH_3CN)_4][Tf_2N] \tag{4.2}$$

$[Cu(MeCN)_4][Tf_2N]$ is a white crystalline solid at room temperature which melts at 66 °C into a colorless liquid. Two acetonitrile molecules were driven off by equilibrating the compound at 90 °C for 24 h to give $[Cu(MeCN)_2][Tf_2N]$. This temperature was chosen because it is the standard temperature at which electrochemical experiments have been performed. So the composition of the electrolyte used for electrodeposition of the copper layers is $[Cu(MeCN)_2][Tf_2N]$.

The electrochemical experiments were performed in an argon-filled glove box (with O_2 and H_2O concentrations below 1 ppm) because the tested low-melting salts are sensitive to moisture and oxygen and undergo oxidation of copper(I). Silicon wafers have been used as the substrates for electrodeposition. The different layers of this wafer were: Si - 100 nm SiO_2 - 10 nm TaN - 40 nm Ta - 150 nm Cu. Before use these substrates, with an active area of 7 mm by 10 mm, were degreased in alkaline cleaner (type P3-RST, Henkel) at 70 °C, rinsed in demineralized water and ethanol, and dried. The copper layer of the wafers was electrochemically dissolved *in situ* just before the deposition experiments. After the deposition of the copper layer, they were rinsed with acetone and ethanol, and finally dried. The copper solution was contained in a copper crucible (5 ml), which also served as counter-electrode, and it was not stirred during the experiments. The experiments were done using an EG&G Princeton Applied Research potentiostat/galvanostat model 273 controlled by a computer with Corrware software (cyclic voltammetry) or an EG&G Princeton Applied Research potentiostat/galvanostat model 263A. All specified potentials in this paper are relative to a copper pseudo-reference electrode. A polyimide Thermofoil^{TM} heater was used to maintain the temperature at 90 °C during the experiments. The morphology of the copper deposits was determined by scanning electron microscopy (SEM) (Philips XL 30 FEG) and atomic force microscopy (AFM) (Digital Instruments Nanoscope III AFM). Thin lamellas for transmission electron microscopy (TEM) investigations have been prepared via a NOVA 200 (FEI) dual beam system combining a focused ion beam (FIB) and a scanning electron microscope (SEM). Lamellas have been prepared in standard lift out geometry and subsequently transferred with a micromanipulator (Omniprobe) to TEM grids (Omniprobe). To prevent lamella bending, window milling technique was applied during pre-thinning procedure followed by a low energy cleaning step at 5 kV and 70 pA under an angle of 5 ° on both sides to reduce amorphized surface layers. All subsequent TEM investigations were performed at 200 kV on a Tecnai T20 FEG/STEM, equipped with a Gatan Quantum EELS spectrometer. For imaging, bright field phase contrast techniques have been applied, whereas for the chemical analysis, the system was set up in scanning TEM mode, employing a beam diameter of approximately 0.5 nm, a beam convergence of about 10 mrad and a collection angle of 15 mrad.

Results and discussion

The tantalum layer of the silicon wafer was protected against oxidation by a copper seed layer. Before electrodeposition, this seed layer was anodically dissolved at +0.5 V to expose the underlying tantalum to the electrolyte. The resulting current-time plot is shown in figure 4.2(a), which reveals that the current quickly peaks high and eventually drops to zero when copper is dissolved. Nonetheless, the anodic polarization was maintained for 400 s in order to dissolve all copper. The cyclic voltammogram, recorded after 400 s of anodic polarization, is shown in figure 4.2(b). The overall appearance of this cyclic voltammogram is typical for an electrode reaction involving the electrodeposition and stripping of metal. The voltammogram indicates that the nucleation of copper onto tantalum requires an overpotential of 0.1 V. This nucleation overpotential causes the appearance of a nucleation loop: the backward scan of the voltammogram crosses the forwards scan at 0 V.

Deposits were made at overpotentials η in the range from -3.0 V and -5.0 V. In conventional ionic liquids e.g. imidazolium or pyrrolidinium salts, such cathodic overpotentials cannot be applied without the decomposition of the ionic liquid. Also the $[Cu(MeCN)_2][Tf_2N]$ complex is cathodically decomposed, but in this case the decomposition is the desired reduction of Cu(I) into metallic copper without the incorporation of acetonitrile or the bistriflimide anion [20]. The liberated acetonitrile molecules become bound to the Cu(I) in $[Cu(MeCN)_2][Tf_2N]$ in the bulk electrolyte, temporarily forming $[Cu(MeCN)_4][Tf_2N]$ or they can diffuse towards the anode where they assist the anodic dissolution of copper. The net reaction in the electrochemical cell is therefore just the dissolution and deposition of copper, whereas in *regular* ionic liquids the solution would get poisoned by decomposition products of the cation. High applied overpotentials give rise to small sized copper grains. This comes from the electrochemical Kelvin equation [28]

$$r_c = \frac{2\gamma V_{mol}}{n\mathrm{F}|\eta|} \tag{4.3}$$

in which γ is the surface energy between deposit and electrolyte (J m^{-2}), V_{mol} the molar volume of the deposited metal (m^3 mol^{-1}), n the ion charge, F the Faraday constant (C mol^{-1}) and r_c is the critical radius for nucleation (m). A nucleus is only stable and able to grow if its size is equal to, or exceeds r_c. If it is smaller than r_c, it is energetically favorable to dissolve again. By using $\gamma = 0.5$ J m^{-2} [28] and $V_{mol} = 7.1{\cdot}10^{-6}$ m^3 mol^{-1}, a critical nucleus consists of a single atom if an overpotential of $\eta \approx 0.5$ V is applied. Because copper was deposited at more negative potentials than -0.5 V, nucleation can proceed without the need to form clusters of atoms[1]. One of the consequences is that nucleation solely depends

[1] A deposit thickness of 20 nm corresponds to a charge density of 2.7 C dm^{-2}. If the potential is applied for 0.5 s, this corresponds to a current density of 5.4 A dm^{-2} or a current of 0.0378 A

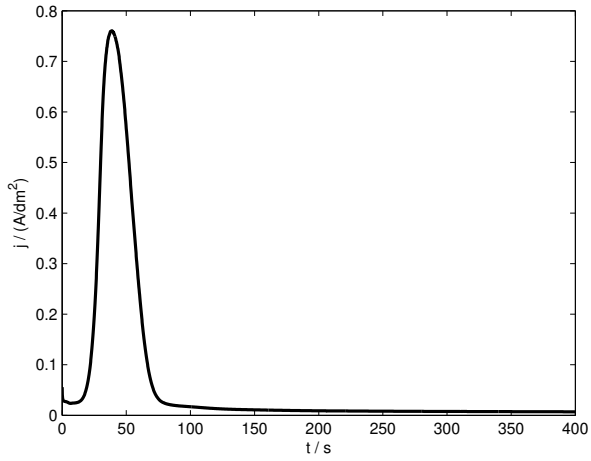

(a)

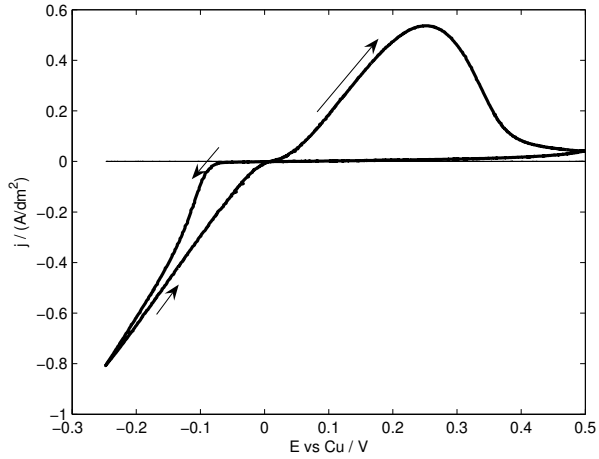

(b)

Figure 4.2: (a) Seed layer stripping at +0.5 V. (b) Cyclic voltammograms of the ionic liquid $[Cu(MeCN)_2][Tf_2N]$ on a tantalum working electrode at 90 °C. The scan rate was 50 mV s^{-1}.

on the available nucleation sites. The high intrinsic concentration of Cu(I) ions in $[Cu(MeCN)_2][Tf_2N]$ (3.1 mol dm^{-3} [20]) causes that more nucleation sites can start growing simultaneously: growing nuclei will deplete their surroundings of Cu(I) ions which inhibits further nucleation and growth of nucleation sites located in the diffusion layer of the original nucleus. Due to the higher concentration, more time will pass before the concentration drops below levels where no further nucleation occurs and during this time interval more nucleation sites can be activated.

The deposit at -3.0 V shown in figure 4.3(a) has a grainy morphology with varying grain sizes and open grain boundaries. This was also confirmed by TEM analyses of deposit cross-sections with varying layer thickness between 13 and 38 nm. For -4.0 V (figure 4.3(b)), the deposit reveals a flat appearance, with a varying grain size but fewer pinholes than the deposit made at -3.0 V (figure 4.3(a)). TEM revealed a film thickness around 19 nm. The best results were obtained at -5.0 V: figure 4.3(c) shows a deposit with flat appearance, very few pinholes and a thickness around 19 nm, found by TEM measurements (figure 4.4). A continuous tantalum oxide layer of 3−5 nm was found along the entire Cu-Ta interface. This oxide layer is indicated by the two parallel lines in figure 4.4 and it originates most probably during the anodic polarization of the substrate. No oxygen was found at the interface of the tantalum substrate and the copper seed before the latter was anodically dissolved. Some pinholes, through which oxygen can diffuse, are present in the deposits but there are too few of them to permit sufficient oxygen transport to obtain the uniform oxide layer on the copper-tantalum interface. The composition of the oxide layer was Ta_2O_5, as determined by quantitative EELS compositional analysis in combination with multiple scattering simulations (FEFF code) of the O-K edge fine structure. The adhesion of copper to the tantalum substrate was tested by submitting the deposited layers to the Scotch tape test. All samples that were tested could withstand this test, indicating a good adhesion between tantalum and the deposited copper.

It was tried to describe the nucleation behavior by the well-known theory developed by Scharifker and Hills [29]. According to this theory, the nucleation behavior is known by fitting the experimentally measured currents to the theoretical curves for progressive and instantaneous nucleation. This method works fine for small overpotentials and low concentrations for which a clear maximum

(electrode area of 0.007 dm^2). For an applied potential of -3 V to lead to an electrode potential more negative than -0.5 V, the resistance R of the solution should follow from -3+0.0378·R <-0.5 V, or $R < 66\ \Omega$. By using the Newman formula $R = (4\sigma r)^{-1}$ with r the radius of a circle with the same area as the used rectangular electrode, one can calculate that $\sigma > 0.81\ \Omega^{-1}m^{-1}$. This is true as the conductivity of $[Cu(MeCN)_2][Tf_2N]$ is 1.62 Ω^{-1} m^{-1}. Similar calculations for a deposition during 0.25 s at -4 or -5 V show that the electrode potential is more negative than -0.5 V in these cases as well.

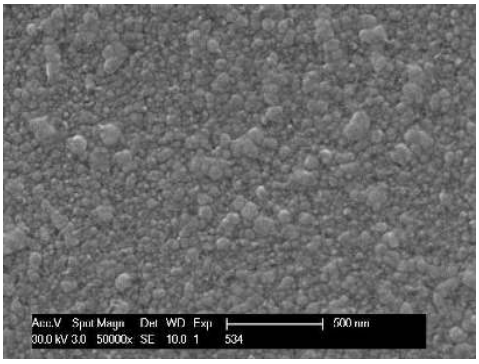

(a)

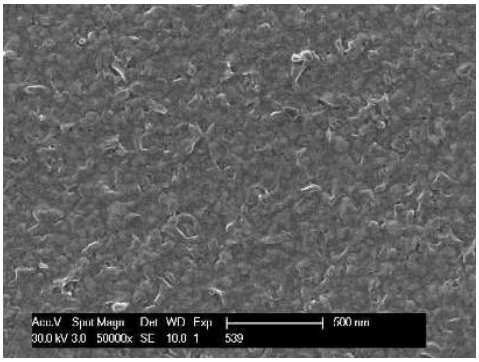

(b)

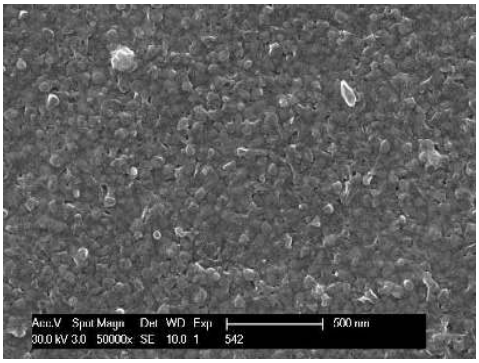

(c)

Figure 4.3: SEM micrographs of copper deposits from the ionic liquid $[Cu(MeCN)_2][Tf_2N]$ on a tantalum working electrode after seed layer stripping at +0.5 V at 90 °C: (a) 0.5 s at -3.0 V, (b) 0.25 s at -4.0 V, (c) 0.25 s at -5.0 V.

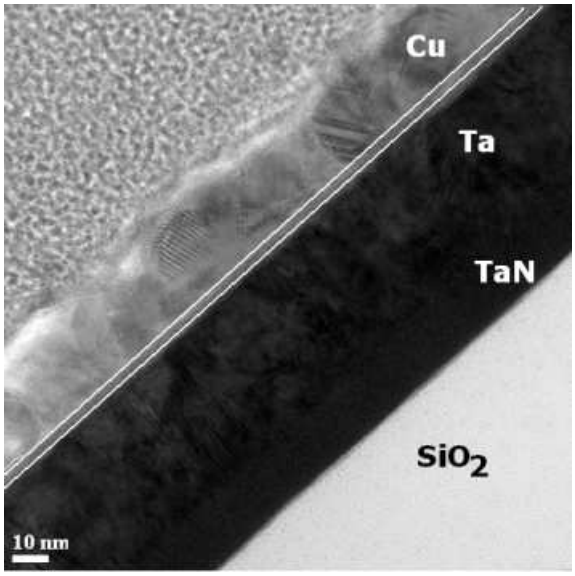

Figure 4.4: TEM cross-section of a copper deposit from the ionic liquid $[Cu(MeCN)_2][Tf_2N]$ on a tantalum working electrode at 90 °C: 0.25 s at -5.0 V. The white lines mark the tantalum oxide layer.

in current develops a few seconds after applying the potential step. In our experiments, this theory could not be applied. Firstly, the concentration of electroactive species is high (3.1 mol dm^{-3}, see reference [20]), which shifts the appearance of the current maximum to shorter times. Secondly, the applied overpotentials are high. This causes a large charging current for the electrical double layer which interferes in determining the location and value of the current maximum. The nucleation was therefore determined by the topographical investigation via atomic force microscopy (AFM). Topologies were measured at three deposition potentials (-3.0, -4.0 and -5.0 V) and deposition times as short as 15 ms to calculate the nucleation densities and nucleation rates. Unfortunately, AFM scans show that even for such short deposition times separate nuclei start to coalesce so that an accurate determination of the nucleation rate is not possible since the separate nuclei can no longer be distinguished. A lower limit for the nucleation density N was calculated by the empirical formula $N = (\pi d^2)^{-1}$, in which d, the deposit thickness, was taken from the TEM cross section. This formula is valid in situations in which closed layers have been deposited. Figure 4.4 shows that this condition is met. The calculated value for N was $N = 8{\cdot}10^{14}$ m^{-2}. This nucleation density is higher than for aqueous deposition on the native tantalum oxide layer where $N \approx$

10^{12} m^{-2} [10, 11]. This high nucleation density, despite the presence of an oxide layer, is due to the large overpotential that can be applied in $[Cu(MeCN)_2][Tf_2N]$ without decomposition products of the ionic liquid poisoning the electrolyte. This makes $[Cu(MeCN)_2][Tf_2N]$ an excellent medium for the electrodeposition of very thin seed layers in non-aqueous environments.

Conclusion

The use of the ionic liquid $[Cu(MeCN)_2][Tf_2N]$ as medium for copper electrodeposition on a tantalum substrate is demonstrated. A nucleation density of $8{\cdot}10^{14}$ m^{-2} is reached at a deposition potential of -5.0 V. The deposits show a flat appearance and very few pinholes for thicknesses around 19 nm. Research towards the origin of the oxide layer (from water, dissolved oxygen, or chemical decomposition of the bistriflimide anion $[Tf_2N]^-$) is ongoing, just as the search for additives that can improve the morphology of the deposited copper. If the oxidation of the tantalum substrate can be avoided, it is most likely that the thickness of the copper deposits can be reduced even further, possibly to about 5 nm. In that case, the layers become thin enough not only as seed layers for TSV, but also for vias and trenches to achieve superfilling.

Acknowledgments

This research was funded by a Ph.D grant of the Institute for the Promotion of Innovation through Science and Technology in Flanders (IWT-Vlaanderen) to S.S.
This work is supported in part by the European Commissions Seventh Framework Programme (FP7) under Grant Agreement number 216474 (CopPeR).
The authors acknowledge financial support by the K.U.Leuven (projects IDO/05/005 and GOA 08/05), by the FWO-Flanders (research community "Ionic Liquids") and by the IWT-Flanders (SBO-project IWT 80031 "MAPIL").
Support by IoLiTec (Heilbronn, Germany) is also acknowledged.

References

[1] Ed.: F. Endres, A. P. Abbott, D. R. MacFarlane, *Electrodeposition from ionic liquids*, Wiley-VCH, Weinheim (2008).

[2] F. Endres, S. Zein El Abedin, Air and water stable ionic liquids in physical chemistry, *Phys. Chem. Chem. Phys.*, **8**, 2101 (2006).

[3] F. Endres, Ionic liquids: solvents for the electrodeposition of metals and semiconductors, *ChemPhysChem*, **3**, 144 (2002).

[4] F. Endres, Ionic liquids: Promising solvents for electrochemistry, *Z. Phys. Chem.*, **218**, 255 (2004).

[5] A. P. Abbott, K. J. McKenzie, Application of ionic liquids to the electrodeposition of metals, *Phys. Chem. Chem. Phys.*, **8**, 4265 (2006).

[6] T. Oku, E. Kawakami, M. Uekubo, K. Takahiro, S. Yamaguchi, M. Murakami, Diffusion barrier property of TaN between Si and Cu, *Appl. Surf. Sci.*, **99**, 265 (1996).

[7] M. T. Wang, Y. C. Lin, M. C. Chen, Barrier properties of very thin Ta and TaN layers against copper diffusion, *J. Electrochem. Soc.*, **145**, 2538 (1998).

[8] K. Holloway, P. M. Fryer, C. Cabral, J. M. E. Harper, P. J. Bailey, K. H. J. Kellegher, Tantalum as a diffusion barrier between copper and silicon - failure mechanism and effect of nitrogen additions, *J. Appl. Phys.*, **71**, 5433 (1992).

[9] S. B. Emery, J. L. Hubbley, D. Roy, Voltammetric and amperometric analyses of electrochemical nucleation: electrodeposition of copper on nickel and tantalum, *J. Electroanal. Chem.*, **568**, 121 (2004).

[10] A. Radisic, G. Oskam, P. C. Searson, Influence of oxide thickness on nucleation and growth of copper on tantalum, *J. Electrochem. Soc.*, **151**, C369 (2004).

[11] M. Zheng, J. J. Kelly, H. Deligianni, Electrodeposition of Cu on Ta-based layers: I. electrodeposition on Ta, *J. Electrochem. Soc.*, **154**, D400 (2007).

[12] Z. Wang, H. Li, H. Shodiev, I. I. Suni, Immersion/electroless deposition of Cu on Ta, *Electrochem. Solid-State Lett.*, **7**, C67 (2004).

[13] D. Starosvetsky, N. Sezin, Y. Ein-Eli, Seedless copper electroplating on Ta from a "single" electrolytic bath, *Electrochim. Acta*, **55**, 1656 (2010).

[14] S. Kim, Seedless copper electrodeposition onto tantalum diffusion barrier by two-step deposition process, *Electrochem. Solid-State Lett.*, **13**, D83 (2010).

[15] P. C. Andricacos, C. Uzoh, J. O. Dukovic, J. Horkans, H. Deligianni, Damascene copper electroplating for chip interconnections, *IBM J. Res. Develop.*, **42**, 567 (1998).

[16] W.-P. Dow, H.-H. Chen, M.-Y. Yen, W.-H. Chen, K.-H. Hsu, P.-Y. Chuang, H. Ishizuka, N. Sakagawa, R. Kimizuka, Through-hole filling by copper electroplating, *J. Electrochem. Soc.*, **155**, D750 (2008).

[17] O. Lühn, A. Radisic, P. M. Vereecken, C. Van Hoof, W. Ruythooren, J.-P. Celis, Changing superfilling mode for copper electrodeposition in blind holes from differential inhibition to differential acceleration, *Electrochem. Solid-State Lett.*, **12**, D39 (2009).

[18] O. Lühn, C. Van Hoof, W. Ruythooren, J.-P. Celis, Filling of microvia with an aspect ratio of 5 by copper electrodeposition, *Electrochim. Acta*, **54**, 2504 (2009).

[19] N. R. Brooks, S. Schaltin, K. Van Hecke, L. Van Meervelt, K. Binnemans, J. Fransaer, Copper(I)-containing ionic liquids for high-rate electrodeposition, *Chem. Eur. J.*, **17**, 5054 (2011).

[20] S. Schaltin, N. R. Brooks, K. Binnemans, J. Fransaer, Electrodeposition from cationic cuprous organic complexes: Ionic liquids for high current density electroplating, *J. Electrochem. Soc.*, **158**, D21 (2011).

[21] J.-F. Huang, H. Luo, S. Dai, A new strategy for synthesis of novel classes of room-temperature ionic liquids based on complexation reaction of cations, *J. Electrochem. Soc.*, **153**, J9 (2006).

[22] M. Iida, C. Baba, M. Inoue, H. Yoshida, E. Taguchi, H. Furusho, Ionic liquids of bis(alkylethylenediamine)silver(I) salts and the formation of silver(0) nanoparticles from the ionic liquid system, *Chem. Eur. J.*, **14**, 5047 (2008).

[23] M. Iida, S. Kawakami, E. Syouno, H. Er, E. Taguchi, Properties of ionic liquids containing silver(I) or protic alkylethylenediamine cations with a bis(trifluoromethanesulfonyl)amide anion, *J. Colloid Interface Sci.*, **356**, 630 (2011).

[24] H. M. A. Abood, A. P. Abbott, A. D. Ballantyne, K. S. Ryder, Do all ionic liquids need organic cations? Characterisation of $[AlCl_2{\cdot}n$ amide$]^+$ $AlCl_4^-$ and comparison with imidazolium based systems, *Chem. Commun.*, **47**, 3523 (2011).

[25] S. G. Biallozor, Electrodeposition of copper on platinum from non-aqueous solutions, *Electrochim. Acta*, **17**, 1243 (1972).

[26] S. G. Biallozor, D. Poletek, Electrochemical behavior of copper in nonaqueous solutions. I, *Élektrokhimiya*, **15**, 472 (1979).

[27] N. Petrescu, L. Ganovici, M. Britchi, Electrolytic copper refining from cuprous sulphate solutions containing organic nitriles, *Rev. Roum. Chim.*, **29**, 407 (1984).

[28] E. Budevski, G. Staikov, J. W. Lorenz, *Electrochemical phase transformation and growth*, VCH, Weinheim (1996).

[29] B. Scharifker, G. Hills, Theoretical and experimental studies of multiple nucleation, *Electrochim. Acta*, **28**, 879 (1983).

Chapter 5

Direct Cu-on-Ta electroplating from ionic liquids in high vacuum

Published as S. Schaltin, A. Shkurankov, K. Binnemans and J. Fransaer, *ECS Trans.*, **25**, 119-128 (2010)

Abstract

Smooth layers of 20 nm of copper have been deposited on a tantalum substrate from ionic liquids under high vacuum conditions. By electrochemical vacuum deposition (EVD) it is possible to achieve extremely low concentrations of oxygen and water, so that the tantalum electrode does not oxidize. Due to the low vapor pressure of ionic liquids, no evaporation of the electrolyte was observed in vacuum. The wide electrochemical windows of the ionic liquids are advantageous to obtain nucleation densities up to $8{\cdot}10^{14}$ m^{-2} of copper on the tantalum electrode by applying a very large overpotential. Copper was deposited at potentials as negative as -3 V versus a Cu pseudo-reference electrode.

Introduction

Due to their intrinsic ionic conductivity and wide electrochemical window, ionic liquids are interesting non-aqueous electrolytes for the electrodeposition of reactive metals which cannot be deposited from aqueous solutions [1–5]. Studies have been made on the electrodeposition of titanium [6, 7], tantalum [8, 9], magnesium [10], silicon [11], germanium [12], cesium [13] and the rare earths [14], but the most successful and convincing results were obtained for aluminium and some of its alloys [15–26]. At first sight, there seems to be no advantages associated with the electrodeposition from ionic liquids of metals which can also be deposited from water like zinc, copper, silver or gold. However, ionic liquids not only allow to deposit alloys of these metals with compositions not obtainable from aqueous solvents, but these solvents also allow in principle to use electrodes made of materials that are passivated in the presence of water. Typical examples are titanium, niobium or tantalum. The wide electrochemical window of ionic liquids are an advantage if one wants to electrodeposit at very large overpotentials to get a high nucleation density. A property of ionic liquids that has not been explored so far for electrochemical applications is their extremely low vapor pressure. This allows to electrodeposit from a liquid electrolyte under high vacuum conditions without the danger of evaporation of the electrolyte. A useful application is the deposition of a thin copper metal layer on a tantalum electrode. The possibility of direct deposition of copper on a tantalum barrier is of great importance for the microelectronics industry. In state-of-the-art wafer technology, a barrier layer of Ta/TaN prevents the diffusion of copper into silicon [27–29]. Presently, the copper layer is fabricated via a two-step process. First, a copper seed layer is grown by Physical Vapor Deposition (PVD) and this layer protects the underlying tantalum against oxidation. On top of this seed layer, copper is deposited electrochemically from an aqueous sulfate solution until the desired thickness is reached. Moreover, the filling of trenches and vias with copper without creating a void is a challenge [30]. In direct electrodeposition of copper on tantalum no seed layer is required and this would allow to reduce the two-step process into a one-step process. The direct electrodeposition of copper on tantalum has already been described from aqueous solutions [31, 32], but the authors are aware of the fact that in aqueous solution, tantalum is covered with its native oxide.

In this paper, copper is deposited on tantalum using copper(I) bis(trifluoromethylsulfonyl)imide ($Cu(Tf_2N)$) dissolved in the ionic liquids 1-ethyl-3-methylimidazolium chloride ($[C_2mim]Cl$), *N*-butyl-*N*-methylpyrrolidinium bis(trifluoromethylsulfonyl)imide ($[BMP][Tf_2N]$), or in mixtures of the latter ionic liquid with *N*-butyl-*N*-methylpyrrolidinium chloride ([BMP]Cl). The electrodeposition process is carried out in high vacuum conditions to prevent passivation of the tantalum electrode. It is shown that large overpotentials are needed for obtaining a well-

adhering closed copper layer.

Experimental

[BMP][Tf_2N], [BMP]Cl and [C_2mim]Cl were purchased from IoLiTec. Cu(Tf_2N)$_2$ was prepared by dissolving an excess of CuO in an aqueous solution of H(Tf_2N). The remaining CuO was filtered off and the water evaporated under reduced pressure. Before use, appropriate amounts of Cu(Tf_2N)$_2$ and the ionic liquid were mixed and dried in vacuo at 120 °C.
Electrochemical experiments were conducted using a Solartron SI 1287 Electrochemical Interface. The electrochemical cell (5 cm^3) was a home-made copper crucible which also served as counter electrode. By using a copper crucible, the equilibrium of the comproportionation reaction was maintained (*vide infra*). The crucible was placed in the vacuum chamber and the pressure was reduced below $4{\cdot}10^{-6}$ mbar. This step effectively removed water, oxygen and any remaining organic impurities out of the ionic liquid. A polyimide Thermofoil^{TM} heater was used to maintain the temperature at 90 °C. The working electrodes for cyclic voltammetry consisted of platinum wire (ϕ = 0.5 mm, Goodfellow, 99.99%) and were mechanically polished with diamond paste (3 μm), rinsed in demineralized water and dried. The working electrodes for deposition experiments were cut from silicon wafers covered with 10 nm of TaN, 40 nm of Ta, and 150 nm of Cu. Before the actual deposition experiment, the copper layer was electrochemically stripped at +0.1 V. All potentials mentioned are referred to a copper pseudo-reference electrode. Optical spectra were measured on a Varian Cary 5000 spectrophotometer at room temperature. Absorption spectra of Cu^{2+} solutions were recorded in a 0.2 cm quartz cell, whereas the stabilized solution (*vide infra*) was measured with a path length of 1 cm. The morphology of the deposits was determined by scanning electron microscopy (Philips XL 30 FEG).

Results and discussion

Spectroscopy of copper solutions

It is known that in non-aqueous solvents, cuprous ions can be more stable compared to aqueous solutions [33]. Even more, it turns out that in ionic liquids these ions are more stable than cupric ions, leading to a comproportionation reaction when a Cu^{2+} solution is brought in contact with metallic copper:

$$Cu + Cu^{2+} \rightleftharpoons 2Cu^{+} \tag{5.1}$$

This phenomenon was already previously encountered in ionic liquids with the bis(trifluoromethylsulfonyl)imide anion [34–36]. The comproportionation reaction

requires a stabilization step of the solution before deposition experiments can be performed. If this step would be skipped, the copper deposit would start to dissolve in the Cu^{2+} solution as soon as the deposition potential is no longer applied. Therefore, solutions of 0.5 mol dm^{-3} of $Cu(Tf_2N)_2$ were poured into a copper crucible, heated and vigorously stirred overnight so that reaction (5.1) reaches equilibrium. In [BMP][Tf_2N], the equilibrium of reaction (5.1) lies almost completely to the right as proven by spectrophotometric experiments. Cupric ions

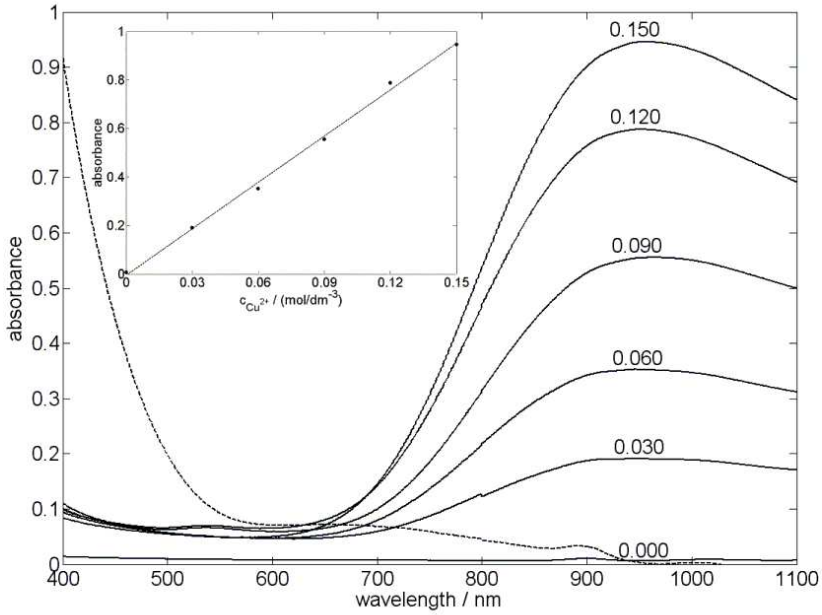

Figure 5.1: Absorption spectra at room temperature of the stabilized [BMP][Tf_2N]-$Cu(Tf_2N)$ solution (dashed line) and six Cu^{2+} solutions with different concentrations (solid lines). Insert: absorbance as function of Cu^{2+} concentration at a wavelength of 955 nm.

strongly absorb at a wavelength of 955 nm and the absorbance is a linear function of the concentration of cupric ions (see figure 5.1). For the stabilized solution however, the absorbance is zero at 955 nm indicating that virtually all cupric ions are converted into cuprous ions. This is in contrast with the data from references [34, 35]: they found a conversion of 60% of Cu^{2+} in trimethyl-*n*-hexylammonium bis(trifluoromethylsulfonyl)imide but these results were obtained at different temperatures. For the chloride containing solutions, no spectroscopic measurements

were done, because the solutions tend to crystallize at room temperature. However, it is reasonable to assume that in these solutions the conversion of cupric into cuprous ions is almost 100%. In a mixture of $AlCl_3$ and *N*-methylpyridinium chloride (67-33 mole%), the equilibrium constant for reaction (5.1) is $5{\cdot}10^{17}$ on a molal basis [37], meaning that the concentration of cupric ions is negligible compared to the cuprous ion concentration. All solutions mentioned in this paper are prepared with a Cu^{2+} concentration of 0.5 mol dm^{-3}, poured into a copper crucible and given time to reach the equilibrium of reaction (5.1). Further on, they will be mentioned as containing a $Cu(Tf_2N)$ concentration of 1 mol dm^{-3}.

Estimation of the tantalum oxidation in high vacuum

Because of the oxophilic nature of tantalum metal, it is important that the amount of oxygen that can react with the bare tantalum metal is limited so that no passivation of the substrate takes place. The following calculation (at 50 °C, because not all data are available for 90 °C) shows that electrodeposition in high vacuum conditions is promising for this purpose. The partial pressure p_{O_2} for O_2 in high vacuum is $8{\cdot}10^{-7}$ mbar. With this pressure and the Henry coefficient H_{O_2}, the molar fraction x_{O_2} of O_2 in the ionic liquid can be calculated:

$$p_{O_2} = H_{O_2} x_{O_2} \tag{5.2}$$

At 50 °C, H_{O_2} is $1.210{\cdot}10^6$ mbar for [BMP][Tf_2N] [38], so $x_{O_2} = 6.61{\cdot}10^{-13}$. Using the molar mass and density of [BMP][Tf_2N] (422.21 g mol^{-1} and 1.37 g cm^{-3} [38, 39] respectively), this value can be converted to molar bulk concentration c_{O_2} of O_2 in [BMP][Tf_2N]: $c_{O_2} = 2.14{\cdot}10^{-12}$ mol dm^{-3}. The concentration c_o of O_2 near the tantalum surface was assumed to be zero because of the fast kinetics of the oxidation of tantalum. These values were used to solve Fick's second law of diffusion, with J the flux of O_2 at the tantalum surface and D_{O_2} the diffusion coefficient of O_2 in [BMP][Tf_2N] which leads to:

$$J(t) = D_{O_2} \frac{c_{O_2}}{\sqrt{\pi D_{O_2} t}} \tag{5.3}$$

Integration of this equation gives the amount of O_2 that can diffuse to the tantalum surface in a given amount of time:

$$\int_0^t J(\xi) d\xi = 2 c_{O_2} \sqrt{\frac{D_{O_2} t}{\pi}} \tag{5.4}$$

Since $D_{O_2} \approx 10^{-8}$ dm^2 s^{-1} [40], this equation can be solved: the resulting graph is plotted in figure 5.2. After 400 s, less than $5{\cdot}10^{-15}$ mol dm^{-2} can reach the tantalum surface. This amount has to be compared with the amount of oxygen that is needed for the conversion of tantalum metal into Ta_2O_5. A metallic surface

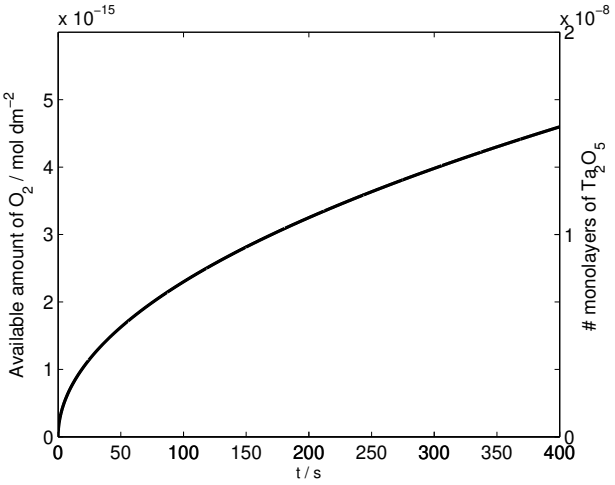

Figure 5.2: Amount of O_2 that has reacted with the electrode per unit area as a function of time.

has $\pm 2 \cdot 10^{17}$ atoms dm^{-2}, so the oxidation of one monolayer of tantalum metal requires $5 \cdot 10^{17}$ atoms dm^{-2} of oxygen, or $4 \cdot 10^{-7}$ mol dm^{-2} of O_2. This calculation shows that the amount of O_2, required for oxidation of one monolayer of tantalum metal, is 8 orders of magnitude larger than the amount of oxygen that is available by diffusion. So EVD should enable the direct deposition of copper on tantalum metal. This calculation does not take into account the presence of water or the effect of adsorbed species onto the copper seed.

Electrochemistry of copper

Figure 5.3(a) shows the cyclic voltammogram of 1 mol dm^{-3} of Cu(Tf_2N) in [BMP][Tf_2N] at 90 °C using a scan rate of 50 mV s^{-1}. Cuprous ions are reduced to metallic copper at negative potentials and oxidized to cupric ions at potentials more positive than 0.8 V vs Cu. The cyclic voltammograms for the [C_2mim]Cl and [BMP]Cl solutions show analogue features. The cyclic voltammogram for a tantalum working electrode is shown in figure 5.3(b). It is limited to the potential values in which only copper metal or Cu^+ ions are present. As can be clearly seen, the deposition of copper onto tantalum requires a considerable overpotential of 200 mV, leading to the presence of a nucleation loop. This nucleation loop is a clear indication of the difficult deposition of copper onto tantalum. Just as for the cyclic voltammograms on platinum electrodes, the [C_2mim]Cl and [BMP]Cl solutions have similar features for the tantalum electrodes as the [BMP][Tf_2N]

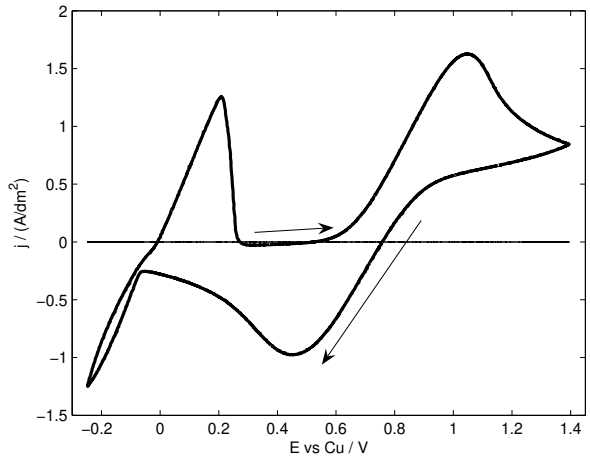

(a)

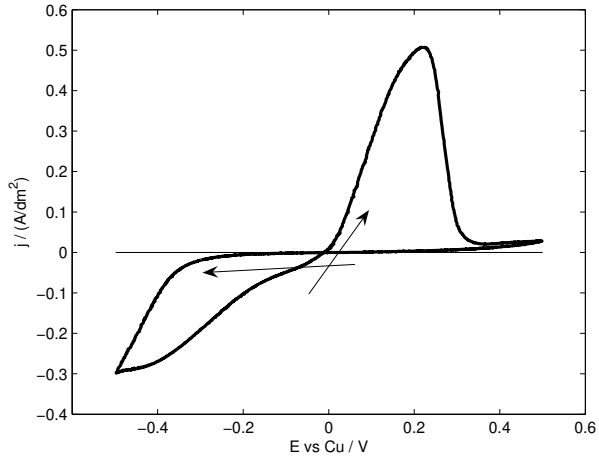

(b)

Figure 5.3: Cyclic voltammograms of 1 mol dm^{-3} of Cu(Tf_2N) in [BMP][Tf_2N] at 90 °C on (a) a Pt working electrode, (b) a Ta working electrode. The scan rate was 50 mV s^{-1}.

solution.

Deposition of copper

It was found that the copper layers had the highest quality when they were deposited from [BMP]Cl. [BMP]Cl was tested in this study since it combines the electrochemical stability of the $[BMP]^+$ cation with the properties of Cl^- based ionic liquids. Unfortunately, this compound is solid at 90 °C. Therefore it was mixed with [BMP][Tf_2N] (50-50 mol%). This is a logical choice since both ions of [BMP][Tf_2N] are present in the final deposition bath. The mixture of [BMP]Cl and [BMP][Tf_2N] still showed some undissolved crystals at 90 °C, but after the addition of $Cu(Tf_2N)_2$, a transparent orange liquid was formed. This Cu^{2+} containing liquid was then transformed into a Cu^+ solution. The cross section of a deposit is shown

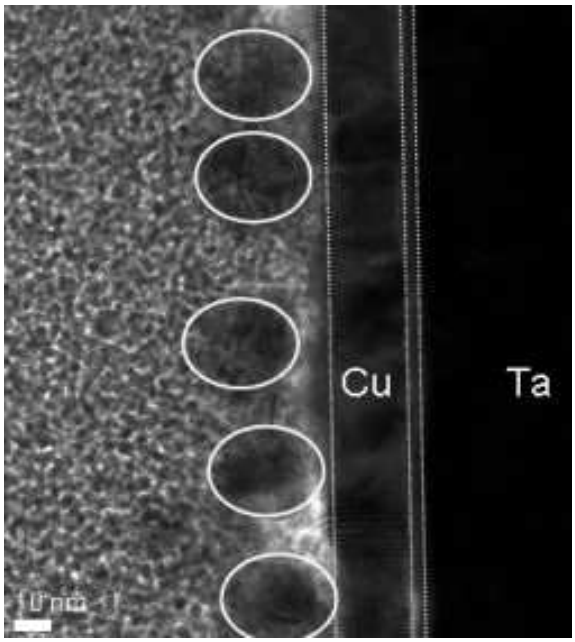

Figure 5.4: TEM cross section of a deposit made in 1 mol dm^{-3} of $Cu(Tf_2N)$ in [BMP][Tf_2N]-[BMP]Cl (50-50 mol%) at 90 °C. The deposition potential was -3 V and was applied for 500 ms. The white circles indicate the renucleated layer. The oxide layer is marked by two lines on the Cu-Ta interface.

in figure 5.4. The deposited layer is 20 nm thick and closed. This means that the nucleation density has an approximate value of at least $8{\cdot}10^{14}$ m^{-2}, a value

which could only be obtained by applying a large overpotential of -3 V. Some renucleation has already occurred as separately copper grains (indicated by white circles) can be noticed on top of the closed copper layer. Unfortunately, the TEM cross section shows that in between the tantalum substrate and the copper layer, a thin layer of tantalum oxide is present. Experiments to determine the origin of this oxide are still in progress.

Conclusions

Our research shows that Electrochemical Vacuum Deposition (EVD) should permit to deposit thin layers of copper on tantalum metal instead of tantalum oxide. The amount of available oxygen is strongly reduced in high vacuum conditions. Although some oxidation of the tantalum substrate still takes place, closed copper layers with a thickness of 20 nm can be deposited.

Acknowledgments

Research funded by a Ph.D grant of the Institute for the Promotion of Innovation through Science and Technology in Flanders (IWT-Vlaanderen). The authors thank the FP7 CopPeR project and the K.U.Leuven for financial support (project IDO/05/005). Peter Nockemann and Evert Vanecht are acknowledged for their help with the spectroscopy measurements and the preparation of $Cu(Tf_2N)_2$. Harald Plank and Gerald Kothleitner are acknowledged for the TEM analyses. Support from IoLiTec (Denzlingen, Germany) is gratefully acknowledged

References

[1] Ed.: F. Endres, A. P. Abbott, D. R. MacFarlane, *Electrodeposition from ionic liquids*, Wiley-VCH, Weinheim (2008).

[2] F. Endres, S. Zein El Abedin, Air and water stable ionic liquids in physical chemistry, *Phys. Chem. Chem. Phys.*, **8**, 2101 (2006).

[3] F. Endres, Ionic liquids: solvents for the electrodeposition of metals and semiconductors, *ChemPhysChem*, **3**, 144 (2002).

[4] F. Endres, Ionic liquids: Promising solvents for electrochemistry, *Z. Phys. Chem.*, **218**, 255 (2004).

[5] A. P. Abbott, K. J. McKenzie, Application of ionic liquids to the electrodeposition of metals, *Phys. Chem. Chem. Phys.*, **8**, 4265 (2006).

[6] J. Ding, J. Wu, D. R. MacFarlane, W. E. Price, G. Wallace, Induction of titanium reduction using pyrrole and polypyrrole in the ionic liquid ethyl-methylimidazolium bis(trifluoromethanesulphonyl)amide, *Electrochem. Commun.*, **10**, 217 (2008).

[7] F. Endres, S. Zein El Abedin, A. Y. Saad, E. M. Moustafa, N. Borissenko, W. E. Price, G. G. Wallace, D. R. MacFarlane, P. J. Newman, A. Bund, On the electrodeposition of titanium in ionic liquids, *Phys. Chem. Chem. Phys.*, **6**, 2189 (2008).

[8] S. Zein El Abedin, Electrodeposition of tantalum and aluminium in ionic liquid [$Py_{1,4}$] TFSA, *Trans. Inst. Metal. Finish.*, **86**, 220 (2008).

[9] N. Borissenko, A. Ispas, E. Zschippang, Q. Liu, S. Zein El Abedin, A. Bund, F. Endres, In situ STM and EQCM studies of tantalum electrodeposition from TaF_5 in the air- and water-stable ionic liquid 1-butyl-1-methylpyrrolidinium bis(trifluoromethylsulfonyl)amide, *Electrochim. Acta*, **54**, 1519 (2009).

[10] G. T. Cheek, W. E. O'Grady, S. Zein El Abedin, E. M. Moustafa, F. Endres, Studies on the electrodeposition of magnesium in ionic liquids, *J. Electrochem. Soc.*, **155**, D91 (2008).

[11] S. Zein El Abedin, N. Borissenko, F. Endres, Electrodeposition of nanoscale silicon in a room temperature ionic liquid, *Electrochem. Commun.*, **6**, 510 (2004).

[12] W. Freyland, C. A. Zell, S. Zein El Abedin, F. Endres, Nanoscale electrodeposition of metals and semiconductors from ionic liquids, *Electrochim. Acta*, **48**, 3053 (2003).

[13] P.-Y. Chen, C. L. Hussey, Electrodeposition of cesium at mercury electrodes in the tri-1-butylmethylammonium bis((trifluoromethyl)sulfonyl)imide room-temperature ionic liquid, *Electrochim. Acta*, **49**, 5125 (2004).

[14] A. I. Bhatt, I. May, V. A. Volkovich, D. Collison, M. Helliwell, I. B. Polovov, R. G. Lewin, Structural characterization of a lanthanum bistriflimide complex, $La(N(SO_2CF_3)_2)_3(H_2O)_3$, and an investigation of La, Sm, and Eu electrochemistry in a room-temperature ionic liquid, $[Me_3NnBu][N(SO_2CF_3)_2]$, *Inorg. Chem.*, **44**, 4934 (2005).

[15] N. M. Rocher, E. I. Izgorodina, T. Ruether, M. Forsyth, D. R. MacFarlane, T. Rodopoulos, M. D. Horne, A. M. Bond, Aluminium speciation in 1-butyl-1-methylpyrrolidinium bis(trifluoromethylsulfonyl)amide/$AlCl_3$ mixtures, *Chem. Eur. J.*, **15**, 3435 (2009).

[16] Q. X. Liu, S. Zein El Abedin, F. Endres, Electroplating of mild steel by aluminium in a first generation ionic liquid: A green alternative to commercial Al-plating in organic solvents, *Surf. Coat. Technol.*, **201**, 1352 (2006).

[17] Y. Zhao, T. J. Vandernoot, Electrodeposition of aluminium from room temperature $AlCl_3$-TMPAC molten salts, *Electrochim. Acta*, **42**, 1639 (1997).

[18] Y. Zhao, T. J. Vandernoot, Electrodeposition of aluminium from nonaqueous organic electrolytic systems and room temperature molten salts, *Electrochim. Acta*, **42**, 3 (1997).

[19] Q. Liao, W. R. Pitner, G. Stewart, C. L. Hussey, G. R. Stafford, Electrodeposition of aluminum from the aluminum chloride-1-methyl-3-ethylimidazolium chloride room temperature molten salt + benzene, *J. Electrochem. Soc.*, **144**, 936 (1997).

[20] J. Vaughan, D. Dreisinger, Electrodeposition of aluminum from aluminum chloride-trihexyl(tetradecyl) phosphonium chloride, *J. Electrochem. Soc.*, **155**, D68 (2008).

[21] R. T. Carlin, H. C. De Long, J. Fuller, P. C. Trulove, Microelectrode evaluation of transition metal-aluminum alloy electrodepositions in chloroaluminate ionic liquids, *J. Electrochem. Soc.*, **145**, 1598 (1998).

[22] M. R. Ali, A. Nishikata, T. Tsuru, Electrodeposition of Co-Al alloys of different composition from the $AlCl_3$-BPC-$CoCl_2$ room temperature molten salt, *Electrochim. Acta*, **42**, 1819 (1997).

[23] A. P. Abbott, C. A. Eardley, N. R. S. Farley, G. A. Griffith, A. Pratt, Electrodeposition of aluminium and aluminium/platinum alloys from $AlCl_3$/benzyltrimethylammonium chloride room temperature ionic liquids, *J. Appl. Electrochem.*, **31**, 1345 (2001).

[24] B. J. Tierney, W. R. Pitner, J. A. Mitchell, C. L. Hussey, G. R. Stafford, Electrodeposition of copper and copper-aluminum alloys from a room-temperature chloroaluminate molten salt, *J. Electrochem. Soc.*, **145**, 3110 (1998).

[25] G. R. Stafford, The electrodeposition of an aluminum-manganese metallic-glass from molten-salts, *J. Electrochem. Soc.*, **136**, 635 (1989).

[26] S. Zein El Abedin, E. M. Moustafa, R. Hempelmann, H. Natter, F. Endres, Additive free electrodeposition of nanocrystalline aluminium in a water and air stable ionic liquid, *Electrochem. Commun.*, **7**, 1111 (2005).

[27] T. Oku, E. Kawakami, M. Uekubo, K. Takahiro, S. Yamaguchi, M. Murakami, Diffusion barrier property of TaN between Si and Cu, *Appl. Surf. Sci.*, **99**, 265 (1996).

[28] M. T. Wang, Y. C. Lin, M. C. Chen, Barrier properties of very thin Ta and TaN layers against copper diffusion, *J. Electrochem. Soc.*, **145**, 2538 (1998).

[29] K. Holloway, P. M. Fryer, C. Cabral, J. M. E. Harper, P. J. Bailey, K. H. J. Kellegher, Tantalum as a diffusion barrier between copper and silicon - failure mechanism and effect of nitrogen additions, *J. Appl. Phys.*, **71**, 5433 (1992).

[30] P. C. Andricacos, C. Uzoh, J. O. Dukovic, J. Horkans, H. Deligianni, Damascene copper electroplating for chip interconnections, *IBM J. Res. Develop.*, **42**, 567 (1998).

[31] M. Zheng, J. J. Kelly, H. Deligianni, Electrodeposition of Cu on Ta-based layers: I. electrodeposition on Ta, *J. Electrochem. Soc.*, **154**, D400 (2007).

[32] M. Zheng, J. J. Kelly, H. Deligianni, B. C. Baker-O'Neal, C. Cabral Jr., Electrodeposition of Cu on Ta-based layers: II. Cu electrodeposition on Cu/Ta bilayers, *J. Electrochem. Soc.*, **154**, D406 (2007).

[33] Eds.: A. J. Bard, *Encyclopedia of the electrochemistry of the elements*, Marcel Dekker, Inc., New York (1974).

[34] K. Murase, K. Nitta, T. Hirato, Y. Awakura, Electrochemical behaviour of copper in trimethyl-*n*-hexylammonium bis((trifluoromethyl)sulfonyl)amide, an ammonium imide-type room temperature molten salt, *J. Appl. Electrochem.*, **31**, 1089 (2001).

[35] T. Katase, K. Murase, T. Hirato, Y. Awakura, Redox and transport behaviors of Cu(I) ions in TMHA-Tf_2N ionic liquid solution, *J. Appl. Electrochem.*, **37**, 339 (2007).

[36] S. Zein El Abedin, A. Y. Saad, H. K. Farag, N. Borissenko, Q. X. Liu, F. Endres, Electrodeposition of selenium, indium and copper in an air- and water-stable ionic liquid at variable temperatures, *Electrochim. Acta*, **52**, 2746 (2007).

[37] C. L. Hussey, L. A. King, R. A. Carpio, The electrochemistry of copper in a room temperature acidic chloroaluminate melt, *J. Electrochem. Soc.*, **126**, 1029 (1979).

[38] J. L. Anthony, J. L. Anderson, E. J. Maginn, J. F. Brennecke, Anion effects on gas solubility in ionic liquids, *J. Phys. Chem. B*, **109**, 6366 (2005).

[39] G. Hong, J. Jacquemin, M. Deetlefs, C. Hardacre, P. Husson, M. F. Costa, Solubility of carbon dioxide and ethane in three ionic liquids based on the bis(trifluoromethylsulfonyl)imide anion, *Fluid Phase Equilib.*, **257**, 27 (2007).

[40] Y. Katayama, K. Sekiguchi, M. Yamagata, T. Miura, Electrochemical behavior of oxygen/superoxide ion couple in 1-butyl-1-methylpyrrolidinium bis(trifluoromethylsulfonyl)imide room-temperature molten salt, *J. Electrochem. Soc.*, **152**, E247 (2005).

Chapter 6

Oscillating electrochemical reaction in copper-containing imidazolium ionic liquids

Published as S. Schaltin, K. Binnemans and J. Fransaer, *Phys. Chem. Chem. Phys*, **13**, 15448-15454 (2011)

Abstract

An example of an electrochemical oscillator in ionic liquids is presented. Solutions of the ionic liquid 1-ethyl-3-methylimidazolium chloride, $[C_2mim]Cl$, which contain both Cu^+ and Cu^{2+} ions, show current oscillations during potentiostatic polarization. The oscillations were analyzed by the Quartz Crystal Microbalance (QCM) technique and by Electrochemical Impedance Spectroscopy (EIS). The electrochemical oscillations are of the N-NDR-type, because the low frequency end of the impedance spectrum has negative real impedances. The oscillating current leads to an oscillating growth speed of a metallic copper layer. Besides the presence of both Cu^+ and Cu^{2+}, the presence of chloride is a necessary, yet not a sufficient, condition for the occurrence of current oscillations. Oscillating currents were also observed for the ionic liquids 1-butyl-3-methylimidazolium chloride and 1-butyl-2,3-dimethylimidazolium chloride, but not for tributyltetradecylphosphonium chloride and *N*-butylpyridinium chloride.

Introduction

The appearance of electrochemical oscillators (oscillating currents during potentiostatic polarization, or potential oscillations during galvanostatic experiments) is often unexpected, yet not uncommon. Literature data on oscillating systems are mostly about reactions for which both the reactants and products are soluble. Some examples are the oxidation of iodide to iodine [1], the oxidation of formic acid [2], methanol [3], or formaldehyde [4] to CO_2. Only a few papers report on oscillations during electrodeposition processes, and most of them are about potential oscillations during galvanostatic experiments [5–11]. Current oscillations during potentiostatic metal deposition have been found during the electrodeposition of Cu [12, 13] and Cu-Sn alloys from electrolyte solutions containing surfactants [14–17].

Electrochemical oscillations have been reviewed by Koper [18]. The theoretical behavior and classifications of electrochemical oscillators is described in several papers by Koper *et al.* [19–21] and a review by Krischer [22]. A basic classification divides electrochemical oscillators in three classes [20]: (1) oscillations of the current under truly potentiostatic conditions, (2) current oscillations only under potentiostatic conditions with sufficiently large ohmic drop, and (3) potential oscillations under galvanostatic conditions and current oscillations under potentiostatic conditions with sufficiently large ohmic drop. A more extended classification and an experimental *modus operandi* to classify electrochemical oscillators is given by Strasser *et al.* [21]

Ionic liquids are compounds which contain solely cations and anions [23–31]. Often they are liquid at, or melt around, room temperature and they have found their place in the field of electrochemistry and electrodeposition [32–37]. However, electrochemical oscillations in ionic liquids have almost not been reported. We are only aware of the work of Andriyko *et al.* on potential oscillations during galvanostatic electrolysis of solutions of TiF_4 dissolved in the ionic liquid 1-butyl-2,3-dimethylimidazolium tetrafluoroborate [38]. Unfortunately, no details on the occurrence of the oscillations were given.

In this paper, we report on an electrochemical oscillator occurring in solutions of 1-ethyl-3-methylimidazolium chloride ([C_2mim]Cl), that contain both Cu^+ and Cu^{2+} ions.

Experimental

1-Ethyl-3-methylimidazolium chloride ([C_2mim]Cl) (>98%), 1-butyl-3-methylimidazolium chloride ([C_4mim]Cl) (>99%), tributyltetradecylphosphonium chloride ([$P_{4,4,4,14}$]Cl) (>95%), *N*-butylpyridinium chloride ([C_4pyr]Cl) (>99%), 1-

butyl-2,3-dimethylimidazolium chloride ([C_4dmim]Cl) (>99%) and 1-ethyl-3-methylimidazolium bis(trifluoromethylsulfonyl)imide ([C_2mim][Tf_2N]) (99%) were purchased from IoLiTec. $CuCl_2 \cdot 2H_2O$ (99%) and CuCl (>97%) were bought from Merck and Fluka respectively. Extra pure batches of [C_2mim]Cl (99.5%, IoLiTec) and $CuCl_2$ (99.999%, Aldrich) were used to test the influence of impurities. They did not affect the obtained results. Tetraethylammonium chloride (99%) and acetonitrile (99.5%) were purchased from Janssen Chimica and Acros Organics respectively. $Cu(Tf_2N)_2$ was prepared by dissolving CuO in an aqueous H[Tf_2N] solution. Solutions of 0.5 M of Cu^{2+} or 1 M of Cu^+ were prepared by weighing and mixing appropriate amounts of copper salts in the ionic liquid. Before use, all solutions were dried at 120 °C under vacuum for 6 h (150 °C for [C_4pyr]Cl). In this paper, the solutions of 0.5 M of Cu^{2+} or 1 M of Cu^+ will be referred to as the cupric and cuprous solutions, respectively. A third solution consists of 0.5 M of Cu^{2+} in [C_2mim]Cl, poured in a copper crucible. Under these circumstances, a mixture of Cu^{2+} and Cu^+ starts to form due to the comproportionation reaction:

$$Cu^{2+} + Cu \rightleftharpoons 2Cu^+ \tag{6.1}$$

The solution was given time to equilibrate overnight (while stirred) and were used the next morning. This solution, which is transforming from 0.5 M solution of Cu^{2+} towards a 1 M solution of Cu^+, will be referred to as the mixed Cu^{2+}/Cu^+ solution. All solutions had a volume of 4 ml. The electrochemical experiments were performed in an argon-filled glove box (Glovebox Technology Limited, O_2 and H_2O concentrations below 1 ppm) and controlled by a Solartron SI 1287 Electrochemical Interface. Electrochemical Impedance Spectroscopy (EIS) was conducted using a Solartron instruments SI 1255 HF frequency response analyzer and the Quartz Crystal Microbalance (QCM) was a Maxtex RQCM. Platinum coated wafer pieces (Si, 500 nm SiO_2, 10 nm Ti, 100 nm Pt) were used as working electrode (0.7 by 0.7 cm^2). The cupric solution was contained in a platinum crucible and the cuprous solution in a copper crucible. These crucibles also served as counterelectrodes (Fig. 6.1). Such a setup gives the opportunity to work in small volumes without the need to insert a third electrode into the solution. All potentials in this paper are referred to a copper pseudo-reference electrode. Such pseudo-reference electrode led to stable and reproducible results. Unless stated otherwise, all experiments were conducted at 90 °C. This temperature was chosen because [C_2mim]Cl solutions are solid at room temperature. Furthermore, an increased temperature assists in decreasing the viscosity thereby increasing the diffusion of ions.

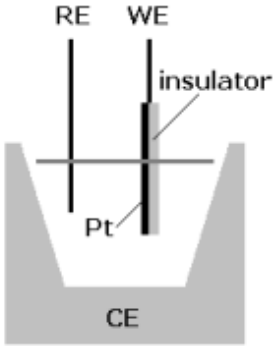

Figure 6.1: Schematic of the experimental setup, with relative positions of the working (WE), reference (RE) and counter electrode (CE).

Results and discussion

Initial observations

During the electrodeposition of copper from the different ionic liquid solutions, a remarkable behavior was observed (Fig. 6.2). When a constant potential of -1.0 V was applied in the cupric or cuprous solution, a decreasing current density j was observed as predicted by the Cottrell equation

$$j = \frac{n\mathrm{F}c\sqrt{D}}{\sqrt{\pi t}} \tag{6.2}$$

in which n is the number of exchanged electrons, F the Faraday constant, c the concentration (mol dm^{-3}) and D (dm^2 s^{-1}) the diffusivity [39]. For the mixed Cu^{2+}/Cu^{+} solution, however, the current signal starts oscillating after a few seconds (identical curve in Fig. 6.2(a) and Fig. 6.2(b)). For the first cycles, the period was on average 3.5 s but the oscillation period increased until the oscillations suddenly disappeared. These results seem to indicate that the oscillating behavior is caused by a mixture of Cu^{2+} and Cu^{+} ions. Another experiment was conducted using a rotating disk electrode (Fig. 6.3).

An platinum RDE at rest was polarized at -1.0 V until no more oscillations were observed. At that time, a rotation speed was applied and as a result, the oscillations reappeared. When the rotation was switched off the oscillations disappeared and this could be repeated. It was also found that the oscillations could be sustained as long as the electrode was rotating (Fig. 6.3). A possible explanation for the disappearance of oscillations in unstirred solutions is that reaction

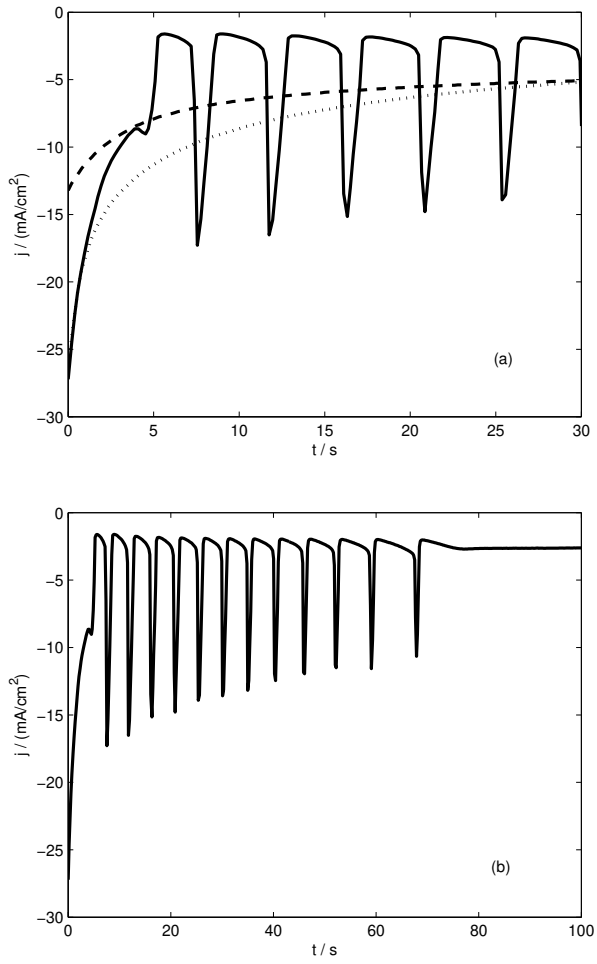

Figure 6.2: (a): Polarization at -1.0 V. (−−) cupric solution, (··) cuprous solution, (−) mixed Cu^{2+}/Cu^{+} solution. (b): Extended view for the mixed Cu^{2+}/Cu^{+} solution of Fig. 6.2(a)

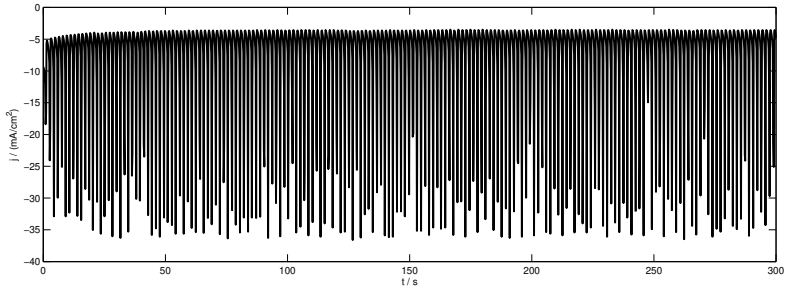

Figure 6.3: Rotating disk electrode experiment at 250 rpm at -1.0 V on the mixed Cu^{2+}/Cu^{+} solution.

(6.1) has proceeded to such an extent that the concentration of Cu^{2+} ions is much lower than the concentrations of Cu^{+} ions. During a potentiostatic experiment, the supply for Cu^{2+} ions is quickly limited by diffusion and this shortage of Cu^{2+} ions causes the oscillations to disappear. By stirring with a rotating disk electrode, new Cu^{2+} ions are supplied and the current can again start to oscillate. To test the involvement of Cu^{2+} ions, the mixed Cu^{2+}/Cu^{+} solution was given another 24 h more to react with the copper crucible (reaction (6.1)) so that the concentration of Cu^{2+} ions in the mixed Cu^{2+}/Cu^{+} solution decreased in favor of Cu^{+} ions. Fig. 6.4(a) shows that after the equilibrating step, only a very small oscillating signal is visible at $t = 8$ s. By gradually adding more Cu^{2+} ions to this solution, the oscillations reappeared and became more and more pronounced (Figs. 6.4(b-c-d)). These findings indicate that both Cu^{+} and Cu^{2+} ions are required to induce and maintain electrochemical oscillations in the ionic liquid.

A Quartz Crystal Microbalance (QCM) was used to test whether the oscillations in current correspond to an oscillating growth speed of the deposited copper metal, or whether an oscillating reaction is superimposed on a constant copper deposition speed. Fig. 6.5 shows the QCM results ($t = 0$ corresponds to the beginning of the oscillatory behavior). It is obvious that there is a one-to-one correspondence between the current oscillations and the growth speed of the deposited copper layer. The lower frequency of the oscillations in the QCM experiment is caused by a different setup which unfortunately suffers from a large iR-drop.

Characterization of the oscillations

According to Koper, electrochemical oscillators can be divided in three main classes: [20]

Class 1: Oscillations of the current under truly potentiostatic conditions

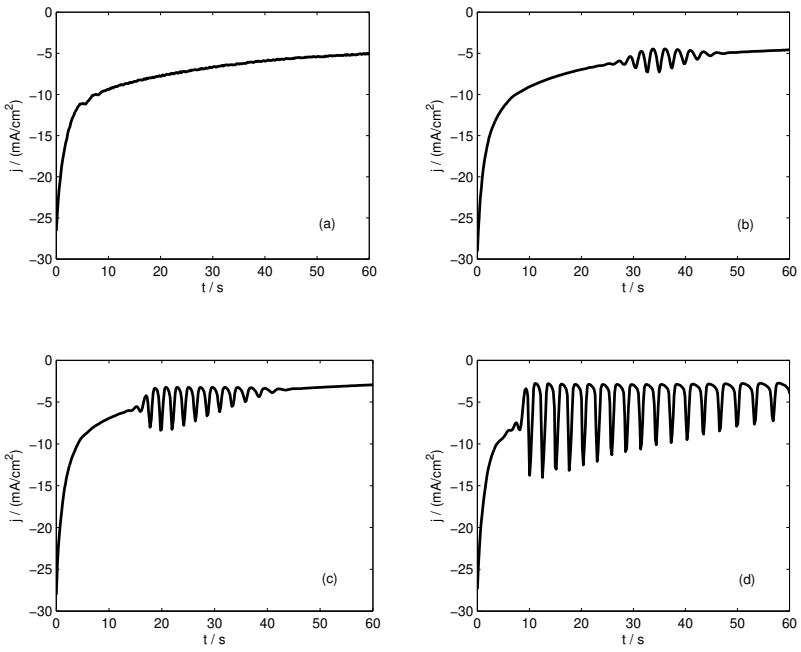

Figure 6.4: Polarization at -1.0 V in the equilibrated mixed Cu^{2+}/Cu^{+} solution. (a) no cupric solution added, (b) two drops of cupric solution added, (c) three drops of cupric solution added, (d) four drops of cupric solution added.

Class 2: Oscillations of the current only under potentiostatic conditions with sufficiently large ohmic drop

Class 3: Potential oscillations under galvanostatic conditions and current oscillations under potentiostatic conditions with sufficiently large ohmic drop

For a system to belong to class 1, the experimental condition should be such that the ohmic potential drop can be safely neglected. Only a very few systems belong to this class. The distinction between class 2 and class 3 lies in current-voltage curves and the impedance at low frequencies. Fig. 6.6 shows the measured current-voltage curves for the mixed solution under potential control (solid line) and under galvanic control (dotted line). The curve for potential control has a steep decline in current at -1.0 V. This region of negative slope indicates the presence of a negative impedance (see further). The current-voltage curve under galvanic control is a

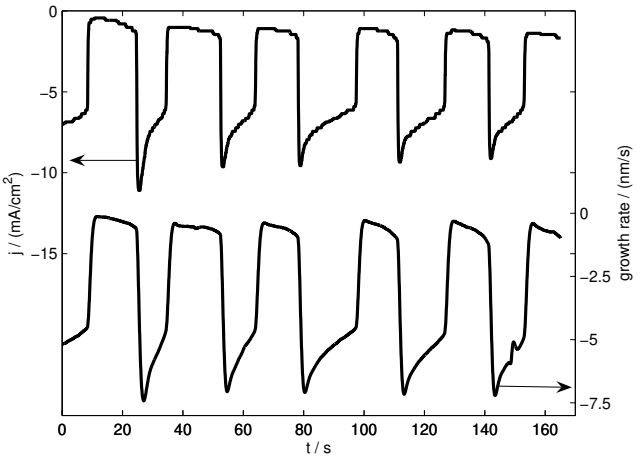

Figure 6.5: Current density (upper curve) and growth rate of the deposited copper layer (lower curve) as a function of time in the mixed Cu^{2+}/Cu^{+} solution.

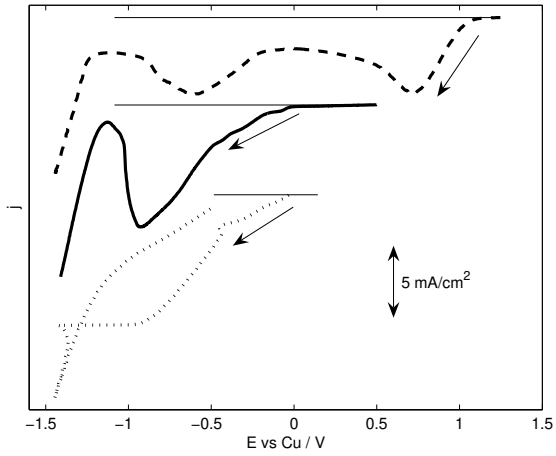

Figure 6.6: Potential scan (−) at 20 mV s^{-1} and current scan (··) at 20 mA dm^{-2} s^{-1} in the mixed Cu^{2+}/Cu^{+} solution. The $j - E$ curve under potential control clearly resembles the shape of the letter N. (−−): Potential scan of the cupric solution.

good resemblance for the potential-controlled curve, but when -1.0 V is reached an abrupt overshoot takes place. In the backward scan, the measured potential follows a different path than that of the forward scan. This is typical for a so-called N-type negative differential resistance (N-NDR) electrochemical oscillator in which the $j - E$ curve resembles the shape of the letter N [21]. Fig. 6.6 also shows a potential scan from the cupric solution (no Cu^+ ions present). The peak around 0.7 V is due to the reduction of Cu^{2+} into Cu^+. The peak around -0.5 V is caused by the deposition of copper metal. The decrease in current for potential values more negative than -0.5 V is less steep than the current drop in the mixed Cu^{2+}/Cu^+ solution. This indicates that the peak in the cupric solution is simply based on a diffusion limited process and so: no oscillations appear in this solution (see also Fig. 6.2(a)).

The Nyquist and phase angle plots of the impedance spectrum for polarizations at -0.5 V and -1.0 V in the mixed solution are given in Fig. 6.7. At -0.5 V, a potential at which no oscillations occurred, the Nyquist plot (Fig. 6.7(a)) showed the classic curve with a semicircle and straight line, inclined at 45 ° with the real axis, due to the double layer capacitance C_{dl} in parallel with a series connection of the charge transfer resistance R_{ct}, the resistance for current flow through the electrolyte-electrode interface, and a Warburg impedance W, caused by diffusion of the electroactive species (Fig. 6.8). This line is built up clockwise if going from high to low frequencies. When the impedance spectrum was measured at a polarization of -1.0 V, the picture changed. The Nyquist plot develops anticlockwise and intersects the real axis a frequency of 0.3 Hz. The slope of the potential scan in Fig. 6.6 corresponds to $\frac{di}{dE}$ which is an inverse resistance R^{-1}. In the region with decreasing current this resistance R is equal to -15 Ω, a value which is close to the value for Z_{Re} at which the impedance spectrum intersects the real axis. The steep decline in the potential scan of Fig. 6.6, and the observation of current oscillations is explained by this negative impedance in the low frequency end of the spectrum. The presence of a negative real impedance in a potential region for a certain range of frequencies is a necessary condition for the occurrence of an electrochemical oscillator. Where the impedance spectrum crosses the real axis, the Bode plot shows a phase angle jump (Fig. 6.7(b)) and the frequency at which this happens (f = 0.3 Hz) corresponds to the initial frequency of the oscillations (Fig. 6.2). The fact that the real impedance of the lowest frequency is negative shows this electrochemical oscillator is an oscillator of class 2. To belong to class 3, the low frequency end of the impedance spectrum should have positive real impedances, thereby hiding the negative impedances from the current-voltage curve.

The influence of temperature on the oscillations is presented in Fig. 6.9. Platinum electrodes were polarized at -1.0 V in the temperature range 70 °C − 120 °C. The graphs show that the time interval during which oscillations occur, decreases with

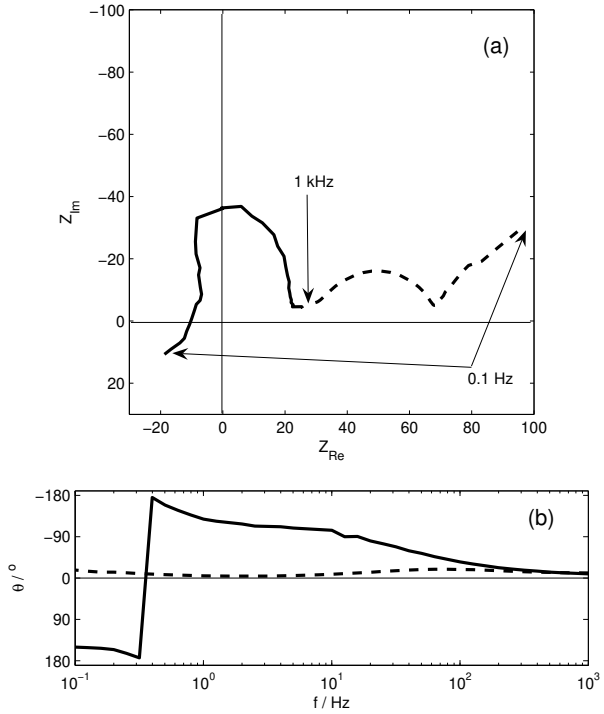

Figure 6.7: Impedance spectrum (0.1−1000 Hz) of the mixed Cu^{2+}/Cu^{+} solution at two polarization potentials. (- -) -0.5 V, (−) -1.0 V. (a) Nyquist plot, (b) Bode plot.

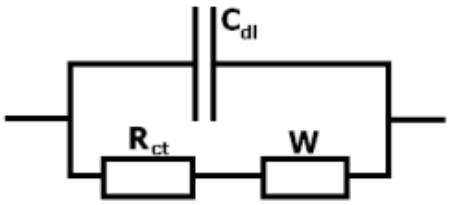

Figure 6.8: Simple equivalent circuit of an electrode indicating the meaning of the double layer capacitance C_{dl}, the charge transfer resistance R_{ct} and the Warburg impedance W.

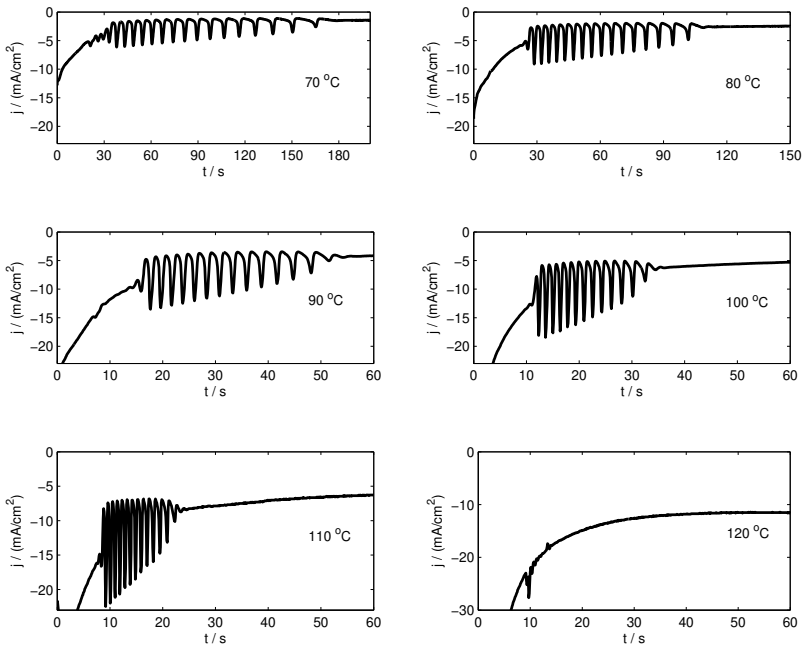

Figure 6.9: Polarization at -1.0 V for different temperatures in the mixed Cu^{2+}/Cu^{+} solution.

increasing temperature. The oscillations go on for almost 3 minutes at 70 °C, while at 110 °C they only last for about 15 s and only a few ripples remain at 120 °C. The frequencies of the oscillations increase with increasing temperature: at 70 °C the frequency is 0.2 Hz, at 110 °C the current oscillates at 1.1 Hz. The data are summarized in Table 6.1. A possible explanation for the effect of the temperature might be the reduced viscosity at elevated temperatures and the different diffusivity for cuprous and cupric ions. The diffusion coefficient for Cu^{2+} is often lower than for Cu^{+}, both in aqueous as in non-aqueous solvents [40, 41]. From Fig. 6.4 it is clear that oscillations only appear if the concentrations of Cu^{+} and Cu^{2+} are within a certain range. At the low temperature of 70 °C, the relatively high viscosity causes a slow diffusion so that it takes more than 30 s before the right concentrations are reached and the oscillations can start (Fig. 6.9), but it takes also a long time before the concentrations are such that the oscillating behavior can no longer be sustained. If the temperature is increased, the oscillations set in sooner, but also end quicker due to the increased diffusion. This causes that

Table 6.1: Influence of the temperature on the oscillating behavior

Temperature (°C)	Duration (s)	Frequency (Hz)
70	160	0.2
80	80	0.3
90	41	0.5
100	24	0.7
110	15	1.1
120	no clear oscillations observed	

the concentration range for which oscillations are observed is traversed faster. At 120 °C, that concentration range is passed through so quickly that hardly any oscillations can be measured.

Other ionic liquids and organic solvents

The system that we have described so far consisted of the $[C_2mim]^+$ cation and Cl^- that acts as anion of the ionic liquid and counter ion for the copper ions. By systematically replacing ions from the system, information was gathered about the oscillating reactions. The results obtained in different solvents are summarized in Table 6.2. Solution `A` was the original mixture. All these solutions were tested at 90 °C, unless this temperature was outside the liquidus range. A potential scan was recorded in all solutions and tested for the presence of a potential region with steeply decreasing current (N-shaped curve), indicating the presence of a negative resistance. If such potential was found, potentiostatic experiments were conducted to test if oscillations occurred. It turned out that, if an N-shaped curve was recorded in the potential scan, oscillations were noticed in the potentiostatic regime and vice versa: if no N-shape was observed, no oscillations appeared. In a first step, Cl^- was replaced by the bis(trifluoromethylsulfonyl)imide ion ($[Tf_2N]^-$) as counterion for copper (solution `B` in Table 6.2). In this solution, oscillations were found. A next step was to try a solution without Cl^- present. Therefore the ionic liquid $[C_2mim][Tf_2N]$ was used with $Cu(Tf_2N)_2$ as source for copper ions (solution `C`). In this mixture, no oscillations could be detected what indicates that chloride complexes of copper are involved in the oscillating behavior. The appearance of oscillations in solution `B` is then no surprise since it is well known that Cl^- forms more stable complexes than the weakly coordinating $[Tf_2N]^-$ anion. Solution `D` was prepared to investigate the influence of alkyl chain length: if the length of the alkyl chain on the imidazolium structure is increased by replacing $[C_2mim]^+$ with $[C_4mim]^+$, oscillations still occur. To test whether oscillations always occur when Cu^+, Cu^{2+} and Cl^- are collectively dissolved, solutions in acetonitrile were prepared with dissolved tetraethylammonium chloride (Et_4NCl)

Table 6.2: Mixtures investigated for oscillations

	Solvent-cation	solvent-anion	Counter ion for copper	N-shape? Oscillations?
A	$[C_2mim]^+$	Cl^-	Cl^-	yes
B	$[C_2mim]^+$	Cl^-	$[Tf_2N]^-$	yes
C	$[C_2mim]^+$	$[Tf_2N]^-$	$[Tf_2N]^-$	no
D	$[C_4mim]^+$	Cl^-	Cl^-	yes
E[a]	acetonitrile-Et_4N^+	acetonitrile-Cl^-	Cl^-	no
F	$[P_{4,4,4,14}]^+$	Cl^-	Cl^-	no
G[b]	$[C_4pyr]^+$	Cl^-	Cl^-	no
H[c]	$[C_4dmim]^+$	Cl^-	Cl^-	yes

[a]at 30 °C, [b]at 150 °C, [c]at 110 °C

as supporting electrolyte (solution E). Et_4NCl also acts as supplier of excess Cl^- ions. They did not lead to oscillations, despite the presence of Cu^+, Cu^{2+} and Cl^-. Neither did solutions in which $[C_2mim]Cl$ was replaced by tributyltetradecylphosphonium chloride ($[P_{4,4,4,14}]Cl$) or *N*-butylpyridinium chloride ($[C_4pyr]Cl$) lead to oscillations (solutions F and G). The observations that the oscillations were observed for both the imidazolium chloride ionic liquids $[C_2mim]Cl$ en $[C_4mim]Cl$ and that the presence of chloride is required, suggested the formation of a copper carbene complex at the cathode, and more particularly a Cu^+-imidazol-2-ylidene chloride carbene complex [42]. In such a complex the Cu^+ ion is coordinated to the C2-position of the imidazole ring and to the chloride ion. To test this hypothesis of carbene formation, experiments were performed in the ionic liquid 1-butyl-2,3-dimethylimidazolium chloride, $[C_4dmim]Cl$ (solution H). In this ionic liquids, the methyl group on the carbon atom in the 2 position prevents the carbene formation. Since oscillations were observed in this system as well, the hypothesis of the copper carbene formation can be refuted.

Conclusions

A solution of the ionic liquid 1-ethyl-3-methylimidazolium chloride in which both Cu^{2+} and Cu^+ are present, gives rise to oscillating currents during constant polarization at -1.0 V. The electrochemical oscillator is an N-NDR-type because the low frequency-end of the impedance spectrum has negative real impedances and the steep decrease in current in the potential-current curve. It is further shown that the oscillating current leads to an oscillating growth speed during the deposition of the metallic copper layer. It was found that the presence of chloride is a necessary, yet not a sufficient condition for the occurrence of current oscillations and that the imidazolium cation also plays a role. The length of the alkyl chain is

less important than the structure of the cation since oscillations can be observed in both [C_2mim]Cl and [C_4mim]Cl.

Acknowledgements

This research was funded by a Ph.D grant of the Institute for the Promotion of Innovation through Science and Technology in Flanders (IWT-Vlaanderen) to S.S. The authors acknowledge financial support by the K.U.Leuven (projects IDO/05/005 and GOA 08/05), by the FWO-Flanders (research community "Ionic Liquids"), by the IWT-Flanders (SBO-project IWT 80031 "MAPIL") and the support of the Belgian Federal Science Policy Office through the IUAP project INANOMAT (contract P6/17). This work is supported in part by the European Commissions Seventh Framework Programme (FP7) under Grant Agreement number 216474 (CopPeR). Support by IoLiTec (Heilbronn, Germany) is also acknowledged.

References

[1] G. Baier, U. Kummer, S. Sahle, An electrochemically induced oscillatory instability, *J. Phys. Chem. A*, **103**, 33 (1999).

[2] J. Lee, P. Strasser, M. Eiswirth, G. Ertl, On the origin of oscillations in the electrocatalytic oxidation of HCOOH on a Pt electrode modified by Bi deposition, *Electrochim. Acta*, **47**, 501 (2001).

[3] J. Lee, C. Eickes, M. Eiswirth, G. Ertl, Electrochemical oscillations in the methanol oxidation on Pt, *Electrochim. Acta*, **47**, 2297 (2002).

[4] I. Jung, D. Kim, J. Lee, I. Oh, H. Y. Ha, Y. Tak, Electrochemical oscillations in the HCHO oxidation on a Pt electrode, *J. Ind. Eng. Chem.*, **9**, 159 (2003).

[5] J. C. K. Ho, D. L. Piron, J. St-Pierre, Cathodic potential oscillations of Fe(III) reduction on Pb and Zn in 1 M NaCl solution under galvanostatic conditions, *J. Electrochem. Soc.*, **144**, 3367 (1997).

[6] E. W. Bohannan, L.-W. Huang, F. S. Miller, M. G. Shumsky, J. A. Switzer, In situ electrochemical quartz crystal microbalance study of potential oscillations during the electrodeposition of Cu/Cu_2O layered nanostructures, *Langmuir*, **15**, 813 (1999).

[7] S. Leopold, H. Herranen, J.-O. Carlsson, Spontaneous potential oscillations in the Cu(II)/tartrate and lactate systems, aspects of mechanisms and film deposition, *J. Electrochem. Soc.*, **148**, C513 (2001).

[8] S. Leopold, I. U. Schuchert, J. Lu, M. E. Toimil Molares, M. Herranen, J.-O. Carlsson, Electrochemical deposition of cylindrical Cu/Cu_2O microstructures, *Electrochim. Acta*, **47**, 4393 (2002).

[9] J. Eskhult, M. Herranen, L. Nuholm, On the origin of the spontaneous potential oscillations observed during galvanostatic deposition of layers of Cu and Cu_2O in alkaline citrate solutions, *J. Electroanal. Chem.*, **594**, 35 (2006).

[10] M.-Z. Zhang, M. Wang, Z. Zhang, J.-M. Zhu, R.-W. Peng, N.-B. Ming, Periodic structures of randomly distributed Cu/Cu_2O nanograins and periodic variations of cell voltage in copper electrodeposition, *Electrochim. Acta*, **49**, 2379 (2004).

[11] R. Saliba, C. Mingotaud, F. Argoul, S. Ravaine, Spontaneous oscillations in gold electrodeposition, *Electrochem. Commun.*, **4**, 629 (2002).

[12] F. W. Schlitter, G. Eichkorn, H. Fischer, Rhythmic lamellar crystal growth in electrolytic copper deposition, *Electrochim. Acta*, **13**, 2063 (1968).

[13] R. Nakanishi, S. Sakai, K. Nishimura, Y. Nakato, Layer-by-layer electrodeposition of copper in the presence of *o*-phenanthroline, caused by a new type of hidden NDR oscillation with the effective electrode surface area as the key variable, *J. Phys. Chem. B*, **109**, 18846 (2005).

[14] A. Survila, Z. Mockus, R. Juškėnas, Current oscillations observed during codeposition of copper and tin from sulfate solutions containing Laprol 2402C, *Electrochim. Acta*, **43**, 909 (1998).

[15] A. Survila, Z. Mockus, Current oscillations and a negative impedance observed during copper and tin codeposition from solutions involving Laprol 2402C as a surface-active substance, *Electrochim. Acta*, **44**, 1707 (1999).

[16] S. Sakai, S. Nakanishi, K. Fukami, Y. Nakato, Oscillation-induced layer-by-layer electrodeposition producing alternate metal and metal-alloy multilayers on a nanometer scale, *Chem. Lett.*, **6**, 640 (2002).

[17] S. Nakanishi, S. Sakai, T. Nagai, Y. Nakato, Macroscopically uniform nanoperiod alloy multilayers formed by coupling of electrodeposition with current oscillations, *J. Phys. Chem. B*, **109**, 1750 (2005).

[18] M. T. M. Koper, *Far-from-equilibrium phenomena in electrochemical systems*, PhD thesis, Utrecht (1994).

[19] M. T. M. Koper, J. H. Sluyters, Electrochemical oscillators: their description through a mathematical model, *J. Electroanal. Chem.*, **303**, 73 (1991).

[20] M. T. M. Koper, Stability study and categorization of electrochemical oscillators by impedance spectroscopy, *J. Electroanal. Chem.*, **409**, 175 (1996).

[21] P. Strasser, M. Eiswirth, M. T. M. Koper, Mechanistic classification of electrochemical oscillators - an operational experimental strategy, *J. Electroanal. Chem.*, **478**, 50 (1999).

[22] K. Krischer, Nonlinear dynamics in electrochemical systems, In: *Advances in Electrochemical Science and Engineering,* Ed.: R. C. Alkire, D. M. Kolb. Wiley-VCH (2003).

[23] P. Bonhôte, A.-P. Dias, N. Papageorgiou, K. Kalyanasundaram, M. Grätzel, Hydrophobic, highly conductive ambient-temperature molten salts, *Inorg. Chem.*, **35**, 1168 (1996).

[24] J. Sun, M. Forsyth, D. R. MacFarlane, Room-temperature molten salts based on the quaternary ammonium ion, *J. Phys. Chem. B*, **102**, 8858 (1998).

[25] C. L. Hussey, Room temperature haloaluminate ionic liquids. novel solvents for transition metal solution chemistry, *Pure & Appl. Chem.*, **60**, 1763 (1988).

[26] M. Hirao, H. Sugimoto, H. Ohno, Preparation of novel room-temperature molten salts by neutralization of amines, *J. Electrochem. Soc.*, **147**, 4168 (2000).

[27] J. Dupont, P. A. Z. Suarez, Physico-chemical processes in imidazolium ionic liquids, *Phys. Chem. Chem. Phys.*, **8**, 2441 (2006).

[28] Ed.: P. Wasserscheid, T. Welton, *Ionic liquids in synthesis*, Wiley-VCH, Weinheim (2003).

[29] S. Zein El Abedin, F. Endres, Ionic liquids: The link to high-temperature molten salts?, *Acc. Chem. Res.*, **40**, 1106 (2007).

[30] D. R. MacFarlane, K. R. Seddon, Ionic liquids - progress on the fundamental issues, *Aust. J. Chem.*, **60**, 3 (2007).

[31] R. Hagiwara, J. S. Lee, Ionic liquid for electrochemical devices, *Electrochemistry*, **75**, 23 (2007).

[32] M. C. Buzzeo, R. G. Evans, R. G. Compton, Non-haloaluminate room-temperature ionic liquids in electrochemistry - a review, *ChemPhysChem*, **5**, 1106 (2004).

[33] F. Endres, S. Zein El Abedin, Air and water stable ionic liquids in physical chemistry, *Phys. Chem. Chem. Phys.*, **8**, 2101 (2006).

[34] M. Galiński, A. Lewandowski, I. Stępniak, Ionic liquids as electrolytes, *Electrochim. Acta*, **55**, 5567 (2006).

[35] A. P. Abbott, K. J. McKenzie, Application of ionic liquids to the electrodeposition of metals, *Phys. Chem. Chem. Phys.*, **8**, 4265 (2006).

[36] Eds.: H. Ohno, *Electrochemical aspects of ionic liquids*, John Wiley & Sons, New York (2005).

[37] Ed.: F. Endres, A. P. Abbott, D. R. MacFarlane, *Electrodeposition from ionic liquids*, Wiley-VCH, Weinheim (2008).

[38] Y. Andriyko, A. Andriiko, O. B. Babushkina, G. E. Nauer, Electrochemistry of TiF_4 in 1-butyl-2,3-dimethylimidazolium tetrafluoroborate, *Electrochim. Acta*, **55**, 1081 (2010).

[39] F. G. Cottrell, Der Reststrom bei galvanischer Polarisation betrachtet als ein Diffusionsproblem, *Z. Phys. Chem.*, **42**, 385 (1903).

[40] G. W. Tindall, S. Bruckenstein, Determination of heterogeneous equilibrium constants by chemical stripping at a ring-disk electrode - evaluation of equilibrium constant for reaction copper + copper(II) = 2 copper(I) in 0.2 M sulfuric acid, *Anal. Chem.*, **40**, 1402 (1968).

[41] R. B. Bessette, J. W. Olver, Measurement of diffusion coefficients for reduction of copper(I) and (II) in acetonitrile, *J. Electroanal. Chem.*, **21**, 525 (1969).

[42] J. C. Y. Lin, R. T. W. Huang, C. S. Lee, A. Bhattacharyya, W. S. Hwang, I. J. B. Lin, Coinage metal - *N*-heterocyclic carbene complexes, *Chem. Rev.*, **109**, 3561 (2009).

Chapter 7

Modeling of aluminium deposition from chloroaluminate ionic liquids

Published as S. Schaltin, M. Ganapathi, K. Binnemans and J. Fransaer, *J. Electrochem. Soc.*, **158**, D634-D639 (2011)

Abstract

A finite-element model of the electrodeposition of aluminium from chloroaluminate ionic liquids is introduced. The purpose of this model is to give an explanation for the reasonable current densities that can be achieved in chloroaluminate ionic liquids despite the fact that the electrochemically active $Al_2Cl_7^-$ complexes are transformed into inactive $AlCl_4^-$ complexes during the electrodeposition of aluminium. The obtainable current density in the electrodeposition from chloroaluminate ionic liquids strongly depends on the chemical rate constants for establishing the equilibrium $Al_2Cl_7^- + Cl^- \rightleftharpoons 2AlCl_4^-$. A high current (up to 3000 A m^{-2}) was found for both high and low rate constants whereas a minimum current (200 A m^{-2}) was found for intermediate rate constants due to kinetics and thermodynamics. The model is compared to experiments conducted in the ionic liquid $AlCl_3$ - $[C_2mim]Cl$ (60/40 mol%) where $[C_2mim]Cl$ is 1-ethyl-3-methylimidazolium chloride.

Introduction

The electrodeposition of aluminium from ionic liquids was reported for the first time by Hurley and Wier in 1951 [1]. Within the field of the electrodeposition of metals from ionic liquids, the electrodeposition of aluminium is by far the most investigated topic. A possible application for electrodeposited aluminium is as surface coatings for corrosion protection in marine environments, where zinc coatings cannot be used due to chemical reactions with sea salt. The electrodeposition of aluminium is often carried out from chloroaluminates [2–22]. These are binary mixtures of $AlCl_3$ with quaternary ammonium, imidazolium or pyridinium salts. In these solutions, the mole fraction of $AlCl_3$ should be higher than 0.5 (Lewis acidic solutions) to get the electrochemically active $Al_2Cl_7^-$ complex in the melt. For a mole fraction smaller than 0.5 (Lewis basic melts), the sole aluminium species is $AlCl_4^-$ which is not electrochemically active within the electrochemical window of the organic cations. The electrodeposition of aluminium alloys is also a widely investigated topic [20–31].

The net reaction in the deposition of aluminium from acidic chloroaluminates is [32]:

$$4Al_2Cl_7^- + 3e^- \rightarrow Al + 7AlCl_4^- \tag{7.1}$$

This reaction is the sum of

$$Al_2Cl_7^- + 3e^- \rightarrow Al + AlCl_4 + 3Cl^- \tag{7.2}$$

$$3Cl^- + 3Al_2Cl_7^- \rightarrow 6AlCl_4^- \tag{7.3}$$

in which $Al_2Cl_7^-$ can be viewed as a molecule of $AlCl_3$ solvated by $AlCl_4^-$ [32]. The sum of both reactions can be considered as an electrochemical-chemical mechanism (EC mechanism) where a product of the electrochemical reaction, Cl^-, reacts with the solvent to produce a species that is electrochemically inactive [33]. Since $AlCl_4^-$ cannot be reduced within the electrochemical window of $[C_2mim]Cl$, only one out of two aluminium ions of $Al_2Cl_7^-$ is reduced. The liberated chloride ions react further according to reaction (7.3) and if this reaction goes fast, both reactions can be written simultaneously as reaction (7.1). The sum reaction indicates that only one out of eight aluminium ions is reduced to metallic aluminium and that the other ions become unavailable for reduction since they are transformed into the electrochemically inactive $AlCl_4^-$ ion. However, reasonable current densities ($500-1000$ A m^{-2}) can be achieved during the electrodeposition of aluminium from chloroaluminate ionic liquids. This suggests that reaction (7.1), although macroscopically correct, might not be the real reaction happening at the electrode's surface. In this paper we propose an extension of reaction (7.1) by taking into account the kinetics of reaction (7.3).

Model

The modeling of the electrodeposition of aluminium on a rotating disk electrode from chloroaluminate ionic liquids is based on a one-dimensional model (figure 7.1). Point A represents the working electrode and point B the bulk solution. It

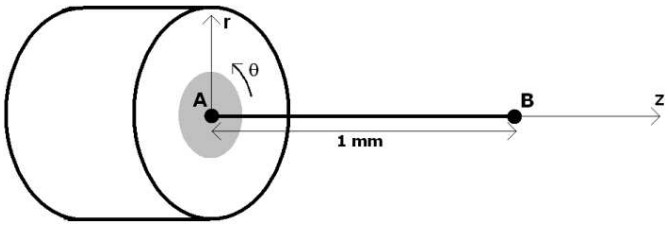

Figure 7.1: Schematic representation of the one-dimensional model: point A represents the active area of a rotating disk electrode and point B the bulk solution.

is assumed that bulk conditions are valid at a distance of 1 mm from the working electrode. This assumption will be validated (*vide infra*). The modeled solution is $AlCl_3$ - $[C_2mim]Cl$ (60/40 mol%) where $[C_2mim]Cl$ is 1-ethyl-3-methylimidazolium chloride. Bulk concentrations of both $Al_2Cl_7^-$ and $AlCl_4^-$ are equal to 1981 mol m^{-3} [34].

The net deposition reaction (7.1) is not suitable as the starting equation for the model. It does not give information on the different steps in the electrodeposition process and it does not consider the presence of *free* Cl^- ions, i.e. ions that are not bound to Al^{3+}. Therefore reaction (7.1) is rewritten in a similar way as Lai and Skyllas-Kazacos [8]:

$$4Al_2Cl_7^- + 3e^- \rightarrow Al + 4AlCl_4^- + 3AlCl_4^- \tag{7.4}$$

Three Al^{3+} ions are no longer considered to form a complex with chlorides and are regarded as *free* ions:

$$4Al_2Cl_7^- + 3e^- \rightarrow Al + 4AlCl_4^- + 3Al^{3+} + 12Cl^- \tag{7.5}$$

These three *free* Al^{3+} ions can be reduced, and this requires 9 additional electrons to the left-hand side of the reaction:

$$4Al_2Cl_7^- + 12e^- \rightarrow 4Al + 4AlCl_4^- + 12Cl^- \tag{7.6}$$

Dividing both sides by 4 gives:

$$Al_2Cl_7^- + 3e^- \rightarrow Al + AlCl_4^- + 3Cl^- \tag{7.7}$$

which is again equation (7.2). Equations (7.4) to (7.6) clarify the origin of equation (7.2). If the $Al_2Cl_7^-$ ion is considered as a molecule of $AlCl_3$ solvated by $AlCl_4^-$ [32], reaction (7.7) represents that one aluminium ion is reduced and that the solvating $AlCl_4^-$ is liberated together with three chloride ions, which acted as ligands for Al^{3+}. Reaction (7.7) can be used to study the complex formation behavior as it contains the three relevant species Cl^-, $Al_2Cl_7^-$ and $AlCl_4^-$. The equilibrium between these anions is expressed by the following autosolvolysis reaction:

$$Al_2Cl_7^- + Cl^- \underset{k_b}{\overset{k_f}{\rightleftharpoons}} 2AlCl_4^- \tag{7.8}$$

in which k_f and k_b are the rate constants for the forward and backward reaction, respectively. This reaction is the $AlCl_3$-$[C_2mim]Cl$ solvent system equivalent of the autoionization reaction of water (with OH^- the basic species and H_3O^+ the acidic species) but with Cl^- as the Lewis basic species and $Al_2Cl_7^-$ as the Lewis acidic species [32]. Reaction (7.7) was also used by Lai and Skyllas-Kazacos [8], and if reaction (7.8) goes fast, it would yield the net reaction (7.1). The equilibrium constant for reaction (7.8) is given by the expression

$$K_{eq} = \frac{\left[AlCl_4^-\right]^2}{\left[Al_2Cl_7^-\right]\left[Cl^-\right]} = \frac{k_f}{k_b} \tag{7.9}$$

Literature values for the equilibrium constant K_{eq} in $AlCl_3$ - $[C_2mim]Cl$ solutions are given in table 7.1.

Table 7.1: Values for the equilibrium constant K_{eq} at different temperatures

$\log K_{eq}$	T (^{o}C)	Ref.
17	RT	[30]
17.1	40	[34]
16.3	40	[7]
16.1	50	[7]
15.5	60	[7]

In our model, the time-dependent reaction-convection-diffusion equation

$$\frac{\partial c}{\partial t} = R - \mathbf{u} \cdot \nabla c + D\nabla^2 c \tag{7.10}$$

is solved for the three species of interest: Cl^-, $Al_2Cl_7^-$ and $AlCl_4^-$. In this equation, c represents the concentration (mol m^{-3}), D the diffusion coefficient (m^2 s^{-1}), R the reaction rates for the species in the bulk (mol m^{-3} s^{-1}) and $\mathbf{u}$ the fluid velocity

vector (m s^{-1}). The time-dependent reaction-convection-diffusion equation gives the time-gradient of the concentration as a function of diffusion $D\nabla^2 c$, convection $\mathbf{u}\cdot\nabla c$ and the bulk reaction rate R. It is assumed that the reaction rate R is given by

$$R = k_b \left[AlCl_4^-\right]^2 - k_f \left[Al_2Cl_7^-\right]\left[Cl^-\right] \tag{7.11}$$

The bulk reaction rate of any ion under investigation is a measure for the amount of that ion that is generated (or consumed) due to reaction (7.8). Therefore following conditions hold for the generation of $Al_2Cl_7^-$ and Cl^-: $R_{Al_2Cl_7^-} = R_{Cl^-} = R$, because $Al_2Cl_7^-$ and Cl^- react in a 1:1 ratio and for $AlCl_4^-$, $R_{AlCl_4^-} = -2R$ since two $AlCl_4^-$ ions are formed for every reaction between $Al_2Cl_7^-$ and Cl^-. The negative sign in the expression for $R_{AlCl_4^-}$ indicates that the formation of $AlCl_4^-$ proceeds in the opposite reaction as for $Al_2Cl_7^-$ and Cl^-. This is obvious from reaction (7.8). The fluid velocity vector $\mathbf{u}$, caused by the rotation of a rotating disc electrode, consists of three components: the normal velocity $\mathbf{u}_z$, the radial velocity $\mathbf{u}_r$ and the angular velocity $\mathbf{u}_\theta$ (see figure 7.1). Since convectional mass transport $\mathbf{u}\cdot\nabla c$ mostly take place in the normal direction, $\mathbf{u}$ is simplified to a scalar function u which gives the fluid speed normal to a rotating disk electrode as a function of the distance z towards the electrode. This scalar velocity u is calculated by use of the coefficients from Fransaer *et al.* [35]

The boundary conditions at point B are the bulk concentrations: $\left[Al_2Cl_7^-\right]_{bulk} = \left[AlCl_4^-\right]_{bulk} = 1981$ mol m^{-3} and $\left[Cl^-\right]_{bulk} = \frac{\left[AlCl_4^-\right]^2_{bulk}}{\left[Al_2Cl_7^-\right]_{bulk}\cdot K_{eq}}$. The boundary conditions for point A are the molar fluxes J for all three species: $J_{Al_2Cl_7^-}$, $J_{AlCl_4^-}$ and J_{Cl^-}. Both $J_{AlCl_4^-}$ and J_{Cl^-} are dependent on $J_{Al_2Cl_7^-}$. This is because as $AlCl_4^-$ and Cl^- are formed during the electrodeposition from aluminium (reaction (7.7)). Since one $AlCl_4^-$ ion and three Cl^- ions are formed for every $Al_2Cl_7^-$ ion that is reduced, the following two equations hold:

$$J_{AlCl_4^-} = -J_{Al_2Cl_7^-} \tag{7.12}$$

$$J_{Cl^-} = -3J_{Al_2Cl_7^-} \tag{7.13}$$

$J_{Al_2Cl_7^-}$, evaluated on the electrode surface, is based on a Butler-Volmer relationship:

$$J_{Al_2Cl_7^-} = k^o_{ox} \exp\left(\frac{\beta n\ \mathrm{F}}{\mathrm{R}_g T}\eta\right) - \left[Al_2Cl_7^-\right]_{surf}\ k^o_{red} \exp\left(-\frac{\alpha n\ \mathrm{F}}{\mathrm{R}_g T}\eta\right) \tag{7.14}$$

In equation (7.14), k^o_{ox} and k^o_{red} are the heterogeneous rate constants for oxidation and reduction, α and β are the charge transfer coefficients, n the number

of exchanged electrons from reaction (7.7), F the Faraday constant, R_g the gas constant, T the temperature and η the overpotential. η is determined by the potential difference ΔE, applied by a potentiostat between the working and reference electrode, but corrected for the concentration overpotential η_c:

$$\Leftrightarrow \eta = \Delta E - \eta_c = E - \frac{R_g T}{n\mathrm{F}} \ln\left(\frac{\left[Al_2Cl_7^-\right]_{surf}}{\left[Al_2Cl_7^-\right]_{bulk}}\right) \tag{7.15}$$

With these relationships the model can be solved. In reality, k_f and k_b are constants but are in this model considered as variables since their exact values are unknown, only their ratio is known via equation (7.9). The model is therefore solved for several values of k_b, the corresponding value for k_f is then $k_f = k_b \cdot K_{eq}$. An estimate for the value of k_b is based on a comparison between the experimental and calculated limiting current densities j_L (*vide infra*).

Results and discussion

The presented current density versus time curves and concentration profiles are valid for a potentiostatic polarization at -0.75 V for a disk electrode at rest, and rotating at 100 rotations per minute (rpm). The resulting calculated current density-time curves are presented in figure 7.2. As expected, the current density is higher for the stirred solution than for the unstirred one and reaches a steady-state value whereas a continuous decline in current is visible for the unstirred solution. Less evident is the relationship between the current and the rate constant k_b: the highest currents are calculated for $k_b = 10^{-25}$ and $k_b = 10^{-5}$ m^3 mol^{-1} s^{-1} and a minimum in current can be found for $k_b = 10^{-8}$ m^3 mol^{-1} s^{-1}. Other values for k_b lead to intermediate values for the current density. This observation holds for both rotation speeds. The concentration profiles near the electrode after 100 s are shown in figure 7.3. To keep the graphs simple, only the curves for $k_b = 10^{-25}$, 10^{-8} and 10^{-5} m^3 mol^{-1} s^{-1} were plotted. These figures show that the assumption of bulk concentrations at $z = 1$ mm is correct: even for the unstirred solution, the concentrations do not deviate from the bulk concentrations for $z > 0.4$ mm. The concentration profile for $Al_2Cl_7^-$ does not depend on k_b on the scale of the figure and the curves for different k_b values can therefore not be separated. Only close to the electrode surface can the curves be distinguished, what explains the different current densities for varying k_b values. This is because the resulting current depends on the value of the slope of the concentration profile, evaluated at the electrode surface. For $AlCl_4^-$, the curves for $k_b = 10^{-8}$ and 10^{-5} m^3 mol^{-1} s^{-1} coincide, but the curve for $k_b = 10^{-25}$ has lower values in the diffusion layer. Also for Cl^- do the curves for $k_b = 10^{-8}$ and 10^{-5} m^3 mol^{-1} s^{-1} coincide with each other and the horizontal axis. The rotation speed does not alter the relative position of the curves for different k_b values. It only influences the thickness of the diffusion layer.

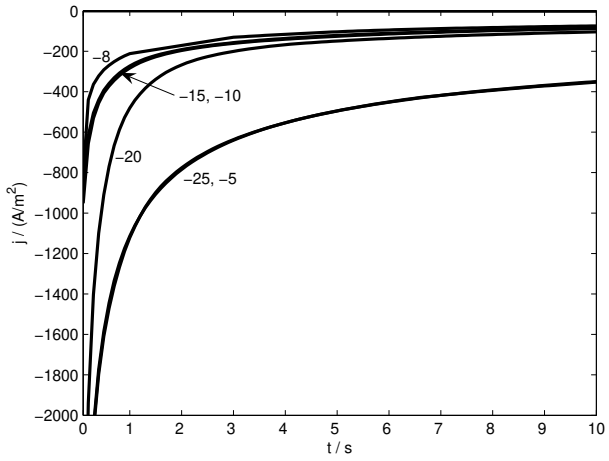

(a) 0 rpm

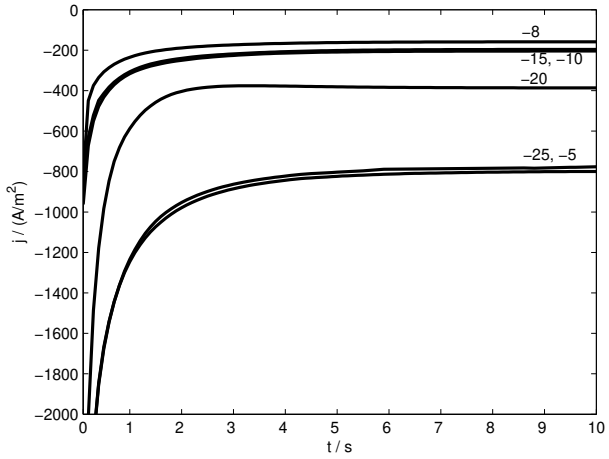

(b) 100 rpm

Figure 7.2: Calculated current densities for different rotation speeds. Only the first 10 s are shown. The numbers on the graph indicate different values for n in $k_b = 10^n$ m^3 mol^{-1} s^{-1}.

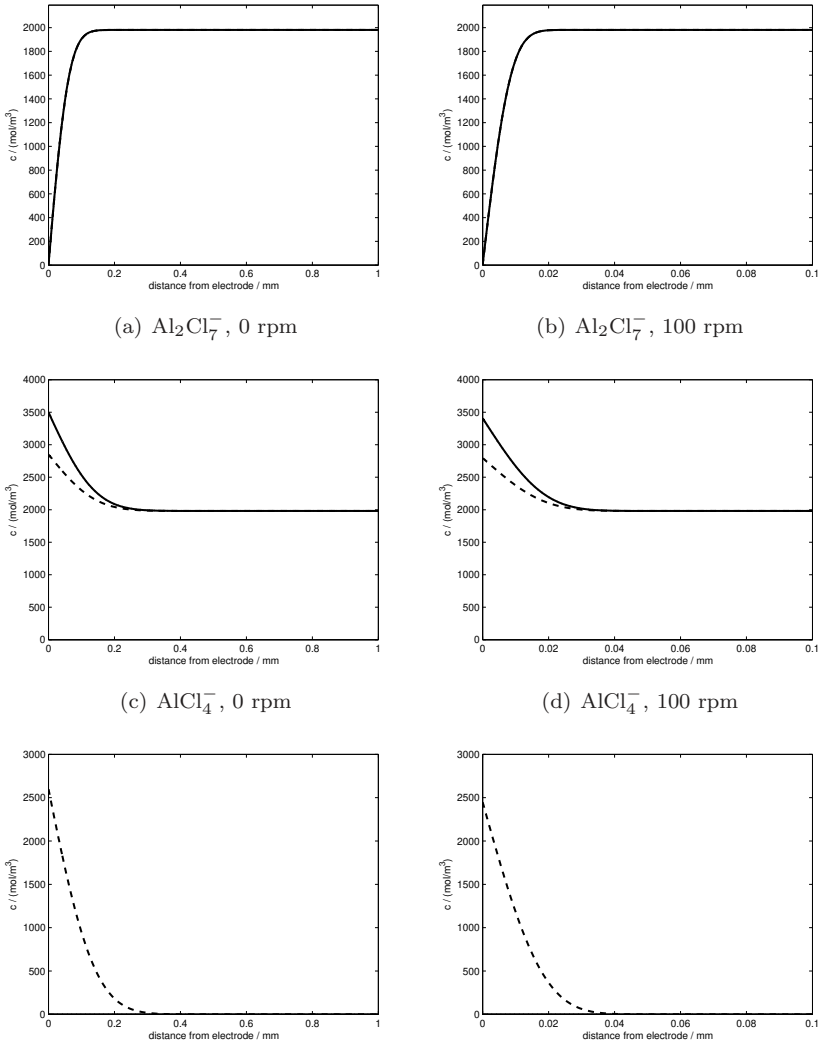

(a) $Al_2Cl_7^-$, 0 rpm

(b) $Al_2Cl_7^-$, 100 rpm

(c) $AlCl_4^-$, 0 rpm

(d) $AlCl_4^-$, 100 rpm

(e) Cl^-, 0 rpm

(f) Cl^-, 100 rpm

Figure 7.3: Calculated concentration profiles for $Al_2Cl_7^-$, $AlCl_4^-$ and Cl^- after 100 s at -0.75 V. (- -) $k_b = 10^{-25}$ m^3 mol^{-1} s^{-1}, (–) $k_b = 10^{-8}$ m^3 mol^{-1} s^{-1}, (··) $k_b = 10^{-5}$ m^3 mol^{-1} s^{-1}. The graphs are explained in the text. Please note that the scale on the horizontal axis is different for the two rotation speeds.

An ion of $Al_2Cl_7^-$ entering the diffusion layer has two possible reaction paths: it can react electrochemically according to reaction (7.7) by reaching the electrode thereby contributing to the current. The second possible outcome is that it reacts chemically according to reaction (7.8), a reaction that can take place in the entire diffusion layer and does not contribute to the current. The current is thus determined by the amount of $Al_2Cl_7^-$ ions that can diffuse through the diffusion layer without reacting according to reaction (7.8). Whether or not an incoming $Al_2Cl_7^-$ ion will transform into $AlCl_4^-$ depends on two opposite effects: kinetics and thermodynamics. The kinetics depend on k_f and k_b: the higher their values, the faster the forward and backward reactions in equation (7.8) will take place. The influence of thermodynamics is clarified in figure 7.4. This figure shows the ratios $\frac{[AlCl_4^-]^2}{[Al_2Cl_7^-][Cl^-]}$ and $\frac{[Al_2Cl_7^-]}{[Cl^-]}$, which are based on the calculated concentration profiles of figures 7.3. For $k_b = 10^{-25}$, 10^{-20} and 10^{-15} m^3 mol^{-1} s^{-1}, the ratio $\frac{[AlCl_4^-]^2}{[Al_2Cl_7^-][Cl^-]}$ is orders of magnitude smaller than the equilibrium value $\frac{[AlCl_4^-]^2}{[Al_2Cl_7^-][Cl^-]} = K_{eq} = 10^{17.1}$. For higher values of k_b, the curves are coincident with the vertical axis. This means that for $k_b = 10^{-25}$ m^3 mol^{-1} s^{-1}, there is a large thermodynamic tendency to convert $Al_2Cl_7^-$ into $AlCl_4^-$. This tendency decreases for increasing values of k_b as can be noticed in figure 7.4(a). With these data, the minimum in current as a function of k_b can now be explained. If $k_b = 10^{-25}$ m^3 mol^{-1} s^{-1}, the ratio $\frac{[AlCl_4^-]^2}{[Al_2Cl_7^-][Cl^-]}$ deviates considerably from the equilibrium value, meaning that an $Al_2Cl_7^-$ ion feels a large driving force to be converted to $AlCl_4^-$. Furthermore figure 7.4(b) shows that the ratio $\frac{[Al_2Cl_7^-]}{[Cl^-]}$ is smaller than 1 near the electrode's surface, meaning that there is a sufficient amount of Cl^- to react with $Al_2Cl_7^-$. Despite these observations a large current can flow because the speed of reaction to convert $Al_2Cl_7^-$ into $AlCl_4^-$ is very slow and a $Al_2Cl_7^-$ ion entering the diffusion layer can reach the electrode relatively unhindered. For a large rate constant k_b, the reaction $Al_2Cl_7^- + Cl^- \rightarrow 2AlCl_4^-$ proceeds quickly but the ratio $\frac{[AlCl_4^-]^2}{[Al_2Cl_7^-][Cl^-]}$ already equals the equilibrium value so an incoming $Al_2Cl_7^-$ ion can easily reach the electrode and contribute to the current. For intermediate values of k_b, the opposite influences of kinetics and thermodynamics lead to a minimum in the calculated current.

Determination of input data and comparison with experimental data

To determine input data for the model, such as diffusion coefficients and the heterogenous rate constant for reduction, linear potential scans were measured.

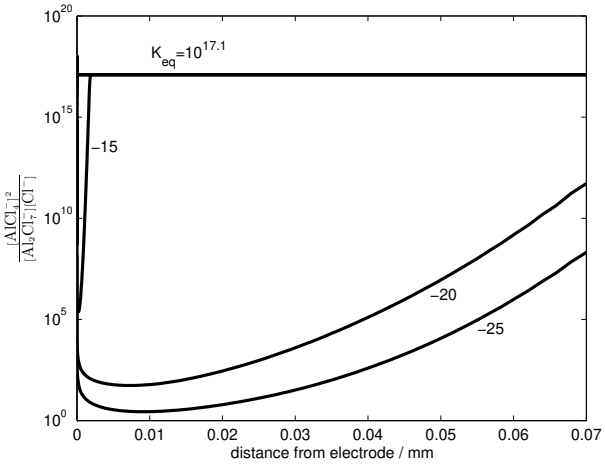

(a) ratio $\frac{[AlCl_4^-]^2}{[Al_2Cl_7^-][Cl^-]}$

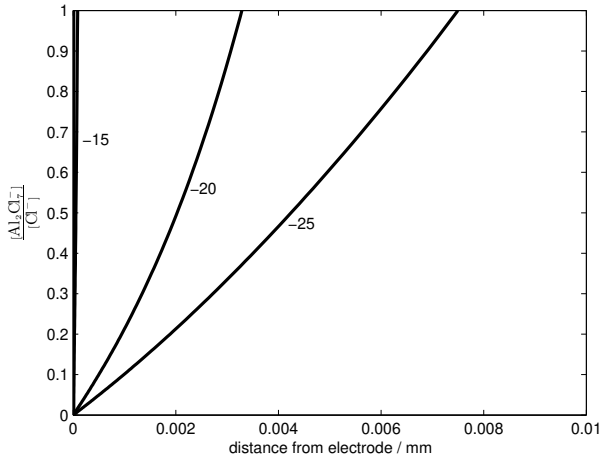

(b) ratio $\frac{[Al_2Cl_7^-]}{[Cl^-]}$

Figure 7.4: Calculated concentration ratios after 100 s at -0.75 V for the stirred solution. The numbers on the graph indicate different values for n in $k_b = 10^n$ m^3 mol^{-1} s^{-1}.

The experimental scans can also be compared with the results calculated by the model. These experiments were conducted at different rotation speeds in a mixture of $AlCl_3$ - [C_2mim]Cl (60-40 mol%) at 40 °C. Platinum was used as a working electrode, while an aluminium rod served as counter electrode, all potentials are referred to an aluminium pseudo-reference electrode. The recorded scans are presented in figure 7.5(a). For a potential of -0.75 V, the limiting current was reached for rotation speeds up to 400 rpm. The purpose was to find the diffusion coefficient $D_{Al_2Cl_7^-}$ of $Al_2Cl_7^-$ and the value for k^o_{red} by using the Koutecky-Levich equation [36]:

$$j_L^{-1} = \left[0.62n\mathrm{F}\left(D^{2/3}_{Al_2Cl_7^-}\right)\left(\nu^{-1/6}\right)\omega^{1/2}\left(c_{Al_2Cl_7^-}\right)\right]^{-1} + \left(n\mathrm{F}k^o_{red}c_{Al_2Cl_7^-}\right)^{-1} \tag{7.16}$$

If the inverse of the limiting current density $\left(j_L^{-1}\right)$ is plotted as a function of the square root of inverse rotation speed $\left(\omega^{-1/2}\right)$ a linear behavior should be observed. This is evident from figure 7.5(b). The dotted line is a fit through the experimental data points. From the slope of this fit, the diffusion coefficient can be calculated with a resulting value of $D_{Al_2Cl_7^-} = 1.17{\cdot}10^{-11}$ m^2 s^{-1}. For the calculation of this diffusion coefficient, n was taken as $n = 3$ thereby reflecting reaction (7.7). Literature values for the diffusion coefficient of $Al_2Cl_7^-$ at the same temperature of 40 °C in the same ionic liquid ([C_2mim]Cl) are given in reference [9]. The reported values for a platinum working electrode range from 0.55 to 3.33 $\cdot 10^{-11}$ m^2 s^{-1}. Although these literature values are based on $n = 0.75$ and reaction (7.1), the diffusion coefficient found in our work lies in the reported range. k^o_{red} is determined from the intercept with the vertical axis of the fit in figure 7.5(b), leading to $k^o_{red} = 1.89{\cdot}10^{-5}$ m s^{-1}. The measured values for $D_{Al_2Cl_7^-}$ and k^o_{red} were used in the calculations. The diffusion coefficient $D_{Cl^-} = 6.1{\cdot}10^{-11}$ m^2 s^{-1} was taken from literature [37], while $D_{AlCl_4^-}$ was assumed to equal D_{Cl^-}.

An estimate for the actual value of k_b was derived from a comparison of the experimental limiting current densities j_L (see table 7.2) and the calculated ones. Figure 7.6 shows the calculated j_L values as a function of k_b for different rotation speeds. Because the j_L versus k_b curves have a minimum, each line has two k_b values for which the calculated current density corresponds to the experimental value. These points are indicated by + and × for the intersections at low and high k_b values respectively and they are summarized in table 7.2. At the left side of the minimum, the estimated k_b value varies between 10^{-20} and $10^{-9.5}$ m^3 mol^{-1} s^{-1}, on the right side of the minimum k_b estimates are comprised between $10^{-7.5}$ and $10^{-6.7}$ m^3 mol^{-1} s^{-1}, which is a much smaller range. As in the ideal case, k_b should be independent of the rotation speed, these results indicate that the real k_b value lies between $10^{-7.5}$ and $10^{-6.7}$ m^3 mol^{-1} s^{-1}, which is within a factor of 6.3. A possible explanation for the fact that a range is observed instead of a

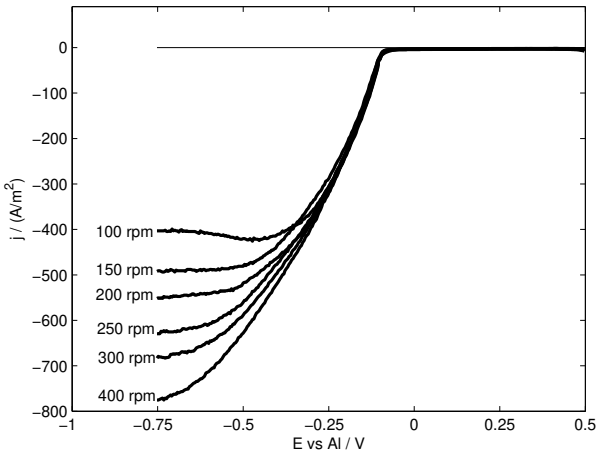

(a) Linear potential scans (20 mV s^{-1})

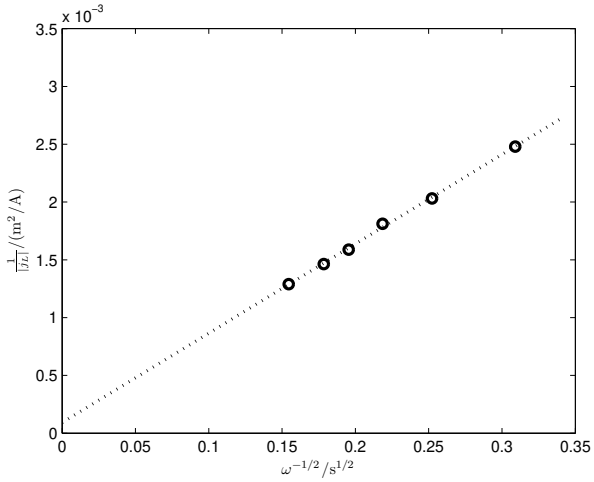

(b) Koutecky-Levich plot

Figure 7.5: Linear potential scans for different rotation speeds at 20 mV s^{-1} and Koutecky-Levich plot of $AlCl_3$ - $[C_2mim]Cl$ (60-40 mol%) at 40 °C.

Table 7.2: Experimental j_L values for different rotation speeds. Also given are the k_b values for which the calculated limiting current density corresponds to the experimental value.

Rotation speed (rpm)	$\lvert j_L \rvert$ (A/m^2)	Left intersection at k_b = (m^3 mol^{-1} s^{-1})	Right intersection k_b = (m^3 mol^{-1} s^{-1})
100	403	10^{-20}	$10^{-6.7}$
150	492	10^{-19}	10^{-7}
200	552	10^{-18}	$10^{-7.1}$
250	630	$10^{-17.1}$	$10^{-7.3}$
300	683	$10^{-15.6}$	$10^{-7.3}$
400	775	$10^{-9.5}$	$10^{-7.5}$

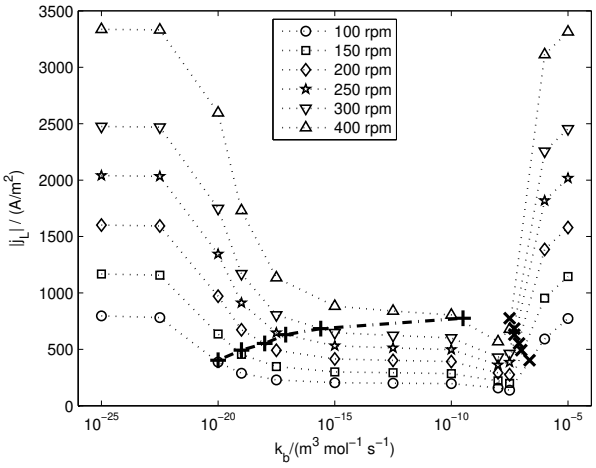

Figure 7.6: Calculated limiting current density j_L as a function of k_b for different rotation rates. The + and × signs indicate the intersection with the experimental j_L values (figure 7.5(a)).

fixed value might be that the kinetics of reaction (7.8) is not described by reaction (7.11) but by a more general expression of the form

$$R = k_b \left[AlCl_4^-\right]^a \left[Al_2Cl_7^-\right]^b \left[Cl^-\right]^c - k_f \left[AlCl_4^-\right]^d \left[Al_2Cl_7^-\right]^e \left[Cl^-\right]^f \qquad (7.17)$$

In table 7.1 it is shown that values of K_{eq} can vary, even if the temperature is kept constant. Therefore, the limiting current density j_L was calculated as a function of k_b (as in figure 7.6) but for different K_{eq} values, ranging from 10^{15} untill 10^{19}. These calculations showed that the j_L versus k_b curves shift to the left hand side for increasing values of K_{eq}. Furthermore, the estimated k_b values, based on these alternative K_{eq} values showed a larger range than the values determined using $K_{eq} = 10^{17.1}$.

Conclusion

We presented a finite element model of the electrodeposition of aluminium from chloroaluminate ionic liquids. It is shown that the calculated current densities strongly depend on the rate constants k_b and k_f of the autosolvolysis reaction. This is caused by the effect of these constants on the kinetics and thermodynamics of the autosolvolysis which change in opposite directions for variations in k_b. These opposing effects lead to a minimum in the calculated current density for intermediate k_b values. A comparison of the calculated data and the experimental limiting current densities indicates that the value of k_b lies between $10^{-7.5}$ and $10^{-6.7}$ m^3 mol^{-1} s^{-1}.

Experimental

Aluminium chloride (99%, anhydrous granules, Acros Organics) was used without further purification. [C_2mim]Cl (99%, Iolitec) was dried under vacuum and under stirring for 6 h at a temperature of 120 °C. Ultra pure aluminium wire (99.99%, Goodfellow) was used as a quasi-reference electrode and as counter electrode. Prior to the electrochemical experiments, all electrodes were cleaned. Both Al reference and counter electrode were cleaned with alkaline cleaner (type P3-RST, Henkel) at 70 °C for 5 minutes, rinsed with deionized water followed by immersion in mixture of H_3PO_4 (70%), H_2SO_4 (25%) and HNO_3 (5%) for a few seconds at room temperature to remove the residual oxide layer on the surface of the Al metal electrodes and rinsed with deionized water. Finally the electrodes were rinsed with ethanol and acetone and dried before being transferred into the dry box (moisture and oxygen levels below 1 ppm). The Pt working electrode was cleaned in a 1:1 water:HCl mixture, rinsed with deionized water, ethanol and acetone and dried. All electrochemical experiments were performed using a Potentiostat/Galvanostat EG&G 273.

Acknowledgments

This research was funded by a Ph.D grant of the Institute for the Promotion of Innovation through Science and Technology in Flanders (IWT-Vlaanderen) to S.S. The authors acknowledge financial support by the K.U.Leuven (projects IDO/05/005 and GOA 08/05), by the FWO-Flanders (research community "Ionic Liquids") and by the IWT-Flanders (SBO-project IWT 80031 "MAPIL") and the support of the Belgian Federal Science Policy Office through the IUAP project INANOMAT (contract P6/17). Support by IoLiTec (Heilbronn, Germany) is also acknowledged.

List of symbols

symbol	value and/or unit	meaning
$[\ldots]$	mol m^{-3}	concentration of species ...
$[\ldots]_{surf}$	mol m^{-3}	surface concentration of species ...
c	mol m^{-3}	concentration
D	m^2 s^{-1}	diffusion coefficient
ΔE	V	applied potential difference
F	96485 C mol^{-1}	Faraday constant
j_L	A m^{-2}	limiting current density
k_b	m^3 mol^{-1} s^{-1}	backward reaction rate constant
k_f	m^3 mol^{-1} s^{-1}	forward reaction rate constant
K_{eq}	$10^{17.1}$ (Ref. [34])	equilibrium constant for reaction (7.8)
k^o_{ox}	$1.89{\cdot}10^{-5}$ mol s^{-1} m^{-2}	heterogeneous rate constant for oxidation
k^o_{red}	$1.89{\cdot}10^{-5}$ m s^{-1}	heterogeneous rate constant for reduction
n	3	number of exchanged electrons from reaction (7.7)
N	mol m^{-2} s^{-1}	molar flux
r	m	radial coordinate
R	mol m^{-3} s^{-1}	bulk reaction rate
R_g	8.31 J mol^{-1} K	gas constant
t	s	time
T	313 K	temperature
$\mathbf{u}$	m s^{-1}	fluid velocity vector
u	m s^{-1}	scalar fluid velocity
z	m	axial coordinate
α	0.5	charge transfer coefficient for reduction
β	0.5	charge transfer coefficient for oxidation
η	V	$E - \eta_c$
η_c	V	concentration overpotential
θ	rad	angular coordinate
ν	$8.34 \cdot 10^{-6}$ m^2 s^{-1}	kinematic viscosity
ω	rad s^{-1}	rotation speed ($=\frac{2\pi \mathrm{rpm}}{60}$)

References

[1] F. H. Hurley, T. P. Wier Jr., The electrodeposition of aluminum from nonaqueous solutions at room temperature, *J. Electrochem. Soc.*, **98**, 207 (1951).

[2] L. G. Boxall, H. L. Jones, R. A. Osteryoung, Solvent equilibria of AlCl -NaCl melts, *J. Electrochem. Soc.*, **120**, 223 (1973).

[3] P. Rolland, G. Mamantov, Electrochemical reduction of $Al_2Cl_7^-$ ions in chloroaluminate melts, *J. Electrochem. Soc.*, **123**, 1299 (1976).

[4] J. Robinson, R. A. Osteryoung, The electrochemical behavior of aluminum in the low temperature molten salt system n butyl pyridinium chloride: Aluminum chloride and mixtures of this molten salt with benzene, *J. Electrochem. Soc.*, **127**, 122 (1980).

[5] J. S. Wilkes, J. A. Levisky, R. A. Wilson, C. L. Hussey, Dialkylimidazolium chloroaluminate melts: a new class of room-temperature ionic liquids for electrochemistry, spectroscopy, and synthesis, *Inorg. Chem.*, **21**, 1263 (1982).

[6] C. J. Dymek Jr., J. L. Williams, D. J. Groeger, J. J. Auborn, An aluminum acid-base concentration cell using room temperature chloroaluminate ionic liquids, *J. Electrochem. Soc.*, **131**, 2887 (1984).

[7] C. L. Hussey, T. B. Scheffler, J. S. Wilkes, A. A. Fannin, Chloroaluminate equilibria in the aluminum chloride-l-methyl-3-ethylimidazolium chloride ionic liquid, *J. Electrochem. Soc.*, **133**, 1389 (1986).

[8] P. K. Lai, M. Skyllas-Kazacos, Aluminium deposition and dissolution in aluminium chloride-*n*-butylpyridinium chloride melts, *Electrochim. Acta*, **32**, 1443 (1987).

[9] P. K. Lai, M. Skyllas-Kazacos, Electrodeposition of aluminium in aluminium chloride/1-methyl-3-ethylimidazolium chloride, *J. Electroanal. Chem.*, **248**, 431 (1988).

[10] R. T. Carlin, W. Crawford, M. Bersch, Nucleation and morphology studies of aluminum deposited from an ambient-temperature chloroaluminate molten salt, *J. Electrochem. Soc.*, **139**, 2720 (1992).

[11] G. R. Stafford, C. L. Hussey, *Advances in Electrochemical science and engineering*, volume 7, chapter Electrodeposition of transition metal-aluminum alloys from chloroaluminate molten salts, 275, Wiley-VCH Verlag GmbH, Weinheim (2002).

[12] Y. Zhao, T. J. Vandernoot, Electrodeposition of aluminium from nonaqueous organic electrolytic systems and room temperature molten salts, *Electrochim. Acta*, **42**, 3 (1997).

[13] A. P. Abbott, C. A. Eardley, N. R. S. Farley, A. Pratt, Novel room temperature molten salts for aluminium electrodeposition, *Trans. Inst. Metal. Finish.*, **77**, 26 (1999).

[14] T. Jiang, M. J. Chollier Brym, G. Dubé, A. Lasia, G. M. Brisard, Electrodeposition of aluminium from ionic liquids: Part I - electrodeposition and surface morphology of aluminium from aluminium chloride ($AlCl_3$)-1-ethyl-3-methylimidazolium chloride ([EMIm]Cl) ionic liquids, *Surf. Coat. Technol.*, **201**, 1 (2006).

[15] T. Jiang, M. J. Chollier Brym, G. Dubé, A. Lasia, G. M. Brisard, Electrodeposition of aluminium from ionic liquids: Part II - studies on the electrodeposition of aluminum from aluminum chloride ($AlCl_3$) - trimethylphenylammonium chloride (TMPAC) ionic liquids, *Surf. Coat. Technol.*, **201**, 10 (2006).

[16] J. Vaughan, D. Dreisinger, Electrodeposition of aluminum from aluminum chloride-trihexyl(tetradecyl) phosphonium chloride, *J. Electrochem. Soc.*, **155**, D68 (2008).

[17] Q. X. Liu, S. Zein El Abedin, F. Endres, Electrodeposition of nanocrystalline aluminum: Breakdown of imidazolium cations modifies the crystal size, *J. Electrochem. Soc.*, **155**, D357 (2008).

[18] G. Yue, S. Zhang, Y. Zhu, X. Lu, S. Li, Z. Li, A promising method for electrodeposition of aluminium on stainless steel in ionic liquid, *AIChE Journal*, **55**, 783 (2009).

[19] S. Zein El Abedin, P. Giridhar, P. Schwab, F. Endres, Electrodeposition of nanocrystalline aluminium from a chloroaluminate ionic liquid, *Electrochem. Commun.*, **12**, 1084 (2010).

[20] F. Endres, M. Bukowski, R. Hempelmann, H. Natter, Electrodeposition of nanocrystalline metals and alloys from ionic liquids, *Angew. Chem. Int. Ed.*, **42**, 3428 (2003).

[21] H. Natter, M. Bukowski, R. Hempelmann, S. Zein El Abedin, E. M. Moustafa, F. Endres, Electrochemical deposition of nanostructured metals and alloys from ionic liquids, *Z. Phys. Chem.*, **220**, 1275 (2006).

[22] A. P. Abbott, C. A. Eardley, N. R. S. Farley, G. A. Griffith, A. Pratt, Electrodeposition of aluminium and aluminium/platinum alloys from $AlCl_3$/benzyltrimethylammonium chloride room temperature ionic liquids, *J. Appl. Electrochem.*, **31**, 1345 (2001).

[23] R. T. Carlin, H. C. De Long, J. Fuller, P. C. Trulove, Microelectrode evaluation of transition metal-aluminum alloy electrodepositions in chloroaluminate ionic liquids, *J. Electrochem. Soc.*, **145**, 1598 (1998).

[24] J. A. Mitchell, W. R. Pitner, C. L. Hussey, G. R. Stafford, Electrodeposition of cobalt and cobalt-aluminum alloys from a room temperature chloroaluminate molten salt, *J. Electrochem. Soc.*, **143**, 3448 (1996).

[25] M. R. Ali, A. Nishikata, T. Tsuru, Electrodeposition of Co-Al alloys of different composition from the $AlCl_3$-BPC-$CoCl_2$ room temperature molten salt, *Electrochim. Acta*, **42**, 1819 (1997).

[26] W. Freyland, C. A. Zell, S. Zein El Abedin, F. Endres, Nanoscale electrodeposition of metals and semiconductors from ionic liquids, *Electrochim. Acta*, **48**, 3053 (2003).

[27] B. J. Tierney, W. R. Pitner, J. A. Mitchell, C. L. Hussey, G. R. Stafford, Electrodeposition of copper and copper-aluminum alloys from a room-temperature chloroaluminate molten salt, *J. Electrochem. Soc.*, **145**, 3110 (1998).

[28] W. R. Pitner, C. L. Hussey, Electrodeposition of zinc from the Lewis acidic aluminum chloride-1-methyl-3-ethylimidazolium chloride room temperature molten salt, *J. Electrochem. Soc.*, **44**, 3095 (1997).

[29] Y.-F. Lin, I.-W. Sun, Electrodeposition of zinc from a Lewis acidic zinc chloride-1-ethyl-3-methylimidazolium chloride molten salt, *Electrochim. Acta*, **44**, 2771 (1999).

[30] H. C. De Long, J. S. Wilkes, R. T. Carlin, Electrodeposition of palladium and adsorption of palladium chloride onto solid electrodes from room temperature molten salts, *J. Electrochem. Soc.*, **141**, 1000 (1994).

[31] G. R. Stafford, G. M. Haarberg, The electrodeposition of Al-Nb alloys from chloroaluminate electrolytes, *Plasmas & Ions*, **1**, 35 (1999).

[32] B. Trémillon, G. Letisse, Proprietes en solution dans le tetrachloroaluminate de sodium fondu I. Systemes acide-base, *J. Electroanal. Chem.*, **17**, 371 (1968).

[33] A. J. Bard, L. R. Faulkner, *Electrochemical methods*, chapter 12 - Electrode reactions with coupled homogeneous chemical reactions, John Wiley & Sons (2001).

[34] Z. J. Karpinski, R. A. Osteryoung, Potentiometric studies of the chlorine electrode in ambient-temperature chloroaluminate ionic liquids: Determination of equilibrium constants for tetrachloroaluminate ion dissociation, *Inorg. Chem.*, **24**, 2259 (1985).

[35] J. Fransaer, J. R. Roos, J. P. Celis, Fluid flow past a rotating disk, *Chem. Eng. Sci.*, **46**, 1194 (1991).

[36] A. J. Bard, L. R. Faulkner, *Electrochemical methods*, p. 341, John Wiley & Sons (2001).

[37] R. T. Carlin, R. A. Osteryoung, Microelectrodes in the examination of anodic and cathodic limit reactions of an ambient-temperature molten-salt, *J. Electroanal. Chem.*, **252**, 81 (1988).

Chapter 8

Conclusions and outlook

8.1 Conclusions

8.1.1 General conclusions

The research presented in this thesis concerned three main topics:

1. The electrochemistry of liquid metal salts: ionic liquids with incorporated metal ions to increase mass transport
2. The investigation of Cu-on-Ta electrodeposition in a high vacuum environment
3. Modeling of the electrodeposition of aluminium from chloroaluminates and the effect of the rate constants (of the equilibrium between $Al_2Cl_7^-$, $AlCl_4^-$ and Cl^-) on the limiting current density

While investigating the Cu-on-Ta electrodeposition, the first electrochemical oscillator in ionic liquids was discovered as well.

Chapters 2 and 3 studied the thermal stability and electrochemical behavior of the liquid metal salts $[Cu(MeCN)_4][Tf_2N]$, $[Cu(PhCN)_4][Tf_2N]$, $[Ag(MeCN)_4]_2$-$[Ag(Tf_2N)_3]$ and $[Ag(EtIm)_2][Tf_2N]$. For both metals, the acetonitrile-based complexes were thermally weaker than the PhCN-based or EtIm-based complexes, but gave better morphological results for the electrodeposits. This was especially true for the highest applied current density of 25 A dm^{-2}, a current density that normally cannot be achieved in unstirred ionic liquids. The deposits were free from incorporated species, showed a smooth appearance and did not show any signs of cracks, which could indicate build up of internal stresses. 1*H*-benzotriazole and thiourea permitted to decrease the roughness down to 45 nm for silver deposits and even to 7 nm for copper, giving a mirror-bright finish.

The liquid metal salts, presented in Chapters 2 and 3, not only can support high current densities. Another advantage of these compounds is that electrodeposition can take place at high applied overpotentials. In regular ionic liquids, the cation will decompose, its break-down products polluting the solution, but in liquid metal salts this breakdown is the desired reaction. In Chapter 4, $[Cu(MeCN)_2][Tf_2N]$ was tested for the deposition of copper on tantalum. Overpotentials up to -5.0 V were applied. The resulting copper deposits were as thin as 20 nm and completely closed due to the nucleation density of $8{\cdot}10^{14}$ m^{-2}. Unfortunately, an oxide layer was still found on the Cu-Ta interface.

Chapter 5 led to similar results, even in high vacuum conditions. The experimental findings contradict a calculation based on solubility data of O_2 which predicted that not enough oxygen is available for complete oxidation of the tantalum surface.

The ionic liquids that were used for these experiments were [BMP][Tf_2N], [BMP]Cl and [C_2mim]Cl. Again, a nucleation density of $8{\cdot}10^{14}$ m^{-2} could be reached.

The least expected, yet very interesting, results were found by accident during copper deposition from [C_2mim]Cl. They are described in Chapter 6. Under certain circumstances, a constant applied potential can cause an oscillating current signal. These circumstances require the presence of Cu^+ and Cu^{2+}, chloride and imidazolium cations. In a solution containing these four ion types, the application of -1.0 V vs Cu leads to a so-called N-NDR electrochemical oscillator. QCM experiments revealed that the oscillations corresponded to oscillations in the growth speed of the depositing copper and not from a superimposed, parasitic reaction in which both reactant and product are soluble. A change in temperature influences the frequency of the oscillations, and their duration.

A model on the aluminium deposition from chloroaluminates is developed in Chapter 7. It shows that the achievable limiting current density is a function of k_b, one of the rate constants determining the equilibrium between $Al_2Cl_7^-$, $AlCl_4^-$ and Cl^-. This is due to opposite effects of kinetics and thermodynamics: the larger k_b, the faster the kinetics of the autosolvolysis reaction takes place, but the less driving force is available for the reaction. This gives a minimum in the calculated current as a function of k_b. The value of k_b lies between $10^{-7.5}$ and $10^{-6.7}$ m^3 mol^{-1} s^{-1} as concluded from a comparison of the calculated data and the experimental limiting current densities. It was shown that the often suggested reaction (8.1) for aluminium deposition from chloroaluminate ionic liquids

$$4Al_2Cl_7^- + 3e^- \rightarrow Al + 7AlCl_4^- \tag{8.1}$$

is only a special case of the more general reactions (8.2) and (8.3):

$$Al_2Cl_7^- + 3e^- \rightarrow Al + AlCl_4 + 3Cl^- \tag{8.2}$$

$$3Cl^- + 3Al_2Cl_7^- \rightarrow 6AlCl_4^- \tag{8.3}$$

Reaction (8.1) is only valid if the equilibrium of reaction (8.3) lies completely to the right and that the kinetics of this reaction are fast. The former condition is met due to the high equilibrium constant ($K_{eq} = 10^{17.1}$), while the latter is only partially true.

8.1.2 Breakthroughs

- It was often thought that electrodeposition from ionic liquids would not get widespread use, except for some niche applications, due to their relatively high viscosity and correspondingly low current densities. It is hoped that the results on liquid metal salts, presented in this thesis, lead to the awareness

that ionic liquids are capable of depositing micrometer thick layers in short timescales, without the need of stirring.

- Metal deposition can take place at any desired (cathodic) potential without a parasitic reaction due to decomposition of the cation of the ionic liquid, as long as the metal can be incorporated in a liquid metal salt.

- The first electrochemical oscillator in ionic liquids was discovered, although finding it required a little bit of luck.

8.2 Outlook for further research

To end, some suggestions for further research are given. These suggestions are split up in suggestions for research in *standard* ionic liquids (based on cations such as shown in figure 1.1) and liquid metal salts.

Standard ionic liquids From an electrochemical point of view, the greatest challenge for research on ionic liquids (and those who synthesize them) is finding ionic liquids that are more cathodically stable than [BMP][Tf_2N], the currently most stable ionic liquid. The most obvious approach is the search for new cationic structures, but an alternative might be to strengthen the weak spots of existing structures, for instance by replacing easily removable hydrogens by methyl groups.

Liquid metal salts The challenges in research of liquid metal salts seem to be twofold.

At first, it might be advantageous to extend the amount of complexes by using other ligands. The best results of Chapters 2 and 3 were all achieved for liquid metal salts based on acetonitrile. Other complexes, such as the published [$Cu(PhCN)_4$][Tf_2N] or [$Ag(EtIm)_2$][Tf_2N] are also electrochemically active but do not lead to the qualitative deposits of acetonitrile-based complexes. The downside of the acetonitrile-based compounds is their low thermal stability. Preliminary tests were conducted on other copper or silver complexes than those mentioned in Chapters 2 and 3. Examples are [$Cu(MeIm)_6$][Tf_2N]$_2$, [$Cu(BuIm)_4Cl$]Cl or [$Ag(EtIm)_2$][TfO]. Both copper complexes lead to distorted cyclic voltammograms due to a high viscosity so that electrodeposition from these compounds does not seem feasible. The behavior of [$Ag(EtIm)_2$][TfO] seemed to resemble that of [$Ag(EtIm)_2$]-[Tf_2N], but at lower current densities so that it has no advantages over the $[Tf_2N]^-$ complex. Examples of complexes of other metals that were tested are [$Mn(BuIm)_5$]Cl_2 and [$Fe(MeIm)_6$][$(NO_3)_3$]$\cdot x H_2O$. None of these compounds could be reduced to manganese or iron metal. Secondly, it would be very interesting to test complexes of metals that are difficult to deposit:

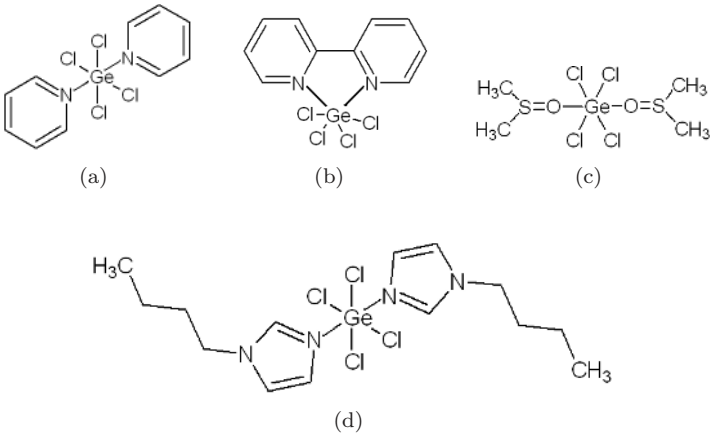

Figure 8.1: Complexes used for germanium deposition: (a) $GeCl_4(py)_2$, (b) $GeCl_4(bpy)$, (c) $GeCl_4(DMSO)_2$, (d) $GeCl_4(BuIm)_2$.

examples of such metals are the rare earth metals and germanium. The difficulty in the electrodeposition of rare earths is their electronegativity. The standard reduction potential of metals such as samarium or neodymium is around -2.3 V vs NHE (or -2.7 V vs Fc/Fc^+) which is at the edge of currently available ionic liquids. Germanium does not suffer from a large electronegativity: the difficulty in germanium deposition lies in finding a relatively cheap source of germanium ions with high solubility in ionic liquids. Often, $GeCl_4$ is used. This is however a molecular compound and probably does not dissociate completely in ionic liquids. Its solubility is limited and the boiling point is only 86 °C, so that the use of elevated temperatures leads to loss of $GeCl_4$ due to evaporation. In our ionic liquids research group, four different germanium complexes were synthesized, all starting from $GeCl_4$. These complexes are $GeCl_4(py)_2$, $GeCl_4(bpy)$, $GeCl_4(DMSO)_2$ and $GeCl_4(BuIm)_2$ (figure 8.1). In contrast with the earlier studied copper and silver based liquid metal salts, these germanium complexes were not used as pure compounds, but were dissolved in either $[BMP][Tf_2N]$ or $[BMP][N(CN)_2]$. These complexes have an increased thermal stability compared to $GeCl_4$, but still a limited solubility. An ideal complex for electrodeposition would have a low melting point (all compounds mentioned in figure 8.1 are solid at room temperature) and dissociates into ions so that it becomes electrically conductive and suitable for electrochemistry. In this case, the complex could be used in its pure form without the need to solubilize it into another solvent.

Appendix A

Derivations

A.1 Average hole size $\langle r_{hole} \rangle$

The following derivation for the average hole size was taken from [1].

The probability of finding a hole of a radius between r and $r + \mathrm{d}r$ is given by

$$P_r(r)\mathrm{d}r = \frac{16}{15\sqrt{\pi}} \left(\frac{4\pi\gamma}{\mathrm{k}T}\right)^{\frac{7}{2}} r^6 \exp\left(-\frac{4\pi\gamma}{\mathrm{k}T} r^2\right) \mathrm{d}r \tag{A.1}$$

The average radius $\langle r_{hole} \rangle$ is obtained from equation (A.1) by multiplying the probability by the radius of the hole and integrating this product over all possible values of r:

$$\langle r_{hole} \rangle = \int_0^\infty r P_r(r)\mathrm{d}r \tag{A.2}$$

so that

$$\langle r_{hole} \rangle = \int_0^\infty r \frac{16}{15\sqrt{\pi}} \left(\frac{4\pi\gamma}{\mathrm{k}T}\right)^{\frac{7}{2}} r^6 \exp\left(-\frac{4\pi\gamma}{\mathrm{k}T} r^2\right) \mathrm{d}r \tag{A.3}$$

or

$$\langle r_{hole} \rangle = \frac{16}{15\sqrt{\pi}} \left(\frac{4\pi\gamma}{\mathrm{k}T}\right)^{\frac{7}{2}} \int_0^\infty r^7 \exp\left(-\frac{4\pi\gamma}{\mathrm{k}T} r^2\right) \mathrm{d}r \tag{A.4}$$

The integral can be evaluated by substituting $t = \frac{4\pi\gamma}{\mathrm{k}T} r^2$

$$\int_0^\infty r^7 \exp\left(-\frac{4\pi\gamma}{\mathrm{k}T} r^2\right) \mathrm{d}r = \frac{1}{2} \left(\frac{\mathrm{k}T}{4\pi\gamma}\right)^4 \int_0^\infty t^3 \exp(-t)\mathrm{d}t \tag{A.5}$$

which leads to

$$\langle r_{hole} \rangle = \frac{4}{15\pi} \sqrt{\frac{\mathrm{k}T}{\gamma}} \int_0^\infty t^3 \exp(-t)\mathrm{d}t \tag{A.6}$$

The integral $\int_0^\infty t^3 \exp(-t)\mathrm{d}t$ is the gamma function $\Gamma(3+1)$ and is equal to 3! from

$$\Gamma(x+1) = \int_0^\infty t^x \exp(-t)\mathrm{d}t = x! \tag{A.7}$$

Hence,

$$\langle r_{hole} \rangle = \frac{8}{5\pi} \sqrt{\frac{\mathrm{k}T}{\gamma}} = 0.51 \sqrt{\frac{\mathrm{k}T}{\gamma}} \tag{A.8}$$

So the average surface area of a hole calculated by this procedure gives

$$4\pi \langle r_{hole}^2 \rangle = 3.5 \frac{\mathrm{k}T}{\gamma} \tag{A.9}$$

A.2 Stokes - Einstein equation

The following derivation is a simplified version of the derivation given by Sutherland [2].

A spherical particle moving through a viscous medium (figure A.1), feels a resistance F_d

$$F_d = 6\pi\mu r_{dc} v \tag{A.10}$$

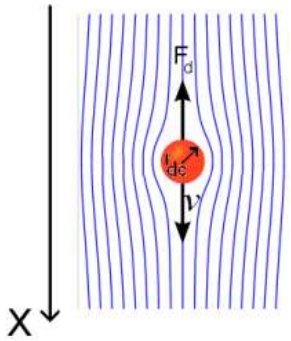

Figure A.1: Motion of spherical particle with velocity v through a medium with viscosity μ.

For a total of N_p particles per unit volume, this force is is given by

$$F_{total} = 6\pi\mu r_{dc} v N_p \tag{A.11}$$

At equilibrium, the resistance to motion is equal to the variation of osmotic pressure p_{osm}

$$F_{total} = -\frac{\mathrm{d}p_{osm}}{\mathrm{d}x} \tag{A.12}$$

so that

$$\Rightarrow 6\pi\mu r_{dc} v N_p = -\mathrm{R}_g T \frac{\mathrm{d}c}{\mathrm{d}x} \tag{A.13}$$

$$\Rightarrow 6\pi\mu r_{dc} \frac{v N_p}{\mathrm{N}_a} = -\mathrm{k}T \frac{\mathrm{d}c}{\mathrm{d}x} \tag{A.14}$$

Since

$$\frac{v N_p}{\mathrm{N}_a} = J = -D \frac{\mathrm{d}c}{\mathrm{d}x} \tag{A.15}$$

the conclusion is that

$$D = \frac{\mathrm{k}T}{6\pi\mu r_{dc}} \tag{A.16}$$

References

[1] J. O. Bockris, A. K. N. Reddy, *Modern Electrochemistry*, volume 1, chapter 6 - Ionic liquids, Plenum press, New York (1970).

[2] W. Sutherland, A dynamical theory of diffusion for non-electrolytes and the molecular mass of albumin, *Phil. Mag.*, **9**, 781 (1905).

List of Publications

1. S. Schaltin, P. Nockemann, B. Thijs, K. Binnemans and J. Fransaer, Influence of the anion on the electrodeposition of cobalt from imidazolium ionic liquids, *Electrochem. Solid-State Lett.*, **10**, D104-D107 (2007)

2. K. Deleersnyder, S. Schaltin, J. Fransaer, K. Binnemans and T. N. Parac-Vogt, Ceric ammonium nitrate (CAN) as oxidizing or nitrating reagent for organic reactions in ionic liquids, *Tetrahedron Lett.*, **50**, 4582-4586 (2009)

3. P. Nockemann, M. Pellens, K. Van Hecke, L. Van Meervelt, J. Wouters, B. Thijs, E. Vanecht, T. N. Parac-Vogt, H. Mehdi, S. Schaltin, J. Fransaer, S. Zahn, B. Kirchner and K. Binnemans, Cobalt(II) complexes of nitrile-functionalized ionic liquids, *Chem. Eur. J.*, **16**, 1849-1858 (2010)

4. S. Schaltin, A. Shkurankov, K. Binnemans and J. Fransaer, Direct Cu-on-Ta plating from ionic liquids in high vacuum, *ECS Trans.*, **25**, 119-128 (2010)

5. S. Schaltin, N. R. Brooks, K. Binnemans and J. Fransaer, Electrodeposition from cationic cuprous organic complexes: ionic liquids for high current density electroplating, *J. Electrochem. Soc.*, **158**, D21-D27 (2011)

6. N. R. Brooks, S. Schaltin, K. Van Hecke, L. Van Meervelt, K. Binnemans and J. Fransaer, Copper(I)-containing ionic liquids for high-rate electrodeposition, *Chem. Eur. J.*, **17**, 5054-5059 (2011)

7. S. Schaltin, K. Binnemans and J. Fransaer, Oscillating electrochemical reaction in copper-containing imidazolium ionic liquids, *Phys. Chem. Chem. Phys.*, **13**, 15448-15454 (2011)

8. S. Schaltin, M. Ganapathi, K. Binnemans and J. Fransaer, Modeling of aluminium deposition from chloroaluminate ionic liquids, *J. Electrochem. Soc.*, **158**, D634-D639 (2011)

9. S. Schaltin, N. R. Brooks, L. Stappers, L. D'Urzo, H. Plank, G. Kothleitner, C. Gspan, K. Binnemans and J. Fransaer, Electrodeposition from a liquid cationic cuprous organic complex for seed layer deposition, *J. Electrochem. Soc.*, **158**, D647-D650 (2011)

10. L. D'Urzo, S. Schaltin, A. Shkurankov, H. Plank, G. Kothleitner, K. Binnemans and J. Fransaer, Direct-on-barrier copper electroplating on ruthenium from the ionic liquid 1-ethyl-3-methylimidazolium dicyanamide, *J. Mater. Sci.: Mater. Electron.*, DOI: 10.1007/s10854-011-0525-4

11. C. Maton, N. De Vos, B. I. Roman, E. Vanecht, N. R. Brooks, K. Binnemans, S. Schaltin, J. Fransaer and C. V. Stevens, Continuous synthesis of peralkylated imidazoles and their transformation into ionic liquids, To be submitted to *ChemPhysChem*

12. S. Schaltin, N. R. Brooks, L. Stappers, K. Van Hecke, L. Van Meervelt, K. Binnemans and J. Fransaer, High current density electrodeposition from silver complex ionic liquids, *Phys. Chem. Chem. Phys.*, **14**, 1706-1715 (2012)

13. B. Neirinck, H. Marzouk, S. Schaltin, J. Fransaer, O. Van der Biest and J. Vleugels, Electrophoretic deposition onto ionic liquid layers, *Key Eng. Mater.*, **507**, 35-40 (2012)

List of Contributions to International Conferences

- S. Schaltin*, K. Binnemans and J. Fransaer, "*Direct Cu-on-Ta Electroplating from ionic liquids in high-vacuum*", EUCHEM conference on molten salts and ionic liquids, 24-29 August 2008, Copenhagen, oral presentation.
- S. Schaltin*, K. Binnemans and J. Fransaer, "*Direct Cu-on-Ta electroplating from ionic liquids in high vacuum*", 216^{th} meeting of the Electrochemical Society, 4-9 October 2009, Vienna, oral presentation.
- L. Stappers, S. Schaltin*, A. Shkurankov, J. W. Seo, K. Binnemans and J. Fransaer, "*Layering in ionic liquids*", EUCHEM conference on molten salts and ionic liquids, 14-19 March 2010, Bamberg, poster presentation (poster award).
- A. Shkurankov, S. Schaltin, L. D'Urzo, K. Binnemans and J. Fransaer*, "*Ionic liquids - a new path to form nanothin seed films for CMOS applications*", EUCHEM conference on molten salts and ionic liquids, 14-19 March 2010, Bamberg, poster presentation.
- N.R. Brooks*, S. Schaltin, Jan Fransaer and K. Binnemans, "*Synthesis and1 characterisation of new metal-containing ionic liquids and their use in electrodeposition*", EUCHEM conference on molten salts and ionic liquids, 14-19 March 2010, Bamberg, oral presentation.
- B. Neirinck*, S. Schaltin, H. Marzouk, J. Fransaer, O. Van der Biest and J. Vleugels, "*Electrophoretic deposition onto ionic liquid layers*", 4^{th} international conference on electrophoretic deposition: Fundamentals and applications, 2-7 October 2011, Puerto Vallarta, poster presentation.
- S. Schaltin*, K. Binnemans and J. Fransaer, "*Electrochemical oscillations in imidazolium ionic liquids*", 220^{th} meeting of the Electrochemical Society, 9-14 October 2011, Boston, oral presentation.

- S. Schaltin*, N. R. Brooks, K. Binnemans and J. Fransaer, "*Liquid metal salts: Ionic liquids for high current density electroplating of copper and silver*", 220$^{\text{th}}$ meeting of the Electrochemical Society, 9-14 October 2011, Boston, oral presentation.

*presenting author